Universidade do Minho
Escola de Engenharia

Andreia Martins

Seismic Behaviour of Masonry Veneer Walls

June 2018

Universidade do Minho
Escola de Engenharia

Andreia Martins

Seismic Behaviour of Masonry Veneer Walls

Doctoral thesis
Civil Engineering

Work performed under the supervision of
Graça Vasconcelos
Alfredo C. Costa

June 2018

DECLARAÇÃO

Nome: Andreia Piedade Gomes Martins

Endereço eletrónico: amartins@civil.uminho.pt Telefone: 914304612

Número do cartão de cidadão: 13743181

Título tese:

Seismic behaviour of masonry veneer walls

Orientadores:

Professora Doutora Graça Vasconcelos, Universidade do Minho

Investigador Principal Alfredo C. Costa, Laboratório Nacional Engenharia Civil

Ano de conclusão: 2018

Designação do Doutoramento:

Doutoramento em Engenharia Civil - Estruturas

Universidade do Minho, ___/___/_____

Assinatura: _____

DECLARAÇÃO

Andreia Piedade Gomes Martins, autora da presente Tese, declara ter atuado com integridade na sua elaboração. Confirma que em todo o trabalho conducente à sua elaboração não recorreu à prática de plágio ou a qualquer forma de falsificação de resultados.

Mais declara que tomou conhecimento integral do Código de Conduta Ética da Universidade do Minho.

Universidade do Minho, ___/___/_____

Assinatura: _____

Ao meu marido, pelo sentimento irrepreensível que nos une.

Agradecimentos

Os agradecimentos para a realização desta tese exigiriam várias páginas, pelo que pretendo resumi-las, pedindo desde já perdão a quem não for nomeado pessoalmente.

Este trabalho foi realizado com a orientação principal e imprescindível da Prof. Graça Vasconcelos, a quem agradeço sinceramente todo o apoio e persistência constantes, e sugestões importantes nas discussões técnicas. Também agradeço o apoio técnico, disponibilidade e simpatia características e muito presentes ao longo de todo o trabalho desenvolvido por parte do coorientador Engenheiro Campos Costa.

Queria partilhar os meus sinceros agradecimentos a todos os técnicos do Laboratório de Engenharia Civil pela preciosa ajuda que sempre disponibilizaram ao longo de todos estes anos. Enfatizo a minha particular apreciação para além do apoio técnico, ao genuíno apoio psicológico sempre presente e tão importante na concretização dos nossos objetivos. Agradeço também as restantes equipas que me apoiaram no desenvolvimento do trabalho experimental: Sr. Manuel na construção de todos os provetes de laboratório; *Cerâmica Vale da Gândara* pelo fornecimento dos tijolos; *Cortartec/Ancon* pelo fornecimento dos ligadores e *Hilti* pelo fornecimento de todos os dispositivos químicos de ancoragens.

Particularmente deixo os meus cordiais agradecimentos à Fundação para a Ciência e Tecnologia (FCT) pelo financiamento através da Bolsa de Doutoramento SFRH/BD/96484/2013. Este trabalho foi parcialmente financiado pelos fundos FEDER através do Programa Operacional Fatores de Competitividade - COMPETE e pelos fundos nacionais da FCT no âmbito do projeto POCI-01-0145-FEDER-0076 33. *I would like to acknowledge the Portuguese Science and Technology Foundation (FCT) for its financial support through grant SFRH/BD/96484/2013. This work was partly financed by FEDER funds through the Competitivity Factors Operational Programme - COMPETE and by national funds through FCT - Foundation for Science and Technology within the scope of the project POCI-01-0145-FEDER-0076 33.*

Além destes importantes agradecimentos, é com um enorme gosto que reconheço o afeto crucial dos amigos que me acompanharam neste processo em especial a Bete, a Abreu e a Joana, entre muitos outros que sabem quem são e que também agradeço por fazerem parte da minha vida. Em tom especial, enumero também o Hélder, amigo de uma vida, por tudo

aquilo que vivemos e haveremos de viver. De coração cheio de boas memórias agradeço o companheirismo ao longo dos tempos, a humildade em situações complicadas, a paciência de me suportarem em dias difíceis, o apoio incondicional que me proporcionaram nas horas certas e o carinho com que me recebem nas suas vidas.

Como não podia deixar de ser, registo aqui a minha maior gratidão e respeito pelos meus pais, irmãos e restante família, não só pela importância que tiveram no desenvolvimento deste trabalho, mas também por todo o meu desenvolvimento enquanto pessoa. Respeitosamente, deixo um especial obrigado ao meu pai que me deixou fisicamente no culminar deste processo. Deixo-vos um agradecimento sincero e aprecio genuinamente todos os valores morais transmitidos que me fazem acreditar ser possível sermos melhores enquanto pessoas para fazermos melhor enquanto profissionais.

Ao meu marido Bruno, ao qual dedico inteiramente este documento com imensa satisfação, gostaria de congratular o facto de o poder ter na minha vida a acrescentar-me todos os dias, pois é sem dúvida a minha fonte de inspiração quer para o desenvolvimento desta tese como em tudo na minha vida. Aprecio verdadeiramente o apoio e proteção incondicionais, a dedicação e afeto desmedidos, o sentimento inesgotável e a resiliência de querer sempre ficar.

Uma vez família, família toda a vida.

Obrigada.

Abstract

It is recognized that masonry veneer walls, commonly used in commercial, industrial and residential buildings can be vulnerable to earthquakes and most of the reported cases of failures are due to poor materials, design and inadequate construction practices. This inadequate behaviour has promoted research on the seismic behaviour of brick veneer walls mostly attached to structural systems composed of light timber and steel frames but this work aims to contribute to the knowledge of seismic behaviour of masonry veneer whose backing support is composed by brick masonry infill walls enclosed in RC frames that is a construction system common in Portugal and South of European countries. In detail, this thesis aims at: (1) analyse at the local level the mechanical behaviour of connections of wall ties between the brick veneer walls and masonry infill walls; (2) assess the mechanical behaviour of brick veneer walls under out-of-plane loads for different configurations of ties; (3) carry out an overview of standards and provide design and construction guidelines under seismic action for brick masonry veneer walls. To accomplish this, an extensive experimental program was designed, being divided mainly in two phases: (1) mechanical and physical characterization of materials components, such mortar, bricks and brick masonry. An extensive experimental campaign on cyclic tension-compression and shear tests on different tie-masonry assemblages was performed. Different parameters were considered, namely the type of tie, width of the air cavity, mortar strength and embedment length of the ties; (2) cyclic out-of-plane tests on brick masonry veneer walls attached to brick masonry walls enclosed in a RC frame. In this experimental campaign it was also varied the type of ties, air cavity width, embedment length and the effect of previous in-plane loading. The experimental work is complemented with analytical tools to define hysteric laws to represent the cyclic tension-compression and shear behaviour of ties, which can be used in further numerical studies.

It was concluded that the tension-compression behaviour of connections is influenced by the type of wall tie and air cavity width. The stiffness of tie and free length influences significantly the compression behaviour and the shape of tie and embedment length of the tie control the tensile behaviour. The out-of-plane behaviour of the brick veneer walls depend also on the type and number of ties, and on the air cavity width. Both parameters control the out-of-plane performance from the brick veneer walls to the backing wall.

Resumo

As paredes de alvenaria de fachada, habitualmente aplicadas em edifícios comerciais, industriais e residenciais, podem ser vulneráveis a terremotos e a maioria dos casos de rotura registados deve-se a materiais pobres, projeto e práticas inadequadas de construção. Esse comportamento inadequado tem promovido investigação sobre o comportamento sísmico de paredes de alvenaria de fachada principalmente conectadas a sistemas estruturais constituídos por madeira e estruturas metálicas. Este trabalho visa compreender o comportamento sísmico de paredes de fachada, cujo suporte é composto por paredes de enchimento inseridas em pórticos de betão armado, sendo um sistema de construção comum em Portugal e no sul da Europa. Em detalhe, esta tese pretende: (1) analisar localmente o comportamento mecânico das conexões com ligadores entre a parede de fachada e a parede de enchimento; (2) avaliar o comportamento mecânico de paredes de alvenaria de fachada sob carregamento fora do plano em diferentes configurações de conexões; (3) desenvolver uma revisão de normas e fornecer diretrizes de projeto e construção para paredes de alvenaria de fachada. Com efeito, foi desenvolvido um extenso programa experimental, sendo dividido principalmente em duas fases: (1) caracterização mecânica e física dos componentes do sistema, tais como argamassas, tijolos e alvenaria. Foi realizada uma extensa campanha experimental de ensaios cíclicos de tração-compressão e corte em diferentes tipos de conexões. Consideraram-se diferentes parâmetros, nomeadamente o tipo de ligador, a largura da cavidade de ar, a resistência da argamassa e o comprimento de embebimento dos ligadores; e (2) ensaios cíclicos fora de plano em paredes de alvenaria de fachada ligadas a paredes de enchimento inseridas em pórticos de betão armado. Nesta campanha experimental também foi avaliado o tipo de ligador, a largura da cavidade de ar, o comprimento de embebimento e efeito de dano prévio no plano. O trabalho experimental foi complementado com ferramentas analíticas para definição de leis histeréticas para a representação do comportamento de compressão-tração e corte das conexões, que podem ser usadas em estudos numéricos adicionais.

Concluiu-se que o comportamento de compressão-tração das conexões é influenciado pelo tipo de ligador da parede e pela largura da cavidade de ar. A rigidez do ligador e o comprimento livre influenciam significativamente o comportamento à compressão. O tipo de ligador e o comprimento de embebimento do ligador controlam o comportamento à

tração. O comportamento fora do plano das paredes de alvenaria depende também do tipo e número de ligadores e da largura da cavidade de ar. Ambos os parâmetros controlam o desempenho fora do plano das paredes de alvenaria de fachada e da parede de suporte.

Index

List of symbols

Latin upper case letters:

A and A_i – loaded area;

A_{eff} – area of the vertical faces which effectively resist to compression;

A_{env} – total energy of the experimental envelope curve;

$A_{env}^{pre-peak}$ and $A_{env}^{post-peak}$ – energy of the experimental envelope curve correspondent to the pre-peak and post-peak behaviour, respectively.

$A_{tri}^{pre-peak}$ and $A_{tri}^{post-peak}$ – energy of the trilinear idealized curve correspondent to the pre-peak and post-peak behaviour, respectively;

A_{gross} – gross area for units intended to be laid on a full bed of mortar;

A_n – area of net mortared and/or grouted section of a wall;

A_{pt} – projected area of masonry wall ties;

A_t – section area of wall tie;

C – coefficient of water absorption for an individual mortar specimen;

CG_f – cumulative dissipation of energy;

C_{sd} – reduction coefficient;

D_p – relative seismic displacement;

D_r – drift ratio;

E – elasticity modulus;

E_e^+ and E_e^- – elastic energies of an equivalent viscous system calculated at the maximum displacement in each loop for the positive and negative direction of loading;

F – generalized force;

F_{cr} and d_{cr} – force and displacement correspondent the beginning of cracking phenomenon.

$F_i(\delta_{max}^{i-1})$ – force of a displacement corresponding to the maximum resistance in the previous cycle;

$F_{i,max}$ – maximum shear force;

F_{max} – maximum load;

F_o or $F_o{}'$ – intersection point of tangent line of the backbone curve and abscissa y-axis;

F_{pi} – precompressive force;

F_p – component seismic force applied horizontally at the center of gravity of the component or distributed according to the mass distribution of the component;

F_r, $F_r{}'$ and F_{res} – residual forces corresponding to displacement 0;

$F_{re,1}$ and $F_{re,1}{}'$ – forces corresponding to displacement $\delta_{re,1}$ and $\delta_{re,1}{}'$, respectively;

$F_{re,2}$ and $F_{re,2}{}'$ – forces corresponding to displacement $\delta_{re,2}$ and $\delta_{re,2}{}'$, respectively;

$F_{t\_shear\ damage}$ – tensile maximum strength of specimen with prior shear damage;

$F_{un,F=0}$ and $F_{un,F=0}{}'$ – forces corresponding to displacement $\delta_{un,F=0}$ and $\delta_{un,F=0}{}'$, respectively;

$F_{un,1}$ and $F_{un,1}{}'$ – forces corresponding to displacement $\delta_{un,1}$ and $\delta_{un,1}{}'$, respectively;

F_x or $F_x{}'$ – upper force asymptote of backbone curve;

G – modulus of rigidity;

G_c – energy of dissipation of a cycle;

I_p – importance factor;

K – constant according type of material to obtain the characteristic compressive strength of bricks;

K_d and $K_d{}'$ – tangent stiffness of the backbone curve for tension and compression loading, respectively, after resistant peak;

K_i – initial stiffness;

Ki,c – compression initial stiffness;

Ki,t – tension initial stiffness

K_0 and $K_0{}'$ – tangent stiffness of the backbone curve for tension and compression loading, respectively, before resistant peak;

$K_{re,1}$ and $K_{re,1}{}'$ – stiffness of first part of the curve;

$K_{re,3}$ and $K_{re,3}{}'$ – tangent stiffness before maximum resistance;

$K_{t\_shear\ damage}$ – tension stiffness of specimen with prior shear damage;

$K_{un,1}$ and $K_{un,1}{}'$ – steep slope of the unloading branch after the maximum displacement;

K_x or $K_x{}'$ – slope or tangent stiffness of the descending backbone;

L – length of the wall;

L_d – initial length of the diagonals of a wall or frame;

L_h – initial horizontal length between diagonals points;

L_v – initial vertical length between diagonals points.

M_1 and M_2 – mass of the specimen;

$N_c{}^{pull}$ – strength capacity governed by masonry breakout;

$N_c{}^{tie}$ – strength capacity governed by steel failure;

P_D – superimposed dead load at the top of the wall under consideration;

P_W – self-weight of the wall;

Q_{CL} and Q_{CE} – design strength;

Q_{UF} – imposed stresses;

R – electrical resistivity;

R_p – response modification factor;

S_a – seismic coefficient applicable to non-structural elements;

S_{XS} – spectral response acceleration parameter at short periods for any Seismic Hazard Level;

V_s – apparent volume of the specimen;

W – width of specimen;

W_p and W_a – weight of the wall or of a specific area of the wall;

X – height of upper support attachment at level x as measured from grade;

Y – height of lower support attachment at level y as measured from grade.

Latin lower case letters:

a_g and g – design ground acceleration;

a_p – amplification factor;

b – depth of the specimen;

d is the general displacement;

d_d and F_d – displacement and force correspondent to intersection the experimental envelope with a function defined by $F = 0.8\ F_{max}$;

d_e – displacement correspondent to intersection of $F = F_d$ with $F = k_e d$;

dist – distance between transmitter and receiver;

d_{max} – maximum tested displacement;

d_{Fmax} – displacement correspondent to maximum load;

d_{resi} – displacement correspondent to beginning of residual plateau;

e_m – moisture expansion;

f_a – axial compression stress caused by gravity loads;

f_b – normalized mean compressive strength of the units;

f_c – compressive strength;

f_{cfm} – flexural strength;

f'_{dt} – masonry diagonal tension strength;

f_k – characteristic compressive strength of the masonry;

f_m – compressive strength of the mortar;

f'_m –masonry compressive strength;

strength;

f_{pi} – precompressive strength;

f_{vo} – initial shear strength;

f_{voik} – characteristic shear strength for each level of precompressive stress;

f_{vok} – characteristic initial shear strength or cohesion;

f_{voi} – initial shear strength;

f_x or f'_x – lower force asymptote of backbone curve;

g_v – vertical gage length;

h – height of specimen;

h_{eff} – average elevation of structure;

h_{inf} – height of infill panel;

k – knowledge factor;

k_e – effective stiffness;

l – distance between the support rollers;

l_b – effective embedment length of wall tie.

l_i – first measurement before test;

l_{m1} – mean initial deviations of l_{s1} and l_{s2};

l_{m2} – mean initial deviations of l_{s3} and l_{s4};

l_{s1} , l_{s2} , l_{s3} and l_{s4} – measurement of length after bricks cooled, 3h of bricks cooled, 1h of bricks immersed and 24h of bricks immersed, respectively.

m – capacity modification factor;

m_c – adjustment factor depending on the moisture;

$m_{s,sat}$ – mass of saturated specimen of hardened mortar;

$m_{s,i}$ – apparent mass of saturated specimen of hardened mortar immersed in water;

$m_{s,dry}$ – oven dry mass of specimen of hardened mortar;

n – percent of the gross area of the unit that is solid expressed as a decimal;

q – structural behaviour factor;

t – total thickness of specimen;

time – time taken by the pulse to overcome the distance *dist*;

t_{eff} – average thickness of structure;

x – elevation in structure of the average point of attachment of the component to the structure;

w – width of specimen.

Greek lower case letters:

ΔV – the vertical shortening;

ΔH – horizontal extension;

Δ_ρ – variation of density;

Δ_η – variation of porosity;

Δ_C – variation of capillarity coefficient;

Δ_{UPV} – variation of ultrasonic pulse velocity;

Δd_1 and Δd_2 – the length change of diagonals of a wall or frame, respectively.

Greek upper case letters:

α – factor dependent of boundaries conditions of wall;

α_0 – internal friction;

α_k – characteristic internal friction;

β – correction factor dependent of geometric characteristics of wall;

γ – shear distortion;

γ_a – importance factor of the element;

δ_{Fmax} – displacement correspondent to maximum load;

δ_{max} and $\delta_{max}{}'$ – displacement corresponding to maximum forces F_{max} and $F_{max}{}'$, respectively;

δ_{re1} and $\delta_{re,1}{}'$ – 30% of displacement of maximum resistance;

δ_{re2} and $\delta_{re,2}{}'$ – 80% of displacement of maximum resistance;

$\delta_{un,1}$ and $\delta_{un,1}{}'$ – 90% of displacement of maximum forces;

$\delta_{un,F=0}$ and $\delta'_{un,F=0}$ – residual plastic deformations;

δ_x or $\delta_x{}'$ – point of inflection located at deflection of backbone curve;

δ_X – lateral displacement at level x of structure;

δ_Y – lateral displacement at level y of structure.

ε – strain;

ε_v – mean vertical strain;

η – open porosity (or apparent porosity);

μ_0 – global ductility factor;

μ_k – characteristic friction coefficient;

ν – reduction factor;

ξ – shape factor;

ρ – dry bulk density of mortar;

ρ_w – density of water;

σ_c – compressive strength;

σ_d – strength design;

σ_{eff} – compressive strength;

σ_{gross} – compressive strength;

σ_{max} – maximum strength;

τ – shear stress.

List of acronyms

ACI – American Concrete Institute;
ANSI – American National Standards Institute;
ASCE/SEI – Structural Engineering Institute of the American Society of Civil Engineers;
CP – Collapse Prevention;
DL – Damage Limitation;
DL – Double Leaf;
EC6 – Eurocode 6;
EC8 – Eurocode 8;
EVDR – Equivalent Viscous Damping Ratio;
IO – Immediate Occupancy;
LS – Life Safety;
LVDT – Linear Variable Differential Transducer;
MIL – Masonry Infill Leaf;
MSJC – Masonry Standards Joint Committee;
MVL – Masonry Veneer Leaf;
NC – Near Collapse;
O – Operational;
PR – Position Retention;
RC – Reinforced Concrete;
SD – Significant Damage;
TMS – The Masonry Society;
UPV – Ultrasonic Pulse Velocity;
URM – Unreinforced Masonry.

List of figures

List of tables

Chapter 1

Introduction

1.1. Background and research focus

Following the natural evolution of structural systems for buildings and with innovative insulation materials, alternative construction technologies have been developed for the enclosure walls, other than masonry structural walls [1]. In many European countries, the façade walls were characterized by single leaf walls, built with stone, brick or adobe [1] ensuring the global stability of the buildings until mid-twentieth century. With the introduction of structural solutions other than structural masonry, such as reinforced concrete frames with or without concrete shear walls, masonry walls lost their structural role and become mostly non-loadbearing walls [2]. Traditionally, the masonry walls were rendered with mortar and painted. However, the maintenance costs and the need to avoid or reduce problems with humidity and thermal bridges led to the development of masonry veneer walls adopted as an alternative solution for traditional building rendered façades due to the enhanced aesthetic, higher thermal comfort and better behaviour with respect to humidity [1, 3].

The masonry veneer walls system (often in brick masonry) is the research focus and consists of an exterior cladding acting as a skin of the structure separated from it by an air cavity, which is often filled or partially filled with insulation material. Due to their aesthetics and durability, the masonry veneer walls are found in several countries of Europe, such as Italy, England, Portugal, France and Germany, as well as in United States and New Zealand in low to medium rise residential buildings [4]. In Portugal, masonry veneer walls have been applied mainly from the 1980's in industrial and residential buildings. Two emblematic examples of brick external veneer are the Electricity museum, initially a thermoelectric power station (Figure 1.1 (a)), and *Campo Pequeno* Bull-ring built in 1982 [4], see Figure 1.1 (b).

The stability of the brick veneer is ensured by connecting it to a baking structural system through wall ties [5]. The backing system, to which the masonry veneers are attached, can be composed of light wood or steel frames, structural masonry or masonry infill walls in conjunction with reinforced concrete frames. The brick veneer walls are attached to the backing system through distinct types of ties, generally from steel, with very different geometry, much dependent on the backing system. The main role of wall ties on masonry veneer walls is transferring the out-of-plane lateral loads to the backup by providing a

connection between the masonry veneer and the backup. For this, the wall ties should have adequate resistance and stiffness in tension and in compression and shear flexibility to accommodate in-plane movements.

(a) (b)

Figure 1.1 – Examples of brick veneers in Portugal; (a) Electricity museum, Lisbon; (b) Campo Pequeno Bull-ring, Lisbon

1.1.Motivation

Problems related with the performance of masonry infills and brick veneer walls under seismic action have been observed in recent earthquakes in Italy and other seismic prone European countries [6, 7]. Some past studies stated that the unreinforced masonry walls buildings (being included this typology of masonry walls) were responsible for 60% of the fatalities caused by earthquakes in the second half of the 20th century and 74000 people died [8, 9]. Vulnerability of masonry veneer walls under recent earthquakes has been identified, taking into account that these elements have exhibited extensive diagonal cracking and, particularly, out-of-plane detachment from the backing support [10]. Earthquake-resistant construction should be considered in constructions possibly subjected to seismic activity to make them capable of withstanding earthquakes up to a specific magnitude. However, this is a challenge not yet solved, because the brick masonry veneer walls enclosures are not considered as structural elements most of times. However, under earthquakes and strong winds they are subjected to actions that force them to behave structurally. Due to their mass and connection to the backing structural system, veneer walls may influence the overall dynamic response under seismic actions [11, 12]. Thus, it is very important to analyse the behaviour of these structures under lateral actions in order to better predict its seismic performance and to developed suitable design approaches. The absence of appropriate design is known to be one of the main factors contributing to the activation of serious failure

mechanisms. Unfortunately, sufficient information is not available on common constructive practices and considerable research is still being conducted toward that objective. The literature has pointed out that the seismic behaviour of brick veneers depends on various features, such as the tie connection spacing and stiffness, the relative stiffness between the facing and backing structure, the support conditions of brick veneer and of the backup, the location of wall edges and openings, the air cavity width, and the type of loading applied to the wall [13]. Several works has been developed in order to characterize the veneer walls with light wood or steel frames [14-17]. However, it was found a gap in literature about seismic performance of masonry veneer walls in which the backing system is composed of reinforced concrete (RC) frames filled with unreinforced masonry walls.

Thus, the research carried out aims at filling a research gap about seismic characterization of masonry veneer wall system composed of RC frames with brick masonry infill, which is applied in majority of masonry veneer walls in Portugal and South of Europe. Although the masonry infill walls are considerable non-structural, many studied has been carried out and they have concluded that masonry infill walls contribute significantly to the seismic building performance [18-21]. The objectives and associated tasks established for the thesis are part of this effort and intend to push forward this field of study.

1.2. Objectives and methodology

This thesis intends to contribute for the better understanding of the behaviour of masonry veneer walls under cyclic out-of-plane loads, which represent in a simple way the out-of-plane inertial forces in the occurrence of seismic events. Therefore, the main goal of this work is the mechanical characterization under out-of-plane loads of brick veneer walls representative of Portuguese construction practice when attached to brick infill enclosed in reinforced concrete frames. In addition, it is intended to provide guidelines for design and construction of brick veneer walls. In detail, this thesis aims at:

1. Analysing at the local level the mechanical behaviour of connections of wall ties between the brick veneer walls and masonry infill walls;

2. Assessing the mechanical behaviour of brick veneer walls under out-of-plane loads for different configurations of wall ties;

3. Carrying out an overview of standards and provide design and construction guidelines under seismic action for brick masonry veneer walls.

To accomplish these objectives, an extensive experimental campaign was designed to (1) characterize the materials used in the construction of the brick veneer walls, namely of the masonry compounds (units and mortars) and of brick masonry as a composite material subjected to different types of load configurations. An experimental campaign was also designed to characterize the behaviour of brick masonry to freeze and thawing ageing; (2) evaluate the cyclic tension-compression and shear behaviour of different types of ties connecting the brick veneer walls to brick infill walls. Mechanical parameters as strength, stiffness, ductility and energy dissipation are very important in this experimental analysis for possible model calibration in future numeric works; (3) characterize in detail the out-of-plane response of brick veneer walls when subjected to out-of-plane loads and better understand the interaction existing between the wythes of system under study, as well as the main parameters that more influence its seismic performance. Tie typology, tie spacing, air cavity width and construction details are some factors that should be analysed in detail. Mechanical parameters, deformational features and typical failure modes are also important to know in order to predict possible seismic responses.

The experimental work is complemented with some analytical work to define hysteric laws to represent the cyclic tension-compression shear behaviour of ties, which can be used in further numerical studies. In addition, typical force-displacement diagrams are derived to enable the assessment of the seismic performance of ties in the context of the design of brick veneer walls based on performance levels.

1.3. Outline of the thesis

The presentation and discussion of the work carried out in this thesis is carried out in six chapters (Chapter 2 to Chapter 7). Besides the development of the thesis, two additional chapters are included, namely Chapter 1, where the framework, objectives and methodology are presented and Chapter 8, where the main conclusions and future works are provided, see Figure 1.2.

Chapter 2 deals with a literature review and provides an overview of relevant topics on brick veneer walls and summarize in a critical way the main works carried out in the scope of the present thesis. Initially, a brief description of the constructive system is presented with the clarification of the main details to take into account in the characterization of the brick veneer

walls under study. In addition, research on experimental and analytical analyses of brick veneer walls carried out in the past is described and discussed.

Chapter 3 aims at describing and discussing of the experimental work designed for physical and mechanical characterization of materials used in the construction of the brick veneer walls systems composed by brick veneer walls, wall ties and infill walls. In particular, bricks, mortar, ties and masonry were characterized considering the appropriate tests in order to obtain key mechanical parameters. The experimental characterization concentrated on the determination of: compression strength and moisture expansion of bricks; compression and flexural strength, density, porosity and capillarity coefficient of mortars; tensile strength of ties; compression, flexural and shear strength of brick masonry veneer. In addition, freeze and thaw resistance of masonry veneer and mortars is also provided. It is considered that this experimental characterization is justified by the possible exposure environment conditions to which façade walls can be subjected.

Chapter 4 presents the results of an extensive experimental campaign for the characterization of tie-masonry connections under different loading configurations. Static cyclic tension-compression and shear tests were carried out on single leaf and double leaf tie-brick masonry assemblages. Tie typology was the main variable under analysis in the different tie-masonry assemblages. An extensive discussion of the results on the damage patterns, hysteretic behaviour and derived seismic parameters is provided. A comparison of the results is carried out based on the different types of ties and among the different tie-masonry assemblages.

Chapter 5 is composed by three main research issues: (1) derivation of an analytical hysteretic model and calibration based on experimental results on cyclic tension-compression and shear tests; (2) assessment of previous shear damage of connections in the cyclic tension-compression behaviour of tie-masonry assemblages; (3) parametric experimental analysis based on the discussion of the influence of different parameters in the cyclic tension-compression behaviour of double-leaf tie connections, namely: (a) compressive strength of mortar; (b) air cavity width and (c) embedment length of the wall ties in the mortar bed joints of the brick masonry prisms.

Chapter 6 presents and discusses the experimental results of an extensive experimental campaign of brick veneer walls under cyclic out-of-plane loading. After the description of the details of the out-of-plane tests, namely regarding the specimens, test setup, instrumentation and test procedure, a detailed discussion of the results is given. The discussion is based on the damage patterns, hysteretic behaviour, and derived seismic

parameters, namely stiffness, plastic deformation, energy of dissipation and equivalent viscous damping ratio. It is also carried out a parametric analysis based on seismic parameters of walls with different tie typology, tie spacing, air cavity width and embedment length of wall ties. It is also evaluated the influence of in-plane damage of the brick infill walls, working as the backing system, in out-of-plane behaviour of system. These results provide important experimental data to calibrate future analytical models.

Finally, Chapter 7 provides an overview of the procedures existing in different standards aiming at design the brick veneer walls under seismic actions. Procedures for the seismic design of brick veneer walls as structural or non-structural elements are presented. In addition, an analytical model for seismic design of connections is derived for two types of connections based on the results obtained in Chapter 4. Bilinear and trilinear curves are derived of the experimental backbone curves, from which it is possible to derive different key deformation values associated to different performance limits.

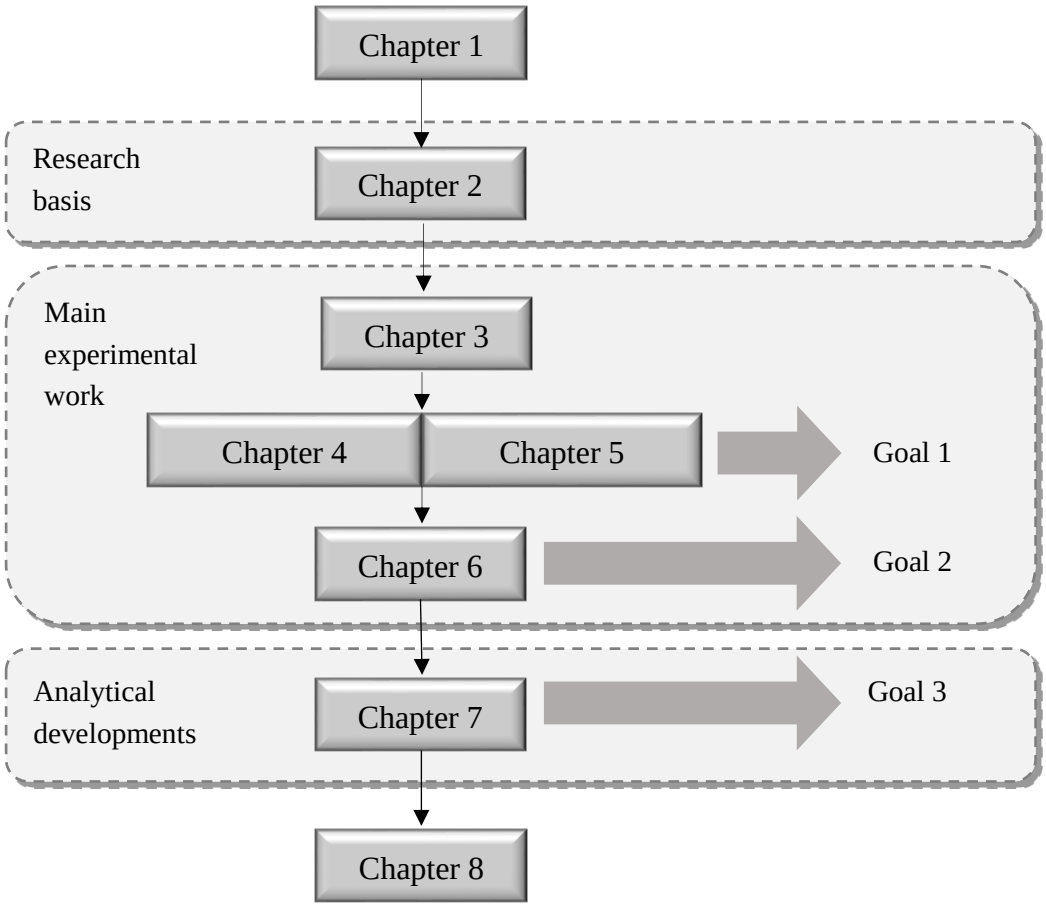

Figure 1.2 – Schematic overview of the thesis' chapters.

Chapter 2

Literature Review

Abstract:

Masonry veneer walls have been used successfully in a wide variety of commercial, industrial, and residential structures and are common place in modern building construction in several countries. However, it is recognized that the veneer walls can be vulnerable to earthquakes and most of the reported cases of failures are due to poor materials, design and inadequate construction practices. This inadequate behaviour has promoted research on the seismic behaviour of brick veneer walls mostly attached to structural systems composed of light timber and steel frames.

This chapter provides an overview of brick veneer walls under seismic actions, presenting a description of the main system characteristics, namely constitutive materials and their roles, mechanical and seismic behaviour, design guidelines and construction specifications. The chapter 2 also summarizes research studies addressing different types of brick veneer walls systems (with steel, stud and concrete block backup walls), different types of analyses (experimental and numerical) and different types of loading (out-of-plane and in-plane static and dynamic).

2.1. Introduction

Brick masonry is an ancient construction material and it has been widely used in the construction of enclosure walls that separate the internal and external environments [22]. The enclosure walls were in the past built by single leaf walls, built with stone, brick or adobe and afterwards by masonry cavity walls, composed of two leaves separated by an air cavity, which was often full or partially filled with insulation material to improve thermal or acoustic performance [1, 3]. The masonry veneer walls system has come into its own in the last 50 years and it is basically a particular typology of a masonry cavity walls but working as a skin of building, involving it in all its external area. Taking into account this leaf is considered structurally unstable and a non-structural element in terms of design most of times, the veneer leaf is anchored, being secured to and supported laterally by the backing through anchors (ties) and supported vertically by the foundation or other structural elements. The veneer should transfer out-of-plane load directly to the backing and is not considered to add load-resisting capacity to the wall system. The backup structure began as concrete block masonry but has evolved into steel or wood stud frames construction as well masonry infill walls.

However, the failure mechanisms related specially with the out-of-plane response of masonry walls in earthquakes events is the most common in historical masonry buildings, causing irreparable damage to culturally significant buildings or even compromise the overall stability of a structure and people safety. The absence of appropriate structural design is known to be one of the main factors contributing to the activation of this type of failure mechanism, as well as the uncertainty about the real behaviour of determined masonry veneer systems under lateral actions. Thus, the main goals of this section are: (1) the detailed description of brick veneer systems; (2) the description of the seismic vulnerability found in recent earthquakes; (3) the detailed discussion of the experimental and analytical research that has been carried out in the past few decades. Taking into account that the majority of these studies are carried out on backing systems other than reinforced concrete masonry infilled frames, it is clear that this typology of backing system is not covered in literature. Therefore, additional research is required to better understand the seismic behaviour of masonry veneer walls applied in reinforced concrete frame buildings, to purpose straightforward design guidelines and, thus, to contribute for their seismic safety.

2.2.Masonry veneer systems

Generally, a masonry veneer wall is an external wythe of masonry, connected to a backup system with different types of ties [23, 24]. The masonry veneer walls provide the buildings with decoration and with barriers to moisture wind penetration but do not contribute to the their structural resistance [25]. The masonry veneer and structural system are commonly separated by an air cavity, which typically contains thermal insulation (Figure 2.1).

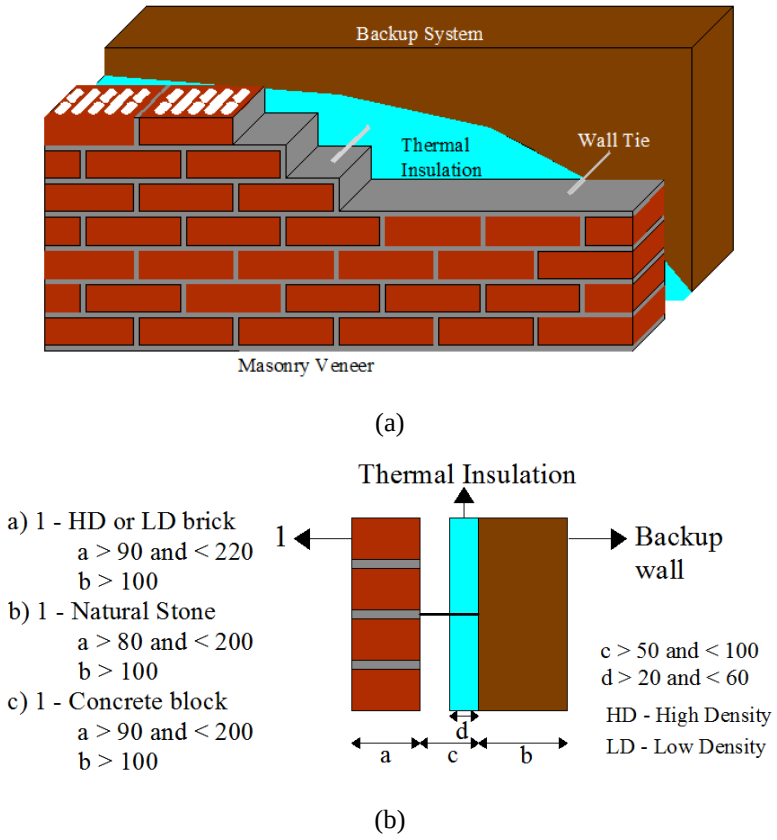

Figure 2.1 – (a) Configuration of veneer wall systems; (b) wall section and configuration (dimension in millimetres) (adapted from French Standard [26])

The backup systems, to which the masonry veneer walls are attached, range from nonloadbearing enclosure walls in reinforced concrete frames, through structural masonry or concrete walls, to light timber and steel stud frames. The brick veneer walls, working as an external cladding to light steel or wood stud walls have proven a successful construction method in North America, New Zealand and Australia [27, 28], in regions of moderate to high seismicity. In European countries, the backup system is commonly comprised of concrete or non-loadbearing masonry infill walls in reinforced concrete frames [29].

The masonry veneer walls are built mostly with vertical perforated clay bricks (group 2 from Eurocode 6 masonry units classification [30]), with a variety of dimensions, colours or

shapes. According to French standard NF DTU 20.1 P1-1 (2008) [26], see Figure 2.1b, veneer walls can also be composed of: (a) high or low density bricks with a thickness equal or greater than 9 cm and not more than 22 cm; (b) natural stone units with a thickness greater than 8 cm and lesser than or equal to 20 cm; (c) concrete blocks designed with thickness greater than or equal to 9 cm and less than or equal to 20 cm.

The masonry veneer walls are considered non-structural elements and, thus, the gravity loads from upper floors and roof are supported by the structural frame. The masonry veneer walls can be supported at the floor slab or through devices like shelf angles located at each floor. According to the French standard NF DTU 20.1 P1-1 (2008) [26], recommendations for supporting and detailing the transition along the height of the building can be seen in Figure 2.2. In the first case (Figure 2.2 (a)), the masonry veneers are completely supported on the slab, and are defined as category A, whereas in the second case (Figure 2.2 (b)), the masonry veneer walls that are partially supported on the slab about 2/3 of the thickness, are defined as category B. In case of buildings have concrete slabs, brick veneer walls can be also supported on shelf angles or lintels located at the slab levels, being the backup wall supported on the slab or by the spandrel beam.

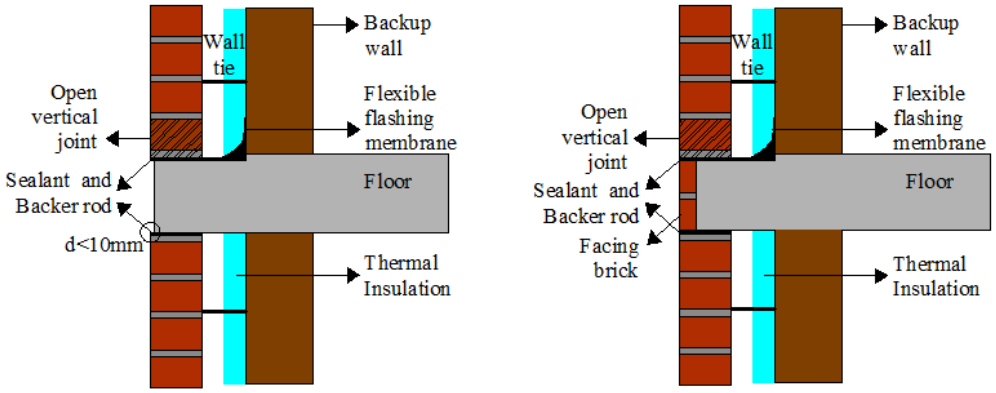

(a) (b)

Figure 2.2 – Devices for water sealing between floors for (a) category A and (b) B (adapted) [26, 31]

The air cavity between masonry veneer and the backing system, typically between 25 mm to 100 mm wide, allows air ventilation between wythes. This space is also ideal for reducing the pressure differentials, allowing quick heat dissipation and improving the thermal efficiency of buildings. In addition, the cavity allows the rain water that penetrates the exterior masonry veneer to be collected through gravity drainage and transfer it to the exterior weep holes located in open head joints, see Figure 2.3. The rain water collection in the air cavity is made with a flashing membrane (of vinyl or rubber, or a copper fabric)

appropriately connected to the backup wall above the floor level and the flashing lies under the first course of bricks.

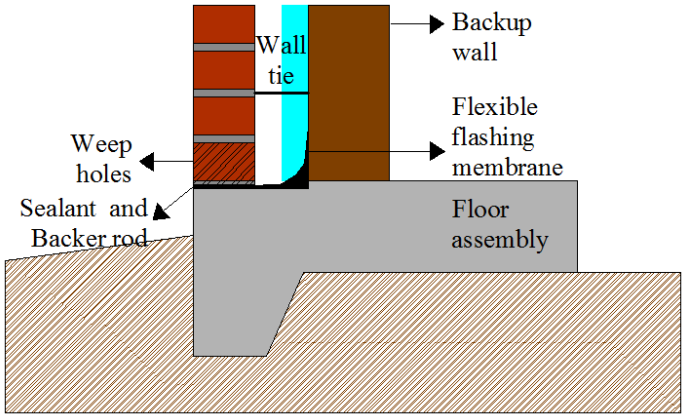

Figure 2.3 – Generic scheme of water proofing configuration adopted for masonry veneer walls [26, 31]

2.2.1. Wall ties

The lateral stability of brick masonry veneer walls is ensured by its connection to the backup system through a variety of ties. The first use of wall ties in brick masonry construction was in England in the 19th century, where wrought iron ties were used in brick masonry cavity walls [32]. Typically, wall ties perform three primary functions, namely: (1) provide a connection; (2) transfer lateral loads; (3) allow in-plane movement to accommodate differential displacements. For a wall tie to be effective in veneer walls it must: (1) connect the brick veneer and to the backing; (2) have sufficient stiffness to transfer lateral loads with minimal deformations; (3) have mechanical resistance; (4) be sufficiently corrosion-resistant; (5) be easily installed to reduce installation errors [13, 27].

The connectors should be selected according to the type of structural and backing wall system and according to the local seismic activity [27]. Wall ties can be corrugated metal straps (nailed or screwed) or wire extensions when the backup system is composed of steel or wood stud walls, see Figure 2.4. The corrugated wall ties are mainly used in low-rise residential structures and for smaller air cavity spaces (25cm), whereas the wire ties are more appropriate for larger cavity widths [5].

The Figure 2.5 presents the most common wire and corrugated ties used for masonry veneers attached both to loadbearing and non-loadbearing masonry and concrete backing walls. Ties based on textile fibres like glass and basalt fibres with reasonable compression and tensile resistance have also been used.

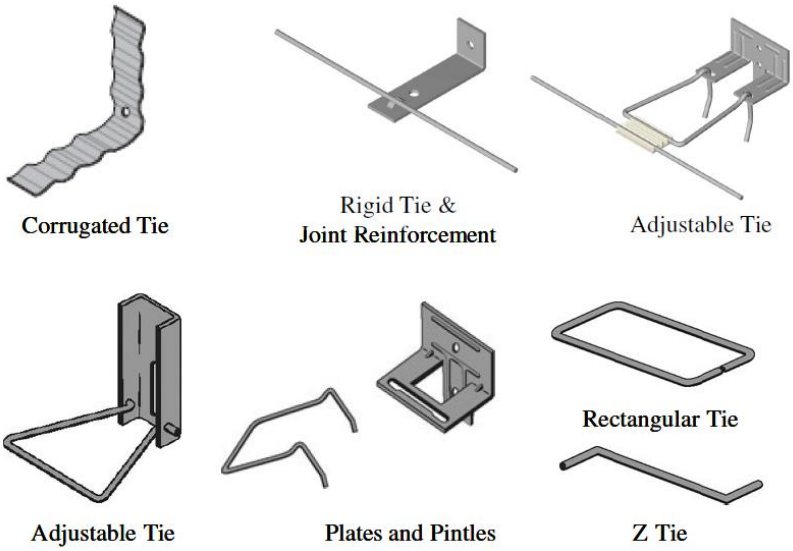

Figure 2.4 – Examples of ties for masonry veneer walls with steel stud and wood frame backup [16]

Figure 2.5 - Examples of wire and corrugated ties when masonry veneer walls are attached to masonry or concrete walls [33]

Several recommendations for design and detailing of wall ties are available in different codes. The Masonry Standard Joint Committee Code [34, 35], mainly applied in United States recommends the use of 2.33-4 ties per square meter. The French standard [26] recommends the application of 2 to 5 ties per square meter. Similarly, the English standard BS 5628 [36] recommends the use of 2 ties per square meter in cavity walls with a leaf thickness lower than 90 mm (air cavity width between 50mm and 75mm) and 5 ties per square meter when cavity leaf walls have a thickness equal or higher than 90mm (air cavity width between 50mm and 150mm). Eurocode 6 [30] indicates that, in the case of the cavity walls, the number of ties under lateral loads should be defined according to the level of lateral load applied on the wall. Additionally, in cavity and veneer walls subjected to lateral wind loads, the wall ties connecting the cavity leaves or the veneer to the backing system shall be capable of distributing the wind loads from the loaded external leaf to the internal leaf and from the veneer wall to the backing system, respectively.

2.2.2. Expansion joints

The masonry brick walls are very susceptible to dimensional changes due to the thermo-hygrometric deformation of clay bricks, meaning that expansion joints must be placed to ensure that expansion of brick veneer walls and potential shrinkage of the backup and do not result in cracking. The addition of expansion joints with a thickness ranging from 10 mm to 20 mm are essential to accommodate possible movements (Figure 2.6). According to Technical Note on Brick Industry Association 18A [31], the actual location of vertical expansion joints is dependent on the configuration of the structure, as well as on the expected amount of movement. In addition, horizontal movement joints are also important to account for movements of the masonry and reinforced concrete frames. The design of movement joints should be carried out according to the type of joint sealant, which should be able to accommodate the movements of masonry. The movement joints should be placed: (1) at building corners, (2) at wall openings, (3) when building height changes (adjacent buildings with different heights), (4) when the thickness of the walls changes, (5) when materials change [22, 31].

(a) (b)

Figure 2.6 – Examples of (a) vertical expansion joints and (b) horizontal movement joints

2.2.3. Functional and mechanical deficiencies

Being that brick masonry veneers are considered external claddings of buildings, their characteristics are mainly related to aesthetics and enhancing of the building and reduction of maintenance, when compared to traditional rendering façades. These improvements are attributed to greater durability, reduction of moisture penetration and rain water infiltration. The continuous ventilation of the air cavity leads to the improvement of efficiency of the building façades in terms of humidity and moisture control. As previously mentioned, the

thermal efficiency is controlled by air cavity insulation, which reduces the energy consumption and avoids thermal bridges [22, 37].

In spite of these advantages, masonry veneers also have construction deficiencies that results in their inadequate structural performance. One of the major deficiencies in existent brick masonry veneers is the lack of ties, larger spacing in relation to the one recommended by codes and or deteriorated ties. Ties play a major role on the performance of brick veneers as they are intended to ensure the lateral stability of the masonry panels. Tie connection failures are often the result of the tie pull-out from poor mortar joints and/or too short tie embedment length into the mortar joint. Tie embedment length can be reduced significantly when veneer walls are constructed with excessive air cavity thickness and when ties are installed at excessive slopes across the cavity due to tie misalignment with the mortar joint, as shown in Figure 2.7 (a).

On the other hand, tie fracture due to corrosion promoted by inadequate moisture drainage out of the wall cavity appears more frequently in coastal regions. As shown in Figure 2.7 (b), the area of corrosion in a brick veneer tie typically occurs in the zone where moisture and contaminant concentrations are higher, such as the length of tie in the air cavity. Additionally, galvanic corrosion may occur as the result of the connection of two dissimilar metals, such as the assemblage of stainless steel ties to galvanized joint reinforcement by welding, or the use of stainless steel screws fastened to steel studs.

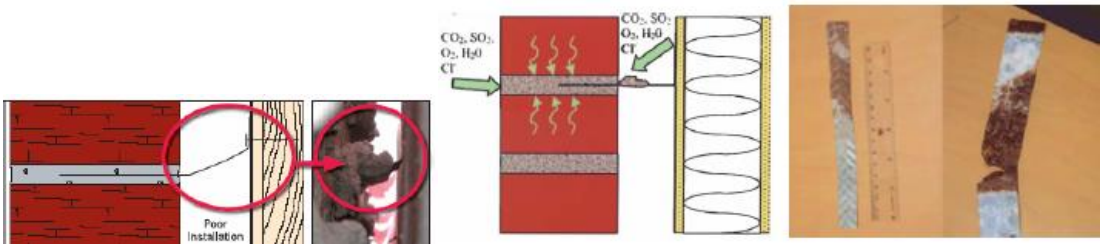

(a) (b)

Figure 2.7 – Examples of deficiencies in ties: (a) misalignment; (b) corrosion

To protect brick veneer ties from corrosion, adequate detailing of ventilation and moisture drainage out of the wall cavity should be provided and the use of chlorides in mortar mixes and in washing compounds must be avoided. Additionally, corrosion protection based on galvanizing zinc coatings or the use of stainless steel materials appears to be the best solution for ties.

The existence of expansion joints can decrease of effect of possible soil settlement and differential movements, resulting in the cracking and crushing of masonry walls (Figure 2.8).

The partial collapse the brick veneer walls attached to a reinforced concrete structure shown in Figure 10 results from hydrothermal expansion of bricks [38].

Figure 2.8 – Cracking on masonry due settlement of soil and differential movements

Figure 2.9 - Collapsed area and detail of a wire tie in the collapsed masonry [38]

Although the veneer walls are regarded as non-structural elements and are not part of the structural system of a building, they are subjected to different types of loadings, including self-weight, wind or seismic loading. With respect to seismic action, the veneer is considered as an added mass, not contributing to the stiffness nor the resistance.

The response of veneer walls to loading during seismic events is influenced by the interaction of the veneer with the backup through wall ties, their thickness, height, length, and height to width ratio [11, 39]. Recent earthquakes in different European countries brought to light vulnerabilities of masonry veneer walls. After many of these events it was possible to observe common failure mechanisms associated to in-plane diagonal cracking and often to the detachment and complete disintegration of the masonry veneer walls, see Figure 2.10. These failures can be primarily attributed to the inadequate connections and absence of suitable design rules that consider the effect of the seismic actions acting on masonry veneer walls systems [40]. These failures are also caused by differential in-plane movement of the structural frame and the brittle veneer.

(a) (b) (c)

Figure 2.10 – Examples of damage caused by the recent earthquakes: (a) Reggio Emilia, Italy, 2012; (b) Lorca, Spain, 2011; (c) L'Aquila, Italy, 2009.

2.3. Research on masonry veneer walls

As a non-structural component, the masonry veneer walls are designed to support only its own weight, transferring out-of-plane loads due to wind or earthquakes to the structural backup system through wall ties. It has been pointed out that the seismic behaviour of masonry veneers depends on the interaction among the wall system elements and it is affected by the tie spacing, strength and stiffness, the relative stiffness between the veneer and backing system, the support conditions of brick veneer and the backup, the location of wall edges and openings and by the cavity width [13]. Experimental and analytical studies have been carried out on the behaviour of ties under a variety of loading configurations and on the in-plane and out of-plane behaviour of brick masonry veneer walls, focusing mainly in the backing wall systems composed of wood and steel studs.

2.3.1. Performance of masonry veneer tie connections

The main role of metal ties on masonry veneer walls is to provide a connection between the masonry veneer and the backup wall, and to transfer out-of-plane lateral loads to the backup. To accomplish this, the ties should have adequate strength and stiffness in tension and compression and sufficient shear flexibility to accommodate in-plane movements.

Recognizing that the tie connections play an important role on in-plane and out-of-plane performance of the masonry veneer system under seismic actions, some authors carried out investigations aimed at assessing the behaviour of the tie connections under shear, tension and compression, see Table 2.1. Notice that under seismic loadings, the ties exhibit complex

loading patterns, where cyclic shear, tension and compression forces are combined. The majority of the experimental studies investigated brick masonry-tie-wood studs assemblages, which are representative of timber frame structures.

Table 2.1 - Summary of experimental research on wall ties assemblies

Reference [REF]	**Loading type[1]**		**Loading action[2]**			**Structural solution[3]**	
	Mon	Cyc	Comp	Tens	Shea	WF	BM
Choi and LaFave (2004) [41]	x	x	x	x	x	x	
Reneckis and LaFave (2009) [14]	x	x	x	x		x	
Zisi and Bennett (2011) [42]		x			x	x	
Mertens et. al (2014) [43]	x		x	x			x
Sebastião et. al (2014) [44]	x			x			x

[1] Mon: Monotonic load; Cyc: Cyclic load

[2] Comp: Compression load; Tens: Tension load and Shea: Shear load

[3] WF: Wood Frame and BM: Brick Masonry

In the experimental work carried out by Zisi and Bennett (2009) [15], the local behaviour of brick-tie-wood subassemblies with variable features under cyclic shear was analysed. Besides two distinct types of bricks for veneer walls, the thickness of the corrugated sheet metal ties, the eccentricity of the nail connecting the corrugated sheet to the wood stud in relation to the bend location, the type of nails and the embedment length of the ties in the mortar joints were analysed, see Figure 2.11.

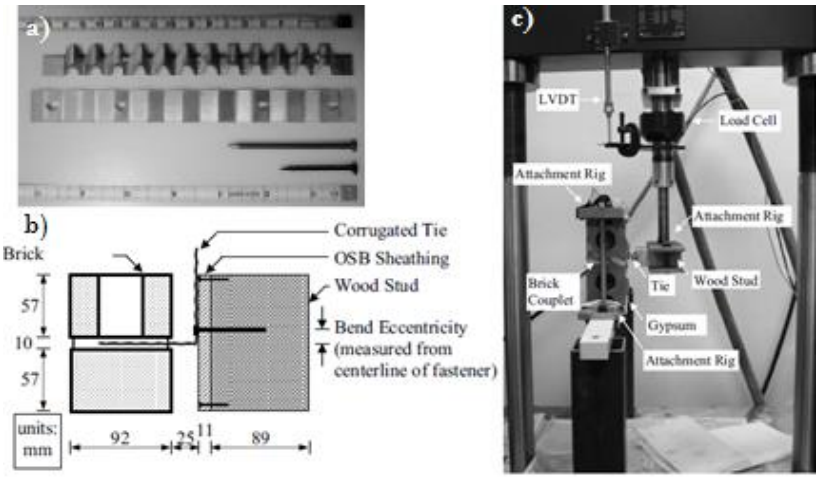

Figure 2.11 – Details of tie connections for shear test: (a) tie and fasteners types, (b) scheme of specimen and (c) test setup [42]

From the experimental results, it was possible to observe that the cyclic behaviour is characterized by an early nonlinearity and reasonable dissipation of energy (Figure 2.12). The hysteresis diagrams were characterized by pinching and asymmetry became pronounced

for increasing displacements. Tie shape and bend eccentricity were found to be the most important factors, whereas tie location in the bed joint and fastener type were influential to a lesser degree [42]. The addition of a second nail constrains tie pivoting around a single fastener, resulting in higher strength of about double of the pull-out strength.

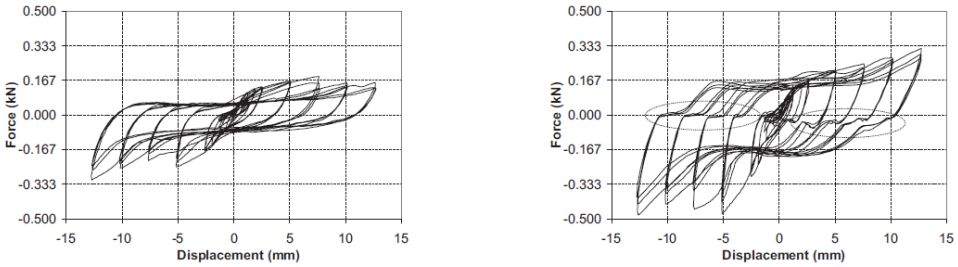

(a) (b)

Figure 2.12 – Typical force-displacement curve for specimens with: (a) serpentine ties; (b) straight ties [42]

Choi and LaFave (2004) [41] and Reneckis (2009) [14] have also developed similar tests with similar results. Besides shear, tension and compression cyclic tests were also carried out in order to analyse the influence of tie thickness (Figure 2.13), initial offset displacement, attaching method of ties (screw, nail or mechanical anchor), type of loading (including cyclic), eccentricity (with sheathing), as well as embedment length.

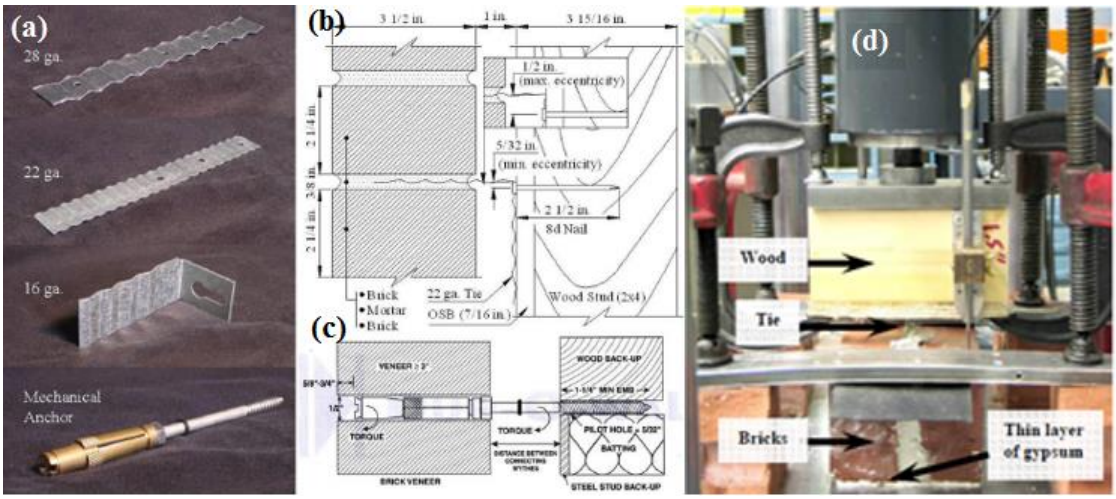

Figure 2.13 – Subassemblies subjected to compression-tension loads: (a) corrugated sheet metal ties of three different thicknesses; (b) tie connection installation details; (c) mechanical repair anchor installation details; (d) setup configuration [14]

Under tensile loading, the tie thickness and eccentricity influence the stiffness, whereas the embedment length of the tie into the masonry mortar joint affected the strength. As seen in Figure 2.14, the tensile strength of tie connections is reduced by over 50% when short roofing nails are used. The predominant failure mode observed in the monotonic tension tests of nailed subassemblies was nail pull-out from the wood stud, which helped to explain

why tie thickness had no effect on the average tensile strength. At the same time, the nail type revealed to have significant influence in the tensile strength. In fact, during cyclic testing of subassemblies with nails, other failure modes developed, namely tie fracture, yield around the tie hole (allowing the head of the nail to pass through) and tie buckling [14].

Workmanship during construction of brick veneer, particularly with respect to installation of the ties, also plays an important role on the cyclic performance of the overall wall system.

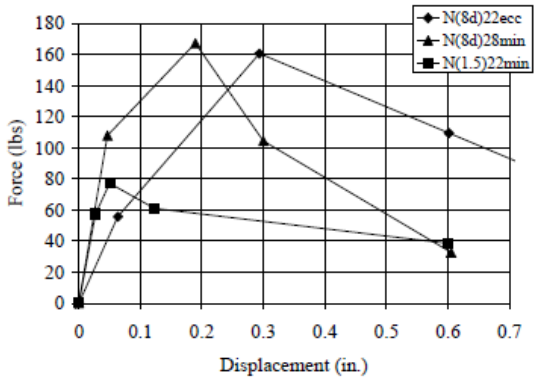

Figure 2.14 - Idealized multi-linear force-displacement behaviour in tension for brick-tie-wood connection subassemblies: effect of different thickness and eccentricity [14]

Note that almost all the wall ties investigated in the literature focused on backing systems related to timber frame buildings, thus additional research is needed to characterize the mechanical behaviour of the wall ties usually used in the connection of brick veneers to masonry infill walls, whose shape and geometry is very different from the ones used for wood. In this regard, analytical material laws for the wall ties must be developed to enable advanced nonlinear numerical analysis. It is also important to assess the main parameters influencing the local behaviour of the wall ties embedded both in brick veneers and brick infill masonry walls.

2.3.2. Experimental assessment of behaviour of masonry veneer walls

The experimental characterization of brick masonry veneers has necessarily considered the system composed of the brick masonry veneer, the backup wall and the ties connecting the masonry veneer and the backup wall. Some experimental investigations had focussed on the static in-plane and out-of-plane behaviour of the brick masonry veneer systems [14, 16, 17, 45, 46]. Some of these works have also focused on the dynamic shaking table tests of both brick veneer elements [11, 14, 16, 17, 45-50] or full scale or reduced scale buildings with attached brick veneer walls [14, 16, 28, 45, 51-55], as shown in Table 2.2.

Table 2.2 - Summary of research on brick veneer walls

Reference [REF]	**Loading type [1]**				**Study approach[2]**		**Structural solution[3]**		
	SIP	SOOP	DVS	DB	Num.	Exp	WF	SF	CBM
Liang (2006) [48] and Liang and Memari (2012) [56]			x			x		x	
Paton-Cole et. al (2012) [51]				x		x		x	
Desai and McGinley (2013) [57]	x	x	x		x			x	
Memari et. al (2002) [11]			x		x	x			x
Marziale and Toubia, (2015) [58]	x		x		x				x
Zisi, (2009) [15]	x	x	x		x		x		
Okail, (2010) [16], Okail et. a, (2010) [47]	x	x	x		x	x	x		
Jo (2010) [17]	x	x	x		x	x	x		
Reneckis and LaFave (2004) [46], Reneckis and LaFave (2010) [14]	x	x	x			x	x		
Reneckis and LaFave (2010) [50], Reneckis and LaFave (2009) [14]	x	x	x		x		x		
Reneckis and LaFave (2012) [59]			x		x		x		
McGinley and Hamoush (2008) [45]	x	x				x	x		
Thurston and Beatti (2008) [49]				x	x	x	x		
Thurston and Beatti (2008) [54]				x	x	x	x		
Thurston and Beatti (2008) [53]				x	x	x	x		
Thurston and Beatti (2008) [55]				x	x	x	x		
Okail, (2010) [16], Okail et. al (2011) [52]				x	x	x	x		

[1] SIP: Static In-Plane; SOOP: Static Out-Of-Plane; DVS: Dynamic Veneer System and DB: Dynamic Building

[2] Num: Numerical; Exp: Experimental

[3] WF: Wood Frame; SF: Steel Frame; CBM: Concrete Block Masonry

Based on experimental research available in the literature, it is concluded that the composite systems with flexible backing structures with brick veneers attached have been reasonably treated by the research community. However, much better insight is needed to analyse the seismic behaviour of composite systems with different backing structures. In fact, almost all of the experimental studies available in the literature only consider wood stud backup walls, probably related to the fact that the research was primarily carried out in the United States.

In these studies, current construction practices have been evaluated and discussed, such as tie typologies, installation technology of wall ties, spacing and its distribution, embedment length of ties in mortar joints and air cavity width.

McGinley and Hamoush (2008) [45] have conducted quasi-static in-plane and out-of-plane load tests on solid brick veneer wall panels with wood backup framing. The brick veneer walls were built with corrugated sheet metal ties attached to the wood backup with nails or screws, with varying vertical and horizontal spacing and varying cavity widths. In some cases, the ties were mechanically attached to horizontal wire reinforcement embedded in the brick masonry. In general, the tests confirmed that the seismic performance of brick veneer walls is closely related to properties and layouts of the tie connections, being ultimately controlled by tie deformation and tie resistance. For walls with ties connected to the backup with nails, the common failure mode was nail pull-out and/or fatigue fracture of the nails. For ties attached with screws, failure mode was dominated by tie pull-out from the mortar joints. The authors also found that the veneer walls were cracked well before failure near mid-height.

Reneckis and LaFave (2004) [46] tested also full-scale brick veneer panels attached to a wood-stud frame with corrugated sheet metal ties considering different nail eccentricities at the tie under out-of-plane static loading. The results obtained showed that brick veneers increased the out-of-plane stiffness of the composite timber frame wall system, compared to the stiffness of the bare wood-stud frame. Post-installed mechanical anchors were able to improve the performance of the brick veneer wall system in relation to the initial configuration of ties.

The shaking table test is considered to be the more realistic testing approach to evaluate the interaction between the brick veneer walls, ties and the backing walls, namely wood-frame backup (Figure 2.15), when subjected to seismic loads. When only brick veneer systems are tested, a reaction structure that is capable of providing the backup walls with adequate boundary conditions to be representative of a real situation is critical. Usually, the in-plane and out-of-plane reaction frame consists of a steel structure which is connected to the double top plate of the wood-stud wall with threaded rods. In the out-of-plane direction, the reaction structure is welded to two inclined trusses at each side of the wall and bolted to the table. In the plane of the wall, the threaded rods are installed through longitudinal slots in the steel structure allowing free in-plane translation. The experimental research based on the same testing typology, evaluated different parameters, namely: (1) type and spacing of ties (sheet metal ties were considered conventional ties) with different dimensions; (2) the attachment

of the veneer to the wood stud with nails or screws; (3) presence of joint reinforcement in mortar joints: (4) the effect of openings [45, 47, 52]; (5) variation of the opening area; (6) geometry of the brick veneers [14].

Figure 2.15 – Shaking table test setup of wall model [47].

Based on the experimental results, it has been observed that the out-of-plane seismic performance of residential anchored brick veneer walls is generally governed by: (1) the tensile and compression strength and stiffness of the tie connections; (2) tie installation details (screwed or nailed); (3) spacing of the ties, especially for ties along the edges of openings and at the upper regions of walls; (4) wall dimensions and configurations [14]. According to Okail et. al (2010) [47] the failure of the corrugated ties is governed by pull-out of the nails from the wood studs, whereas the failure of the screw connected sheet metal (rigid) ties is governed by detachment from the mortar joints or pull-through of the screw heads through fastener holes (Figure 2.16). Okail's measured tie connection deformation in tension was similar to the deformation at ultimate tensile loading determined from subassembly tests done by Reneckis and LaFave (2004) [14, 46].

The presence of horizontal wire reinforcement at the bed joints of brick veneers did not appear to improve the performance of clay masonry veneer under out-of-plane seismic loading [47].

For a given backing wall stiffness, the vertical tie spacing influences the cracking load of the veneer [14, 47]. The detachment of a masonry veneer wall from the backing system is preceded by veneer cracking, which influences the distribution of tie force as the results of force redistribution.

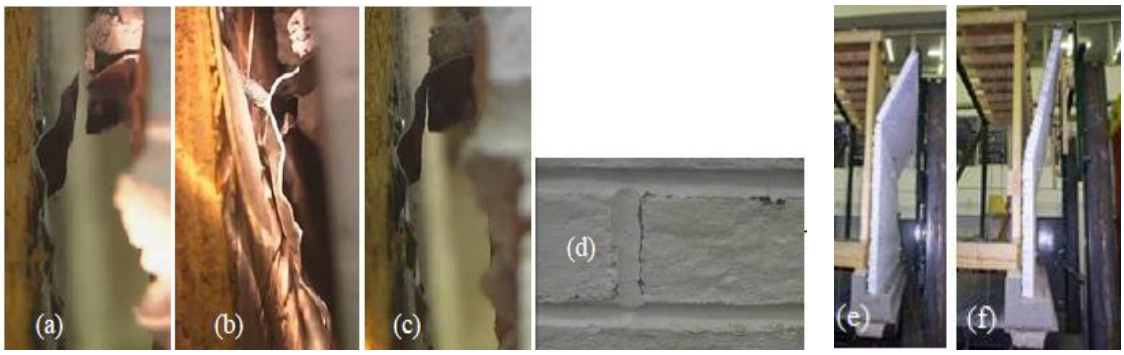

Figure 2.16 - Veneer wall damage: (a) tie fracture; (b) nail pull-out; (c) partial tie fracture; (d) cracks in the brick veneer bed and head joints, (e) and (f) wall collapse [14]

The shaking table testing of buildings with attached masonry veneer enables the analysis of the full interaction between the structure and the masonry veneers under seismic loads [49, 52-55]. Besides the behaviour of the ties, it is important to evaluate the effect of the global seismic behaviour of the buildings on the brick masonry veneer and understand the extent the masonry veneer can contribute for the global seismic response. In the experimental testing carried out by Okail et al. (2011) [52] a full-scale building (one-story, wood-framed structure and brick masonry veneers) was tested under dynamic loading in a shaking-table (Figure 2.17).

Figure 2.17 – Shaking table test setup of building model [52].

The brick veneers were attached to the wood stud backing with two distinct metal anchors, namely corrugated ties fastened with nails and rigid ties fastened with screws. Joint reinforcing in the mortar joints was also considered. The veneers on the west, north, and south walls were attached to the wood studs with corrugated sheet metal ties using nails. In the north wall, the ties were mechanically attached to the wire joint reinforcement. The veneer on the east wall was attached to the wood studs with rigid ties, using screws and wire joint reinforcement in the veneer. Based on the experimental results some interesting observations were obtained: (1) the veneer walls parallel to the direction of shaking helped

to restrain the displacements of the wood structure, meaning that they have a significant impact in the global response of the buildings. This also indicates that in this case the brick veneer should not be simply treated as an added mass; (2) the rigid ties, which were attached to the wood studs with screws, were much stronger than the corrugated ties [52].

By comparing the in-plane and out-of-plane behaviour of brick veneer walls, it is clear that the out-of-plane resistance is lower, irrespectively to the combinations of materials constituting the masonry. Borchelt (2004) [39] states that in-plane behaviour is controlled by shear capacity of each element of the masonry veneer system (masonry veneer, ties and backing wall). In the same way, Okail et al. (2011) [52] pointed out that the behaviour of brick veneer under in-plane loading is ruled mainly by the shear strength and deformation capacity of the nailed connections attached to the studs and to the top and bottom plates.

2.3.3. Analytical and numerical analysis

Complementary to the experimental studies, some analytical works have been carried out aiming at achieving a better insight on the seismic behaviour of masonry veneers, ties and backup walls systems and on the interaction among the different components of the system. These studies play an important role on the understanding of the main parameters affecting the seismic behaviour of the systems, given that once the numerical model is calibrated, parametric studies can be carried out. The analytical works are mostly related to the finite element modelling of masonry veneers attached to different backup walls systems. However, similarly to what was mentioned for the experimental results available in literature, the analytical studies have been also concentrated in the steel and wood stud backing systems mostly used in United States, Australia and New Zealand.

Reneckis and La Fave (2010) [50] carried out an analytical work based on finite element modelling of brick masonry veneer attached to wood stud by using the software ABAQUS (Abaqus Inc. 2006) [60]. The numerical models were calibrated based on dynamic shaking table tests. The models consisted of the wood frame wall panel with the brick veneer attached through corrugated sheet metal ties. To do this, appropriate boundary conditions adopted in the experimental investigation were modelled, linear elastic rotational spring supports at the base of wood frame and translational (axial) spring supports for the sidewalls, celling and roof to take into account the cumulative effects of the concrete foundation, the steel reaction frame and the surrounding wood backup components respectively, see Figure 2.18. Nonlinear elastic spring supports were implemented along the base of the brick veneer wall

panel, representing a rigid body rocking behaviour. Nonlinear inelastic models for the tie connections were developed and implemented in the FE wall models, to capture key features of the absolute and relative performance of different types of ties, see Figure 2.18. Analyses were performed by subjecting the FE wall models to out-of-plane static and dynamic loads.

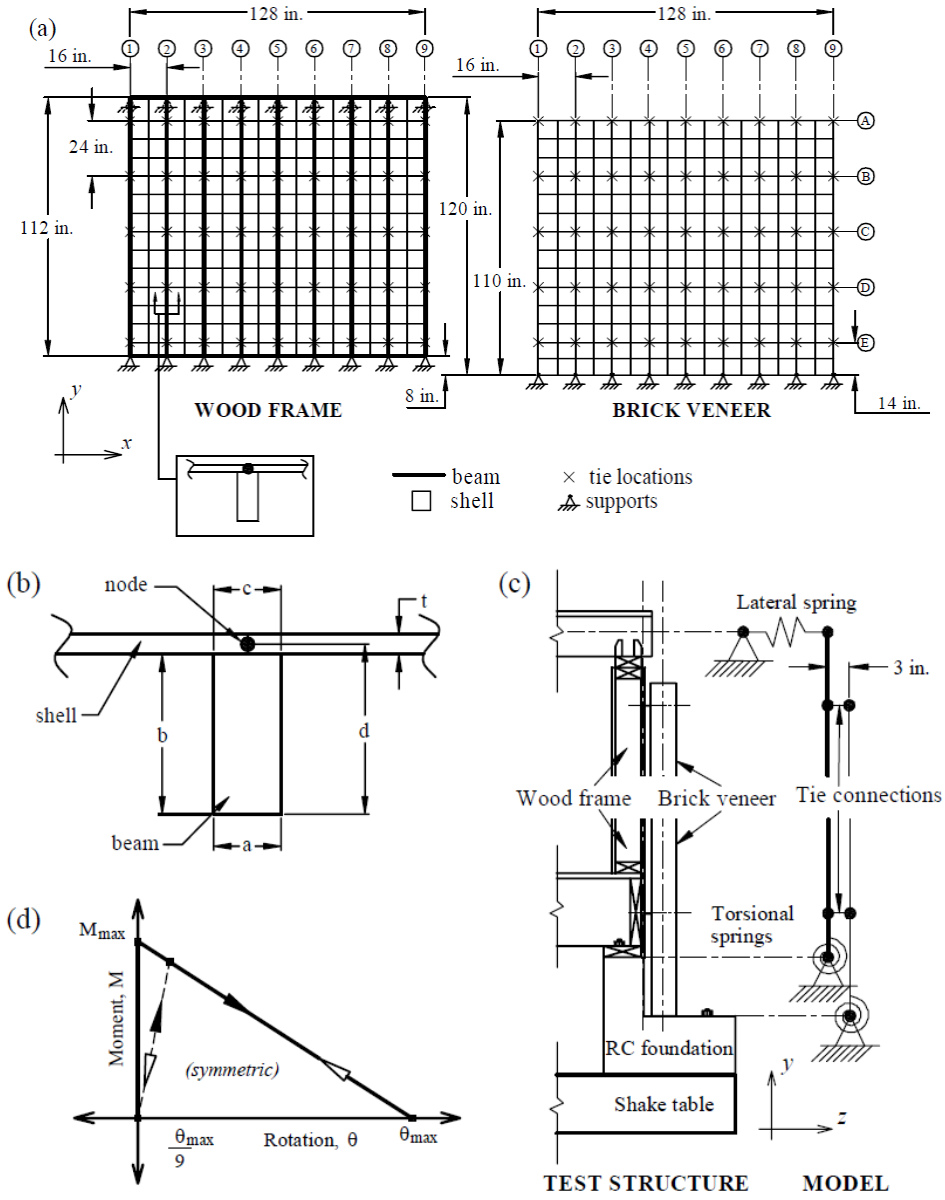

Figure 2.18 – Details of the numerical model by Reneckis and La Fave (2009) [14]: (a) finite element model of the wood frame and masonry veneer; (b) stiffened shell model (OSB sheathing with stud), (c) wall support details, and (d) bilinear elastic brick masonry rocking behaviour model.

A parametric study was carried out to analyse the effects of the variation of the geometry of the veneer, namely with the presence of a central opening with different areas, and different brick veneer tie connection details. From the dynamic analysis on the masonry veneers attached to wood studs it was observed that tie connection strength and stiffness play a major influence in the out-of-plane seismic behaviour of brick veneer walls. The grid spacing and

tie installation also played an important role on the behaviour of the brick veneers as they also determine the out-of-plane capacity of the veneer wall. Brick veneer walls with wide openings were shown to be very sensitive to the tie connection properties [14].

In the analytical work carried out by Jo (2010) [17], a simplified finite element model was developed in Opensees [61] to represent the in-plane and out-of-plane behaviour of brick veneer-tie-concrete block masonry systems. The representation of the brick masonry veneer and the concrete block masonry walls was done with elastic beam elements to which rotational hinges appropriately located were assigned to take into account the in-plane or out-of-plane nonlinear behaviour. For this, adequate moment-curvatures functions were considered for the springs. The ties were represented through truss elements with general hysteretic material behaviour, see Figure 2.19 (a). Okail et al. (2010) [16] developed nonlinear finite element models to simulate the seismic behaviour of brick veneers attached to wood frame backing system also on the Opensees software. The masonry veneer was modelled through nonlinear displacement, beam-column elements with fibre cross section, elastic beam elements were used to simulate the wood shear walls and nonlinear truss elements were used to simulate the tie connectors, see Figure 2.19 (b).

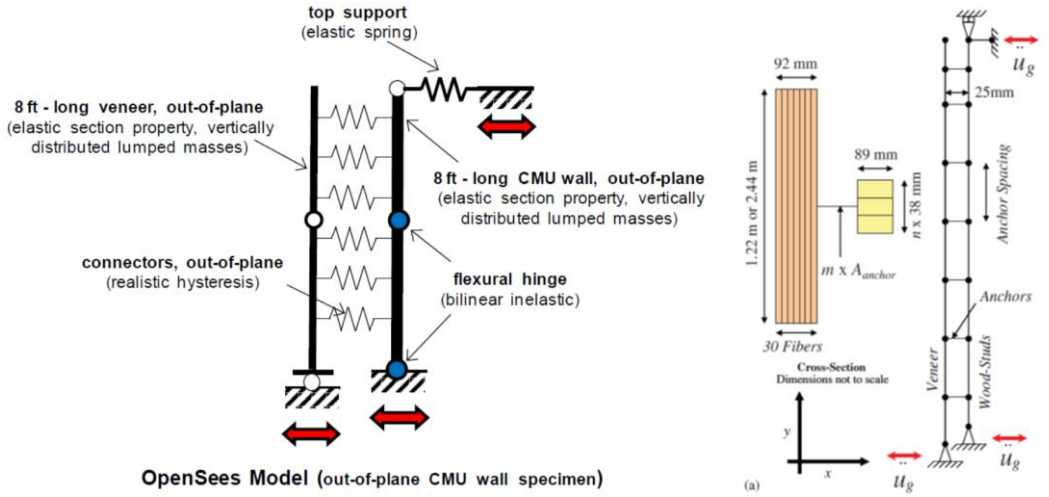

(a) (b)

Figure 2.19 - Finite element models used for brick masonry veneer systems: (a) steel stud backup walls [17] and (b) concrete block masonry backup wall [16]

Appropriate hysteretic models were considered for the nonlinear truss elements simulating the ties. Based on the results it was found that the cracking of the veneer influences the force on the ties. For an uncracked masonry veneer, the force distribution on the ties was influenced by the flexibility of the backing walls and the wall boundary conditions. After cracking of the masonry veneer, the redistribution of the forces occurs and the ties in the

neighbourhood of cracks resisted higher forces. The redistribution of forces depends also on the stiffness of the ties, being lower in case of stiff ties. From a parametric study, it was also possible to analyse the effect of the strength and stiffness of the ties on the out-of-plane of the walls.

The out-of-plane behaviour of brick veneer walls systems was also studied in medium rise buildings under seismic loads [57]. The authors extended the models already used by Jo (2010) [17] and Okail et al. (2010) [16], considering different backing wall systems (steel stud backing walls and concrete block masonry backing wall) and different structural resisting frames in terms of global stiffness, namely reinforced concrete moment resisting frame with and without concrete shear walls, steel moment resisting frame with and without bracing, to evaluate the interaction between masonry veneer systems and multi-storey structural frames (10 storey frames). The models used for the veneer masonry systems were similar to the ones presented in Figure 2.19. Nonlinear material models were used to describe the mechanical behaviour of the distinct elements. Both masonry veneer systems were attached to the main planar frames that compose the building [62] and subjected to dynamic loading. From this study, some interesting results were found: (1) the replacement of the masonry veneer walls by an equivalent mass is a conservative approach for structural design in case of more flexible systems like steel moment resisting frames. On the other hand, in case of stiffer systems like reinforced concrete moment resisting frames with concrete shear walls, the consideration of additional masses produced reasonable design of masonry veneer systems; (2) the peak out –of-plane acceleration for the masonry veneers were higher in case they were attached to flexible steel moment resisting frames and lower for the walls attached to reinforced concrete moment resisting frames and shear wall systems; (3) the stiffness of ties is more important in case of flexible structural frames composing the building; (4) in case of steel stud backed veneer walls, the top rows of ties experience higher forces, even if these forces can be redistributed after cracking of the masonry veneer. Similarly, Lapish and Allen (1982) [63], who developed linear elastic models representing the geometry of one and two story (continuous) brick veneer walls to analyse their out-of-plane behaviour under distributed static loads, concluded that higher loads are imposed on the ties located in the upper region of single story walls, or on the ties anchored near the floors in multi-story construction. The linear elastic dynamic analytical model defined by Memari et al. (2002) [11] allowed also to conclude that the distribution of forces on the ties along the height of the masonry veneer is not constant and it is higher at the top and bottom boundaries. The analytical modelling considered a 2D model for the masonry veneer system composed of

brick never attached to a concrete masonry walls that instead were connected to a structural system based on shear walls (shear wall type building with 5 floors) at the 5th floor. Both brick veneer and masonry concrete block masonry were modelled with two rotational springs at the base to enable to simulate the possible cracking. The ties were modelled with pin-ended tension-compression elements at the face of each wythe.

More recently, Lintz and Toubia (2013) [64] created an analytical method to estimate the amount of load transferred through ties and predicted the resulting reaction of the brick veneer. After analysing a variety of wood shear walls, they found that an unreinforced brick veneer can overturn or slide along the flashing plane at the base of the wall before the wood shear wall reaches its capacity. Other authors [14, 16] also recorded through numerical and experimental analysis substantial rigid body rotation (rocking about its base) and sliding of brick veneers when subjected to out-of-plane static and moderate dynamic loading. Suitable geometry and distribution of ties can be important and affect directly the behaviour of system. This was also concluded by Zisi (2009) [15], which referred that the initial wall stiffness can increase between 41 % and 60 % if optimal installation practice of the ties was considered. The gain in wall strength was estimated to be rather small up to 5 %.

The numerical investigations point out important aspects of the behaviour of brick veneers attached to flexible backup systems, especially the parameters influencing its seismic behaviour. Nevertheless, it is important to stress, that: (1) variations of the stiffness of the resisting backing systems should be taken into account to clarify the role of the brick veneers in the seismic behaviour of the composite structures; (2) global seismic analysis of building systems with brick veneers, considering nonlinear behaviour of the different constructive elements, needs to be carried out to assess the vulnerability of the brick veneers and to analyse the global interaction between brick veneers and the resisting system. Note that the part of the numerical analysis is focused on single panels where simplification of the boundary conditions and of the mechanical behaviour of the resisting system is considered by adopting linear elastic materials. It is also important to have some insight on how to calculate the seismic forces that should be considered in the design of the wall ties.

2.4. Conclusions

Brick masonry veneer walls have been applied in a wide variety of buildings in different regions of world mainly due to aesthetic, thermal and durability functional features.

However, in recurrent seismic events, these types of building systems have been reported as exhibiting vulnerable behaviour resulting in severe damages and local collapse, and thus representing a threat for the human life safety.

Several studies in recent decades have been carried out by several authors aiming at understanding the real behaviour of the system. A review on the up to date knowledge about the seismic behaviour of brick masonry veneer is summarized in the present chapter. This review was divided in following main areas: (1) description of materials and main characteristics of brick veneer system; (2) discussion of the experimental and numerical research; (3) brief overview of the codes and guidelines. This experimental and numerical research have been focused on the: (a) mechanical characterization of components, mainly ties; (b) mechanical characterization of the brick veneer systems as a constructive element; and (c) characterization of the interaction of the resisting system with the brick veneer. The typologies of loading are defined as: (1) static monotonic in-plane and out-of-plane action loading; and (2) dynamic loading (shaking table tests).

Based on the experimental and numerical studies it has been concluded that the out-of-plane response of brick veneer walls is governed the backing wall stiffness and by the properties of the veneer anchors, including typology, stiffness and grid spacing.

On the other hand, the in-plane response of brick veneers is characterized by sliding along the base flashing in case of squat veneer walls and by a combined sliding/rocking failure mode in case of slender panels. It was seen that the brick veneers are able to withstand higher level of in-plane ground motions without collapse in comparison to the out-of-plane direction.

Numerical analysis based on finite element modelling has been played a central role on the analysis of the main parameters influencing the mechanical seismic behaviour of brick masonry systems, namely geometry of the veneer, presence and area of openings, types of ties and spacing. Additionally, the interaction between the brick veneers and the backing system has been also analysed based on shaking table tests on buildings with brick veneers attached. It was concluded that the stiffness of the resisting frame plays an important role in the behaviour of the brick veneer, being more significant in the case of flexible resisting systems. On the other hand, the contribution of the brick veneer for the response of the resisting system appears to be more important in case of flexible structural systems.

In spite of the findings pointed out in this chapter and taking into account the seismic vulnerability observed in recent earthquakes in Europe, the authors think that brick veneers

need to be further investigated. It is considered that there is a gap on the research regarding the seismic performance of brick veneers attached to reinforced concrete moment resisting framed structures, namely at the level of the interaction between the veneer and the resisting system and at the level of local behaviour of tie connections. Note that in spite of very different types of commercial ties can be used both for infill and for masonry veneer walls, no experimental research exists on the characterization of their seismic performance. In this regard, it is considered that the global behaviour of the brick veneers attached to the reinforced concrete frames with brick infills should assessed in detail through shaking table tests so that the interaction between brick infills and reinforced concrete infilled frames can be better understood. In addition, the evaluation of the most appropriate ties to resist seismic action should be carried out through assemblages of infill and brick veneer connected through the wall ties submitted to tension-compression cyclic loading and cyclic shear.

Chapter 3

Materials Characterization

Abstract:

An important and extensive experimental campaign has been developed in order to characterize the mechanical and physical behaviour of constituents of masonry veneer walls. Therefore, the outputs of this chapter are: (1) physical characteristics of bricks (geometry, moisture expansion) and mortar (density, porosity and water absorption); (2) mechanical characteristics of mortar and bricks (compressive strength), and wall ties (tensile strength and stiffness); (3) mechanical characteristics of brick masonry veneer (compressive, flexural and shear strength) and (4) freeze and thaw resistance of brick masonry veneer.

3.1. Introduction

In spite of the masonry veneer wall is not considered as structural element, it is important to know the mechanical behaviour of the compound materials to better understand its behaviour.

The veneer wall system combines different types of bricks and mortar (veneer and infill wall) and wall ties. Therefore, it is needed to obtain the mechanical behaviour and mechanical properties of these materials. The present chapter focusses mainly in the materials composing the brick veneer walls and wall ties given that much information on the characterization of brick masonry infill exist [20, 65-67].

For the physical characterization, an experimental program was designed to characterize the geometric characteristics of veneer and infill bricks, moisture expansion behaviour of veneer bricks and absorption of water of veneer and infill mortar.

Besides of physical properties, it was intended to find some mechanical characteristics of components, namely the compression behaviour of bricks elements of veneer and infill wall, the compression and flexion behaviour of mortar of veneer and infill wall, the tensile behaviour of wall ties and the compression, flexion and shear behaviour of veneer masonry.

Additionally, given the possibility of the brick veneer walls be exposed to severe environment conditions leading to freeze and thaw cycles, it was decided to design an experimental campaign to characterize the freeze and thaw resistance of mortars and brick masonry.

3.2. Physical characterization of masonry elements

Tests in masonry elements will be done according to EN 771 and EN 1015. Determination of dimension of bricks, determination of moisture expansion of veneer bricks, determination of initial rate water absorption by capillarity of mortar and determination of density and porosity of mortar will be evaluated according EN 772-16 [68], EN 772-19 [69], EN 1015-18 [70] and EN 1015-10 [71], respectively.

3.2.1. Geometric characterization of brick units

The brick veneer walls are built with ceramic bricks with vertical holes with approximately 237mm x 115mm x 70mm (length x thickness x height), as shown in Figure 3.1 (a). The masonry infill enclosed in reinforced concrete frame [29] was built with brick units with horizontal perforation and with approximately 300mm x 150mm x 200mm (length x thickness x height), Figure 3.1 (b). Bases on technical notes, some characteristic of bricks units can be seen in Table 3.1.

(a) (b)

Figure 3.1 - Brick units for: (a) veneer walls; (b) masonry infill walls

Table 3.1 – Characteristics of ceramic veneer bricks based on technical notes [29]

Characteristics of ceramic material	**Values**
Volumetric weight (kg/m^3)	>2100
Water absorption by immersion in cold (%)	< 6
Capillary water absorption (kg/m^2.min)	0.6
Thermal conductivity (W/mK)	0.37
Expansion moisture (mm/m)	0.2
Content of active soluble salts	S2
Characteristic compressive strength (MPa)	> 45
Freeze-thaw resistance	F2

The geometric characterization of the clay masonry units was based on NP EN 772-16 [68]. To determine the dimensions of bricks and determining the percentage of perforation, six samples of each brick were selected. Two measurements near the edges of each specimen were carried out in each direction.

The average of results is presented in Figure 3.2 and plotted in Figure 3.2. Regarding to brick veneer unit, two typical configurations of holes as shown in figure, much similar between them. The differences is regarding to perforation configuration, being the brick veneer unit presented in Figure 3.2 (a) only more 9% perforated than the brick veneer unit presented in Figure 3.2 (b).

Table 3.2 - Mean dimensions of the clay masonry units (coefficient of variation (%) is inside brackets)

Units	**Dimensions (mm)**			**Thickness (mm)**		**Average of voids area (mm²)**	**Percentage Perforation (%)**
	Length	Height	Width	Shells	Webs	Total	
Veneer bricks Figure 3.2 (a)	235.5 (0.23)	68.7 (0.72)	113.8 (0.45)	9.9 (0.25)	9.9 (0.34)	9248	34.3
Veneer bricks Figure 3.2 (b)	236.3 (0.57)	67.7 (0.67)	112.8 (1.4)	9.9 (0.14)	9.9 (0.24)	8431	31.5
Infill bricks Figure 3.2 (c)	295.0 (0.9)	190 (0.85)	148.0 (0.95)	17.5 (0.5)	10.0 (0.9)	15120	53.8

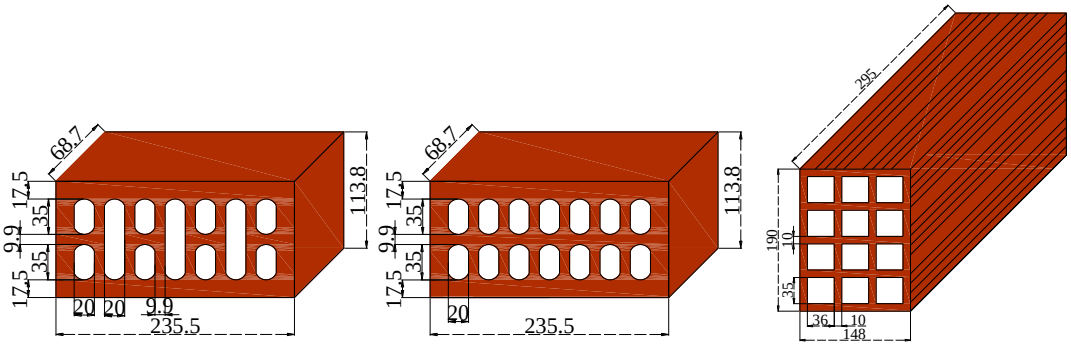

(a) (b) (c)

Figure 3.2 – Typical brick units used in masonry (a) and (b) veneer and (c) infill walls (dimensions in millimetres).

It was found that the dimensions are lower than the theoretical dimensions defined, especially in relation to the length of the bricks. Deviations on the dimensions may be due the difficulty of controlling the shrinkage by drying and firing. As it is possible to see in Figure 3.3, the infill bricks had some defects, including longitudinal cracks and separation of elements (Figure 3.3 (a)), faces that were not square and still poor cooking (Figure 3.3 (b) and (c)).

(a) (b) (c)

Figure 3.3 – Examples of defected bricks: (a) longitudinal cracks, separation of elements, (b) faces that were not square and (c) still poor cooking.

3.2.2. Moisture expansion of brick veneer units

The moisture expansion of bricks veneer elements was obtained based on EN 772-19 standard [69]. This standard is applied to obtain the moisture expansion of large horizontally perforated clay masonry units. However, taking into account that there is not another standard for determination of moisture expansion for other types of bricks, this was used in veneer units.

Six bricks were considered in two approaches. In first approach, only the expansion on parallel direction of perforations of brick was determined (vertical expansion), taking into account that this curing direction could be the most expansive direction. In the second approach, all dimensions of bricks were analysed in order to understand how the bricks expand in different directions.

For the first approach, the bricks units were cut taking into account the standard recommendations. The final dimensions were 115x115x70mm. In the second approach, the original dimensions of bricks were kept and only the suitable cleaning and regularization of surface were carried out.

All dimensions were recorded to the nearest 0.01mm and the first measurement was obtained before dry and water treatment (l_i). After bricks were stored in environment conditions for 24 hours, they were dried in a kiln, maintaining a temperature rise of 50ºC/h until a temperature of 600ºC has been reached and this was maintained for 4 hours (Figure 3.4 (a)). After this, all bricks cooled inside the kiln until 70ºC and they were introduced in a desiccator for 20 hours. In this moment, the second measurement was obtained (l_{s1}). After more 3h, the third record was obtained (l_{s2}). The mean values for these two records (l_{s1} and l_{s2}) allows to calculate the mean initial deviations (l_{m1}). In the second part, the specimens were immersed in boiling water for 24h ((Figure 3.4 (b)), and after that, the specimens were removed and cooled at room temperature. The measurement records were done after 1h (l_{s3}) and 24h (l_{s4}) after the specimens have been removed from boiling water (Figure 3.4 (c)). The mean final deviations were obtained by averaging these records (l_{s3} and l_{s4}).

Finally, the mean irreversible moisture expansion due to the boiling water treatment (e_m) is calculated in mm/m through as follows:

$$e_m = \frac{|l_{m2} - l_{m1}|}{l_i} \times 1000 \quad (3.1)$$

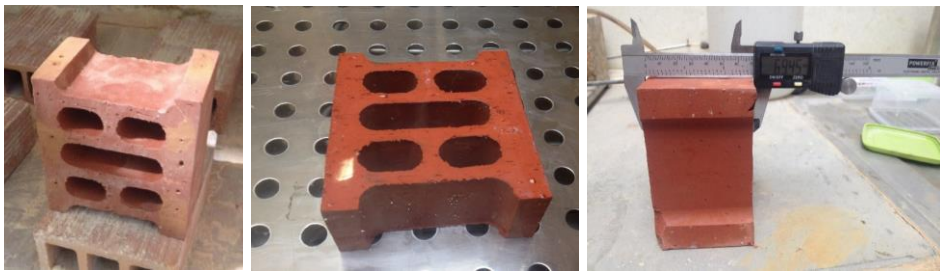

(a) (b) (c)

Figure 3.4 – Phases of procedure of moisture expansion determination: (a) drying of specimens; (b) immersion on boiling water and (c) measurement of dimensions of specimens

The mean values of expansion are presented in Table 3.3. It is possible to see that the coefficient of moisture expansion is different according analysed direction. On the other hand, the same direction studied under two approaches (vertical direction of brick) presents similar coefficient, which increase the accuracy of results.

Table 3.3 – Mean moisture expansion of bricks (coefficient of variation (%) is inside brackets)

	First approach	**Second approach**		
	Vertical expansion	Vertical expansion	Horizontal expansion (minor dimension)	Horizontal expansion (major dimension)
$\boldsymbol{l_i}$ (mm)	68.74 (0.47)	68.63 (0.69)	113.81 (0.28)	235.38 (0.16)
Average $\boldsymbol{l_{s1}}$ and $\boldsymbol{l_{s2}}$ (mm)	68.87 (0.34)	68.75 (0.51)	113.85 (0.24)	235.60 (0.06)
$\boldsymbol{l_{m1}}$ (mm)	0.13	0.12	0.04	0.21
Average $\boldsymbol{l_{s3}}$ and $\boldsymbol{l_{s4}}$ (mm)	68.94 (0.30)	68.84 (0.48)	113.95 (0.26)	235.65 (0.07)
$\boldsymbol{l_{m2}}$ (mm)	0.19	0.20	0.14	0.27
$\boldsymbol{e_m}$ **(mm/m)**	**1.09 (0.37)**	**1.21 (0.53)**	**0.84 (0.24)**	**0.24 (0.09)**

It is noticed also that the recorded variation is low, reinforcing again the accuracy of results. It is worthwhile to look more closely at vertical moisture expansion coefficient because this is the highest value comparing with the other directions. This is the curing direction and this could be the reason for this difference.

Eurocode 6 [30] does not provide enough information to quantify the irreversible expansion because this value depends significantly on the clay used for the masonry units, and the recommended value is between -0.2 to 1.0mm/m. Uncertainty still exists about the real expansion/shrinkage of bricks because it depends on characteristics of units, namely elasticity modulus, expansion/shrinkage coefficients, geometry and specially its age [72]. According Brooks (2014) [72], largest part of moisture expansion of clay bricks occurs during the first month after production, and its evolution after that it is not very clear, which difficult the real knowledge about the irreversible moisture expansion coefficient. However,

an obtained value about horizontal expansion on major dimension is very similar to normalized values consulted in technical notes, 0.2mm/m (presented in Table 3.1 on previous section).

3.2.3. Density, porosity and water absorption by capillarity of mortar

The mortars used in veneer and infill walls were tested in order to calculate the dry density and absorption of water by capillarity according to EN 1015-10 [71] and EN 1015-18 [70], respectively. Only the most typical infill mortar was analysed, namely mortar general purpose mortar M5. The veneer mortar was a typical pre-mixed water repellent mortar presented in previous section.

For each type of mortar, the dry bulk density of hardened mortar was calculated as the quotient of the mass and volume. The mass was obtained in oven dried conditions at a temperature of 70 ºC until constant mass was reached. The volume was obtained by measuring the saturated and submerged weight of the specimens. For this, the specimens were immersed in a vacuum of approximately 1000Pa for a period of six hours, to eliminate the air contained in the pores, and after this its saturated mass was determined, according to [73]. The volume is given by:

$$V_s = \frac{m_{s,sat} - m_{s,i}}{\rho_w} \quad (3.2)$$

Where

V_s is the apparent volume of the specimen, m^3;

$m_{s,sat}$ is the mass of saturated specimen of hardened mortar, kg;

$m_{s,i}$ is the apparent mass of saturated specimen of hardened mortar immersed in water, kg;

ρ_w is the density of water, kg/m^3.

The bulk density of mortar, ρ, and open porosity (or apparent porosity), η, are given by the following expressions:

$$\rho = \frac{m_{s,dry}}{V_s} \quad (3.3)$$

$$\eta = \frac{m_{s,sat} - m_{s,dry}}{m_{s,sat} - m_{s,i}} \times 100 \quad (3.4)$$

where,

ρ is dry bulk density of mortar, kg/m^3;

$m_{s,dry}$ is the oven dry mass of specimen of hardened mortar, kg;

η is the open porosity (or apparent porosity), %.

For the tests, specimens with dimensions are 40mmx40mmx160mm and 6 samples were considered. The results of the physical properties are presented in Table 3.4. The values are very approximated to the normalized values given in technical specifications for each type of mortar (1950±200 kg/m^3 for infill mortar and veneer mortar).

Table 3.4 – Results of real volume and dry bulk density for each type of mortar bricks (coefficient of variation (%) is inside brackets)

	η (%)	**ρ (kg/m^3)**
Pre-mixed veneer mortar	17.83 (3.32)	1752.73 (2.09)
Infill mortar	21.19 (4.36)	1858.58 (1.15)

The obtaining of the capillary water absorption coefficient is carried out on prismatic specimens with dimensions 40x160x160mm^3. After drying, the samples were broken in two parts and the four longitudinal faces were sealed using the specified sealing material, Figure 3.5 (a).

(a) (b)

Figure 3.5 – Capillarity test: (a) sealed samples and (b) samples during the test

In order to ensure full immersion of broken and rough textured surface of specimens, they were immersed in water to a depth of 5 mm to 10 mm for the duration of the test and in a sloping attitude, as shown in Figure 3.5 (b). The measurements were carried out in each 5minutes until 20min of test. After this, in each 10minutes, a measurement was carried out until 60minutes. More two measurements were taken at 90 minutes. After that, the record was done every 30minutes until 6hours. The records continued two times per day until complete 8 days.

The values of water absorption by capillary along time can be seen in Figure 3.6. The first phase until 90 min is essential to obtain the capillary water absorption coefficient, which is calculated as the slope of the straight line linking the representative points of the

measurements carried out at 10 min and 90 min. It can also be calculated through the following expression:

$$C = 0.1\ (M_2 - M_1) \tag{3.5}$$

Where,

C is the coefficient of water absorption for an individual mortar specimen, kg/(m^2.min$^{0.5}$);

M_1 is the mass of the specimen after soaking for 10 min, g;

M_2 is the mass of the specimen after soaking for 10 min, g.

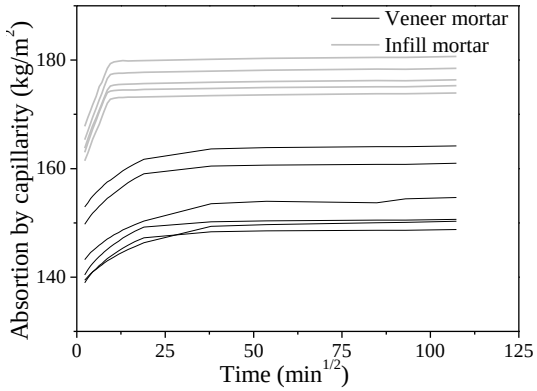

Figure 3.6 – Results of absorption of water by capillarity

The results are presented in Table 3.5 for each type of mortar. It is seen that the mortar used in the infill walls presents a much higher capillary coefficient. Note that the mortar used in the brick veneer walls is water-repellent, meaning that the water absorption is much lower. The stabilization of water absorption was much faster in infill mortar than in veneer mortar due to its very fast initial absorption.

Table 3.5 – Coefficient of water absorption by capillarity for each type of mortar (coefficient of variation (%) is inside brackets)

	C (kg/(m^2.min$^{0.5}$))
Infill mortar	1.58 (3.21)
Veneer mortar	0.62 (11.85)

The obtained values are slightly higher than the normalized values given in technical notes (1.5 kg/(m^2.min$^{0.5}$) for infill mortar and 0.45 kg/(m^2.min$^{0.5}$) for veneer mortar. The difference may be justified by the higher porosity [74] and consequently the absorption of water by capillarity [75].

3.3. Mechanical characteristics of masonry materials

The mechanical characterization of masonry materials is carried out based on European standards. Masonry elements characterization will be done according to EN 771 and EN 1015. In terms of mechanical characterization, compression and flexion tests were done in mortar (EN 1015-3 [76]), compression tests were done on bricks (NP EN 772-1 [77]) and tension tests were carried out on ties (BS EN 845-1 [76]).

3.3.1. Brick

The compressive strength of the brick units were obtained through NP EN 772-1 [77]. For the compression tests, three directions were considered given the anisotropic nature of the hollow/perforated brick units, namely in parallel direction parallel to perforations (direction a), and direction perpendicular to perforations (direction b, c), see Figure 3.7.

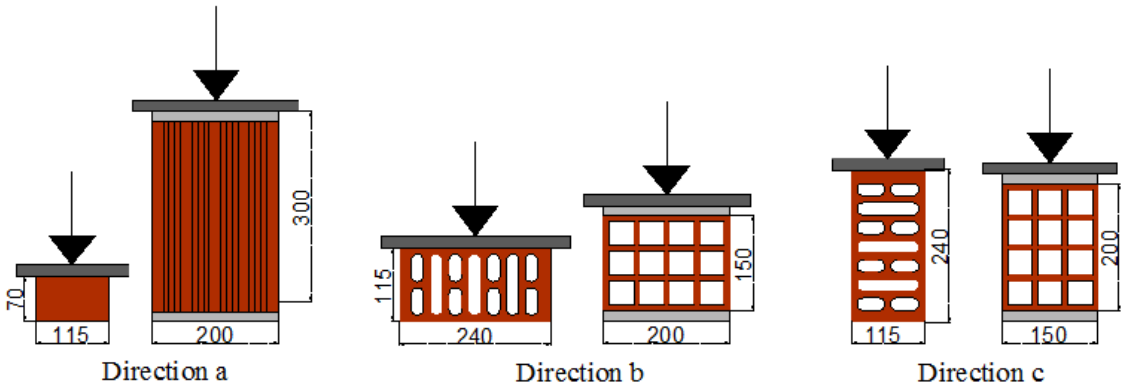

Figure 3.7 – Configuration setups for compressive tests in bricks according direction of load.

Six specimens were tested for each typology. Regarding the preparation of surfaces, in veneer units, the bed faces of the specimen were cleaned and sanded and any loose grit was removed. For infill bricks, the surfaces were regularized with levelled thin mortar bed joint to enable an even loading (Figure 3.8).

Figure 3.8 – Preparation and regularization of surfaces of bricks

The bricks were stored at laboratory conditions (temperature higher than 15º and relative air humidity equal or less than 65 ºC) according to NP EN 772-1 [77].

The test machine is a load frame for compression tests with limit capacity of 2500 kN in close-loop control and 5000 kN in pressure control. The bearing surfaces of testing machine were wiped, and the specimen was aligned carefully in the centre of the ball-seated platen so that a uniform seating. The test was controled by force applied and the speed test was selected according the direction of load. Thus, for direction a, the test speed was 2 kN/s, for direction b, the test speed was 0.7 kN/s and for direction c, the test speed was 0.2 kN/s, making the duration of all test about 5 minutes.

Linear Voltage Displacement Transducers (LDVT) were used in each configuration setup in order to record the vertical deformations of specimens during the compressive test (Figure 3.9). The compressive strength of the brick is given by the following expression:

$$\sigma_{gross} = \frac{F_{max}}{A_{gross}} \tag{3.6}$$

$$\sigma_{eff} = \frac{F_{max}}{A_{eff}} \tag{3.7}$$

Where,

σ_{gross} is the compressive strength, MPa;

F_{max} is the maximum force, N;

A_{gross} is the gross area for units intended to be laid on a full bed of mortar, mm^2;

σ_{eff} is the apparent compressive strength, MPa;

A_{eff} is the area of the vertical faces which effectively resist to compression, mm^2;

The normalized compressive strength was obtained according EN 772-1 [77], considering air-dry conditioning regime through the adjustment factor depending on the moisture (m_c), and a shape factor (ξ). The coefficient of variation was calculated by dividing the standard deviation by average of values. The average values of the compressive strength for brick units are presented in Table 3.6.

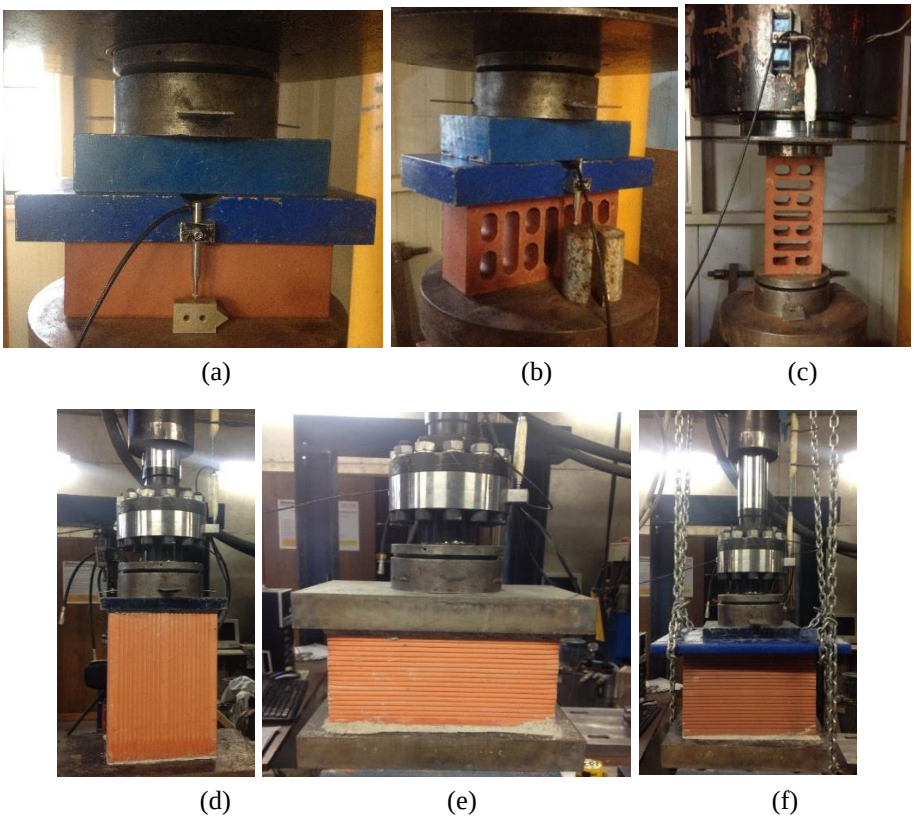

(a) (b) (c)

(d) (e) (f)

Figure 3.9 – Setup configuration of veneer bricks (direction a (a), direction b (b) and direction c(c)) and infill bricks (direction a (d), direction b (e) and direction c (f))

Table 3.6 – Results of compression tests of veneer and infill bricks

		Veneer bricks	**Infill bricks**
Direction a	$\sigma_{gross}\ (MPa)$	24.5	4.15
	$\sigma_{eff}\ (MPa)$	37.84	8.99
	m_c	1.0	1.0
	ξ	0.86	1.35
	$\sigma_b\ (MPa)$	21.07	5.60
	COV (%)	11.8	22.5
Direction b	$\sigma_{gross}\ (MPa)$	13.76	1.45
	$\sigma_{eff}\ (MPa)$	21.26	3.15
	m_c	1.0	1.0
	ξ	1.16	1.0
	$\sigma_b\ (MPa)$	15.97	1.45
	COV (%)	20.9	25.0
Direction c	$\sigma_{gross}\ (MPa)$	6.19	1.18
	$\sigma_{eff}\ (MPa)$	9.56	2.55
	m_c	1.0	1.0
	ξ	1.46	1.25
	$\sigma_b\ (MPa)$	9.04	1.47
	COV (%)	23.5	23.1

The maximum strength of the brick units is presented in Figure 3.10 and the complete stress-strain diagrams from uniaxial compression tests are presented in Figure 3.11.

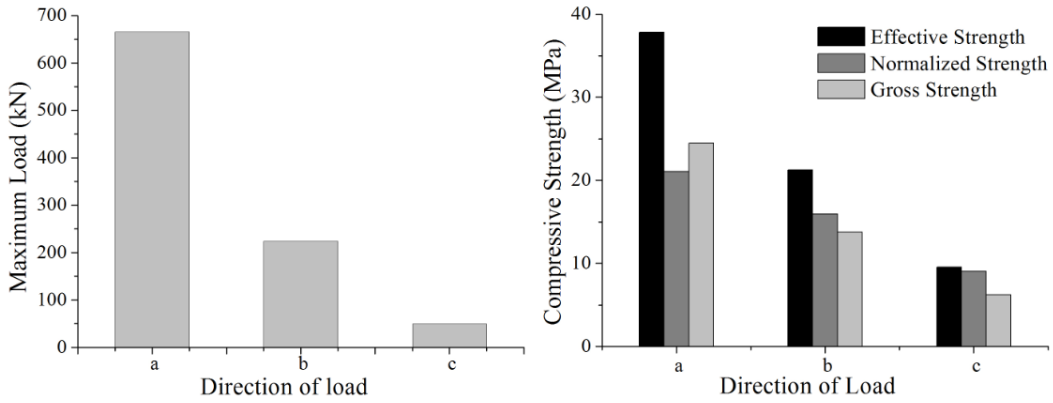

Figure 3.10 – Maximum load and compressive strength obtained in veneer bricks

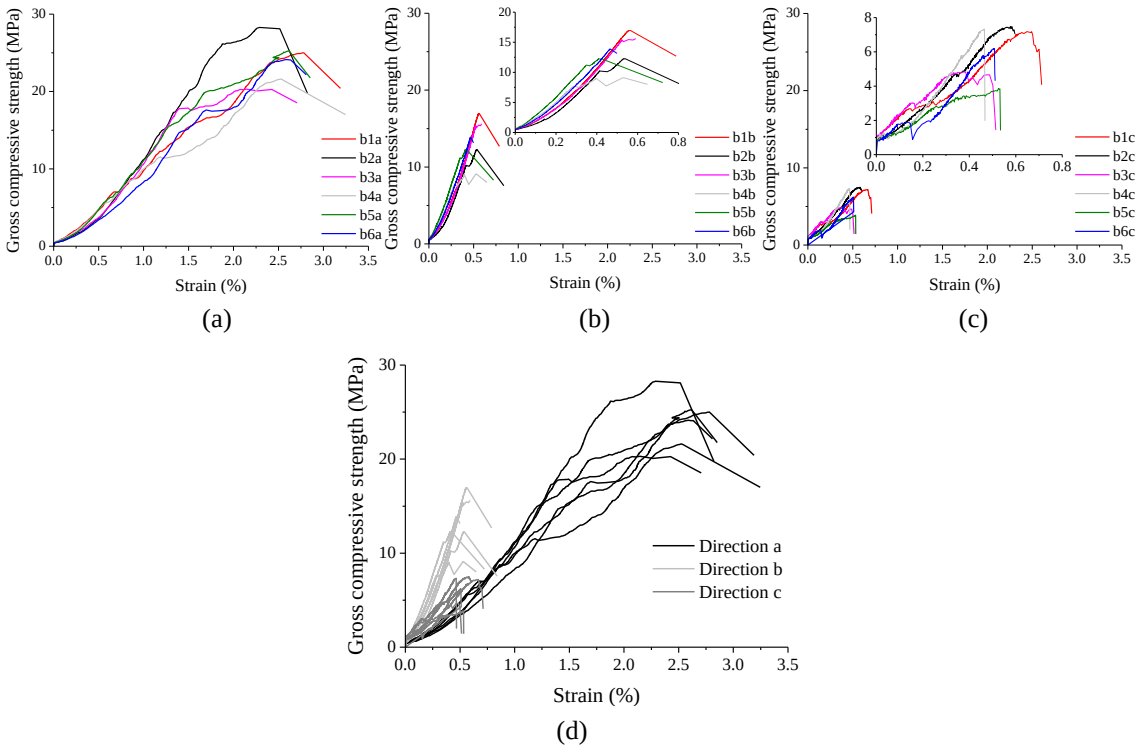

Figure 3.11 - Compressive strength vs extension response of the veneer bricks in (a) direction a, (b) direction b, (c) direction c and (d) all directions

The mean compressive strength was lower than the reference values provided by manufacturers. The coefficient of variation is acceptable because is always lower than 25%, like Eurocode 6 (EC6) [78] recommends.

As it was expected, the post peak behaviour was completely brittle, especially in direction c due to low resistance capacity.

The failure modes are presented in Figure 3.12, according to the direction of loading. The most frequent failure mode was initiated by breaking the connections between internal shells

of the units, particularly with the appearance of a crack in the intersections of shells, followed by bending up to achieve rupture. In direction a of loading, the brick broken totally, whereas in direction b and c, the internal shell of bricks broken before than external faces of bricks.

(a) (b) (c)

Figure 3.12 – Failure modes: (a) direction a; (b) direction b and (c) direction c

The compressive strength of brick units of masonry infill walls and the compression are presented in Figure 3.13 and Figure 3.14 respectively.

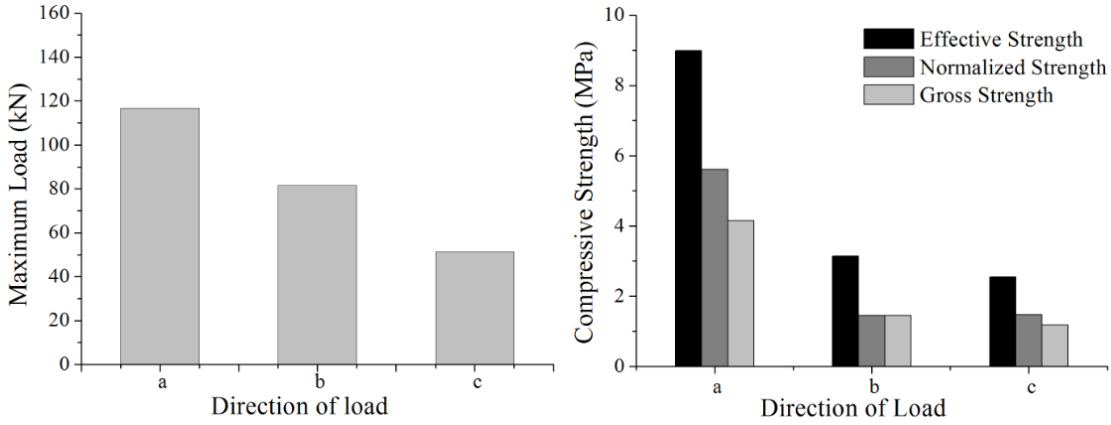

Figure 3.13 – Maximum load and compressive strength obtained in infill bricks

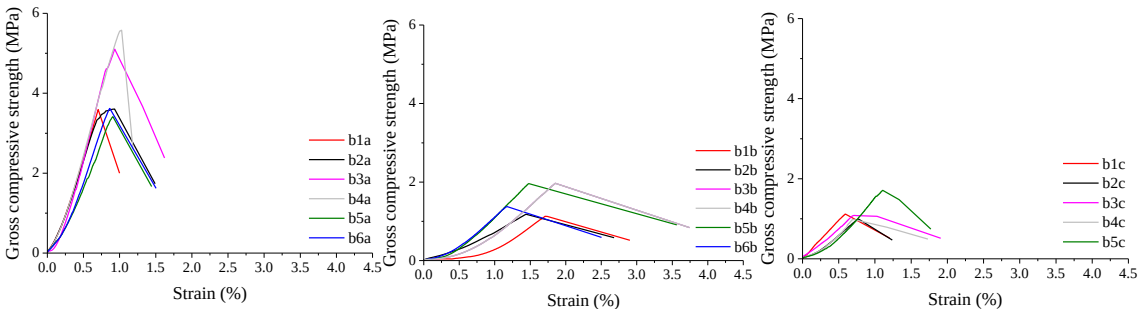

(a) (b) (c)

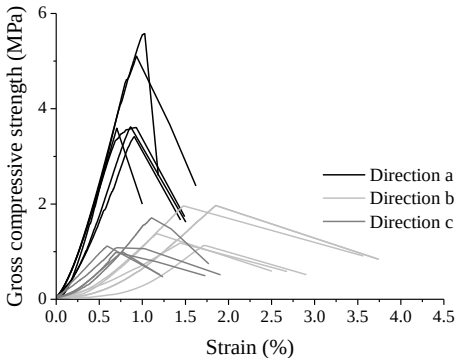

(d)

Figure 3.14 – Compressive strength vs extension response of the infill bricks in (a) direction a, (b) direction b, (c) direction c and (d) all directions

The mean compressive strength is very closed to reference values provided by manufacturers. The compressive stress-strain behaviour of brick presented a similar pre-peak in majority of samples whereas the post-peak behaviour was completely brittle, as expectable.

The failure modes are presented in Figure 3.15, in relation to direction a because the others directions presented a completely rupture. In this configuration, the failure mode was initiated by breaking the connections between external faces and internal shell, following by bending to achieve detachment and rupture of external shell of brick.

Figure 3.15 - Failure modes of direction a of infill bricks

3.3.2. Mortar

Three types of mortar were considered for masonry veneer walls and for masonry infill walls. The veneer units are assembled with pre-mixed water-repellent cement mortar recommended by veneer bricks manufacturer. For the backup leaf, a pre-mixed mortar M5 and M10

typologies were used to bond the masonry units. The thickness adopted for the brick prims was 15mm to make the perfect levelling of the tie possible.

A general purpose mortar of class M10 is considered for the experimental campaign involving the brick masonry infill walls, namely M10* and M10. The difference on this nomenclature is associated to the different mechanical properties obtained. In addition, a general purpose mortar M5 was also used in the experimental campaign involving brick masonry infills. For masonry veneer leaf, only one type of mortar was considered in the experimental campaigns, defined as a pre-mixed water-repellent cement mortar.

The water ratios were decided in advance, based on the recommendations of the mortar manufacturers and based on plasticity tests (Figure 3.16). The mortar was studied in the laboratory to find the appropriate water content so that adequate workability (EN 1015-3 standard [76]) could be obtained. The objective was to obtain a value of flow table between 145 and 160mm based on technical notes of mortars [79-81] and recommendations of the experienced workmanship.

Figure 3.16 – Mortar with different water ratios

The average flow table result from averaging the results of two diameters, see Table 3.1.

After the selection of the W/C ratio, the specimens were prepared to determine the flexural and compressive strength of mortar according to European standard EN 1015-11 [82] at 28 days. For this purpose, 3 samples with 160 mm x 40 mm x 40 mm dimensions were carried out for flexural tests, from which 6 small prisms were derived to compression tests (Figure 3.17). In flexural tests were carried out in force control at a rate of 30 N/s, so that the failure happens among 30s a 90s. The compression tests were also carried out under force control at rate of 250 N/s.

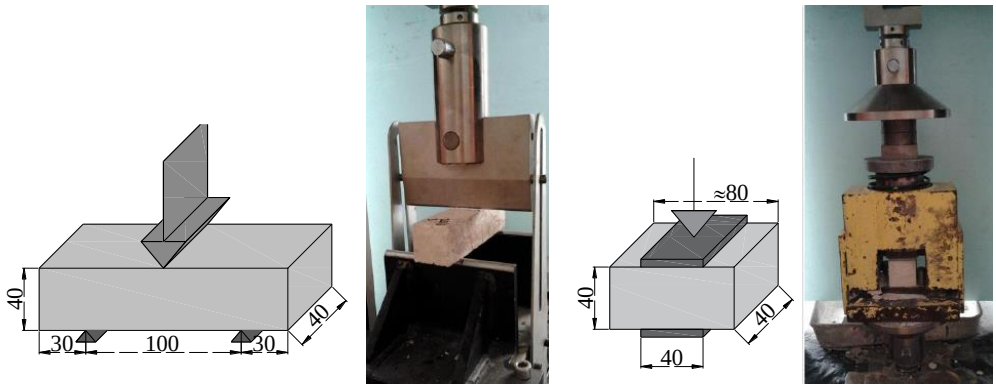

(a) (b)

Figure 3.17 – Setup for (a) flexural and (b) compression tests in mortar (dimensions in millimetres)

The samples previously carried out in laboratory conditions were kept in controlled conditions, namely 60% of humidity and 20ºC for 28 days. The samples from mixtures used in construction were kept in laboratory conditions. The compressive strength is obtained by expression 3.1.

$$f_c = \frac{F_{max}}{A} \tag{3.8}$$

where,

f_c is the compressive strength, MPa;

F_{max} is the maximum force, N;

A is the loaded area, mm^2;

The flexural strength of mortar is calculated through expression 3.2:

$$f_{cfm} = 1.5\frac{F_{max} \times l}{wb^2} \tag{3.9}$$

Where,

f_{cfm} is the flexural strength, MPa;

l is the distance between the support rollers, mm;

w is the width of specimen, mm;

b is the depth of the specimen, mm.

Table 3.7 shows average mechanical properties, namely flexural and compressive strength at 28 days from mixtures used in construction of specimens and mortar casted for mechanical characterization.

Table 3.7 – Mechanical properties of each mortar type (coefficient of variation (%) is inside of brackets)

Mortar typology		**f_c – mason (MPa)**	**f_c – lab (MPa)**	**f_{cfm} – mason (MPa)**	**f_{cfm} – lab (MPa)**	**Flow value (mm)**
Veneer mortar		5.3	4.8	2.9	2.1	147
		5.2	5.5	3.2	2.1	146
		6.1	4.3	3.2	1.8	147
	Average	5.6 (8.7)	5.2 (7.2)	3.1 (5.4)	1.9 (9.9)	147 (0.39)
Infill mortar M10*		6.1	7.5	2.5	3.1	157
		6.5	6.5	2.4	2.6	157
		6.3	6.7	2.7	3.0	155
	Average	6.3 (3.4)	6.9 (7.7)	2.5 (6.2)	2.9 (9.1)	156 (0.74)
Infill mortar M10		12.9	12.1	7.6	7.1	154
		12.1	11.3	8.1	6.9	153
		12.3	10.7	8.0	6.5	154
	Average	12.1 (4.5)	11.4 (6.2)	8 (3.2)	6.4 (6.8)	154 (0.38)
Infill mortar M5		6.3	6.8	2.8	2.6	161
		6.3	5.9	3.5	2.1	159
		6.7	6.1	3.5	2.3	159
	Average	6.5 (4.3)	6.3 (8.9)	3.2 (12.1)	2.3 (10.7)	160 (0.72)

It is important to underline that in spite of M10 and M10* are of the same class, the mortar M10* presents flexural and compressive strength considerably lower than the expected values. It is considered that this should be attributed to quality issues related to the manufacturer of mortar.

The results found for the specimens taken from the mixtures used for the construction of walls are slightly different from the ones prepared in the laboratory, which should be attributed to the different mix conditions. Notice that, the flexural strength obtained in infill mortar M10 from mixtures used in construction of walls is considerably high, however, this value was considered valid due to low scatter of values.

3.3.3. Ties

Taking into account that it is intended to attach the brick veneer walls to masonry infill walls and after a research in the market of wall ties, it was decided to select six most typical commercial ties, see Figure 3.18. The geometric features of the ties are presented in Figure

3.8. With exception of T6 tie, which is composed by basalt fibre, the other ties are made of stainless steel according to technical notes.

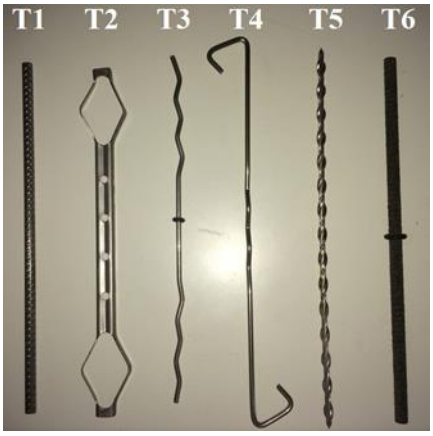

Figure 3.18 - Wall tie typologies used in the experimental campaign

As shown in Figure 3.8, it was considered different lengths in some tie typologies, taking into account the different studies for the experimental campaign. With exception of T5 wall tie, the ties are applied on mortar bed joint in infill and veneer leaves, with suitable embedment length.

Table 3.8 - Geometric features of the wall ties

	T1	T2	T3	T4	T5	T6
Dimension (mm)	225/200	225	225/200	225/200	225	225
Thickness (mm)	6	5.5/12	3	3	5/8	7
Section area (mm^2)	28.27	23	7.07	7.07	19.63	38.5

These elements belong to a big group of solutions from *Ancon building products*. In case of tie T5, the attachment to the brick infill unit is carried out through a chemical anchor. A hole on brick is drilled and it is inserted a sock sleeve to be filled with specific grout. In this study, the *Cementie system* from *Helifix soluctions* was used and it is very useful in rehabilitation cases. The application of wall tie T5 on veneer leaf follows the same recommendations of

application of tie on mortar bed joint. Examples of application of the ties on masonry specimens are shown in Figure 3.19.

(a) (b) (c) (d) (e)

Figure 3.19 – Application of wall ties on mortar bed joint of (a) masonry infill leaf and (b) masonry veneer leaf. Application of T5 wall tie: (c) hole on bricks, (d) sock sleeve to be inserted in hole and filled by grout and (e) chemical anchor resultant inside brick

In terms of mechanical characterization, tensile tests were carried out in available wall ties, namely, T1, T5 and T6 typologies. The ties T2, T3 and T4 were not possible to test in laboratory conditions. However, technical information from declaration of performance in conformity is available and it is presented on Table 3.9.

Table 3.9 – Summarize of features based on technical notes

	T2	T3	T4
Compressive load capacity (kN)	3.9/5.1	0.48	1.05
Tensile load capacity (kN)	3.2/5.5	1.02	1.8
Displacement at 1/3 load capacity in compression (mm)			0.37
Displacement at 1/3 load capacity in tension (mm)			0.33
Failure mode in compression	Bending of tie		
Failure mode in tension	5mm deflection		
Water shedding capacity	Resistant		
Durability: material coating reference	23/3		
Durability: steel grade	1.4482/1.4301		

The tension tests carried out in ties T1, T5 and T6 were based on European norm BS EN 845-1 [76], taking also into account laboratory conditions. The wall ties were confined with two clamps so that the rebar could be pulled out. The tensile load was applied through a hydraulic actuator and measured by a load cell with a maximum capacity of 200 kN. The monotonic tests were carried out under displacement control at a rate of 0.05 mm/s. Three samples of each type of tie were selected. The deformation was measured by the internal transducer of the machine and a clip gauge to measure real strain of rebar applied in middle

of tie. The stress-strain response is plotted in Figure 3.20 for each tie typology selected to test in laboratory conditions. Mechanical parameters were derived from the response of each tie, namely maximum force and tension (F_{max} and σ_{max}) and elasticity modulus (E) and they are presented on Table 3.10. The parameters are obtained by following expressions (3.5) and (3.6):

$$\sigma_{max} = \frac{F_{max}}{A} \tag{3.10}$$

$$E = \frac{1}{3}\frac{\sigma_{max}}{\varepsilon} \tag{3.11}$$

where,

A is the loaded cross-section area of a specimen, mm^2;

ε is the strain and it is obtained by dividing the displacement recorded on clip gauge by distance between its supports points (50mm).

Tie T1 presented a typical behaviour of steel in terms of stress vs strain diagrams and mechanical parameters [83, 84]. Although the technical notes define the T5 wall tie as steel material and the obtained response was not as expected, as well as resulting mechanical parameters. Tie T6 defined by basalt fibre, presented typical results for this type of material [85, 86].

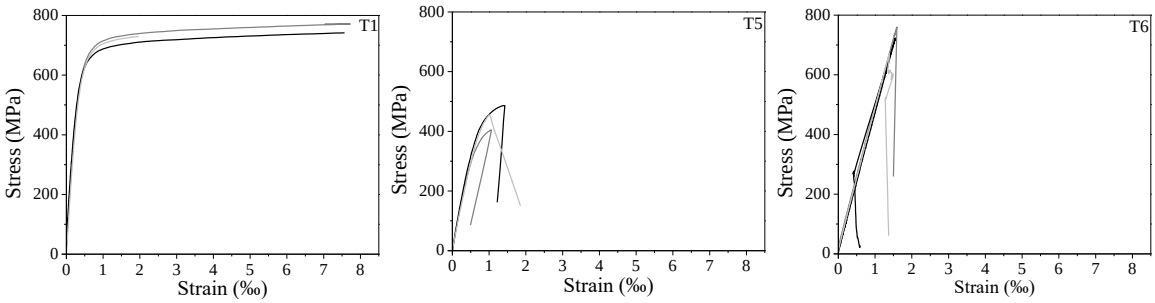

Figure 3.20 – Stress-strain response of each studied tie typology under tension loading

Table 3.10 – Mean mechanical parameters from tension tests (coefficient of variation (%) is inside of brackets)

	σ_{max} (MPa)	E (GPa)
T1	800.52 (1.51)	215.61 (12.12)
T5	452.40 (9.38)	67.30 (6.31)
T6	718.08 (6.18)	50.86 (4.57)

In wall tie T1, the material showed significant hardening after yielding as expected, with minimal softening after peak load, as possible to see in Figure 3.21. The bars have a high

strength and a good deformation capacity of about 20% of elongation, which is important to ensure a ductile response of the wall system. All remaining tested rebars had a brittle failure.

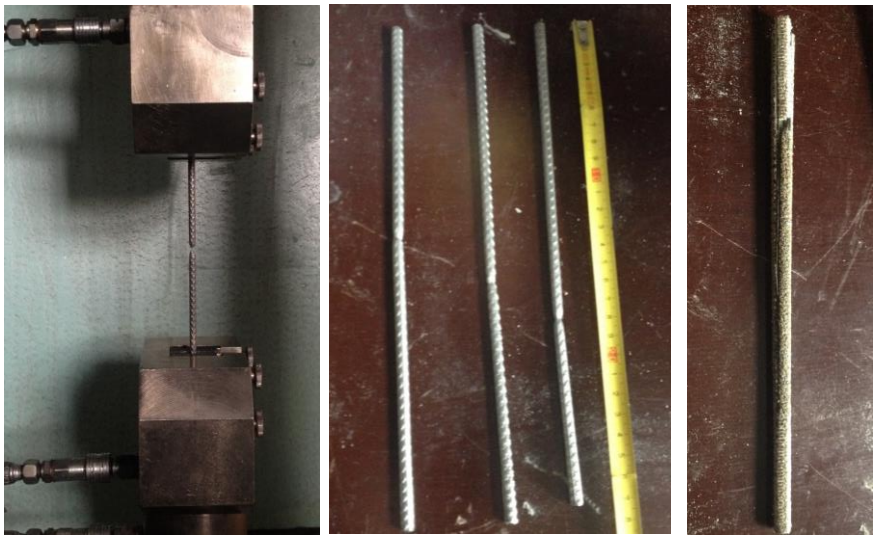

Figure 3.21 – Failure modes of wall ties under tension loading

3.4. Mechanical characteristics of brick masonry veneer

The brick masonry veneer was characterized under different loading conditions, namely compression, flexure and shear through diagonal tension tests and initial shear tests. The characterization of tests follows European standardization. The compressive tests on masonry prisms were performed according to standard EN 1052-1 [87], the bending tests were based on standard EN 1052-2 [88] and shear tests were performed according to standard ASTM E519-02 [89] and EN 1052-3 [90].

For each type of test, the masonry veneer units were assembled with pre-mixed water repellent mortar recommended by veneer bricks. The mortar joints have a thickness of about 15 mm. The construction methodology was based on recommendations of bricks manufacturer and workmanship experience. Three wallets were prepared for each characterization according to standardised dimensions.

3.4.1. Compressive behaviour

The configuration of the uniaxial compression test to characterize the compressive behaviour of brick veneer masonry was based on NP EN 1052-1 [87] and it is shown in Figure 3.22. The top of the specimens was levelled in order to have a uniform vertical load. The test was

performed in displacement control at a rate of 5μm/s. Figure 3.22 shows the instrumentation adopted for the test in order to obtain the compressive stress-strain diagrams and the related mechanical parameters, namely the modulus of elasticity, compressive stress and Poisson coefficient. In particular, LVDT 1, 2, 3 and 4 were used to obtain the modulus of elasticity, considering the mean value, and they were able to give information of the possible rotation of the specimen. LVDT 5 allows to measure horizontal deformations.

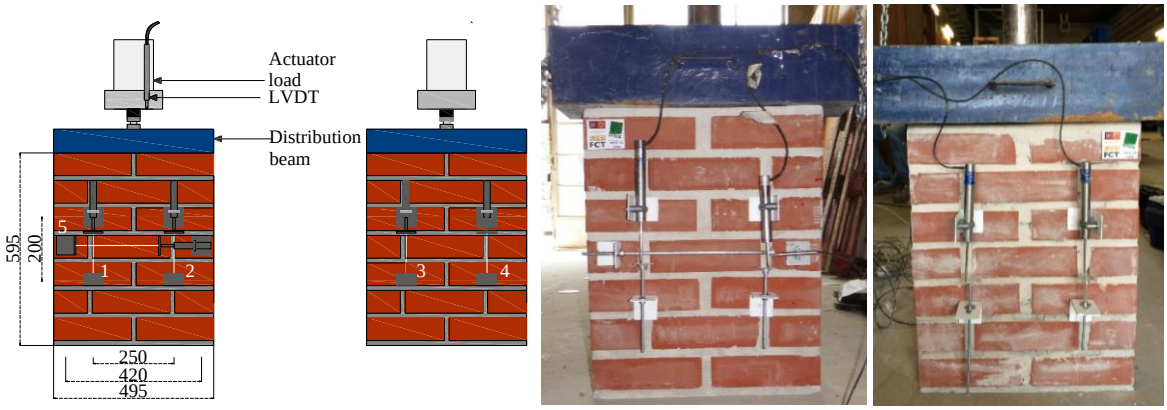

Figure 3.22 – Instrumentation for compression test on masonry assemblages

The mechanical properties were obtained as follows:

$$\sigma_c = \frac{F_{max}}{A} \tag{3.12}$$

$$E = \frac{1}{3}\frac{\sigma_{max}}{\varepsilon_v} \tag{3.13}$$

where,

σ_c is the maximum compression strength, MPa;

F_{max} is the maximum load reached by the specimen, N;

A is the loaded cross-section area of a specimens, mm^2;

ε_v is the mean vertical strain of the specimen at one third of the maximum load (positive value);

The load-displacement and correspondent stress-strain diagrams can be seen in Figure 3.23. The mechanical parameters derived from the diagrams are presented on Table 3.11.

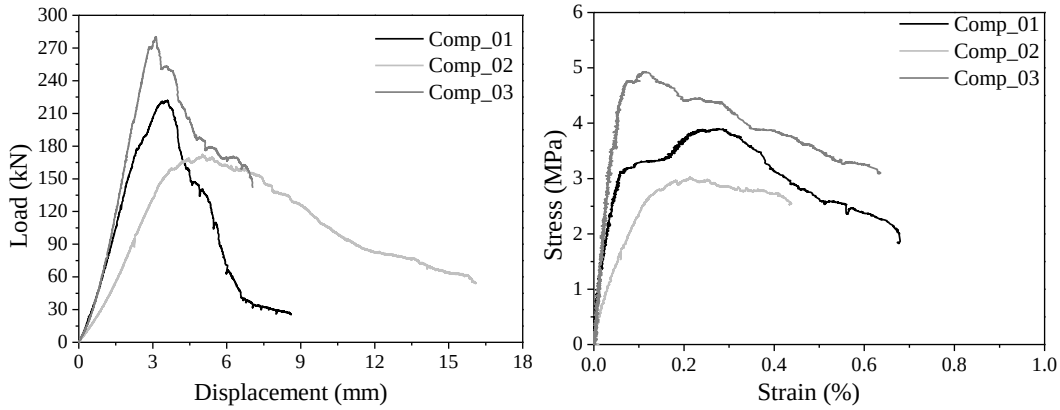

Figure 3.23 – Load vs displacement and stress vs strain response of masonry assemblages under compression loading

Table 3.11 – Mechanical parameters from compression loading

	σ_c (MPa)	E (Gpa)
Comp_01	3.90	8.43
Comp_02	3.03	3.80
Comp_03	4.93	12.64
Average	3.95	8.30
COV (%)	24.01	53.85

Some variation was found in specimen comp_02 sample in terms of maximum resistance and especially in terms of modulus of elasticity.

Based on standard [87], the characteristic value of masonry compression strength can be calculated as the minimum value of the following expressions:

$$f_k = \frac{\sigma_c}{1.2} \text{ or } f_k = \sigma_{c,i,min} \tag{3.14}$$

The resultant experimental characteristic value is 3.03 MPa.

The characteristic compressive strength according to EC6 [30] is obtained through expression (3.15):

$$f_k = K f_b^{0.7} f_m^{0.3} \tag{3.15}$$

where,

f_k is the characteristic compressive strength of the masonry, MPa;

K is a constant according type of material, i.e. 0.45;

f_b is the normalized mean compressive strength of the units, in the direction of the applied action effect, MPa;

f_m is the compressive strength of the mortar, MPa.

The characteristic value based on standard [30] is about 6.4 MPa, higher about 111% than the obtained experimental results.

The failure modes observed during the test is presented on Figure 3.24. The cracks started at centre of upper boundary of wallet. With increasing of displacement, the cracks propagated to the lateral bondaries through the mortar joints and external shells of superior bricks were also detached due to crushing effect. At end of test, cracks and crushing on mortar and bricks were observed in wallets.

Figure 3.24 – Failure mode of wallets under compression loading

3.4.2. Flexural strength

The flexural tests were based on NP EN 1052-2 [88]. The flexural strength in pure bending is obtained under four-point loading. There are two typologies of test in order to obtain: (1) the flexural strength with failure parallel to the bed joints (f_{x1}) and (2) flexural strength with failure perpendicular to the bed joints (f_{x2}). The specimens support lines were levelled in order to have a uniform load application. The test was performed in displacement control at a rate of 10μm/s. Five LVDTs were used, two at centre of samples (one in front and other at the back), two at loading application points and a LVDT to control the actuator displacement, as shown in Figure 3.25.

One of the samples was subjected to cyclic loading in order to evaluate strength and stiffness degradation. The displacement time-history imposed is presented in Figure 3.26.

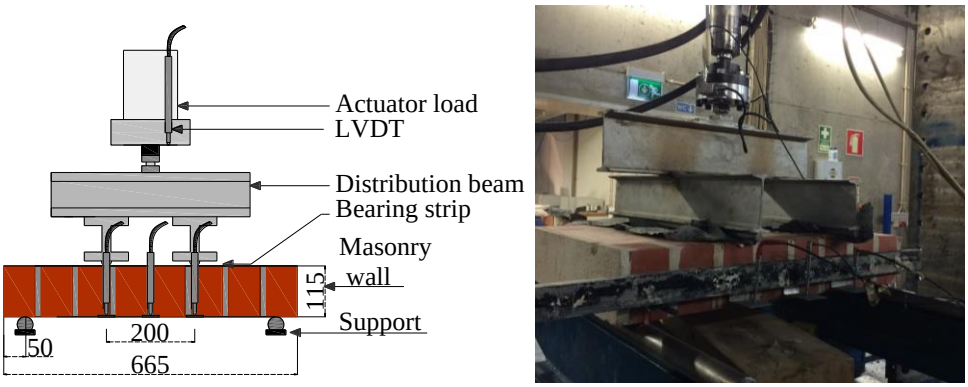

(a)

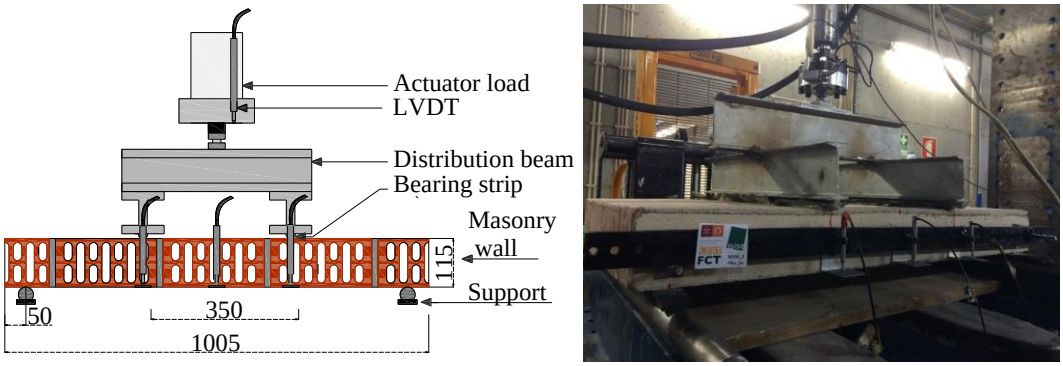

(b)

Figure 3.25 – Configuration of flexural test for (a) plane of failure parallel to the bed joints and (b) plane of failure perpendicular to the bed joints (dimensions in millimetres)

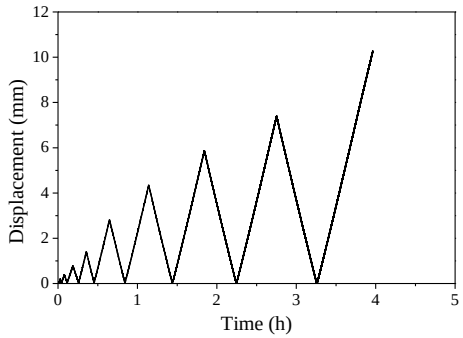

Figure 3.26 – Imposed time-displacement history for cyclic flexural tests

The load-displacement diagrams for each type of flexural test are presented in Figure 3.27.

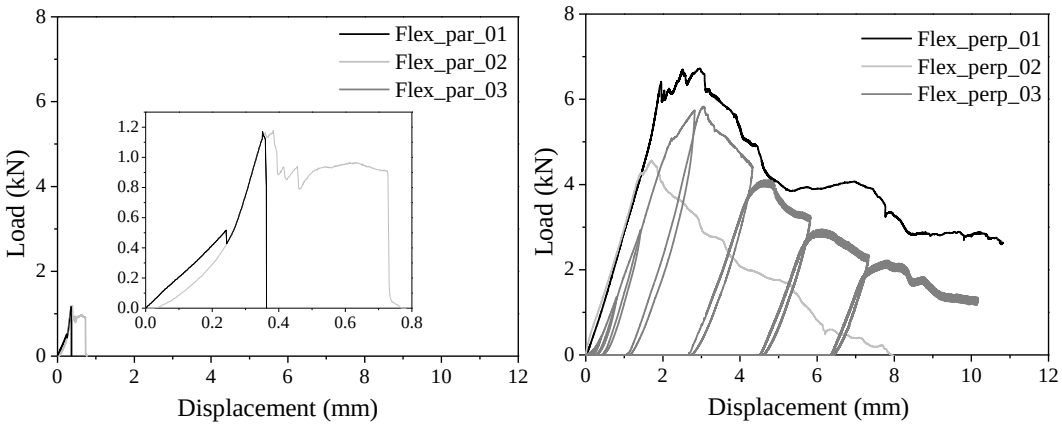

(a) (b)

Figure 3.27 – Flexural load-displacement diagrams t(a) plane of failure is parallel to the bed joints and (b) plane of failure is perpendicular to the bed joints

The derived mechanical parameters, namely maximum force (F_{max}) and correspondent maximum tension (σ_{max}) are summarized in Table 3.12. One of the sample was broken and for that it was impossible to test it. As expected, the flexural strength whose failure is parallel to the bed joints is much lower than the flexural strength whose failure is perpendicular to the bed joints.

Table 3.12 – Mechanical parameters from flexural tests

	f_xk_1	f_xk_2
Flex_01	1.18	6.73
Flex_02	1.16	4.56
Flex_03	-	5.83
F_{max} (kN)	1.17	5.70
σ_{max} (MPa)	0.10	0.70
C.O.V (%)	1.09	19.05

The characteristic flexural strength of the specimens could be calculated by dividing the average compressive strength of the specimens by a factor of 1.5 as following:

$$f_{xk} = \frac{f_x{}^{mean}}{1.5} \tag{3.16}$$

The resultant characteristic flexural strength of masonry whose failure is parallel to the bed joints is 0.07 MPa. The resultant characteristic flexural strength of masonry whose failure is perpendicular to the bed joints is 0.5 MPa.

The results are very closed to characteristic values from EC6 [30], being the f_{xk1} is 0.1 MPa and for f_{xk2} is 0.4 MPa. The standard flexural strength in case of failure is parallel to the bed joints is higher 30% than obtained experimental values, whereas in case of failure is perpendicular to the bed joints is lower 20% than obtained values.

Figure 3.28 presents the failure modes obtained in all tested samples.

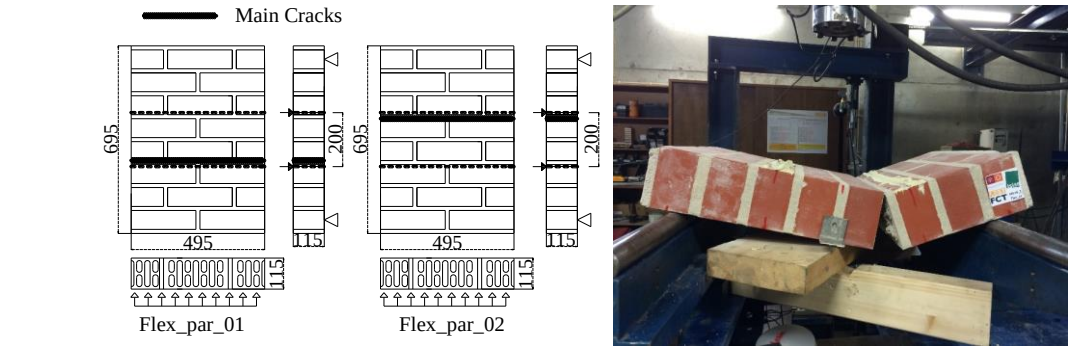

(a)

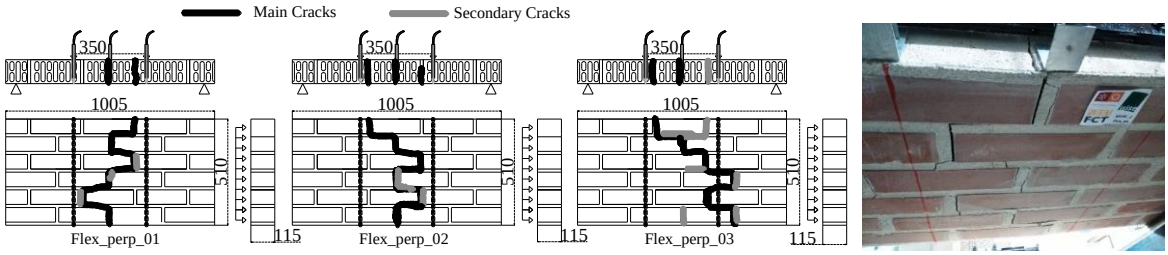

(b)

Figure 3.28 – Failure modes: main and secondary cracks on wallets (a) whose plane of failure is parallel to the bed joints and (b) whose plane of failure is perpendicular to the bed joints

It is possible to see that the rupture on wallets whose failure is parallel to the bed joints is very brittle, whereas the samples whose failure is perpendicular to the bed joints present very distributed cracks, as expected. In third sample of last group, it can be seen more cracks in the pure bending range, which is attributed to cyclic loading.

3.4.3. Shear properties of the unit-mortar interfaces

Nine triplet specimens were tested in shear according to NP EN 1052-3 [90] in order to obtain the initial shear strength. Taking into account that the units have compressive strength greater than 10 MPa, the pre-compression load were 0.2 MPa, 0.66 MPa and 1.0 MPa. Six LVDTs were used, two of them were placed in each external brick to measure the relative vertical displacement in relation to the centre of the brick. It allows to compare the displacement and understand if there is rotation. Other two horizontal LVDTS were used to measure some possible gaps and clearances between bricks. Indeed, all tests were validated taking into account that no great clearance were evidenced. A LVDT was used to control the actuator displacement, as shown in Figure 3.29. The shear force was applied under displacement control at a rate of 10µm/s.

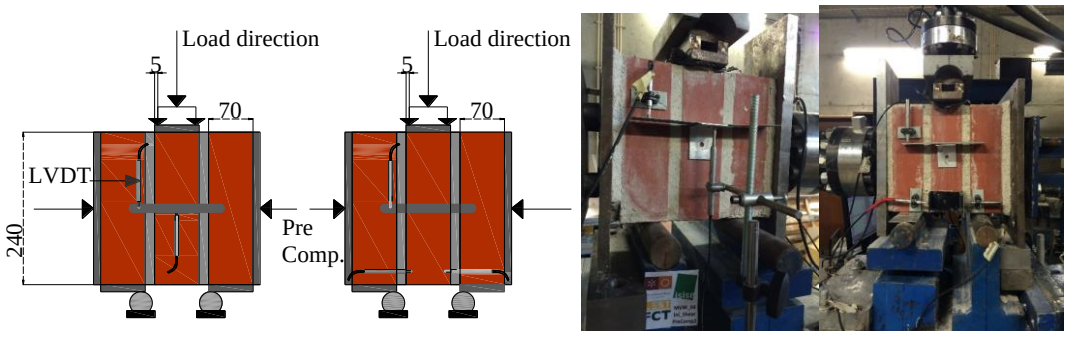

Figure 3.29 – Configuration for initial shear test in masonry (dimensions in millimetres)

For each specimen, the shear strength is calculated using the following expressions:

$$f_{voi} = \frac{F_{i,max}}{2A_i} \tag{3.17}$$

$$f_{pi} = \frac{F_{pi}}{A_i} \tag{3.18}$$

where,

f_{voi} is the initial shear strength for each level of precompressive force, MPa;

$F_{i,max}$ is the maximum shear force, N;

f_{pi} is the precompressive strength, MPa;

F_{pi} is the precompressive force, N;

A_i is the loaded area, mm^2;

The characteristic initial shear strength (f_{vok}) can be calculated according following expression:

$$f_{voik} = 0.8\, f_{voi} \tag{3.19}$$

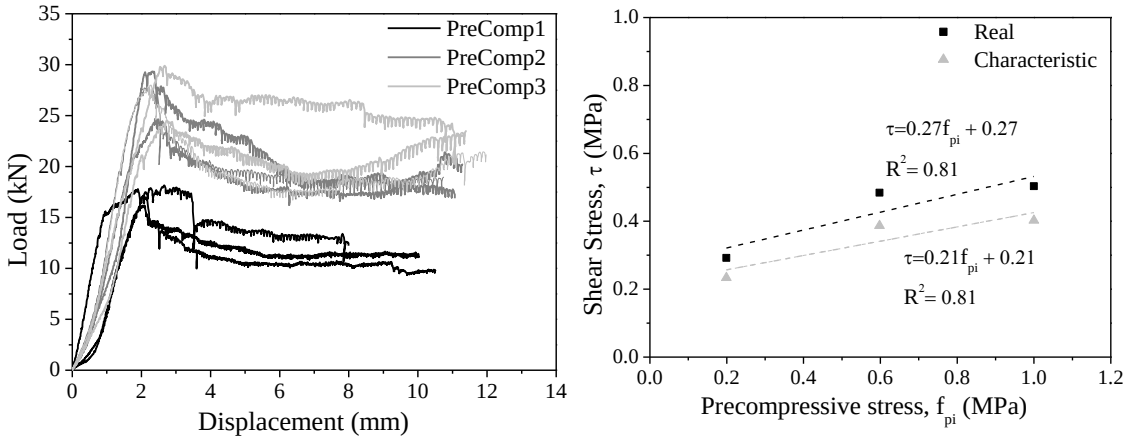

(a) (b)

Figure 3.30 – Obtained results: (a) global response of initial shear test and (b) relation between maximum shear strength vs precompressive stress

The global response measured by external LVDT is presented on Figure 3.30 for each load case, as well as the maximum shear strength points vs pre-compression stress, being possible to obtain the line trend between them, and to calculate the follow parameters:

f_{vo} it is the initial shear strength and it is obtained by line trend y-intercept (0% of precompression stress).

f_{vok} it is the characteristic initial shear strength or cohesion and it is obtained by $f_{vok} = 0.8\, f_{vo}$.

μ_0 is the friction coefficient and it is obtained by slope of obtained line;

α_0 is the internal friction and it is obtained by angle of obtained line;

μ_k is the characteristic friction coefficient and it is obtained by slope of obtained line;

α_k is the characteristic internal friction and it is obtained according to $\tan \alpha_k = 0.8 \tan \alpha_0$

The experimental obtained results are presented on Table 3.13.

Table 3.13 – Mechanical parameters from initial shear tests

	PreComp1	**PreComp2**	**PreComp3**
$\boldsymbol{A_i}$ (mm^2)	27600	27600	27600
$\boldsymbol{F_{pi}}$ (kN)	5.50	16.50	27.60
$\boldsymbol{f_{pi}}$ (MPa)	0.20	0.60	1.00
$\boldsymbol{F_{voi}}$ (kN)	16.12	26.72	27.77
$\boldsymbol{f_{voi}}$ (MPa)	0.29	0.48	0.50
$\boldsymbol{f_{voik}}$ (MPa)	0.23	0.39	0.40
COV (%)	16.54	8.29	8.38
$\boldsymbol{f_{vo}}$ (MPa)		0.27	
$\boldsymbol{f_{vok}}$ (MPa)		0.21	
$\boldsymbol{\mu_0}$		0.26	
$\boldsymbol{\mu_k}$		0.208	
$\boldsymbol{\alpha_0}$ (º)		14.32	
$\boldsymbol{\alpha_k}$ (º)		11.92	

The obtained failure modes was analysed taking into account the type of failure presented in 1052-3 standard [90]. Two types of failures were observed: shear failure in unit/mortar bond area divided between two unit faces and crushing and splitting failure in the units, as shown in Figure 3.31.

(a) (b)

Figure 3.31 – Failure modes: (a) shear failure in unit/mortar bond area divided between two unit faces and (b) crushing and splitting failure in the units

3.4.4. Shear strength

The shear strength of brick veneer masonry was obtained based on diagonal compression tests according to ASTM 519 [89]. The diagonal compression and induces shear stresses in the brick masonry. Through this test, it is possible also to obtain the tensile strength, assuming a pure shear stress state as the minimum principal stress. The test setup and instrumentation are presented in Figure 3.32. The specimens' corners were levelled in order to have a uniform load application. The diagonal compression test was performed in displacement control at a rate of 2μm/s.

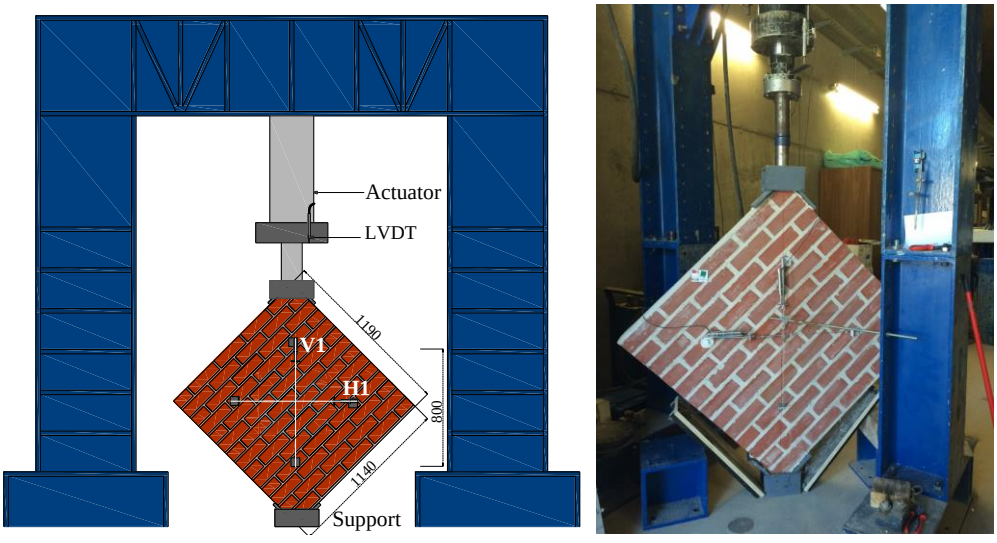

Figure 3.32 – Configuration of shear test in masonry: Diagonal test (dimensions in millimetres)

Five LVDTs were used, being one of them used to control the test and two vertical and two horizontal devices to measure the vertical and horizontal deformation on two faces of wallet. These measurements enable the measurement of vertical shortening and the horizontal

extension on both sides of the specimens and, thus, to obtain the relative strains, so that the shear modulus can be obtained.

According to standard, the shear stress and shear modulus are calculated as follows:

$$\tau = \frac{0.707\,F}{A_n} \tag{3.20}$$

$$A_n = \frac{W+h}{2} tn \tag{3.21}$$

$$\gamma = \frac{\Delta V + \Delta H}{g_v} \tag{3.22}$$

$$G = \frac{\tau}{\gamma} \tag{3.23}$$

where,

τ is the shear stress, MPa;

A_n is the net area of the specimen, W is the width of specimen (mm), h is the height of specimen (mm), t is the total thickness of specimen (mm), and n is the percent of the gross area of the unit that is solid expressed as a decimal;

γ is the shearing strain;

ΔV is the vertical shortening (positive value), (mm);

ΔH is horizontal extension (positive value), (mm);

g_v is the vertical gage length, mm;

G is the modulus of rigidity, MPa.

The load-displacement and strain-stress diagrams are presented in Figure 3.33 and Figure 3.34. In case of force-displacement diagrams, records of vertical and horizontal deformations of wallet are presented.

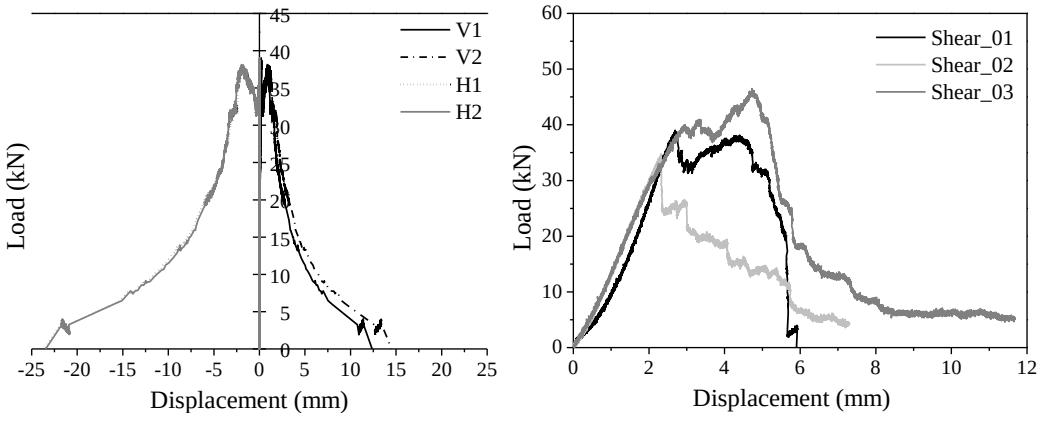

Figure 3.33 – Load-displacement response through (a) vertical and horizontal opening and (b) global deformation

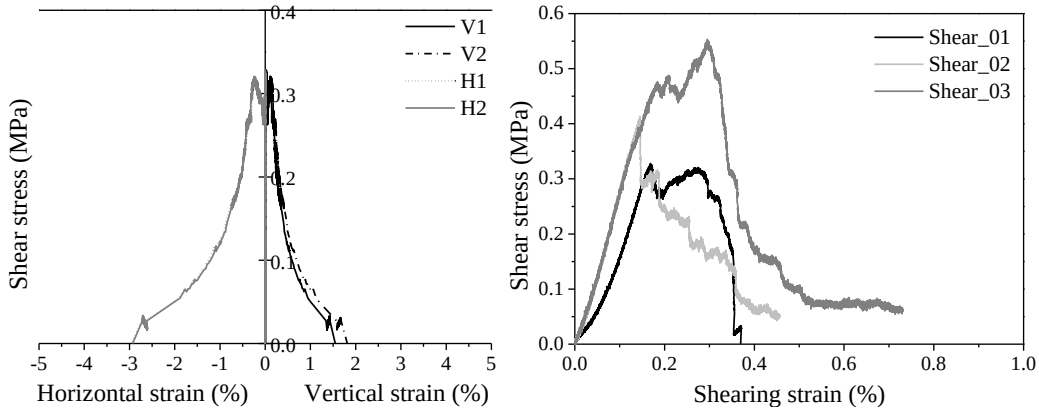

Figure 3.34 – Stress-strain response through (a) vertical and horizontal opening and (b) global deformation

The Table 3.14 presents the results of the tests in terms of shear load and strength (F_{max} and τ_{max}) and shear modulus (G).

Table 3.14 – Mechanical parameters of diagonal tensile tests

	F_{max} (kN)	τ_{max} (MPa)	G (MPa)
Shear_01	38.99	0.33	1355.50
Shear_02	34.78	0.29	1409.45
Shear_03	46.51	0.39	-
Average	40.09	0.34	1382.48
COV (%)	14.82	14.82	2.76

It is observed that variations of both shear strength and shear modulus are low. The shear modulus of sample 03 was not possible to be obtained because technical problems of measurement devices.

Figure 3.35 shows the different failure modes found for the three specimens. While in specimen 02 the crack was not diagonal, in the other two specimens the crack was more along the line of the diagonal. Specimens 01 and 03 present similar crack patterns, with a similar vertical crack aligned with the applied load.

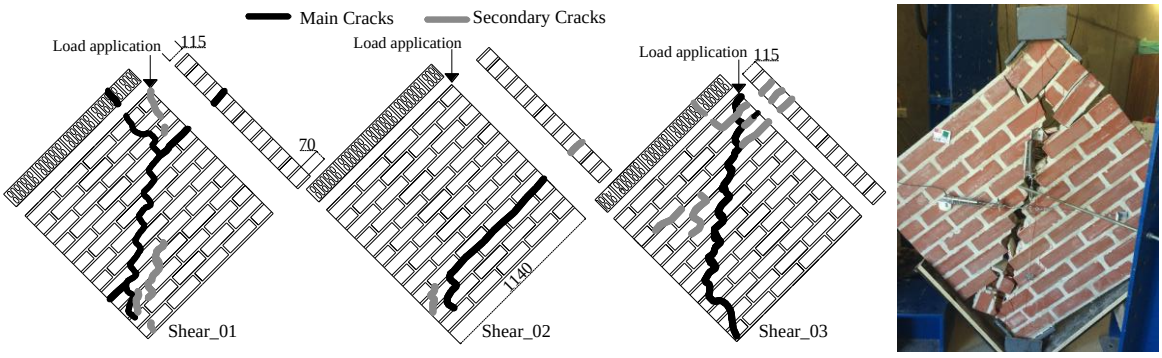

Figure 3.35 – Failure modes of shear wallets

3.5. Freeze and thaw resistance of masonry

Given that the brick veneer walls are directly exposed to environmental conditions, it was decided to evaluate the behaviour of brick veneer masonry to freeze and thaw cycles. Besides brick masonry, mortar used in the construction of brick veneer wall was also submitted to several freeze and thaw cycles. The assessment of specimens after the freeze and thaw cycles was carried out based on the obtainment of physical and mechanical properties in case of mortar (density, porosity, water absorption by capillarity, ultrasonic pulse velocity, electrical resistivity and flexural and compressive strength) and based on visual inspection in case of brick masonry specimens.

Different standards were followed as reference for designing an appropriate experimental campaign for mortar and masonry subjected to freeze and thaw cycles, namely CSN 72 2452 and NP EN 772-22, respectively [91, 92].

3.5.1. Overview of past research on freeze and thaw tests

Freeze and thaw cycles are amongst the most significant weathering process causing severe damage to building materials [93]. Several successful work has been carried out on different types of materials to evaluate its freeze and thaw resistance, especially on rocks, mortar and concrete [94-98].

Lime mortars with compositions similar to ancient mortars is the most studied mortar because it has presented durability problems mainly when exposed to weathering agents like water and freeze-thaw cycles [93, 99, 100]. They are very porous and their mechanical strength and durability are low when exposed to water and frost even though if only occasionally. One way to improve the strength and durability of air lime mortars is to partially replace air lime by other materials such as pozzolanas, being able to achieve much higher mechanical strength than pure lime mortar [101]. The cement mortar has also been studied since long time in order to understand the deleterious effects that the exposition to freeze and thaw can cause on it [100, 102-107]. In majority of these types of mortar, an important manner to improve durability is to avoid water penetration. Thus, frost resistance can be improved by using additives for mortars relying in hydrophobic properties [93, 108-110]. The most common studied water-repellent admixtures for cement and lime mortars is vegetable oil [111-115].

According to Monteiro et. al (2006) and Çavdar (2014) [115, 116], when water begins to freeze in a capillary cavity, the increase in volume requires a dilation of the cavity equal to 9% of the volume of frozen water. The magnitude of this hydraulic pressure depends on the permeability of the cement paste, the degree of saturation, the distance to the nearest unfilled void and the rate of freezing. If the pressure exceeds the tensile strength of the paste at any point it will cause local cracking. In repeated cycles of freezing and thawing in a wet environment, water will enter the cracks during the thawing to freeze again later and there will be progressive deterioration with each freeze–thaw cycles. Thus, the strength of sample can decreases with freeze–thaw cycles [116, 117]. In addition, the surfaces of samples are common to scale off and crumble due to the expansion caused when water freezes to ice. Fibre reinforcement was a investigated solution in order to improve performance against the harmful effects of freeze–thaw cycles [116, 118, 119]. The incorporation of different fibres increases ductility/deflection ability and flexural strength of the cement mortar, improving consequently the freeze-thaw resistance.

Physical and mechanical parameters have been studied to evaluate the effects of freeze and thaw after different number of freeze–thaw cycles. The assessment was carried out using destructive and non-destructive tests to characterize the mechanical property degradation (e.g. modulus and strength), geometry change, microstructural change, ultrasonic signature change and electrical resistivity change. A summary of some studies carried out in the past is presented in Table 3.15.

Table 3.15 – Summary of some research on freeze and thaw tests

Reference [REF]	Type of material	Assessment methodology	Observed effects
Çavdar (2014) [116]	Cement mortars with five different types of fibres in four different ratios.	Dynamic modulus elasticity; flexural and compression strength and deflection.	Dynamic modulus of elasticity and resistance decreases with increasing of freeze and thaw cycles number. The addition fibres increase flexural strength and deflection ability of the samples but decrease compressive strength.
Nunes and Slízková (2016) [93, 101]	Lime mortar mixtures with lime, metakaolin and linseed oil	Mortar mineralogy; microstructure, mechanical strength and resistance.	The combination of lime- metakaolin with linseed oil produced vaterite (less stable polymorph of CaCO3) and showed the highest resistance to frost damage. Linseed oil had comparable effectiveness to industrial water repellents. It might improve elasticity of the mortar matrix and the freezing process itself does not cause material degradation.
Cao and Chung (2002) [100]	Cement mortar	Electrical resistivity measurement.	An increase in temperature caused the resistivity to decrease reversibly, but with hysteresis, which grew with cycling; the effects of freezing and thawing on the resistivity were small compared to the effect of temperature on the resistivity.
Uranjek and Bokan-Bosiljkov (2015) [108]	Brick-mortar triplets and wallets; Lime mortar and lime-slag mortar	3D scanning; ultrasonic velocity (UV); water absorption and flexural and compression strength.	UV is significantly reduced, indicating the damage of mortar. The angle of internal friction, stiffness and compressive strength are reduced after freezing and thawing indicating the damage.
Garbalińska and Wygocka (2014) [75]	Four cement mortars (the reference mortar and 3 modified mortars)	Mechanical strength; porosity and capillarity; microstructure.	The material modifications (based on superplasticizer, silica fume and an air-entraining agent) resulted in an increase frost-resistance of the mortars. The reference mortar presented a decrease of compressive strength more than 60%.

3.5.2. Characterization of specimens

a) Mortar

The mortars used in the assessment of the influence of freeze and thaw actions in its physical and mechanical behaviour are the pre-mixed water repellent cement mortar applied on masonry veneer walls and the general purpose mortar pre-mixed mortar M5 applied in the construction of brick masonry infill walls. The main goal of using these two types of mortar was to understand the behaviour of a common mortar and of a hydrophobic mortar under the same freezing cycles. As shown in Figure 3.36, 16 specimens with dimension 160mm x 80mm x80 mm were prepared for each type of mortar [82]. From these, 8 samples were subjected to freeze and thaw cycles and 8 samples used as reference.

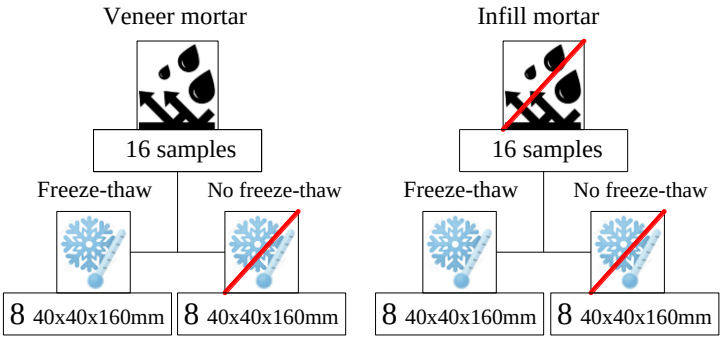

Figure 3.36 – Samples scheme for freeze and thaw tests

The samples were kept during the first day inside the moulds and were stored at 90 ± 5% of relative humidity for 6 days afterwards the samples. The mortar prisms were then stored until the starting of the tests under controlled environment conditions with a temperature of 20 ± 5ºC and relative air humidity of 60 ± 10%.

b) Masonry

To characterize the behaviour of brick veneer masonry to freeze and thaw cycles, two types of mortar were used in the construction of two brick veneer masonry specimens, namely the mortar general purpose pre-mixed mortar of class M5 (infill wallet) and pre-mixed water repellent cement mortar (veneer wallet). The freeze and thaw tests were based on European standard to determine freeze/thaw resistance of clay masonry units [91].

The dimensions adopted for the brick veneer wallets are presented in Figure 3.37. The construction of these wallets followed the recommendations of brick manufacturer and workmanship experience. The infill wallet was built with more 8.5 cm in height in order to

approximate the recommended dimension by the European standard (between 0.25 and 0.5m^2). However, it is considered that this should not be much relevant in the comparison of results between both specimens. The samples were stored in laboratory environment with average temperature of 20 ± 5ºC and relative humidity of 60 ± 10% during 7 days. Then, the test panel was allowed to cure in ambient laboratory conditions for more 21 days until starting procedure.

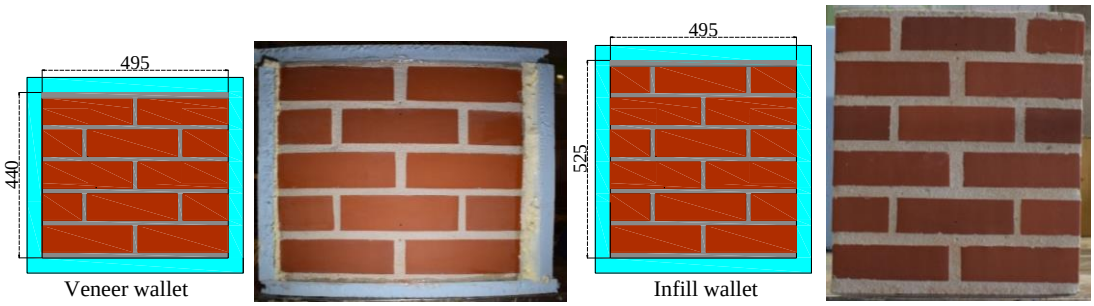

(a) (b)

Figure 3.37 – Tested masonry wallets using (a) veneer and (b) infill mortar (dimensions in millimetres)

3.5.3. Testing procedure and equipment

a) Mortar

The procedure used in freeze and thaw tests on mortar was based on CSN 72 2452 [92]. After curing, the mortar specimens were dried until achieving constant mass at 60ºC according EN 1015-10 standard [71]. After this, the samples were immersed in water at a temperature of 20 ± 5ºC until achieving constant mass. The freeze and thaw cycles procedure requires that the saturated mortar specimens reach a temperature of −20 ± 5◦C in a freezer in 4 hours and then thawed in water at ambient temperature of 20 ± 5◦C for at least 2 hours before performing another cycle [92].

In an attempt to accomplish this procedure, a freezer was adapted in order to carry out the freeze and thaw cycles in an automatic sequence accomplishing also the temperature ranges indicated in the standard. For this, an electric resistance, a water agitator, a ventilator, a pump and a heater were added to a freezer (Figure 3.38).

(a) (b) (c)

Figure 3.38 – Mortar freeze and thaw test: (a) global equipment, (b) developed software and (c) recipient with tested samples with pump, water agitator, heater and temperature sensors

The electric resistance enables to increase the temperature until a value that is compatible with the standard during the thaw cycle and the water agitator enables to have the water where the specimens are immersed at uniform temperature. The ventilator enables to have the internal environment of the freezer at uniform temperature and allow the renovation of air. The pump empties and fills the chamber with water during the thaw cycle. The heater is added so that the internal environment of the freezer during the thaw cycles achieve the range values recommended by the standard. A labview software application was developed to: (1) control the temperature in the freezer and enable the sequence of the freeze-thaw cycles automatic; (2) record the temperatures of the control sensors. The internal environmental temperature of the freezer and a temperature of sample centre were measured and compared by control temperature sensors.

Preliminary tests were carried out to validate the testing procedure, being necessary to make some adjustments to obtain temperature readings according to standard temperature requirements within the required intervals. The time to empty and to fill water in soaking tank was also studied in order to make the correct sequence of freeze and thaw cycles possible. The freezing in the specimens is accomplished with the low air temperature that circulates in the freezer after the water is taken out the recipient, whereas the thaw is materialized with submersion of the samples in water. In the freezing cycle, the decrease in the temperature was not so powerful as should be to accomplish the target temperatures during the required period of time, being recorded some a variation of about 30% regarding to recommended temperature. Thus, 6 hours were defined as a suitable freezing and thaw period as shown in Figure 3.39.

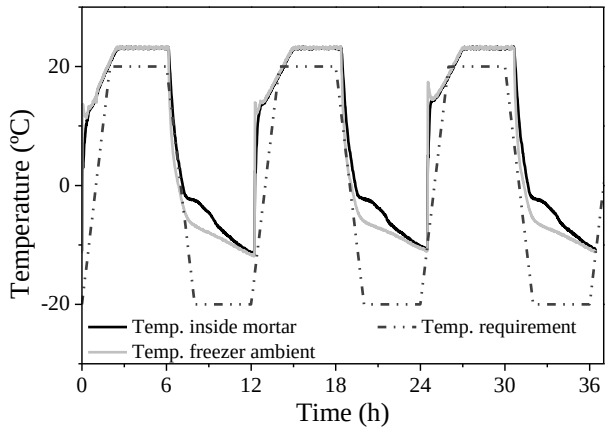

Figure 3.39 – Freeze - thaw cycles records and requirement law for mortar specimens

For each type of mortar, 8 samples were subjected to the freezing cycles (F-T) and a group of more 8 specimens was used as a reference for the frost-exposed materials (No F-T). They were kept at room temperature in water for the whole time of the cycling procedure. Freezing cycles were interrupted when specimens showed degradation signals. The samples were subjected to 175 freeze-thaw cycles.

Based on argument used by Martins et. al (2015) [98], an approximated comparison between freeze-thaw cycles and reality can be done. The freeze-thaw actions are more evident at the northeastern region in Portugal, where temperatures reach values below -8°C during the night and reach values above 5ºC during the day. This is feeling about 8 annual days according Institute of Meteorology of Portugal 2011-2013, which means that 8 freeze-thawing cycles per year are imposed. So that, it can be said that the effect of the total 175 freeze thaw cycles considered herein relate to the effect for a useful life of mortar material of about 22 years. The conditions of the freeze-thaw tests are different from the ones occurring in real in-situ conditions, meaning that this comparison should be seen carefully and more details and temperature monitoring would be necessary.

b) Masonry

Masonry wallets were subjected to freeze and thaw cycles following the standard that determine freeze/thaw resistance of clay masonry units as reference [91]. The masonry wallets were protected with insulation material with 40mm of thickness in all faces with exception of the face to be exposed to freeze and thaw cycles after 7 days of complete saturation.

During the freeze and thaw cycles, the temperature distributions over the exposed face of the panel should be as uniform as possible. To get the time-temperature requirements

suggested by standard, another freezer with higher dimensions than freezer used in mortar material was required. Once again, an electric resistance, a ventilator and a heater were added to the freezer (Figure 3.40). The electric resistance and the heater enable to increase the temperature until a value that is compatible with the standard with the help of the ventilator that enable an uniform internal environment temperature uniform and renovation of air. In this test, there is no submersion of specimens during all freeze and thaw cycles, only the pulverization with water on exposed face in each starting freeze cycle. For this, a water spraying system were applied to the freezer, distributing sprayed water in all face area. The air temperature was measured at a distance of 30 mm ± 10 mm from the centre of the exposed face by two sensors and its average is taken as the test control measurement recommended in the standard.

(a) (b) (c) (d)

Figure 3.40 – Masonry freeze and thaw test: (a) global equipment, (b) ventilated heater (c) spraying system and control temperature sensors and (d) developed software

It was decided to add more two temperature sensors in order to monitor different points on masonry mortar and compare it with the temperature distribution in the wallet. Two points in mortar and two points in the brick of each longitudinal faces were drilled and a thermocouple was introduced in each hole (Figure 3.41). The application of sensors in opposite exposed face was carried out before the application of insulation enabling to understand the difference in temperature between both surfaces

According to the standard, the first freezing cycle should last for 6 h ± 5 min, whereas each following freezing cycle should be completed in 120 min (± 5 min). The air temperature measured at the distance of 30 mm ± 10 mm away from the centre of the exposed face should be between 20 °C ± 3 °C to -15 °C ± 3 °C in not less than 20 min but not more than 30 min. The temperature of -15 °C ± 3 °C should be maintained for a further 90 min to 100 min so that the total freezing period is 120 min ± 5 min. Regarding to thaw cycle, the total warm air period, including the period of temperature rise, should not be lower than 15 min and not more than 20 min ± 1 min, varying the temperature from -15 °C ± 3 °C to 20 °C ± 3 °C. The

water spray period should last 120 s ± 10 s. The water was supplied at a rate of 6 ± 0,5 l/min.metre with the test panel at a temperature between 18 °C to 25 °C. At the end of the spray period, 2 minutes are allowed for water to drain from the system.

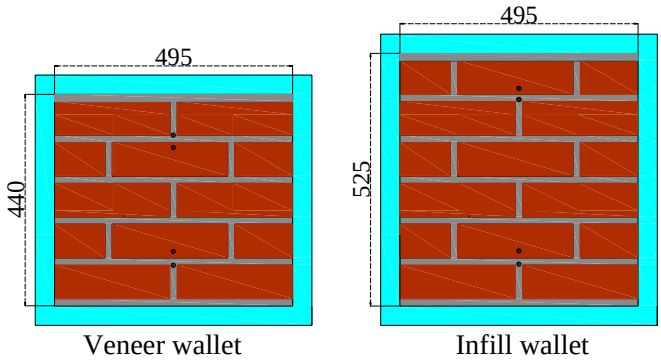

Figure 3.41 – Distribution of holes to apply the temperature sensors on wallets

A labview software application was also developed to: (1) control the temperature in the freezer and make the sequence of the freeze-thawing cycles automatic; (2) control the starting and the end of water spraying, as well as corresponding drainage time; (3) record the temperatures of the control sensors. Preliminary tests were carried out to validate the testing procedure, and the optimization of temperature readings according to the standard temperature requirements within the required intervals is presented in Figure 3.42.

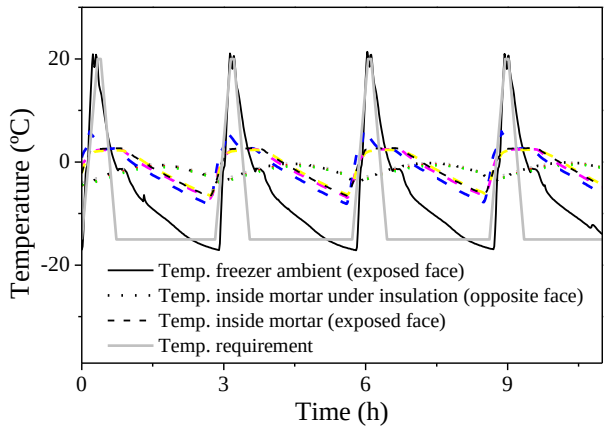

Figure 3.42 – Freeze - thaw cycles records and requirement law for wallets specimens

It is noticed that the material temperature did not achieve the control sensor temperature, as expected, However, it is considered that it achieved freezing and thawing temperatures in suitable stages. The rate of temperature of non-exposed and insulated face is much lower than to exposed face, as expected.

The panels were subjected to 400 freeze/thaw cycles. Using the same mortar comparison idea, the total effect of the 400 freeze thaw cycles considered herein relate to the effect for a useful life of mortar material of about 50 years.

3.5.4. Assessment methodology

a) Mortar

The evaluation of the influence of freeze and thaw cycles in the behaviour of mortar was based on visual inspection and on the variation of mechanical and physical properties, namely: (1) density, ρ, (2) porosity, η, (3) water absorption by capillarity, C, (4) ultrasonic pulse velocity, UPV, (5) electrical resistivity, R, and (6) flexural strength, f_{cfm}, and compressive strength, f_c. These properties were obtained at different freeze-thaw cycles in order to obtain the evolution behaviour of mortar for different ageing phases. Three control measurements were considered after completion of 50, 100 and 175 freeze and thaw cycles. The control measurements were carried out after defrosting period (after the immersion of samples in water for 6 hours).

In each measurement control the mortar specimens were observed carefully to evaluate the superficial textural changes. As no information about visual damage classification available in the standard, it was considered the classification used in natural stones presented in European standard EN 12371 [120] where a scale is suggested, namely: (0) intact specimen; (1) very little damage (slight rounding of corners and edges) that do not compromise the integrity of the specimen; (2) one or several cracks (crack opening <0,1mm) or detachment of small fragments (≤10mm^2 by fragment); (3) one or several cracks, holes or detachment of small fragments superior to those defined for classification "2", or alteration of the material contained in grains; (4) specimen broken in two or with large cracks; (5) specimen broken into several pieces or disintegrated. In this classification, the samples are considered deteriorated when reaches classification "3".

For the evaluation of density, porosity and water absorption by capillarity, expression 3.2 to expression 3.5 were considered. The analysis of these parameters is important because the behaviour of mortar subjected to freeze and thaw cycles depends on open porosity and network of pores. According to Lanas et al. (2006) [121] mortars with high porosity and low strength are more susceptible to degradation due to freeze-thaw cycles, as case of lime mortars. As aforementioned, the capillary water absorption and its retention in the pores has a significant impact on the degradation through the freeze and thaw cycles [98], as the result of loss of cohesion and change on porosity.

Many authors have been estimating the dynamic modulus of elasticity through the measurement of ultrasonic pulse velocity (UPV) [93, 116]. In this case, taking into account

that the estimation of modulus depends of density and Poisson ratio and the first was varying with the number of freeze and thaw cycles, it was decided to analyse directly the variation of the UPV to assess the damage of mortar prisms [108]. Since the measurements were performed on dry and water saturated specimens, it is important to know that the ultrasonic transition time is affected by the moisture content and its distribution through the material [108, 122-124]. Measurements of ultrasonic transition time were performed according to [125] with the transmitter frequency of 150 kHz using the direct and semi-direct method where the transmitter and receiver are placed on opposite and perpendicular surfaces (longitudinal and transverse direction) respectively (Figure 3.43 (a and b)). The measurements on mortars prisms were performed at least three times. Prior to measurements in water saturated state, all specimens were conditioned in water at least for 7 days. Prior to measurements in dry state, the specimens were dried to the constant mass.

Based on the known ultrasonic transition time, the propagation velocity of ultrasound was calculated by the following expression:

$$UPV = \frac{dist}{time} \tag{3.24}$$

Where,

UPV is the ultrasonic pulse velocity;

$dist$ is the distance between transmitter and receiver transducer;

$time$ is the time taken by the pulse to overcome the distance between the transmitter and receiver transducer.

The electrical resistivity was measured taking into account ASTM G57 [126] using a four-point probe with four equally spaced electrodes and convert the measured resistance into apparent resistivity (Figure 3.43 (c)). The sensibility of electrical resistivity is influenced by many factors such as water/cement ratio, dimension and shape of aggregates, type of cement, mineral addictions, temperature and especially aggressive conditions. These factors influence the pore size and its network. This method has been previously used to monitor the damage evolution during compressive stress and freeze and thaw cycling of cement mortar [100, 127].

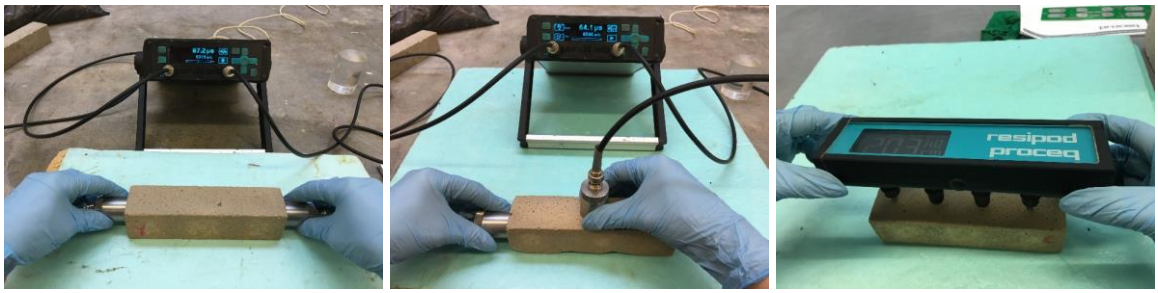

(a) (b) (c)

Figure 3.43 – Non-destructive control tests: (a) longitudinal ultrasonic velocity lecture; (b) transverse ultrasonic velocity lecture and (c) electrical resistivity lecture

Complementary to the physical damage indexes, it was decided to evaluate the variation of mechanical properties before and after the freeze-thaw cycles, namely flexural and compression strength. This enables also correlate physical and mechanical parameters. Besides flexural and compression tests on dried samples, saturated samples were also tested according to NP EN 12390-2 and NP EN 12390-3 concrete standard [128, 129], considering that specimens submitted to freeze and thaw and non-exposed samples had a similar cure after 28 days.

To sum up, the tests that were carried in the scope of this experimental campaign and the age of specimens at the time of each test for each type of mortar and for each control point are presented schematically in Figure 3.44. The number of samples that were tested in destructive tests is also mentioned.

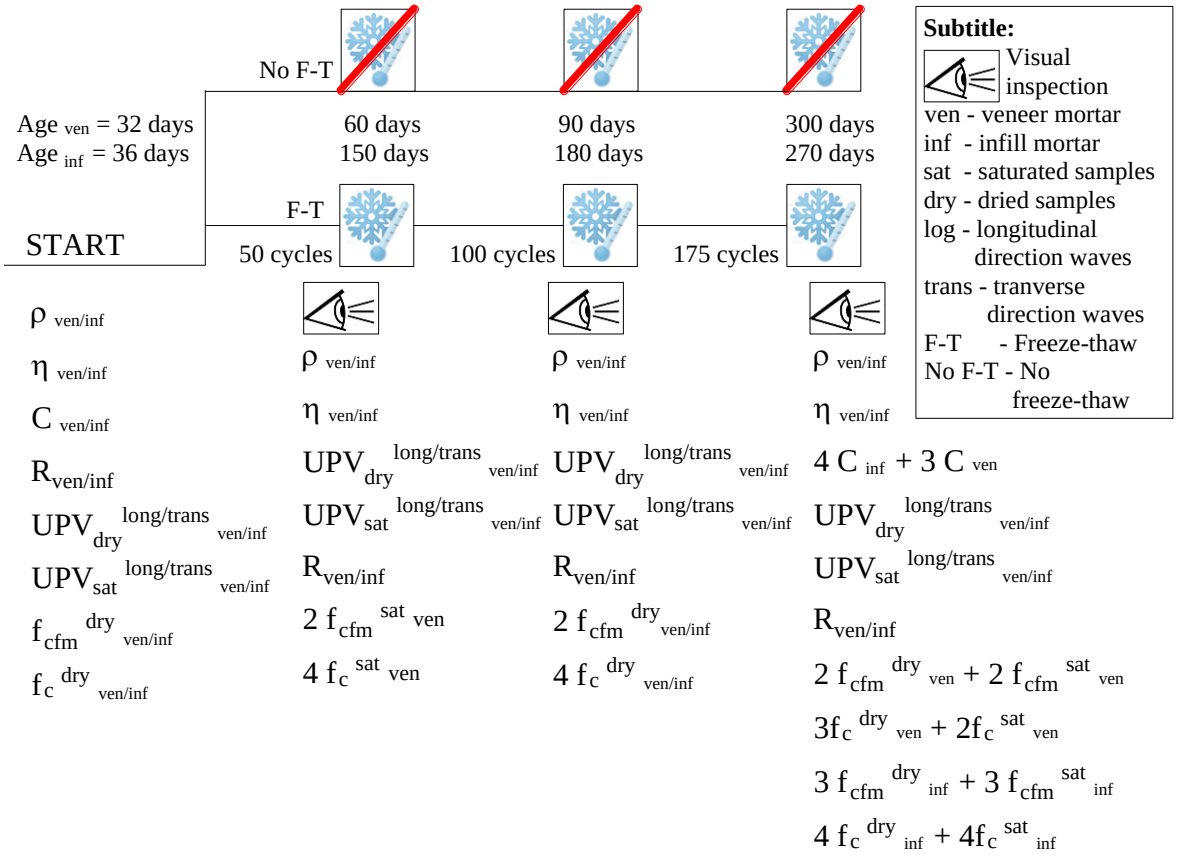

Figure 3.44 – Summarize of assessment methodology of mortars freeze-thaw resistance

b) Masonry

As already mentioned, the freeze thaw cyclic tests were carried out on two masonry wallets, each one built with a different mortar. The assessment of damage was carried out based on visual inspection.

Regarding to visual inspection, the criteria used to characterize the damage on mortar specimens was also used to characterize the brick masonry wallets according to annex A of EN 772-22 standard (2005) [91]. The visual inspection was carried out at the completion of 400 cycles.

3.5.5. Experimental results and discussion

a) Mortar

The main observations resulting from visual inspections on the mortar specimens are described in Table 3.16 and Table 3.17 for veneer and infill mortar, respectively. The

description of damage observed is carried out after the completion of 50 and 175 freeze and thaw cycles.

Table 3.16 – Main remarks from visual inspection of veneer mortar

Photographic record of veneer mortar	Main observations
	**Starting:** The samples presented some initial irregularities that they are considered in following analyses.
 	**50 cycles:** The rough surface layer of the sample disappeared, and the particles are stored in the container. It can be classified in level 1 due to very little damage caused by wearing.
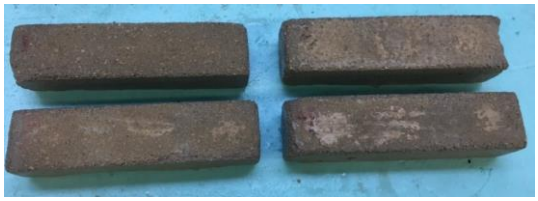  	**175 cycles:** Higher loss of material is observed, especially at bottom face of the mortar specimens. The quantity of detached particles increased due to abrasion. The damage can be classified in level 2, being the fragments ≤10mm^2 by fragment.

Table 3.17 – Main remarks from visual inspection of infill mortar

Photographic record of infill mortar	Main observations
	**50 cycles:** In half of samples detachment of surface layer was seen. The damage is classified in level 3 as the fragments are higher than 10mm^2.
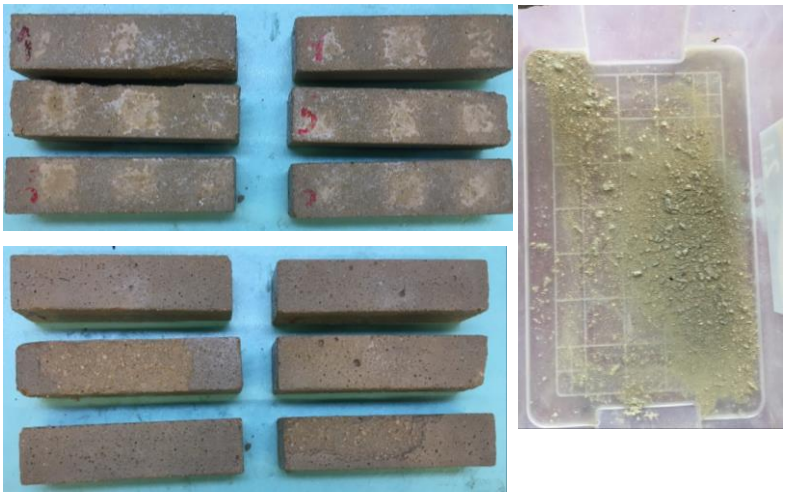	**175 cycles:** No additional significant degradation was recorded in remaining samples not previous deteriorated. Nevertheless, the quantity of sediments increased due to continuous superficial wearing. The level classification can be maintained in level 3.

According to the EN 12371 [120], the infill mortar could be considered degraded as the damage could be classified in level 3 due to the detachment of superficial layer, being the fragments area higher than 10mm^2 by fragment. The mortar veneer was not considered degraded taking into account only small rounding of corners and edges was observed. This does not compromise the integrity of the specimen and only detachment of small fragments (area≤10mm^2 by fragment) was recorded.

In order to obtain a visual and real perception about the influence of the deterioration induced by the freeze and thaw cycles, the variation of the physical and mechanical parameters during freeze and thaw tests was calculated as follows:

$$\Delta_n = \frac{(V_n - V_0)}{V_0} \times 100 \quad (3.24)$$

Where,

Δ_n is the variation of the variable at control point *n*, (%);

V_n is the value of the variable at control point *n;*

V_0 is the value of the variable before the test.

Average values density, porosity and capillarity water absorption obtained for different number of freeze and thaw cycles and corresponding variation along the tests are presented in Figure 3.45.

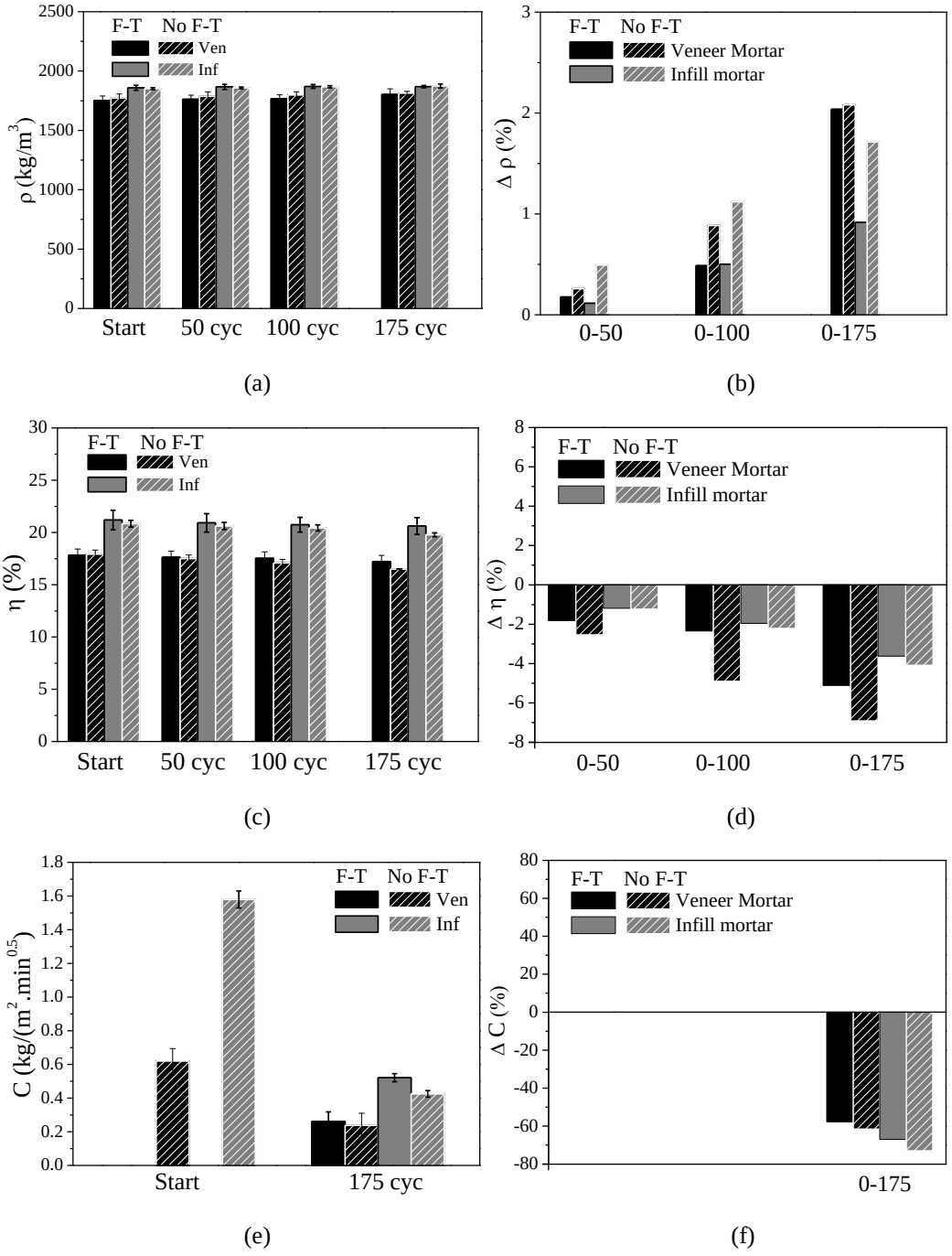

Figure 3.45 – Results of (a, b) density, (c,d) porosity and (e,f) capillarity of freeze-thaw samples and non-exposed samples during test period

The variation of density is very low in both types of mortar, taking into account that the difference was not more than 2%. In case of veneer mortar the porosity decreases about 7% at final of test on non-exposed samples and about 5% in the specimens subjected to freeze and thaw cycles. The porosity of infill mortar decreased about 4% and 3.6% for the reference

specimens and for mortar submitted to freeze and thaw cycles, respectively. Theoretically, the porosity should increase in F-T samples due to the loss of materials. In principle the number and dimension of existing voids would be higher after the freeze and thaw cycles. However, the decreasing trend is seen both in specimens submitted to different test conditions. This can be explained by the process of curing of the specimens, which was developed under saturated conditions. Thus, taking into account all samples are immersed in water, the consequent accelerated hydration due to ageing and/or favourable conditions in water tank should explain the results observed. With the increasing of cement hydration degree and the consequent hardening of the material, the formation of hydration products results in the gradual decrease of the mean diameter of the capillaries and of porosity [130, 131]. In both types of mortar, the reduction of the porosity is lower in case of F-T samples, particularly in reference specimens. This means that the beneficial effect of the curing conditions is not overtaken by the harmful effect of freeze and thaw cycles. In addition, the porosity of the veneer mortar after freeze and thaw cycles is practically the same as the one observed in the reference specimens, which appears to confirm the lower harmful effect of the freeze and thaw cycles in this mortar. The ability of the water-repellent mortars to trap air bubbles can also contribute to the decrease on the porosity, increasing its resistance against frost damage. Trapped air can dissipate the stress induced by ice formation during freezing, and the hydration reactions is enhanced because the water loss is prevented by the low surface energy that characterises the water-repellent materials [110].

This effect is also reflected on the capillarity water absorption coefficient, which reduces about 57% and 73% after 175 freeze and thaw cycles in exposed and non-exposed samples respectively. The lower the thickness of the capillary channels, the higher the capillarity tension and consequently higher the height of absorbed water. This pressure depends on the moisture content, temperature, network and dimensions of the pores and their variation [132].

The variation on the capillary coefficients observed in the different types of mortar was almost the same after the freeze and thaw cycles (infill mortar coefficient is about 2.5 times higher of veneer mortar coefficient).

The average values ultrasonic pulse velocity is each control point are presented in Figure 3.46 for each type of mortar, and for both conditions of exposure. The average is given for dried and saturated specimens and for each type of wave studied. For a better understanding of the influence of the freeze thaw cycles in the ultrasonic pulse velocity, the variation of the UPV is also given in Figure 3.47.

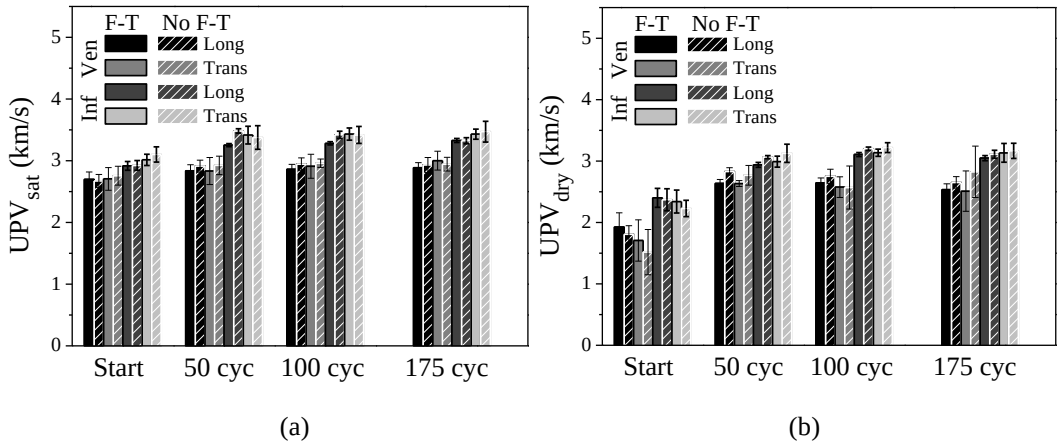

Figure 3.46 – Ultrasonic pulse velocities in (a) saturated conditions and (b) dried conditions

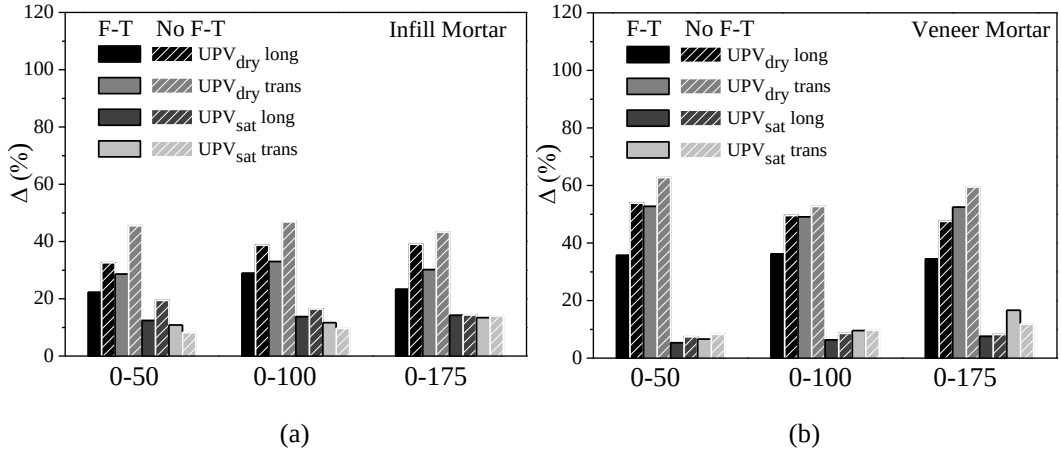

Figure 3.47 - Variation of UPV values in (a) infill mortar and (b) veneer mortar

The results obtained in the ultrasonic pulse velocity are coherent with the values found for porosity water absorption by capillary. There is an increase on the ultrasonic pulse velocity in reference specimens and in the specimens submitted to 175 freeze and thaw cycles. The hardening of the cement based mortars caused by accelerated hydration of cure overlapped the freeze and thaw harmful effect, and the velocity increased [133]. The saturated samples UPV velocities, despite increasing, did not reveal significant difference with increase of age and freeze and thaw cycles (about 9% in veneer and 14% in infill mortar). As seen before with other works, this saturated method does not allow to obtain confident values since the internal structure is fully filled with water. Nevertheless, the saturated samples velocities are higher than velocities measured on dried specimens [108]. The velocities increased with ageing on dry exposed and non-exposed to freeze and thaw cycles, between 35 and 48% in veneer mortar and between 23 and 39% in infill mortar, respectively. The increase was higher in non-exposed material because in these specimens the harmful effect of the freeze and thaw cycles does not exist. The ultrasonic pulse velocities recorded in the infill mortar are higher than the velocities recorded in the veneer mortar, which can be justified by the

higher density. The variation of velocity in veneer mortar is higher because the harmful effect of the freeze and thaw cycles is lower.

The average values of the electrical resistivity are shown in Figure 3.48 (a) for both types of mortar. The variation of the electric resistivity for the different number of freeze and thaw cycles are shown in Figure 3.48 (b).

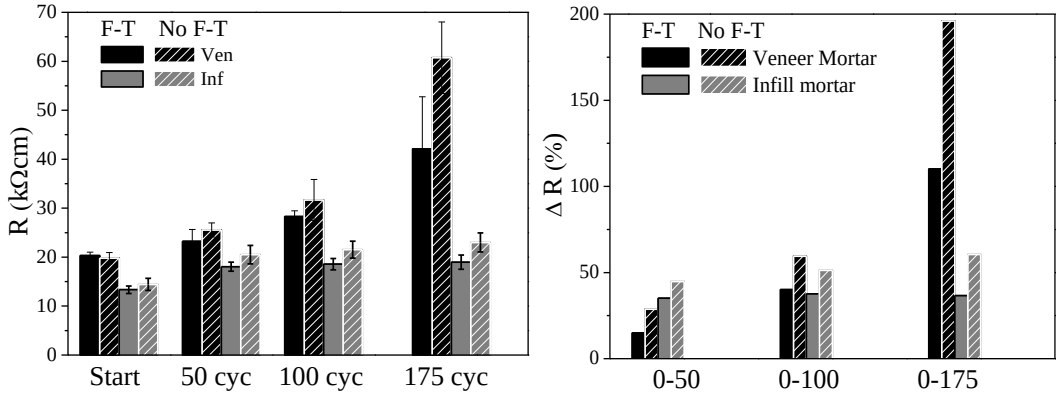

Figure 3.48 – Electrical resistivity test: (a) average resultant values and (b) variation regarding to starting values

The results of electrical resistivity show great differences for the different types of mortar and between exposed and non-exposed mortar specimens. Once again, due to accelerated hardening process, the resistance of material to electrical conductivity increase significantly, especially in veneer mortar. In non-exposed material, the variation almost achieved 200% regarding to initial values. In F-T samples the highest increase, also in veneer mortar, is about 100%. This is result of porosity decrease, i.e. lower water inside mortar porous and, in its turn, more resistant material, which opposes strongly to the flow the electrical current [134]. The veneer mortar presented higher decreases in porosity. In infill mortar, the gain of electrical resistivity achieved 60% in No F-T samples and in F-T samples the increase is about 36%. It is also important to note that the veneer mortar presented almost the double of electrical resistivity before the test, which may suggest that this water repellent material enables higher electrical resistivity.

In order to get possible relations between studied parameters, correlations between physical parameters were carried out, see Figure 3.49. From the results, it is seen that higher scatter is found in case of the UPV and R. The scatter is also high in the relation between porosity and electrical resistivity, but it is seen that the decrease on the porosity is followed by an increase on the electric resistivity, see Figure 3.50 (d). As expected, the increase on UPV in

dry specimens is also accompanied by the increase on the velocity in wet specimens, see Figure 3.50a.

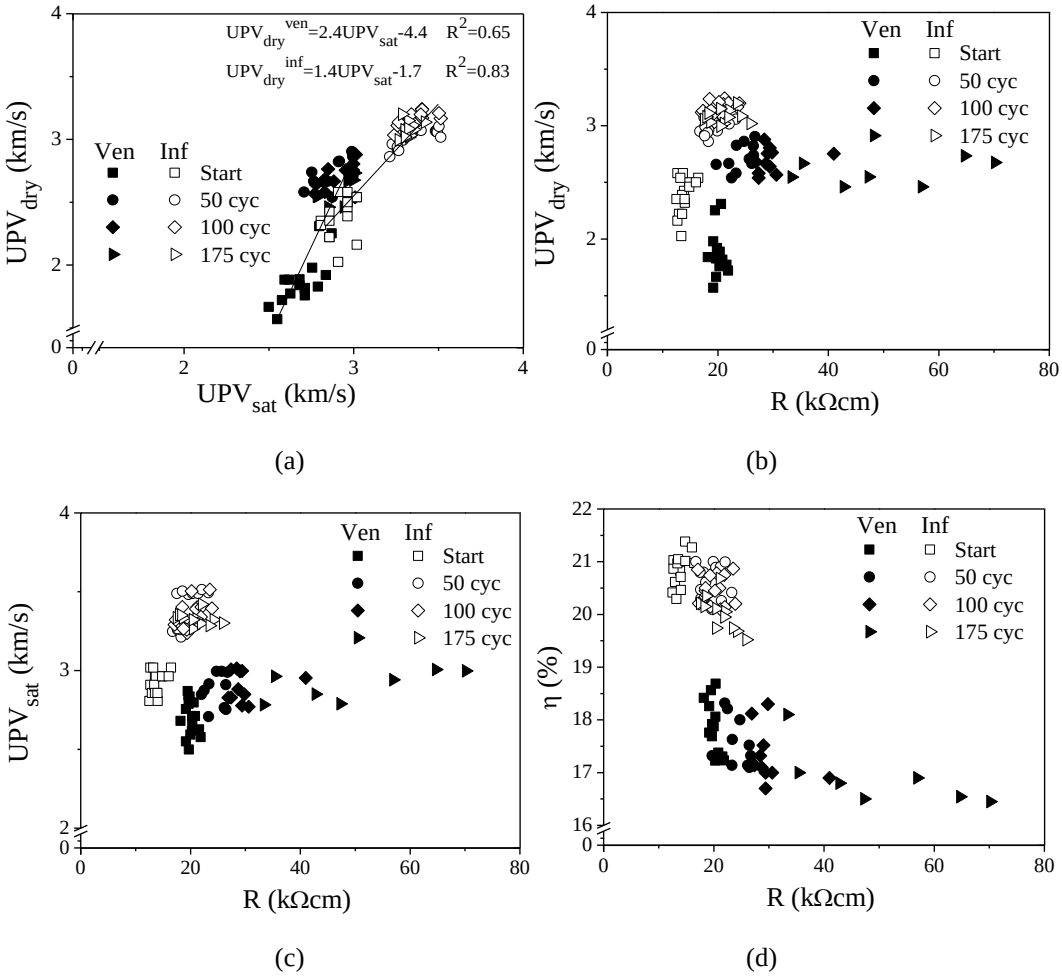

Figure 3.49 – Correlations between (a) UPV in dried samples and UPV in saturated samples; (b) UPV in dried samples and electrical resistivity, (c) UPV in saturated samples and electrical resistivity and (d) porosity and electrical resistivity.

The average values of the flexural f_{cfm} and compressive strength, f_c obtained for the two types of mortar before and after the freeze and thaw cycles is presented in Figure 3.50.

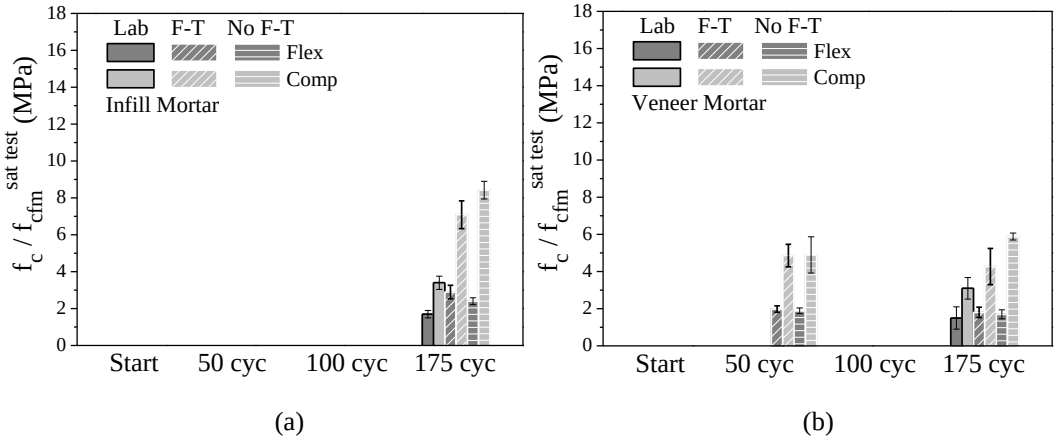

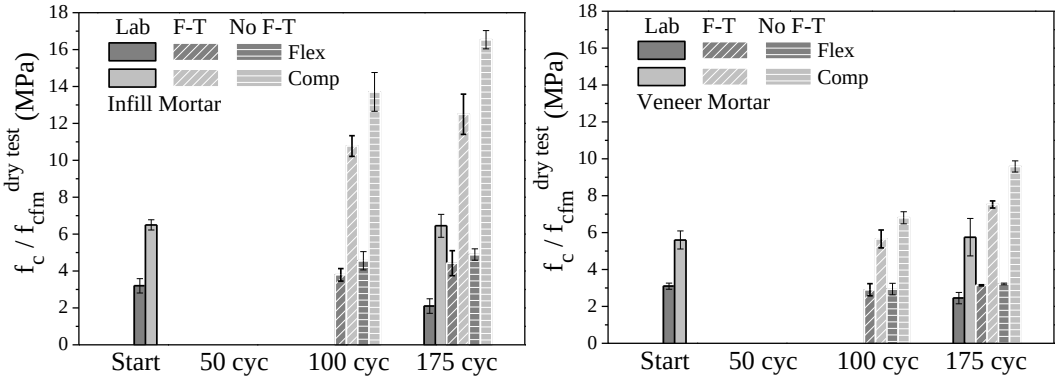

Figure 3.50 – Mechanical results of infill mortar under (a) saturated and (c) dry conditions and the veneer mortar under (b) saturated and (d) dry conditions

The variation of the mortar strength in dried conditions is presented in Figure 3.51. The variation of properties obtained in saturated condition tests was not calculated taking into account the saturated conditions before the tests were not obtained.

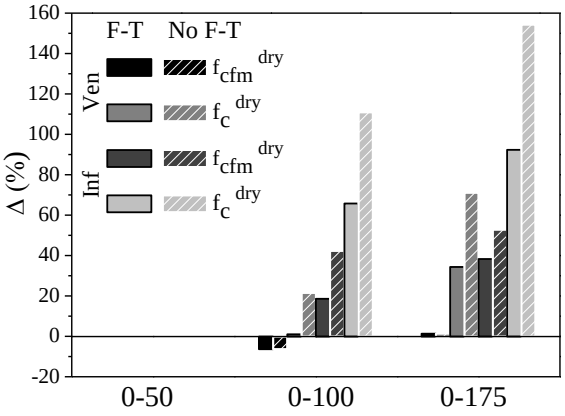

Figure 3.51 – Variation of dried mechanical parameters regarding to initial properties

From the results, it is possible to observe that the mechanical flexural and compressive strength increased in both of types of mortar with increasing number of freeze and thaw cycles. The increase of the compressive strength in infill mortar samples was between 154% No F-T samples and 92% for F-T and after the freeze and thaw cycles. For veneer mortar, the increase on the strength was about 35% in exposed and 70% for non-exposed samples. Regarding to the flexural strength, the effect was not so significant, being the increasing considered neglected in case of veneer mortar. The mechanical properties obtained in saturated samples did not reveal great differences. However, in each tested point, its resistance is about half of strength obtained in correspondent dried samples. On the other hand, it was also observed that practically there is no increase or decrease of strength in dried tests between samples at test starting and at final test, both kept in laboratory conditions.

This appears to indicate that the internal structure of mortar changed especially due to curing wet conditions.

b) Masonry

The effect of freeze and thaw cycles on the masonry wallets is here mainly described based on inspection, see in Table 3.18 and Table 3.19. The same scale of deterioration suggested EN 12371 (2010) [120] was also used to characterize the brick masonry specimens.

Table 3.18 – Main observations obtained in masonry veneer wallet

Photographic record of veneer wallet	**100 cycles**  **400 cycles** 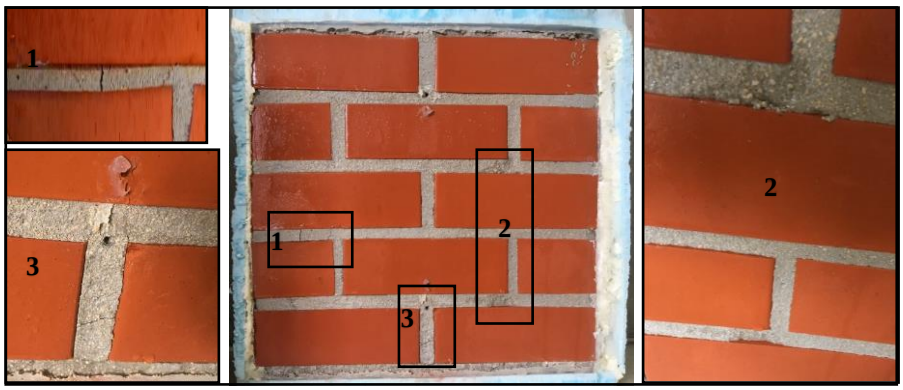
Main observations	Until the masonry veneer wallet achieves 400 cycles, very litle changes were detected, unless surface wearing, detected mainly in deposited sediments after water spraying, being classified by level 1. When the masonry veneer wallet achieved 400 cycles, an expansion of mortar with consequent cracks was recorded in zone 1 and 3, as well as more degradation of mortar was indentifed in zone 2. It can be classified in level 3 due to the thickness of craks higher than 0.1mm and due to holes or detachment of small fragments higher than 10mm^2 by fragment. In bricks, no damage was recorded.

Table 3.19 - Main observations obtained in masonry veneer wallet

Photographic record of infill wallet	**50 cycles**  **400 cycles** 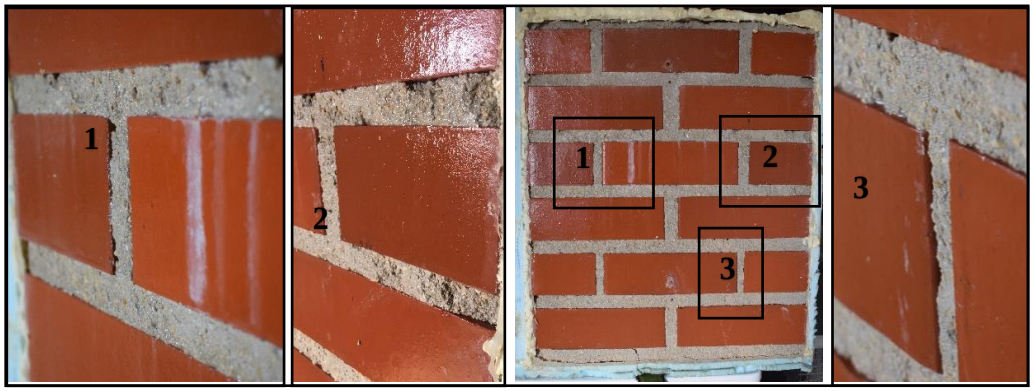 
Main observations	When the masonry infill wallet achieved 50 cycles, the covering surface was degradated in all area, having some regions more affect as ilustrated by zone 1, 2 and 3. The resultant surface presented an irregular and porous layer with holes and desintegration of material at the corners and edges due to freeze abrasion. It can be classified by level 3 due holes or detachment of small fragments higher than10mm^2 by fragment. After 350 cycles, the mortar damage almost remained constant. In bricks of zone 1, salt efflorescence t was indentified caused by soluble salts coming from mortar.

According to EN 12371 [120], both masonry typologies could be considered degraded. The masonry veneer wallet achieved the degradation level 3 after 400 cycles and the masonry

infill wallet achieved the degradation level 3 after 50 cycles. In both masonry wallets, the degradation occurred at the mortar joints and interfaces with brick units, revealing the importance of the type of mortar for the deterioration process during the freeze and thaw cycles. However, the final damage at 400 cycles is very different between the wallets. On the one hand, the degradation of the veneer wallet was caused by volumetric expansion, possibly as the result of water frozen and/or chemical reactions inside the water repellent mortar. On the other hand, the degradation of the infill wallet is mainly attributed to early abrasion and disintegration due to the freeze and thaw cycles, resulting from the more porous and weak structure of the infill mortar.

3.6. Conclusions

Appropriate tests were carried out in almost all materials used during experimental campaign. Mechanical characterization has been developed in order to help calibrate numerical models aiming at reproducing the seismic response of veneer wall systems. While not all the results obtained are essential for the execution of the walls, they give an insight on possible behaviour and failure modes possible to find in this type of construction.

A physical characterization campaign was developed in order to obtain more information regarding to material used in this type of constructive system. Emphasizing part of the experimental campaign, it was possible to characterize the freeze and thaw resistance of masonry and its elements, namely veneer bricks, mortar applied in masonry veneer walls and mortar applied in infill walls. Many research works presented the degradation of different type of material as concerning the appearance as well as internal properties, however, in this study, other behaviour trend was obtained in terms of freeze and thaw resistance. While the visual degradation and disintegration of superficial layer have been detected, especially on infill mortar, the internal structure did not reveal loss of mechanical capacity. Unexpectedly, it was recorded an increase of mechanical properties, being achieved almost 100% of increase on compressive strength of infill mortar. This has been perhaps enabled by accelerated hydration due to ageing and/or favourable conditions in water tank, avoiding the mixture water evaporation and improvement the hardening process. The remaining studied physical parameters reinforce this trend, being observed the decrease of porosity percentage and capillarity water absorption coefficient and the increase of ultrasonic pulse velocities and electrical resistivity.

Chapter 4

Experimental Characterization of Tie Connections

Abstract:

Masonry veneer walls have been used successfully in a wide variety of structures in modern building construction. However, their vulnerability under seismic actions is recognized as the result of poor material selection, design and construction practices. The knowledge of the local behaviour of ties under different loading conditions should provide important information to help in the selection of the most appropriate wall ties, improving seismic performance. An experimental campaign of different brick-tie-brick assemblages subjected to cyclic tension–compression and shear loading is presented in this chapter and the results (stiffness, strength, dissipation of energy and failure modes) are discussed in detail. It was concluded that the tie shape and geometry are important factors regarding tensile and compression strength, whereas the tie thickness influences in a great extent the compression and shear behaviour.

4.1. Introduction

The veneer walls should be connected to the structural system (backup), transferring directly the out-of-plane loads to it, without adding any resistance or stiffness to the structure, being considered as non-structural elements. The backing system, to which the masonry veneers are attached, can be composed of light wood or steel frames, structural masonry or masonry infill walls in conjunction with reinforced concrete frames. The brick veneer walls are usually attached to the backing system through distinct types of ties, generally from steel, with very different geometry, much dependent on the backing system.

Taking into account that these walls have revealed vulnerability under recent earthquakes, exhibiting extensive diagonal cracking and detachment from the backing support [10], it is important to analyse the performance of the tie connections. The seismic behaviour of brick veneers depends on various features [13]: (1) tie connection spacing and stiffness; (2) relative stiffness between the facing and backing materials; (3) support conditions of brick veneer and of the backup; (4) location of wall edges and openings; (5) cavity width and the type of loading applied to the wall.

The main role of ties on masonry veneer walls is the transfer of out-of-plane lateral loads from the veneer to the backup through the connection between both elements. For this, ties should have adequate resistance and stiffness in tension and in compression, and shear flexibility to accommodate in-plane movements.

In Portugal and in other South European countries, the brick veneers are mostly attached to brick masonry infills. enclosed in reinforced concrete frames, through wall ties [135]. Therefore, an experimental campaign was designed on assemblages composed of masonry prisms representing brick veneers and brick infills connected through selected wall ties.

The main goal of this chapter is to provide and discuss the results of the experimental campaign of connections with different types of ties subjected to cyclic tension-compression and shear cyclic loading to simulate the behaviour of ties under out-of-plane and in-plane loads induced in the brick veneers by earthquakes.

4.2. Characterization of the specimens

In order to assess the bond resistance of different types of ties and mechanical behaviour under cyclic tensile and compression loads, it was decided to analyse separately the mechanical behaviour of ties embedded in different brick walls and the behaviour of the complete connection. For that, the specimens considered in the experimental campaign are: (1) brick masonry prisms representing masonry infills with embedded ties at the bed joints (specimens named MIL-Masonry Infill Leaf) (Figure 4.1(a)); (2) masonry prisms representing typical brick veneers with embedded ties at the bed joints (specimens named MVL-Masonry Veneer Leaf) (Figure 4.1(b)) and (3) brick masonry prisms representing brick veneers attached to brick masonry infills through ties (specimens named DL-Double Leaf) (Figure 4.1(c)). Head joints were considered either in the veneer leaf (half of total of specimens) or in masonry infill (half of total of specimens) to have more representative masonry prisms.

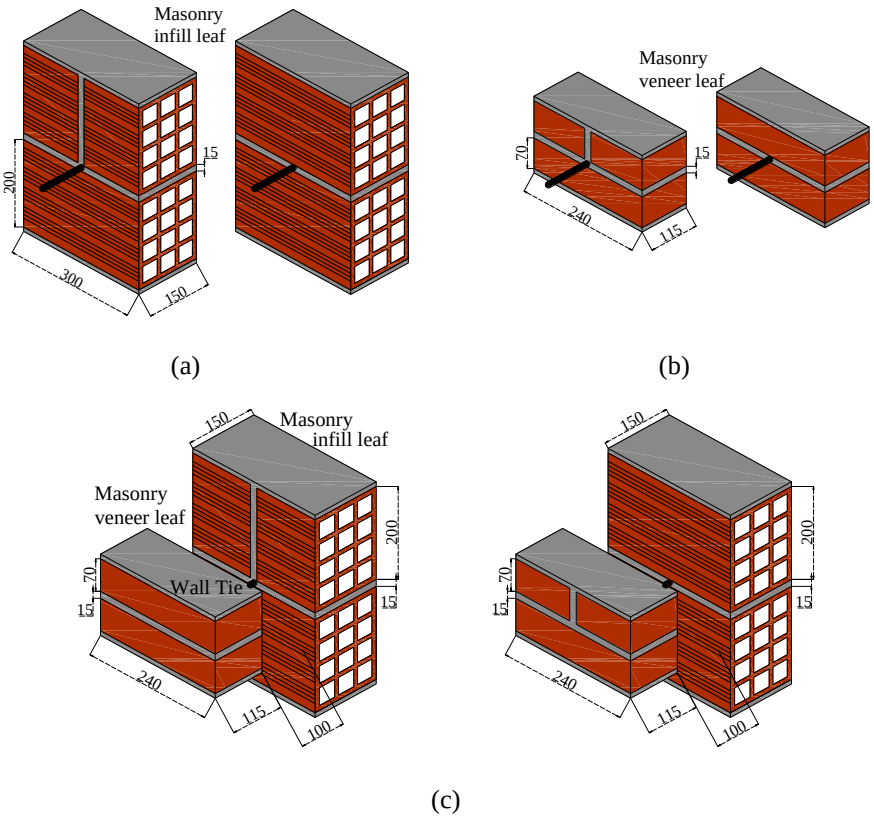

Figure 4.1 - Representative schemes of specimens: (a) brick masonry infill with embedded tie; (b) brick masonry veneer with embedded tie; (c) complete assemblages of brick masonry prisms connected (infill and veneer) through ties

In case of complete assemblages, an air cavity of 100mm thickness was adopted to better represent typical façades including thermal insulation (about 30-50mm) inside the air cavity. In case of single assemblages, it was considered a length of 100mm of free length until to fix it in clamp.

The brick veneer and infill units were presented in Chapter 3. The veneer units were constructed with pre-mixed water-repellent cement mortar and the infill units were assembled with cement-mortar M10* presented previously. The thickness adopted for the brick prims was to 15mm to make the perfect levelling of the tie possible. Notice that in practice, some misalignments can be seen, depending on the alignment of the bed joints of both masonry veneer and infill wall. It is considered that the misalignment can contribute for the worse mechanical performance of the connections. However, it was decided not to take it into account in the present experimental campaign.

The six wall ties considered for this study are presented on previous chapter 3, as well as its main characteristics. The dimensions of wall ties and embedment length for each type of wall tie for this study is presented in Table 4.1. In case of tie T5, the attachment to the brick infill unit was carried out through a chemical anchor. For this, a hole was drilled and filled with expanded mortar following the recommendations of the manufacturer and construction practice. Examples of application of ties on masonry specimens are shown in Figure 4.2.

Table 4.1 - Geometric features of the wall ties

	T1	T2	T3	T4	T5	T6
Dimension (mm)	225	225	225	225	225	225
Thickness (mm)	6	5.5/12	3	3	8	7.5
Embedment length on brick veneer (mm)	60	60	60	60	60	60
Embedment length on brick infill (mm)	65	65	65	65	65	65

(a) (b) (c) (d)

Figure 4.2 - Construction details of the specimens: (a) wall tie on brick infill leaf; (b) wall tie on brick veneer leaf and (c) T5 tie attached to brick masonry leaf and (d) T5 tie in double assemblages

For each type of tie, six tests were carried out, namely three of them in masonry prisms with head joints and other three in masonry prisms without head joints. For tension-compression and shear tests, 216 specimens were tested. All tests were performed at least of 28 days after specimen construction.

4.3. Experimental setup, instrumentation and loading pattern

The cyclic tension-compression and shear tests were carried out on a stiff steel frame. Control and data acquisition systems allowed the control of the test and the record of relevant information from the tests, namely load cell forces and displacements. The cyclic load was applied through a hydraulic servo-controlled actuator. The forces were measured by a load cell with a maximum capacity of 10 kN connected to the hydraulic actuator.

The masonry prims were always confined through two levelled steel plates connected together by means of steel rods in order to prevent any movement of the specimen (Figure 4.3, Figure 4.4, Figure 4.6 and Figure 4.7). In order to simulate vulnerable confinement conditions, an indicative vertical confinement of approximately 3% of the compression strength of masonry units was applied to the specimens. It is stressed that the absence of vertical confinement shall influence the pull-out strength of the tie. Wall ties at the top of brick masonry walls should have lesser vertical confinement and therefore lower pull-out strength. In case of the complete assemblage (brick infill and veneer leaves connected by ties), the vertical confinement was also ensured in the same conditions as previously described.

In order to ensure free sliding of the brick veneer prism in relation to the support and ensure absence of any friction during the cyclic loading, a sliding material was placed between the bottom surface of the prism and the base steel plate.

4.3.1. Tension and compression tests

Regarding to tension and compression tests, the deformation and sliding of the tie from the brick in MIL and MVL specimens, were measured by means of 2 LVDTs (Linear Variable Differential Transducers), LVDT 1 was attached to actuator and measured the total displacement of the tie and LVDT2, fixed to the masonry prism and to the tie, measured the relative displacement of the tie from the mortar bed joint of the masonry prism, see Figure 4.3.

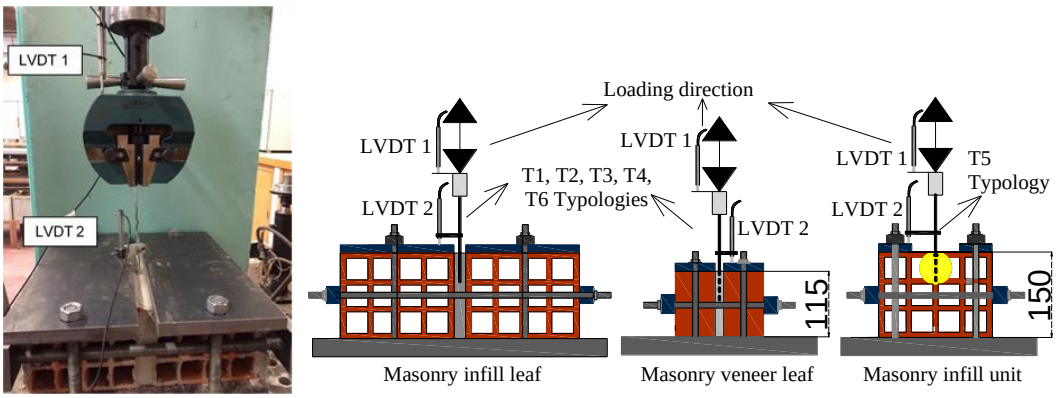

(a) (b)

Figure 4.3 – Details of tension-compression tests for single assemblages: (a) test setup and (b) representative scheme of test setup

In complete assemblages (DL specimens), the displacement of the tie occurring along the mortar bed joints of the brick veneer and/or along the mortar joints of the brick infill prisms was measured by LVDT 1, attached to the front of brick veneer leaf, and by LVDT3 attached to front of the brick infill prims and to the rear face of the brick veneer prims, see Figure 4.4.

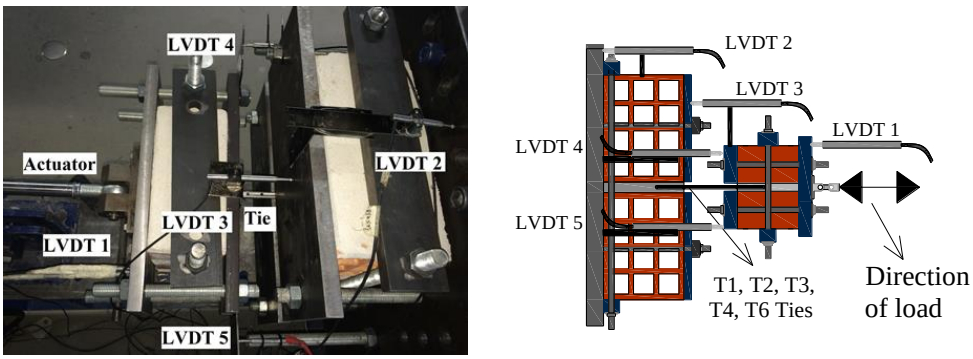

(a)

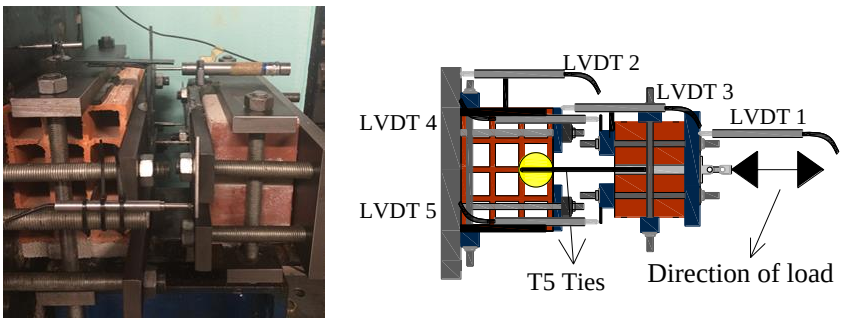

(b)

Figure 4.4 – Tension-compression test setup details: (a) distribution of LVDTs on specimens with T1, T2, T3, T4 and T6 typologies and (b) distribution of LVDT on specimens with T5 wall tie

These two LVDTs (LVDT 1 and 3) were used simultaneously to access the adequacy of the tests setup, as in the absence of clearances in the connection between the brick veneer prism

and brick infill prism, the displacement measured by them shall be the same. Furthermore, it was confirmed that the displacements measured by LVDT 3 and LVDT1 were the same. Additionally, LVDT 4 and LVDT 5 measure the relative displacement of the brick veneer prism at top and bottom points in relation to the steel frame, meaning that these displacements should be also similar to the displacement measured by LVDT1 and LVDT 3 in the absence of clearances between brick infill prisms and the stiff steel frame. These LVDTs could also acquire possible in-plane rotation in case of the tests setup was not correctly mounted. The adequacy of the test setup was verified through LVDT 2, which should record zero displacements if the test setup is correctly mounted.

For the cyclic tension-compression tests, the displacement time history presented in Figure 4.5 was imposed directly to tie in case of single assemblages or to brick veneer prism in case of double specimens, through the internal displacement transducer of the actuator. Each cycle was completed in 200 seconds, making the total duration of the cyclic tests of about 90min (28 cycles). The repetition of the amplitude cycles was considered to record strength and stiffness degradation. The tests were stopped mostly for a displacement at least of 12mm. This displacement was adopted following the accumulated damage of the connections and/or any limitations from setup-test.

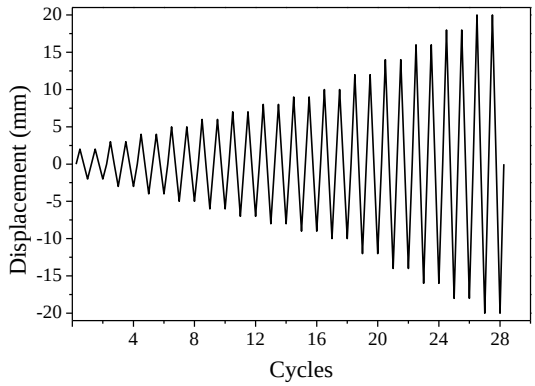

Figure 4.5 – Imposed cycles-displacement history for cyclic tension-compression tests

4.3.2. Shear cyclic tests

The shear tests follow the same procedure used in tension-compression tests, with some alterations according to the different loading conditions. In single assemblages, the deformation and sliding of the tie from the brick prims (MIL and MVL) were measured by LVDT 1 attached to actuator, see Figure 4.6. This measured the total displacement of the tie.

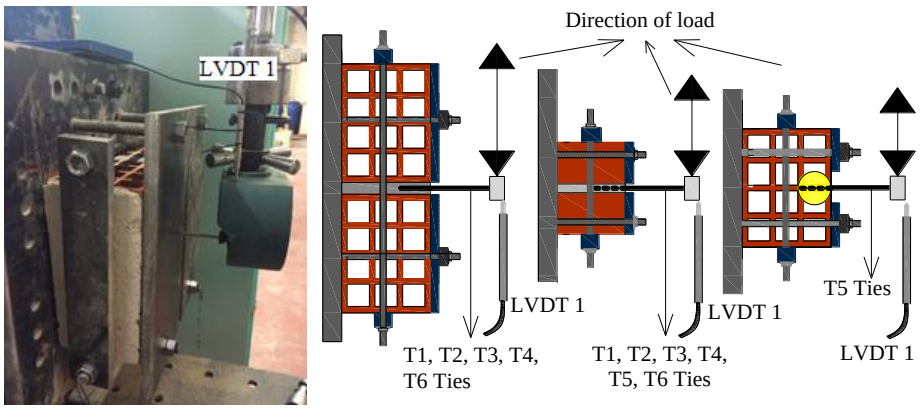

(a) (b)

Figure 4.6 – Details of shear tests for single assemblages: (a) test setup and (b) representative scheme of test setup

In the complete assemblages (DL specimens), the deformation of ties was measured by 3 LVDTs. LVDT 1 measured the total displacement of actuator; LVDT2 that was fixed to the masonry prisms, measured the relative displacement between MIL and MVL. LVDT 1 and LVDT 2 measured the same and they were used simultaneously to assess the absence of clearances in the connection the load system and brick veneer prism. LVDT 3 measured the relative displacement between support structure and MIL and validate the accuracy of test setup, which should record zero displacements if the test setup is correctly mounted (Figure 4.7).

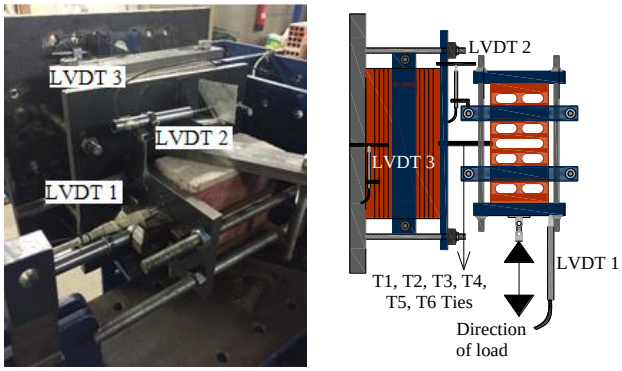

(a) (b)

Figure 4.7 – Details of shear tests for double assemblages: (a) test setup and (b) representative scheme of test setup

The displacement time-history is presented in Figure 4.8 and it was imposed to the tie (single specimens) or to the brick veneer prism (double specimens) through the internal displacement transducer of the actuator. Each cycle was completed in 200 seconds, making the total duration of the cyclic tests of about 90min (28 cycles). The repetition of the amplitude cycles was considered to record strength and stiffness degradation. The tests were

stopped mostly for a displacement at least of 30mm, taking into account the limitations of test setup and accepting this level a real possible deformation of a wall during an earthquake.

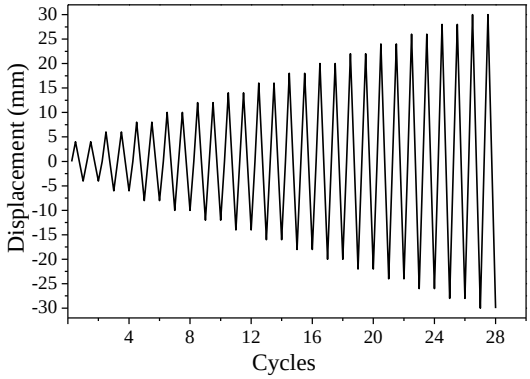

Figure 4.8 - Imposed time-displacement history for cyclic shear tests

4.4. Tension and compression behaviour

4.4.1. Experimental results

The results obtained in the experimental campaign to be presented and discussed are based on the force-displacement curves and the derived mechanical parameters characterizing the cyclic tension-compression behaviour. The characteristic curve for each tie typology was calculated based of average of all points of tested samples, taking into account the acceptable similarity between them, facilitating the lecture and analyse of results. The effect of tie location with respect to head joint was found to be insignificant for all considered variables, and for that the characteristic curve is an average of six samples. The obtained results for the different testing assemblages are compared and discussed. Due to the production process, i.e. the manual work of the builder, there can be some irregularities and clearances which influence their performance, and in some cases the trend is not so evident as expected. Nevertheless, it was considered for an equilibrated result analysis.

c) Force-displacement diagrams

The average force-displacement diagrams obtained in the tension-compression cyclic tests of the double assemblages are shown in Figure 4.9. The force was recorded in the load cell connected to the actuator and the displacement of the tie recorded in the internal displacement of the actuator, given that it is practically equal to the displacement measure by LVDT 3, but with lesser noise. The displacement measured in LVDT2 was practically

zero, which confirms the suitability of the test setup. The displacements measured by LVDT 4 and LVDT 5 present only very slight differences regarding the ones measured by LVDT 1 and LVDT 3 due to slight differential movements of veneer prism. This confirm also the inexistence of relevant in-plane rotation of the brick veneer prism.

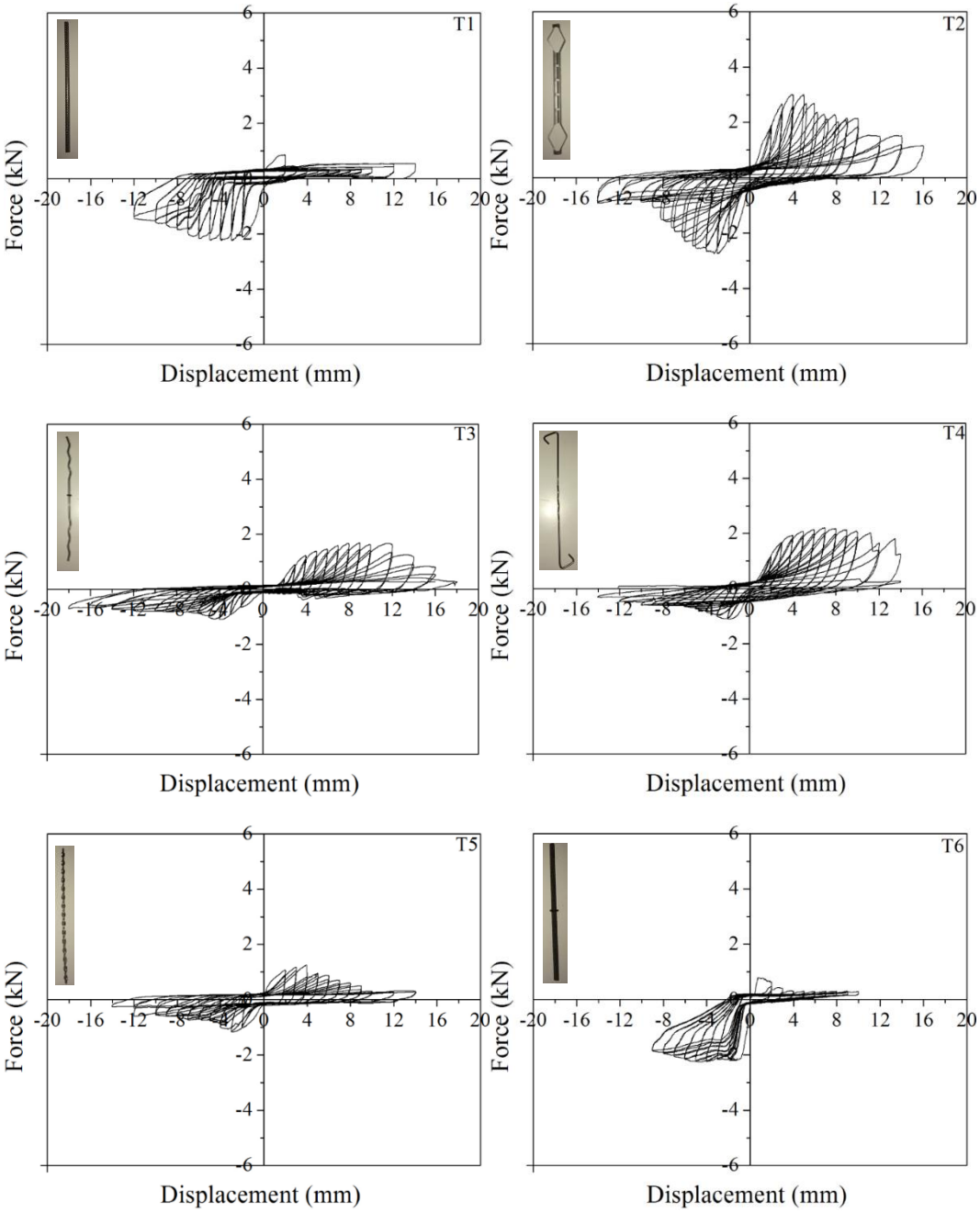

Figure 4.9 - Force vs displacement diagrams of DL specimens in tension-compression tests.

The cyclic tension-compression behaviour of the assemblages with different ties varies considerably. Apart from connections of masonry prisms with ties T2 and T5, which present a comparable hysteretic behaviour under tension and compression cyclic loading, all the other connections exhibit very different behaviour. In these cases, the hysteresis loops are

never symmetrical, which is associated to the different behaviour of the tie connection under tension and compression loading. In all cases, after a linear initial phase in graphs, the deflection changes nonlinearly.

The distinct behaviour under cyclic compression and tensile loading is particularly evident in the connections with T1 tie and T6 tie, which exhibit poor hysteretic behaviour under tension loading, as well as low tensile strength, when compared to the compression strength. On the other hand, connections with ties T3 and T4 present better hysteretic behaviour under tension than in compression and the tensile strength is higher than the compression strength. The differences found for the cyclic behaviour under tension and compression are justified by: (1) the different geometry of the ties and (2) superficial adherence conditions of the ties. In spite of very different materials are used for tie T1 (steel) and tie T6 (basalt fibre), the similar hysteretic behaviour found for the connections with these ties is attributed to the similar shape and smooth surfaces. The low tensile strength results mainly from the low bond adherence due to the surface smoothness.

The better performance of connections with ties T3 and T4 under tension is justified by the corrugated shape of the ties. In case of tie T4, an additional hook improves considerably the tensile bond adherence. The force-displacement diagrams in tension for these two ties are mostly characterized by pinching. This feature is attributed to the accumulation of damage around the tie-mortar interface, which results in cumulative plastic deformations and clearances between the tip tie and the mortar joint. The connections with ties T4 and T3 present poor performance under compression loading due to the low diameter of the ties. After the achievement of the critical buckling load, lateral permanent deformation of the ties develops.

After evaluation of the hysteresis loop, it is worthwhile to look more closely at force-displacement curves of the T2 tie on double specimen, taking into account presents the best hysteretic performance. The quasi-symmetric response leads to a better dissipative response, in spite of force-displacement diagrams are characterized by pinching, particularly in the post-peak regime.

The post-peak behaviour of connections is characterized by strength reduction for increasing displacements both under tension and compression. This is explained by the progressive physical degradation of the bond adherence of the tie along mortar joints and to plastic deformation of the ties. The ductile post-peak was assured by interlocking phenomena,

excepting T1 and T6 under compression behaviour, which is characterized by a greater dissipative capacity, which help to avoid brittle failure.

The mechanical behaviour of the connection with tie T5 differs considerably from the other connections due to the chemical anchorage that enables the tie to be inside the brick units. The behaviour is a result of combination of chemical anchorage and mortar bed joint, nevertheless it is noticed the positive contribution of embedment of tie in mortar and not so much of incorporation of tie on brick because the failure modes was more evident on masonry veneer leaf.

For understanding these differences, furthermore individual samples will be analysed. The force-displacement diagrams obtained for individual connections (MIL and MVL specimens) present similar shape, see Figure 4.10 and Figure 4.11. However, differences on tensile and compressive strength, as well as on the dissipation behaviour were found.

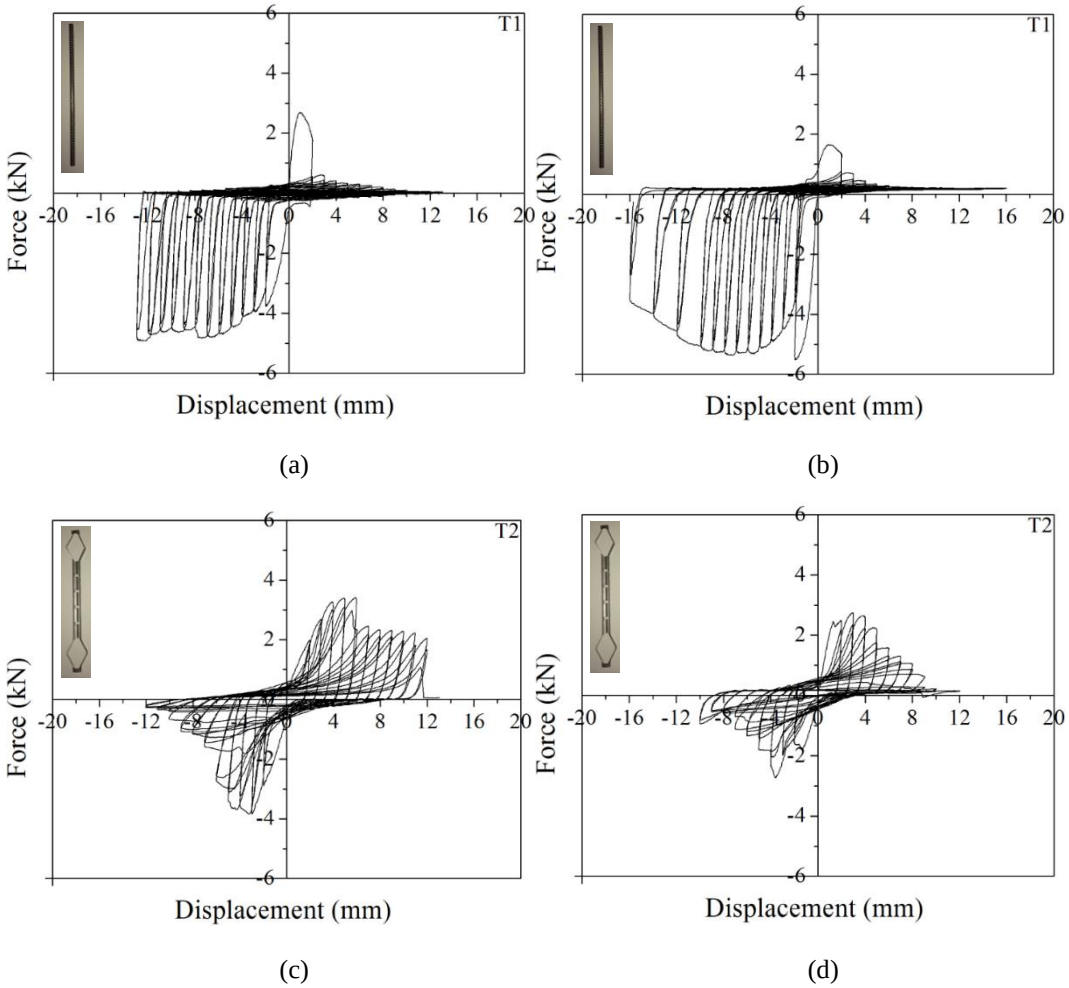

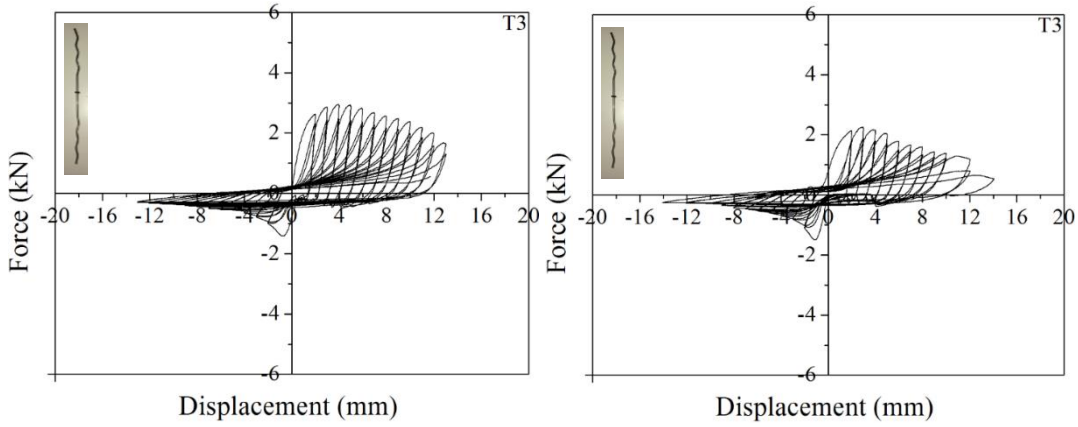

(e) (f)

Figure 4.10 - Force vs displacement diagrams for MIL and MVL connections; (a) MIL and (b) MVL with tie T1 (c) MIL and (d) MVL with tie T2; (e), MIL and (f) MVL with tie T3

In almost all cases, the higher tensile and compressive strength obtained in assemblages MIL is attributed to the higher compressive strength of the mortar used in brick infill masonry prisms. This result demonstrates the important role played by the mortar on the tensile and compressive behaviour of the tie connections.

The connection with tie T5 exhibits very low strength when anchored in the bricks with horizontal perforations (MIL). The mechanical behaviour of this connection is much dependent on the behaviour of brick units under tensile and compression loads induced by the chemical anchorage. Brick units with horizontal perforation have very low tensile strength, justifying the very low value of strength of the connection. The detachment of the chemical anchorage occurs just after the achievement of the maximum force, have been recorded rupture of brick units due to cyclic loading imposed. In case of MVL assemblages, the failure develops along mortar bed joint, which justifies the similarity with DL assemblages.

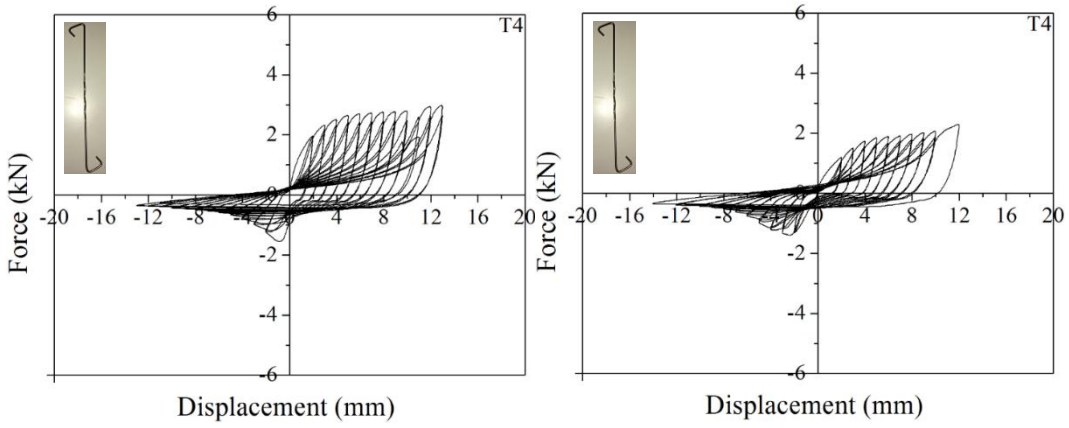

(a) (b)

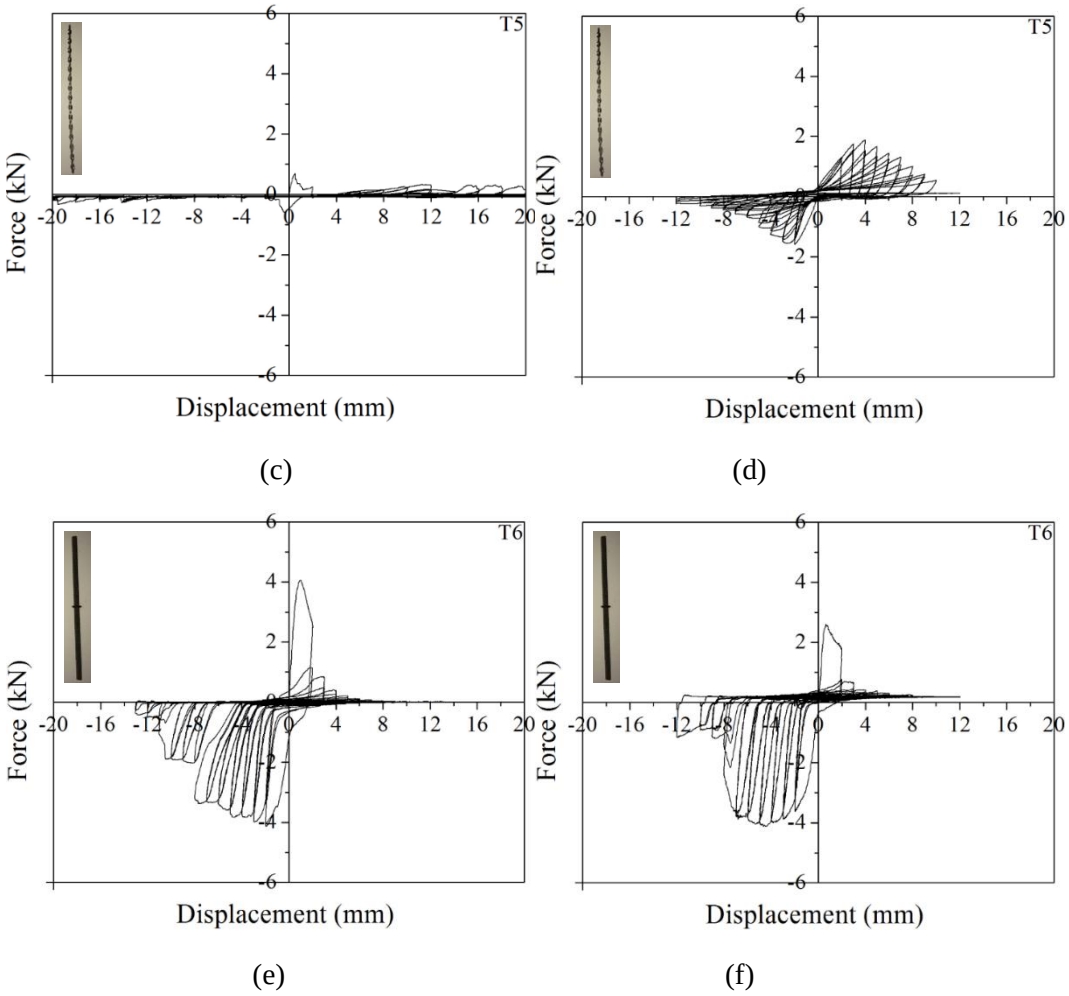

Figure 4.11; Force vs displacement diagrams for MIL and MVL connections: T4 tie on (a) MIL and on (b) MVL; T5 tie on (c) MIL and on (d) MVL; T6 tie on (e), MIL and on (f) MVL

Monotonic envelopes of cyclic force-displacement diagrams were defined for a better comparison of the behaviour of different tie typologies on double leaf and single leaf assemblages. Besides, the difference between first and second cycle load was defined for understanding the loss of resistance caused by degradation and damage accumulated (Figure 4.12 and Figure 4.13).

The second cycle is mostly a moved curve of first cycle. In tension loading the higher loss of resistance is related to T1 and T6 ties typologies, being achieving about 80% of loss of resistance (T6 in MIL). The loss resistance of rest specimen is smaller, being recorded in mostly of cases 80% of resistance of first cycle. The immediate loss of resistance of T6 and T1 can probably be justified by clearances that is formed when the tie is initially pull-out, pointing out the importance of a good interlocking in the connection. In compression loading, there is not so evident the loss of resistance in second cycle taking into account the

behaviour depends of individual ties and not so much due to accumulation of damage around the tie-mortar interface.

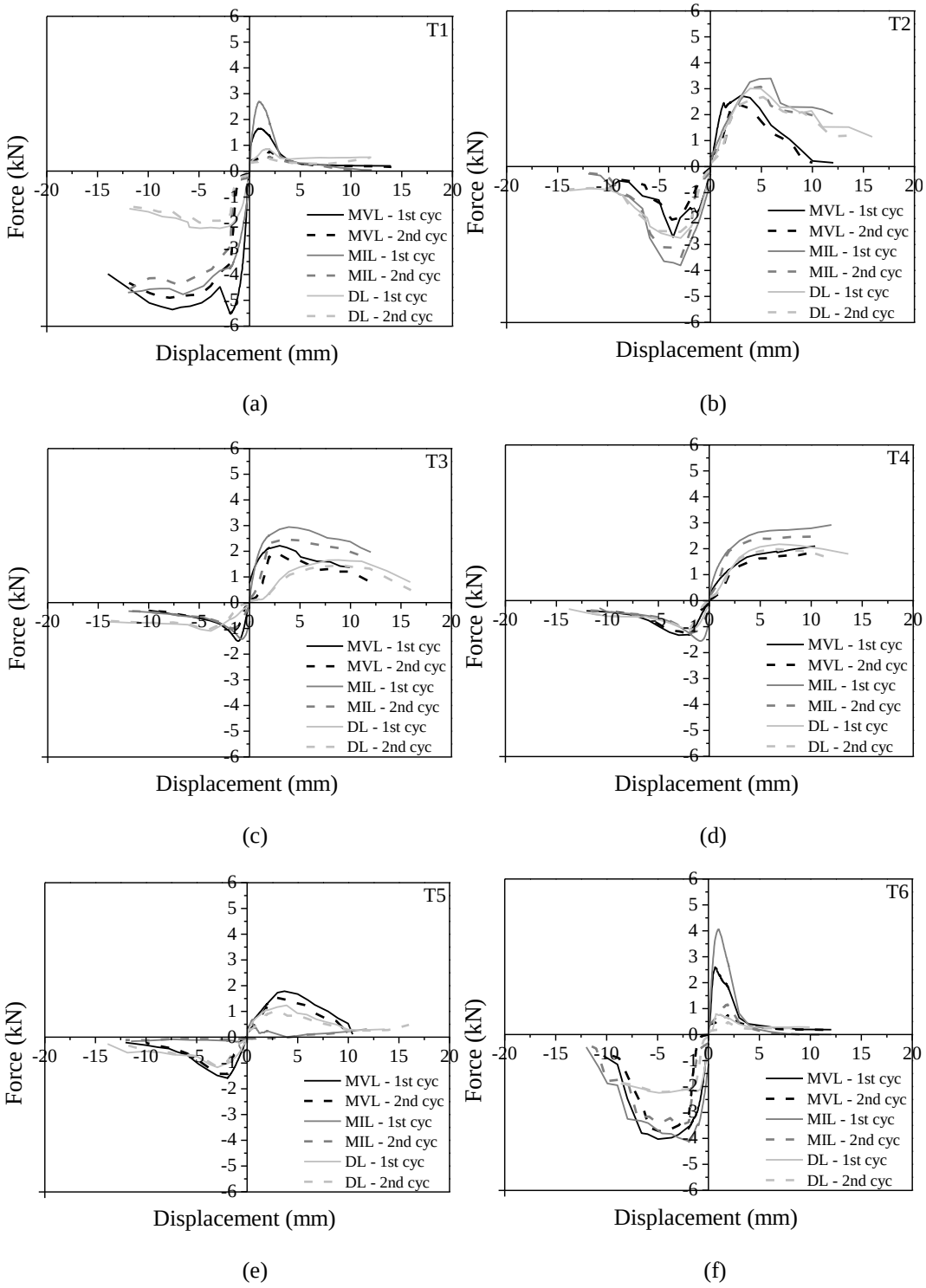

Figure 4.12 – Envelope curves from cyclic tests of (a) T1, (b) T2, (c) T3, (d) T4, (e) T5 and (f) T6 typologies of ties for each type of specimen

From the analysis of envelope curves shown in Figure 4.13 and Figure 4.12, it is possible to easily identify two groups of tied connections with similar behaviour. It is clear that ties T1,

T2 and T6 with higher thickness exhibit ductile behaviour and higher compression strength, whereas ties T3, T4 and T5 present lower compression strength. This behaviour is justified for higher trend for thin ties to buckle laterally. The assemblies with ties T2, T3 and T4 exhibit very good strength and deformation capacity under tensile loading, which is achieved by good interlocking between tied and mortar at the bed joints, resulting in higher tensile bond adherence. On the other hand, complete assemblages with ties T1, T5 and T6 present the lowest strength under tensile loading. The greater tensile strength is obtained in single specimens (MIL) due to the high strength of mortar regarding to MVL.

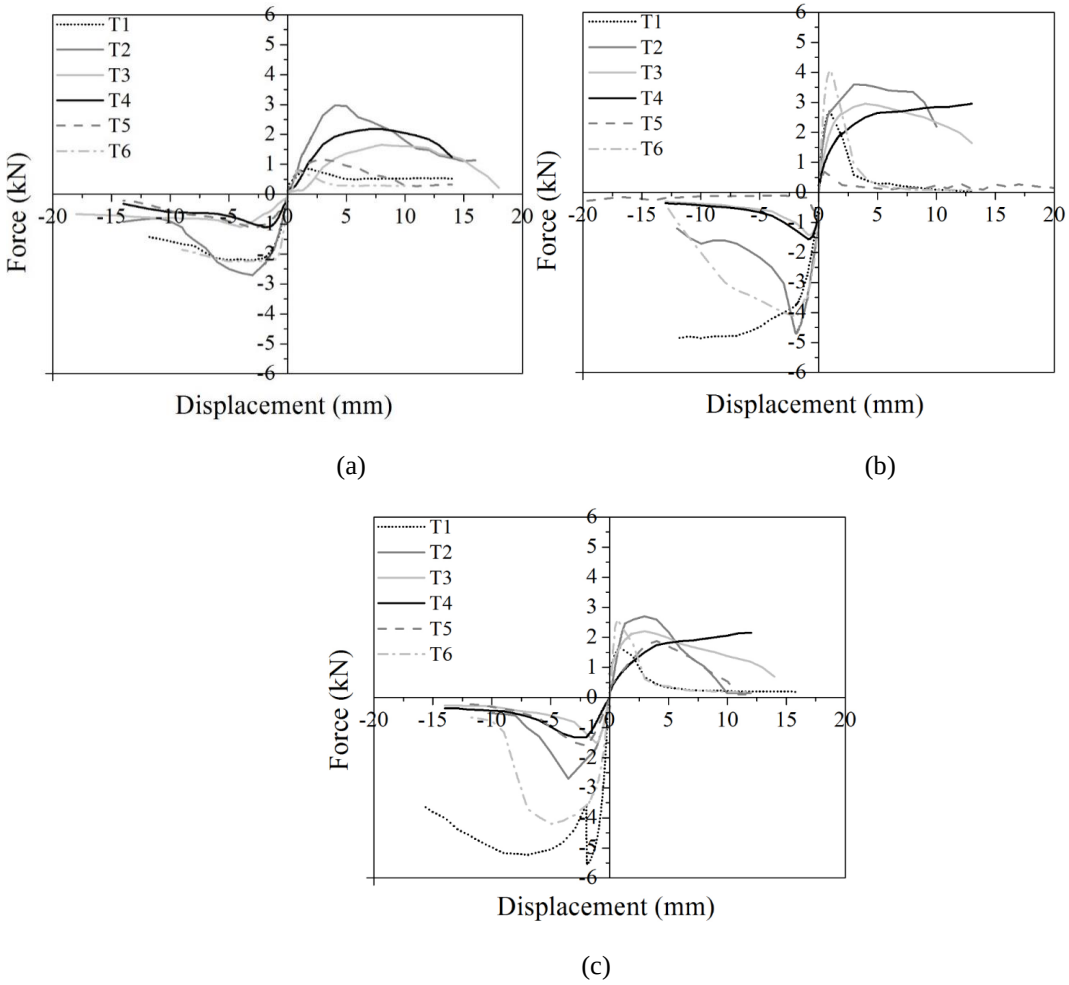

Figure 4.13 – Envelope curves from cyclic tests of (a) DL (b) MIL and (c) MVL specimens

It is important to state that the setup test of individual samples is different in relation to double leaf samples. This difference can influence of behaviour of connections and for that is should be taken into account on analyse of global response of ties. In double samples, there a more number of features that dissipate energy and the connection lose resistance, namely two non-rigid boundaries of ties, mortar of MIL and mortar of MVL. Regarding to individual samples, the application of load through a rigid clamp that fix a tie boundary in

individual samples can cause higher values of strength due to concentrated forces. Probably, it is a reason of the individual samples present mostly more resistance than double samples, which would not make sense if the setup was the same.

d) Failure modes

Different failure modes were observed in the cyclic tension-compression tests of the connections (Figure 4.14, Table 4.2 and Figure 4.15), including tie buckling, tie pull-out, tie fracture at middle length or tie fracture at interface of mortar joint on double and single leaves.

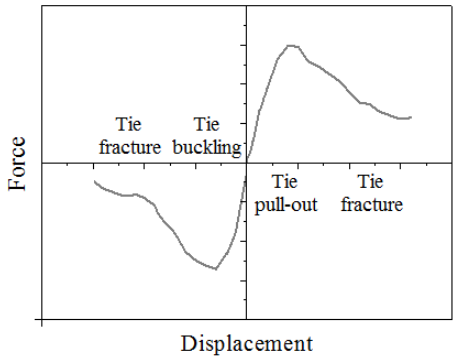

Figure 4.14 – Scheme of phenomena of failure modes in tension-compression behaviour of a type of wall tie

Table 4.2 – Summary of types of failure in each type of wall tie and specimen

Tie	DL	MIL	MVL
T1	Pull-out from MVL; Push-out into MVL.	Pull-out; Push-out.	Pull-out; Push-out.
T2	Pull-out from MVL; Tie buckling; Tie fracture.	Pull-out; Tie buckling; Tie fracture.	Pull-out; Tie buckling; Tie fracture.
T3	Pull-out from MVL; Tie buckling; Tie fracture.	Pull-out; Tie buckling; Tie fracture.	Pull-out; Tie buckling; Tie fracture.
T4	Pull-out from MVL; Tie buckling; Tie fracture.	Pull-out; Tie buckling; Tie fracture.	Pull-out; Tie buckling; Tie fracture.
T5	Pull-out from MVL; Tie buckling; Tie fracture.	Pull-out with anchor from brick; Tie buckling; Tie fracture.	Pull-out from mortar; Tie buckling; Tie fracture.
T6	Pull-out from MVL.	Pull-out.	Pull-out.

Through visual inspection, it was possible to conclude that almost no damage was observed until maximum compression and tensile load was achieved. The maximum tensile load corresponds to tie pull-out from the mortar joint (Figure 4.15 (a)) and the maximum compressive load is associated to tie buckling (T2, T3, T4 and T5 ties) (Figure 4.14, Figure 4.15 (b)).

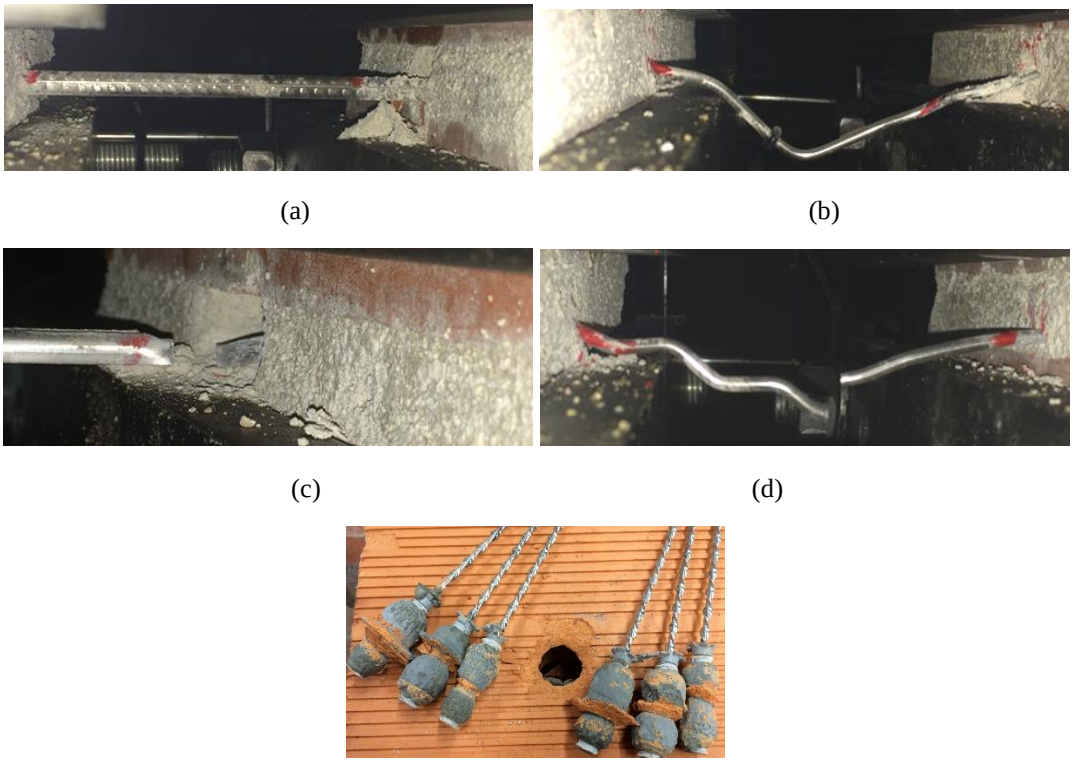

(a) (b)

(c) (d)

(e)

Figure 4.15 – Examples of tie connection failure modes: (a) pull-out tie (T4); (b) tie buckling (T1); (c) tie fracture in interface of mortar (T2); (d) tie fracture in middle of tie (T3); (e) pull-out of T5 tie from the chemical anchor

After this stage, permanent deformations accumulate and tie fracture can occur practically at the end of the test, clearly in the post-peak regime of the connection (Figure 4.14, Figure 4.15 (c), (d)). Fracture observed in ties T2, T3 and T4, is much related to the combination of cyclic tension and compression load (fatigue) and influenced by the plastic deformation of the ties under compression. Ties with higher cross section and higher compression strength (T1 and T6 types) penetrate mainly into the mortar bed joint of MVL and do not buckle.

In double leaf specimens, the pull-out of ties occurred mostly on masonry veneer leaf, which is explained by the lower strength of the mortar applied in the brick veneer prims. When the tie is connected by means of chemical anchor to brick masonry infill (MIL), the failure was

governed by the pull-out of the tie involving detachment of the chemical anchor, see Figure 4.15 (e).

4.4.2. Mechanical parameters: strength and stiffness

Aiming at comparing the mechanical performance of the connections with distinct types of ties, several mechanical properties were derived from the force-displacement diagrams, namely: (1) tensile strength (f_t) and compressive strength (f_c) and (2) tension and compression initial stiffness (Ki,t and Ki,c). These parameters are summarized in Table 4.3. The tensile and compression strength of each connection is defined as the maximum tensile and compression load recorded in the load cell. The initial stiffness was defined as the secant stiffness measured for a displacement of 2 mm (end first cycle to have comparable results in the linear regime). This displacement was selected because the elastic response of the connections was only guaranteed for very low displacements.

Based on the mechanical properties, it is possible to confirm that T2 tie presents the best performance under cyclic tension-compression loading. The geometric configuration of this tie is quite different from the other ties, and this justify its better behaviour. The tensile bond adherence is enhanced due to high contact surface with mortar and the compressive behaviour is improved due to the thickness and shape of the tie.

It is also confirmed that the connections with T3 and T4 ties present different behaviour under tension and compression loading. The tensile strength is considerably higher than the compression strength, which is attributed to the distinct resisting mechanisms developed under tensile and compression. The tensile strength is controlled by the bond adherence of the ties at the bed joint mortar, whereas the compression strength is much more related to the behaviour of the ties under compression and this is dependent on the geometry of the cross section and corresponding buckling load. In double leaf assemblages, the tensile strength of the connection with tie T4 is approximately 42% higher than the tensile strength of the connection with tie T3. This increase is attributed to the hook at the extremity of tie T4, improving the anchorage under tensile loading.

After T2 tie, the better results under compression are achieved in the connections with ties T1 and T6 due the higher area of the cross section. On the other hand, the smooth surface of these ties reduces bond adherence to the bed joint mortar and, thus, to very low tensile strength of the connection. The connections with tie T5 present similar tensile and compressive strength on DL and MVL specimens. The tensile strength is mainly related with

the bond between the tie and mortar at the bed joint of brick veneer prisms and the compression strength is dependent mostly on the compressive behaviour of the tie and its connection. In single connections composed by the tie T5 and brick infill masonry prisms (MIL), the tensile and compression strength depends mainly on the compression and tensile strength of the brick unit. Although the lower force of this tie is recorded in MIL, the connection in double assemblages mobilized the higher forces of MVL. This can be justified taking into account that in single tests, the load is directly applied in tie with rigid clamp, which cause very concentrated forces on tie-brick and become the connection more vulnerable. In double connection, the boundaries are lesser rigid and work simultaneously achieving limits resistance of MVL prism.

Table 4.3 - Average mechanical properties of tension-compression tests (coefficient of variation (%) is inside brackets)

		Compressive behaviour		**Tensile behaviour**	
		F_c *(kN)*	$K_{i,c}$ (kN/mm)	F_t *(kN)*	$K_{i,t}$ (kN/mm)
Double Leaf	T1	2.60 (2.38)	1.25 (23.53)	0.98 (13.16)	0.47 (10.13)
	T2	2.76 (25.09)	1.24 (20.91)	3.00 (24.00)	0.97 (18.32)
	T3	1.23 (17.6)	0.7 (20.00)	1.66 (25.00)	0.98 (25.00)
	T4	1.11 (14.89)	0.6 (8.92)	2.17 (4.22)	0.58 (17.27)
	T5	1.32 (16.85)	0.55 (20.91)	1.33 (27.13)	0.51 (25.37)
	T6	2.49 (23.67)	1.1 (29.00)	0.78 (21.12)	0.37 (30.46)
Masonry Veneer Leaf	T1	5.54 (4.60)	2.81 (9.60)	1.62 (22.89)	0.70 (13.58)
	T2	2.82 (12.67)	1.82 (23.71)	2.62 (13.14)	1.25 (25.69)
	T3	1.46 (5.68)	0.62 (33.27)	2.29 (6.6)	1.1 (24.00)
	T4	1.50 (15.23)	0.65 (3.60)	2.42 (10.37)	0.70 (28.18)
	T5	1.82 (12.38)	0.77 (21.44)	2.06 (14.28)	0.69 (31.33)
	T6	4.13 (22.39)	1.76 (24.07)	2.61 (17.95)	0.95 (10.65)
Masonry Infill Leaf	T1	4.52 (12.21)	1.98 (14.79)	2.52 (19.17)	1.35 (31.45)
	T2	4.09 (13.28)	1.5 (29.07)	3.59 (16.88)	0.98 (17.83)
	T3	1.50 (9.37)	0.52 (8.84)	3.07 (15.76)	1.33 (34.46)
	T4	1.55 (6.75)	0.55 (11.50)	3.13 (23.03)	1.01 (6.46)
	T5	0.92 (19.01)	0.1 (25.00)	0.91 (14.09)	0.13 (32.81)
	T6	4.15 (18.22)	2.1 (26.86)	4.30 (17.73)	1.27 (31.27)

Regarding to type of specimen, the tensile and compressive strength of complete assemblies (DL) are mostly lower than the strength obtained in individual assemblies (MIL and MVL), as shown in Figure 4.16. The strength obtained in complete assemblies can be seen as a

combination of resisting mechanisms developed in infill and veneer masonry prisms. In individual assemblies, one of the anchorages of the tie is rigid (steel grip) and, thus, the resisting mechanism is only dependent on what happens between the ties and one of the masonry prisms. In double leaf assemblages, both extremities of the tie are embedded on masonry prisms, which represent non-rigid boundaries, leading to weaker interaction between the tie and the anchoring systems. The individual assemblies (MIL) with tie T5 present considerably lower strength than complete assemblages because the failure occurs as the detachment of chemical anchorage from the horizontal perforated brick unit. In this case, the tensile and compressive strength of the connections depends mostly on the mechanical behaviour of the brick units under the tensile and compressive loads transferred from the tie to the brick unit through the chemical anchor.

Apart from the assembly with tie T5, the higher values of tensile and compressive strength obtained in the individual assemblages with the brick infill masonry prims are justified by the higher compressive strength of the bed joint mortar, leading to higher bond strength between the tie and the mortar. Under compression loads, the single connections present more scattered mechanical properties because the behaviour is influenced primarily by characteristics of ties.

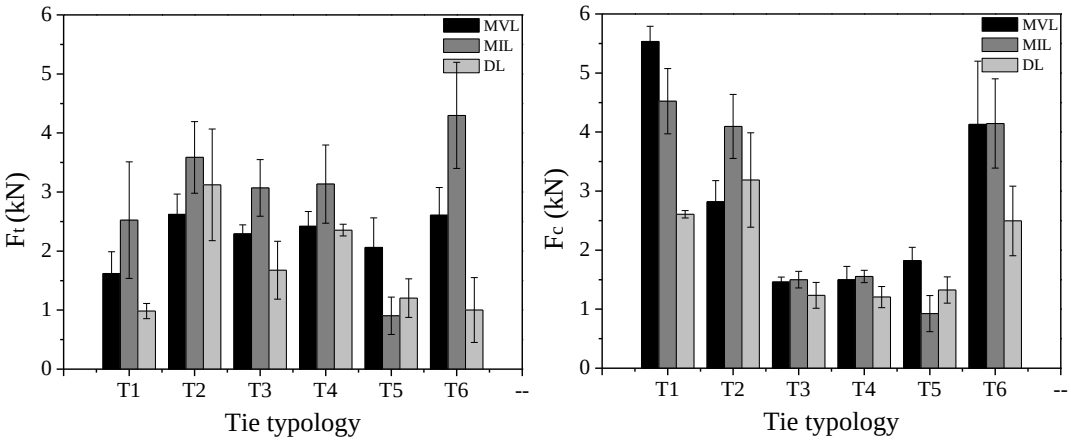

Figure 4.16 – Maximum strength among the distinct assemblies on (a) tension and (b) compression loading

The individual assemblages present also the higher values of the initial stiffness, as it is illustrated in diagrams shown in Figure 4.17. In certain extent, this should be attributed to more rigid boundary associated to the test grip attached to the tie in single specimens. From Figure 4.17 (b), it is also clear that the contribution of the ties for the initial stiffness is particularly relevant in compression regime, as revealed by the differences found between the group of ties T1, T2 and T6 and the group of ties T3, T4 and T5, which have lower cross

section. The higher stiffness of the individual assemblages where ties are embedded in brick masonry infill prisms is attributed to more resistant and stiffer mortar used at the bed joint, as happen with strength values. It shall be stressed that the stiffness found in DL specimens is more realistic because these specimens reproduce the real boundary conditions with better accuracy.

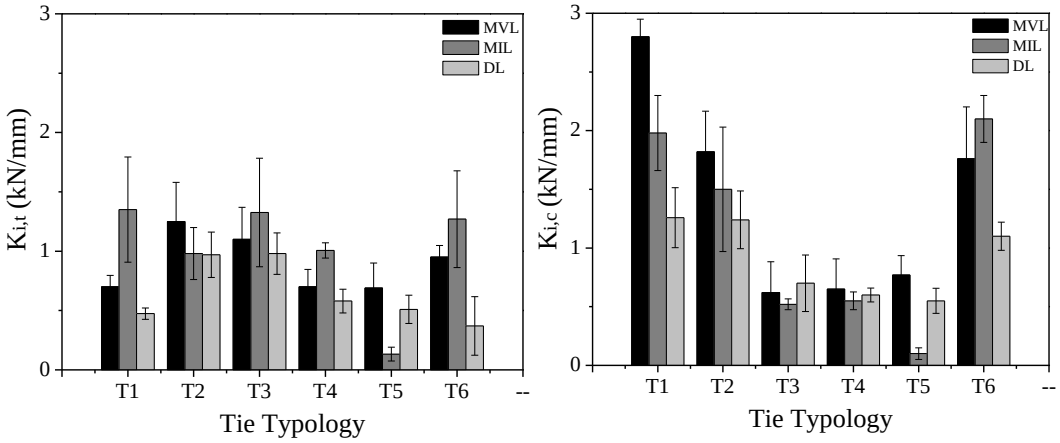

Figure 4.17 –Initial stiffness among the distinct assemblies on (a) tension and (b) compression loading

As far as stiffness degradation is concerned, it was calculated for each test for all type of specimen and it is presented in Figure 4.18, as well as the loss of stiffness in second cycle for each displacement level. Although it has been calculated for all displacement levels, it was decided to present only for some displacement levels, understanding the degradation trend and facilitating the graph lecture. The stiffness degradation of connections was heavily influenced by the previous damage. All connections presented a similar trend, specimens with higher clearances exhibited the highest degradation in stiffness, pointing out the importance of a good interlocking in the connection as happen with T1 and T6 ties typologies.

If the results of the different solutions adopted are compared, two clear trends can be seen: (1) a very high initial stiffness is guaranteed by rigid properties ties element tie as T1, T2 and T6 as seen before; (2) where the decrease in stiffness was as severe (but still great) and a more ductile behaviour was observed in the connection; The loss of stiffness in second cycle of each displacement level is more evident in ties with lower strength to tension loads and higher strengths to compression loading as T1 and T6 ties, being achieving about half of initial stiffness in lower displacement. In rest of samples, the trend of loss of stiffness when increase the displacement level is not so much severe, about at maximum 20%, which is a positive feature of T2, T3 and T4 ties typologies under tension and compression loading.

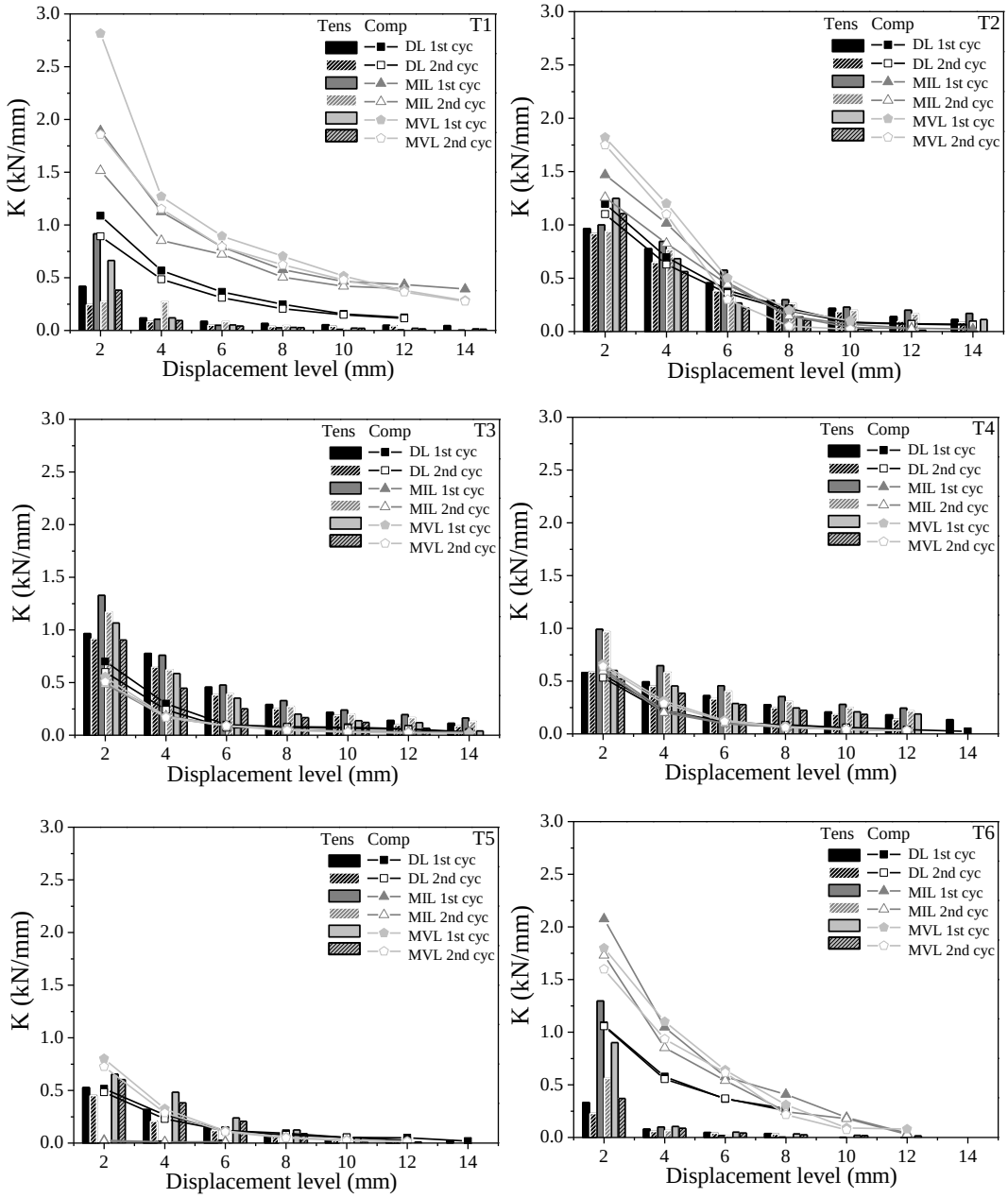

Figure 4.18 – Stiffness degradation under tension-compression loading.

The same happens when the loss of stiffness on second cycle is analysed. Maybe this is explained by geometric characteristics of these elements, once again. Although the initial stiffness is not the best stiffness comparing with other solutions, the loss is softer in major displacements in tension and compression record than T1 and T6 tie group, which become interesting solution to resist earthquakes events. As recorded on maximum strength, the MIL individual assemblages present in many of ties typologies higher values, being probably associated to higher mechanical properties of mortar. Nevertheless, the values are scattered, which can also depend on the workmanship of the builder. The special case of T5 tie, the degradation trend is not very severe, even because the initial values is stiffness is very low.

The T5 MIL assemblages present really low values as happen with strength property due to weak connection tie-brick.

4.4.3. Seismic indicators: Energy of dissipation and Equivalent Viscous Damping Ratio (EVDR)

The energy dissipation capacity and damping ratio are important parameters evaluating the ability of a structure to resist to earthquake. In other words, buildings which are more capable of dissipating energy have better reaction against earthquake because in these structures the imposed earthquake energy can be better absorbed. These parameters are presented in order to obtain a comparison between tie assemblages and evaluate the capacity of the connection under cyclic tension-compression loads.

The energy dissipated by the connections at each tension-compression loading cycle was calculated as the area enclosed in the cyclic loops of the force-displacement diagrams. The cumulative dissipation of energy, CG_f, was calculated as the sum of the energy dissipated at each cycle until a certain displacement, G_f, and it represents the amount of energy dissipated during the cyclic loading. The energy can be dissipated through friction in the connections, yielding of bonding tie-mortar and residual deformation in the tie, as observed during the tests. The energy dissipated during the cyclic tests for each type of tie and for the three assemblages types can be compared through the diagrams shown in Figure 4.19. The diagrams are divided in (1) dissipated energy of each type of specimen, double (DL) and single (MIL and MVL); (2) dissipated energy of first and second cycle of each displacement level and (3) dissipated energy of a determined displacement level (G_c) and cumulative dissipated energy (CG_c).

The strength mechanisms developed in both assemblages depend on to the bond adherence between ties and mortar bed joints. The good bond strength justifies also the higher energy dissipation obtained in assemblies with ties T2, T3 and T4, contrarily to assemblies with ties T1 and T6. The assemblies connecting tie T5 and brick units with horizontal perforation are strongly influenced by the low tensile and compressive strength of the units in the perpendicular direction to the perforations.

Regarding to loss of dissipation capacity of energy due to repetition of cycle, it was possible to conclude in mostly of cases a constant loss of dissipated energy since lower displacement, which confirms the accumulated damage and fatigue of tie during the cyclic tests. The tie

typologies with higher evidences of loss of dissipated energy are T1 and T6 in single assemblages, about of 50%. This happen due to loss of total bond of tie in mortar bed joint, when occur of second cycle of each cycle taking into account that these elements are very straight.

Regarding to the dissipated energy of each level (G_c), it can be seen a gradual increase of dissipated energy as displacement levels increase (Figure 4.19). The increase on the dissipated energy per cycle is naturally related to the increase of damage as the displacement increases. In effect, the energy dissipation is always associated to the propagation of damage in connection. Once again it can be noticed how T2, T3 and T4 ties typologies have similar values, which were able to dissipate slightly higher amounts of energy, due to its higher load capacity. In cumulative dissipated energy (CG_c), when the dissipated energy increases in progressive displacement levels, the curve is more exponential, obviously. On the other hand, the curve of cumulative energy stabilizes or decrease when the progressive displacement levels not present an increase of dissipated energy.

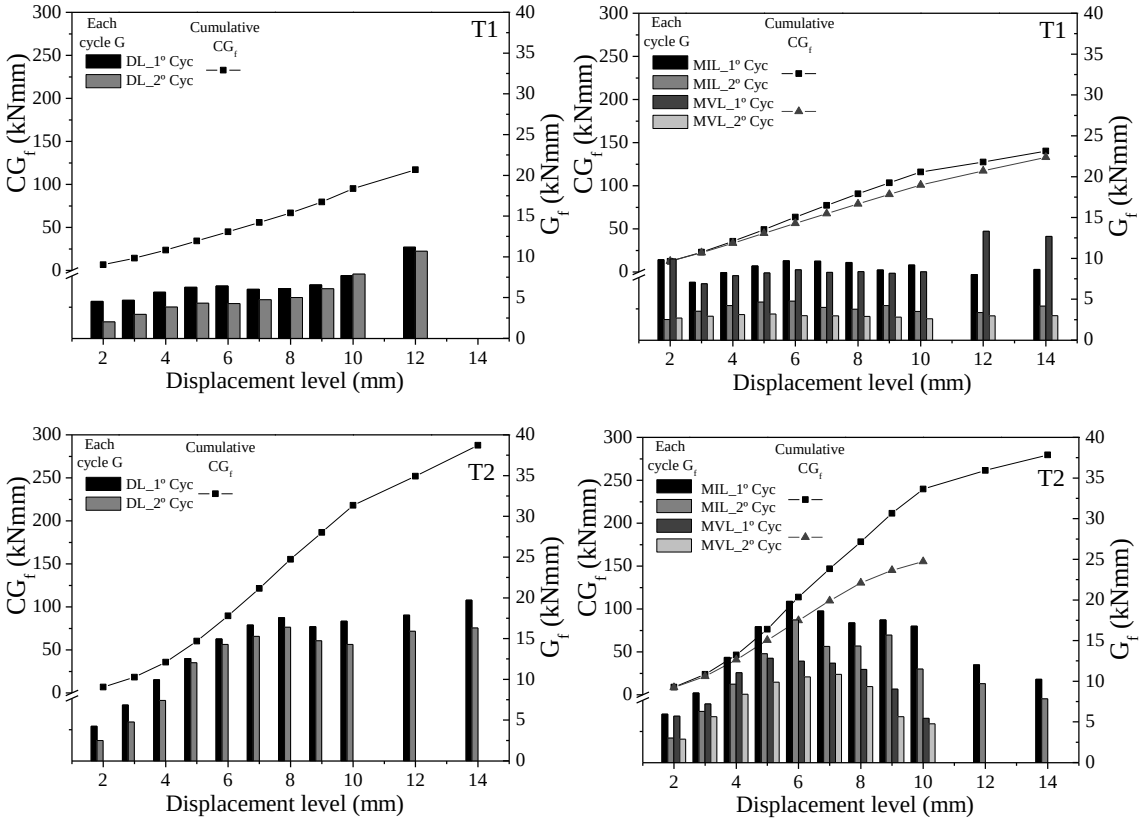

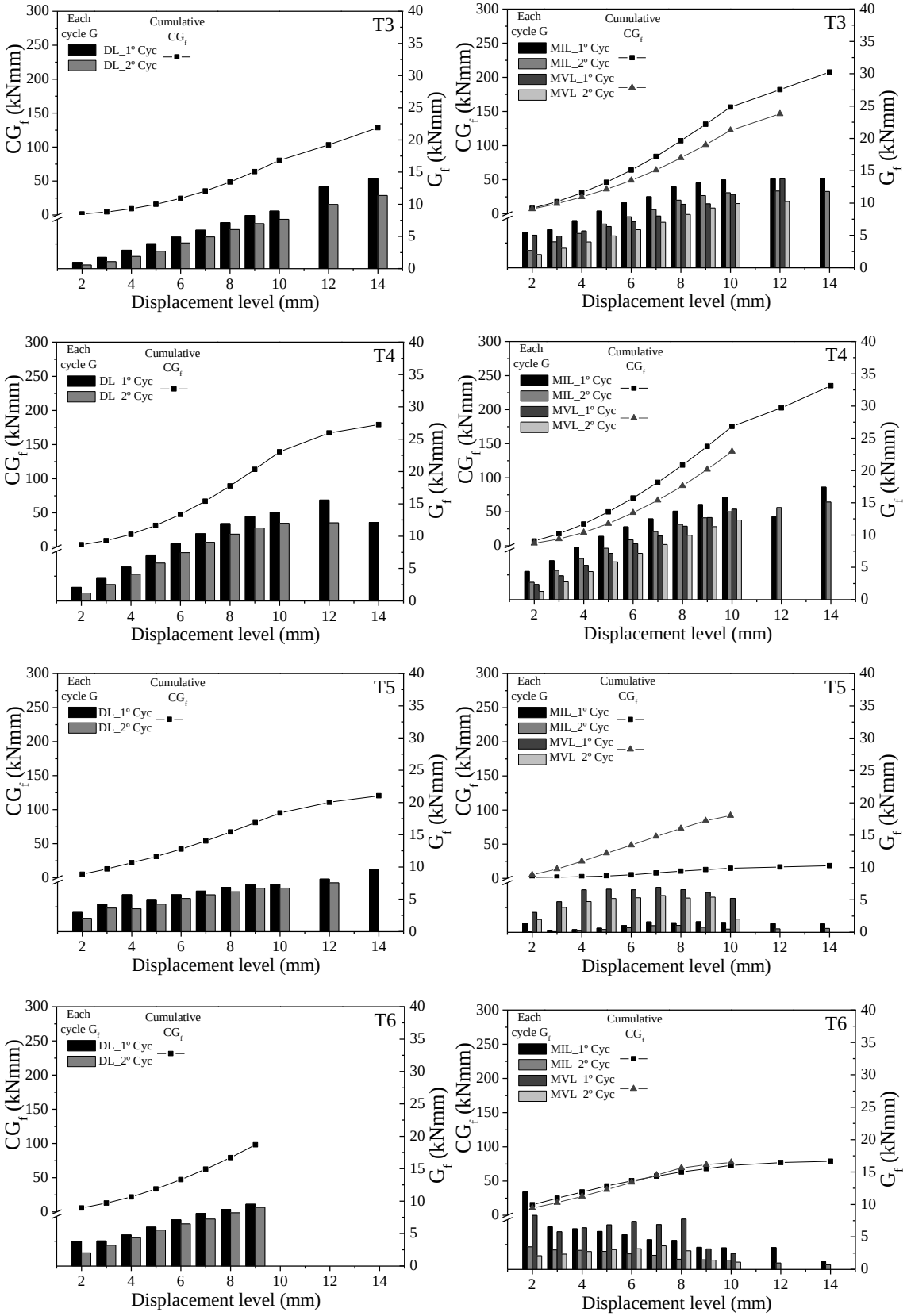

Figure 4.19 – Cumulative dissipated energy for all tie typologies in each type of sample in tension-compression tests

From the analysis of results obtained in the double leaf assemblies, it is observed that the connection with tie T2 exhibits the best performance in terms of dissipation of energy. The second-best performance is obtained in DL assemblages with tie T4, but the total amount of dissipated energy is about 40% lower than the energy dissipated by the connections with tie T2. The cumulative energy dissipated by the connections with other ties is relatively close.

Regarding to type of specimen, it is possible to observe in Figure 4.19 that the dissipated energy obtained in specimens MVL is lower than the energy obtained in specimens DL and MIL, but the trend is very similar. When the ties are combined individually with brick veneer prims, the dissipation of energy is low: (1) the cumulative dissipated energy is lower among the distinct types of ties; (2) the maximum dissipation of energy, obtained for tie T2, is 25% lower than the highest value found in the complete assemblage. When ties are embedded in brick infill masonry prims (MIL), the cumulative dissipated energy is similar or even higher than the energy dissipated in complete assemblies. This happens because the compressive strength of the bed joint mortar is 25% higher than the strength obtained in the mortar used in the brick veneer prisms. The low energy dissipated in the connection with tie T5 is related with low compression and tensile strength obtained in the cyclic testing, which is instead attributed to the low strength of the horizontal perforated units commonly used in brick masonry infill walls. To sum up, it should be noted that: (1) the best energy dissipation is achieved for the connections with tie T2, being the maximum values very close to the ones observed in the complete assemblies; (2) the cumulative dissipated energy found for the specimens with tie T1 and particularly with tie T3 and ties T4 is higher than the values found in the complete assemblies; (3) the cumulative energy dissipated on singular assemblies with ties T5 and T6 are lower than the cumulative energy dissipated in complete assemblies; (4) the compressive strength of mortar influences clearly the cyclic behaviour of the connections regarding the tensile strength and cumulative dissipated energy. This justifies the differences found in the dissipated energy between the assemblies MIL and MVL; (5) MVL and MIL specimens present lower values of dissipated energy than DL specimens, because in the latter specimens the interaction of the tie with mortar joints occurs at both extremities.

The equivalent viscous damping ratio is correlated with the energy dissipation. Damping diminishes the energy of the structure through various mechanisms, such as, for the present case, friction in the connections and opening and closing of gaps. The equivalent viscous damping ratio (EVDR) is calculated according to expression (4.1) [136]:

$$EVDR = \frac{G_c}{2\pi(E_e^- + E_e^+)} \tag{4.1}$$

where G_c is the dissipated hysteretic energy for each cycle (Figure 4.20 (a)), E_e^+ and E_e^- are the elastic energies of an equivalent viscous system calculated at the maximum displacement in each loop for the positive and negative direction of loading respectively (Figure 4.20 (b)).

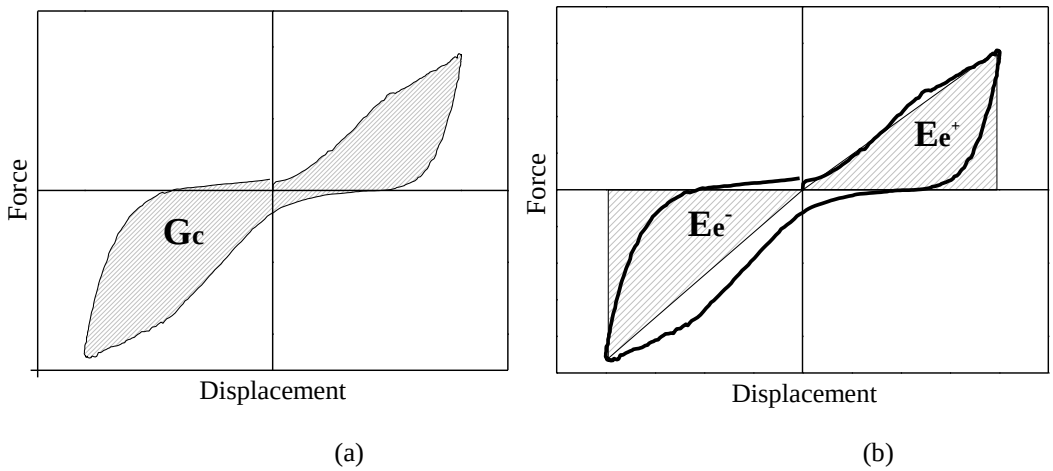

Figure 4.20 - Dissipated energy and equivalent viscous damping: (a) area enclosed in loop; (b) input energy

From the analysis of the diagrams presented in Figure 4.21, it is possible to highlight that for low values of displacement there is some variation on the EVDR among the different connections, being lower in some cases for displacement greater than 5mm.

EVDR is much influenced by type of tie and cumulative damage degradation between first and second cycle. The values of second cycle are mostly lower comparing with values of the first cycle. Based on the assumption that the second hysteresis is lesser dissipative and lower resistance than first cycle, the dissipative energy of each cycle is lower than in first cycle, resulting lower values of EVDR.

Apart from the connections with tie T3, it is seen that the values of EVDR obtained in double assemblages are higher than the values of EVDR found in the individual assemblages. This is the result of higher dissipation of energy. Regarding the individual specimens, differences have no a clear trend.

The connections with ties T3 and T4 present values of EVDR comparable to the connection with tie T2. This means that they have a comparable damping capacity for high values of deformation. In almost all cases, there is no increase of EVDR as the damage progresses, while an interesting increase can be observed for symmetric curves of T2 tie in medium tested displacements, presenting the maximum values of all testes ties. This different behaviour is connected once again to the ductile global behaviour of this typology.

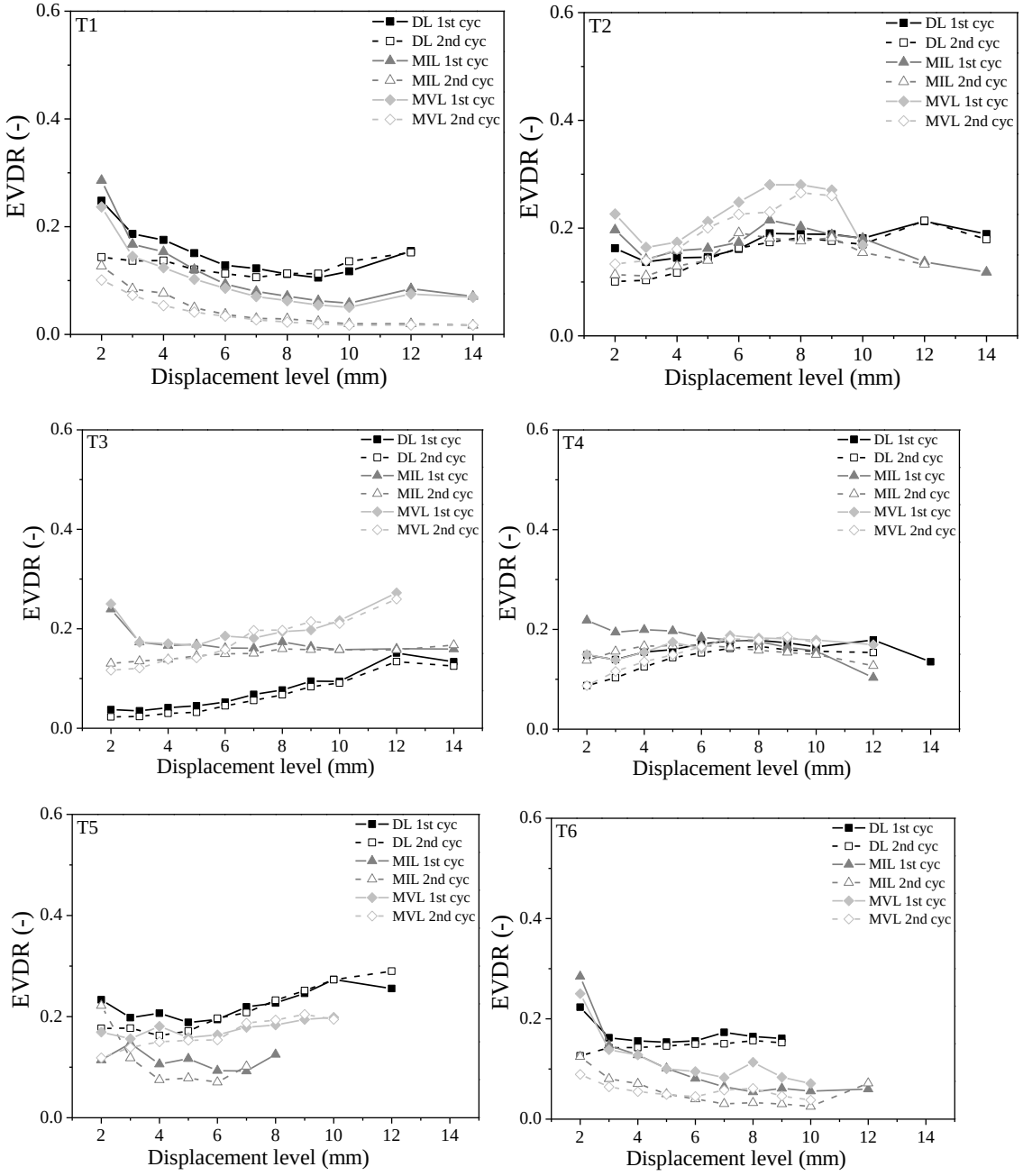

Figure 4.21 – EVDR values for all tie typologies in tension-compression tests

The trend observed in the EVDR of connections with ties T1 and T6 is very similar. In both connections, it is seen that independent on the typology of the specimens, EVDR decreases as the displacement increases. This should be associated to very brittle behaviour under tension loading, leading to a poor dissipative response, contributing for low levels of energy dissipation during the cyclic testing.

In case of the connections with tie T5, it is seen that the double assemblages the higher values of EVDR when compared with the individual assemblages. In all assemblages, the values of EVDR increases for increasing displacements. This may be the result of progress of damage developed in the brick prisms, which in the other connections do not damage.

4.5. Shear behaviour of connections

Similarly to cyclic tension-compression tests, the analysis of results in shear tests is based on damage patterns and on average curve force-displacement of six samples, taking into account that the effect of tie location with respect to head joint was found to be insignificant, representing the shear cyclic behaviour characteristic curve for each tie typology. The corresponding mechanical parameters are also obtained and discussed.

4.5.1. Force-displacement diagrams

The cyclic shear behaviour of connections is represented by the average force-displacement diagrams of all tested double leaf specimens, see Figure 4.22. The displacements considered in the diagrams corresponds to the displacement recorded in LVDT 1, which was practically the same displacement recorded in LVDT 2. The values of displacement measured in LVDT 3 was practically zero, which confirms the adequacy of test setup. The force was recorded in the load cell connected to the actuator.

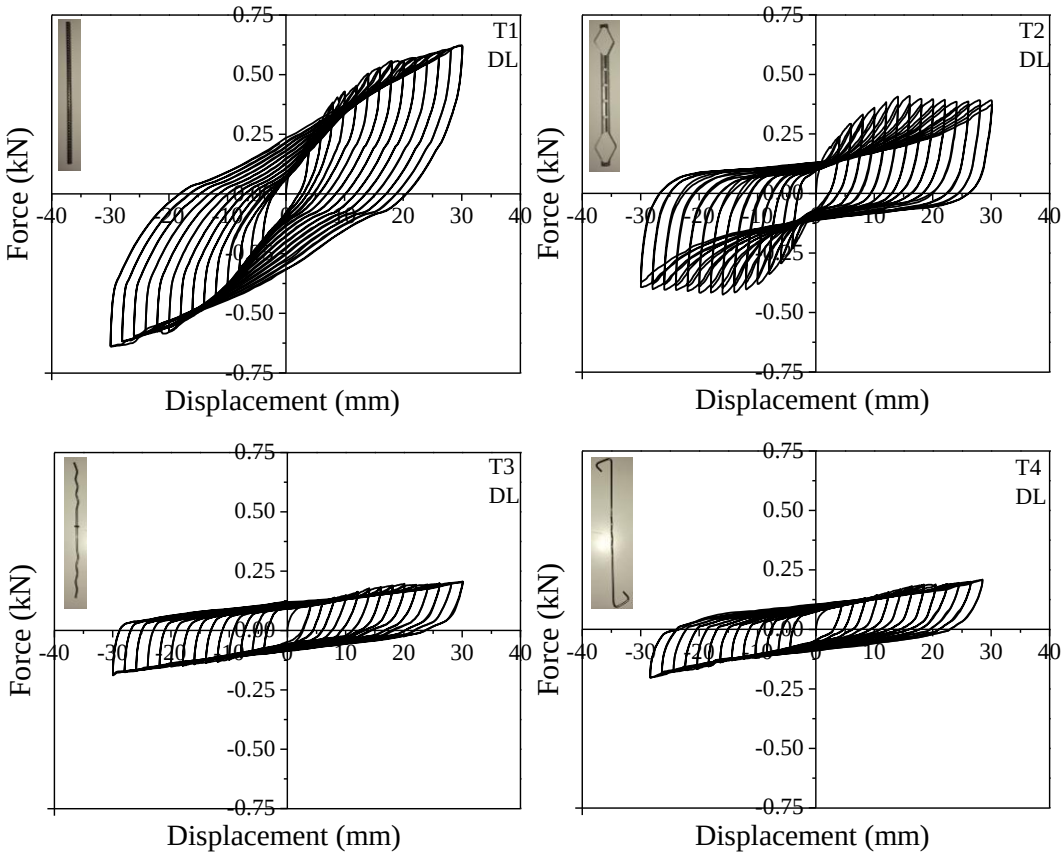

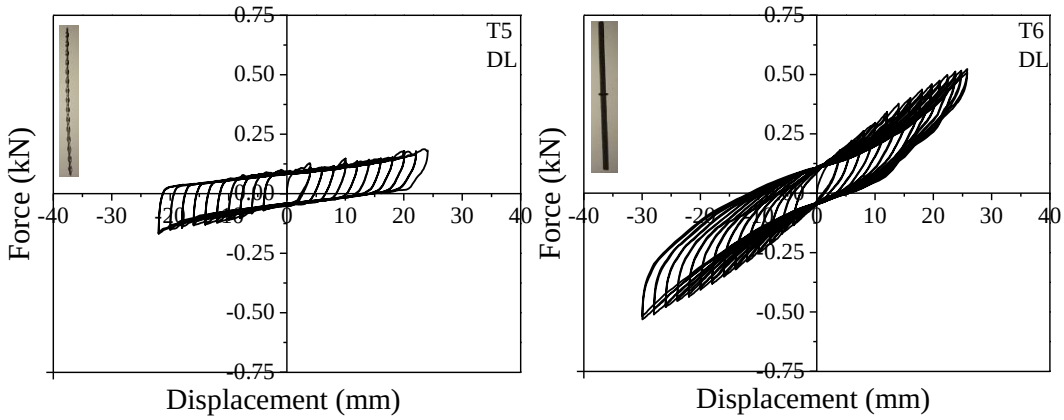

Figure 4.22 - Average force vs displacement curves for each tie typology on DL under shear loading

The hysteresis loops obtained in all connections are always symmetrical, meaning that as expected the shear behaviour does not depend on the direction because symmetric configuration of the tests setup is ensured. In some connections, after an initial linear response, there is the onset of the nonlinear behaviour (connection with Tie T1 and T2). The second cycle for each displacement level is practically equal to first cycle, which means that no progress of damage occurs in the second cycle of displacement.

Based on detailed analysis the shear hysteresis response, it is possible to divide the typical behaviour in two groups, namely the group of connections with ties T3-T5 and the group of connections with ties T1, T2 and T6.

The connections with ties T3, T4 and T5 exhibit low strength and poor hysteretic behaviour under shear loading. Based on the force-displacement diagram of connections with tie T5 connections, it is possible to observe the similarity with T3 and T4 wall ties, although this tie (T5) is attached to the brick prims though a chemical anchorage. However, the similar shear response is mostly associated to the bending of the tie and to the anchorage force of tie embedment on mortar joint.

Connections with ties T1, T2 and T6 presented better hysteretic behaviour and higher strength. The influence of the material of the tie can be seen from the indifferent response of the connections with ties T1 and T6, particularly regarding to the capacity to dissipate energy. The geometry is the same (cylindrical bars with smooth external surface) but the material is different: tie T1 is from steel ad tie T6 is from basalt fibre. The difference in terms of strength is not so much significant, but the dissipative response is much higher in the connection with tie T1.

The connections with tie T2 achieved a high resistance and a good dissipative response. The response is mostly characterized by pinching due to the accumulation of damage along the

tie, resulting in cumulative plastic deformations. The connection with tie T1 presented a dissipative hysteretic loop without pinching. The connections with ties T3 and T4 presented poor performance due to the low diameter of the ties and consequently low mechanical resistance.

Apart from the connection with tie T2, the maximum resistance of the other connections was not recorded because the test was stopped before it occurred. This means that it would be attained for higher levels of displacement. However, it should be noted that the imposed displacement level was considered to be reasonable for the shear deformation that a masonry wall can be submitted during an earthquake. Although that visible damage could be seen, the resistance was increasing, meaning that in real situation the connection appears to present a very good behaviour. For the maximum displacement level, it was possible to observe the plastic deformation of the ties and the degradation of the bond adherence of the tie along the mortar joints.

The shear response of individual connections MIL and MVL is presented in Figure 4.24. In single specimens, diagrams are based on the displacement measured in by LVDT.

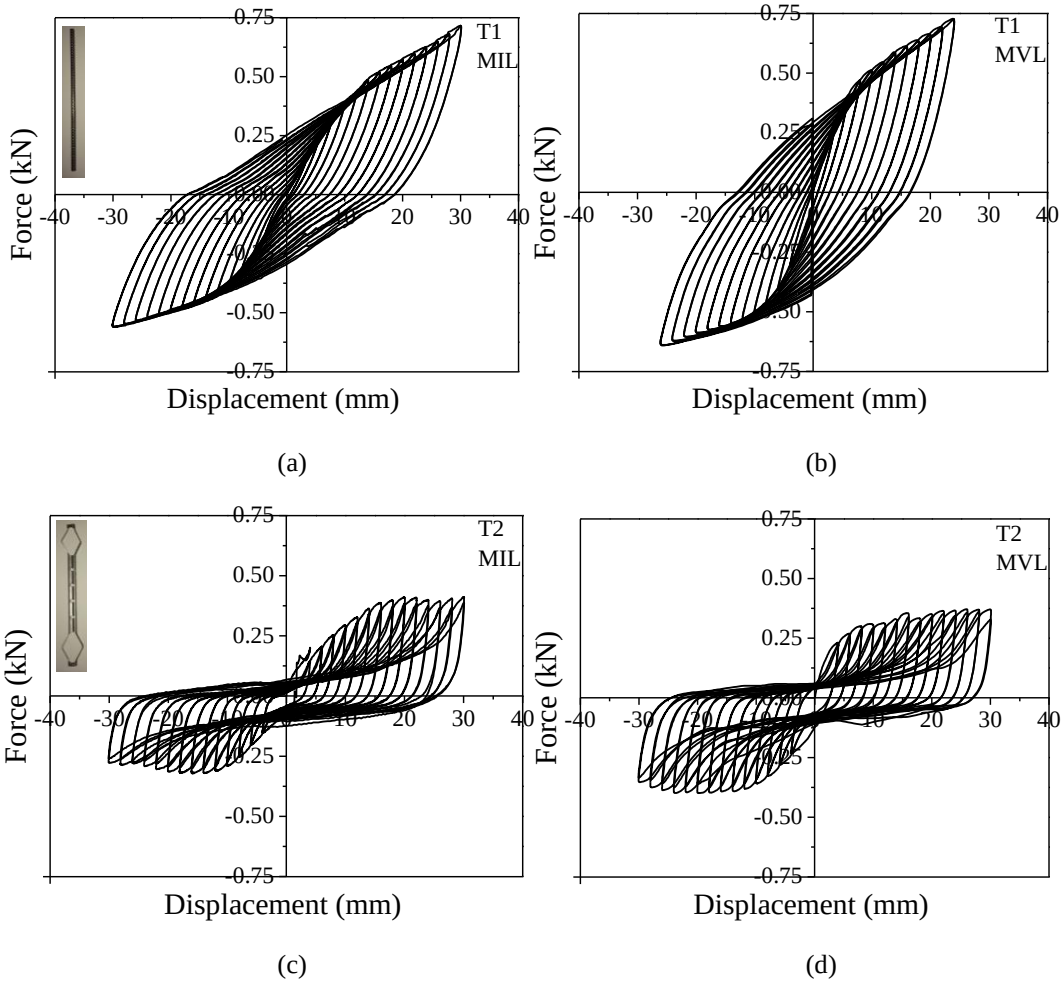

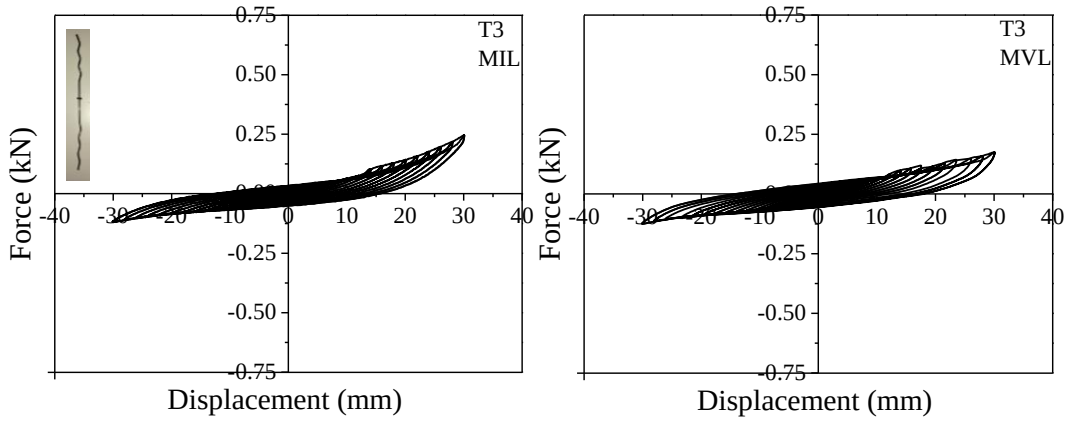

(e) (f)

Figure 4.23 - Force vs displacement diagrams for (a), (c), (e) MIL connections and (b), (d), (f) MVL connections of T1, T2 and T3 tie typologies

The behaviour of the connection with ties embedded in brick veneer prims (MVL) and brick infill prims (MIL) is almost always very close. This can be justified by the resisting mechanism of the connection under shear which is mostly governed by ties properties, particularly as regards the bending behaviour. As the tie is common in both connections, similar results are obtained. In case of the connections with ties T5, the shear strength is higher in MVL specimens. This is explained by the chemical anchorage used in MIL specimens. The chemical anchor applied in horizontal perforated bricks used in the brick infill prims (MIL) has lower compression strength, and thus lower resistance to local crushing. The rigid anchorage of the tie in MIL causes very concentrated forces on brick units, leading to the failure of the connections. The T5 wall tie embedment on mortar of MVL presented a similar behaviour of T3 and T4 wall ties in MVL specimens.

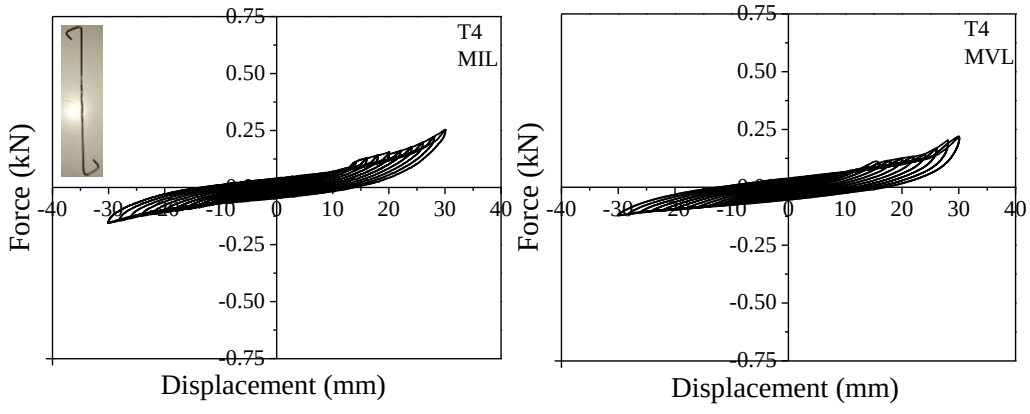

(a) (b)

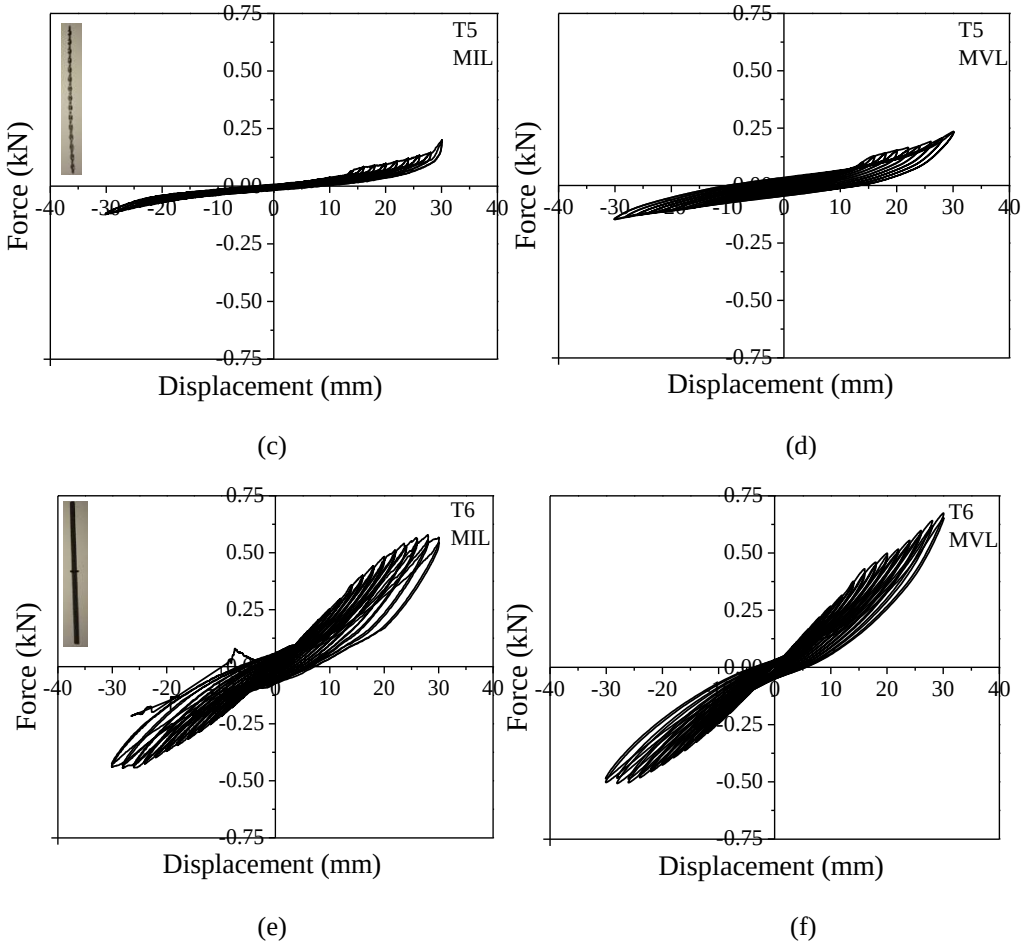

Figure 4.24 - Force vs displacement diagrams for (a), (c), (e) MIL connections and (b), (d), (f) MVL connections of T4, T5 and T6 tie typologies

To better understand the differences found in the shear behaviour of different types of connections, envelope diagrams were defined, see Figure 4.25 and Figure 4.26. As already mentioned, it is possible to identify two groups with different behaviour, namely T1, T2 and T6 and T3, T4 and T5. The envelops obtained for the connections with ties T3, T4 and T5 are almost overlapped in the three types of assemblages, which confirm the similar behaviour of the three types of ties under shear. As above mentioned, the connections with ties T1 and T6 present also very similar behaviour. Even if the initial behaviour of the connections with ties T1 and T2 is very close, indicating that the initial stiffness of the connections is very close, the strength is lower than the one obtained in the connections with ties T1 and T6.

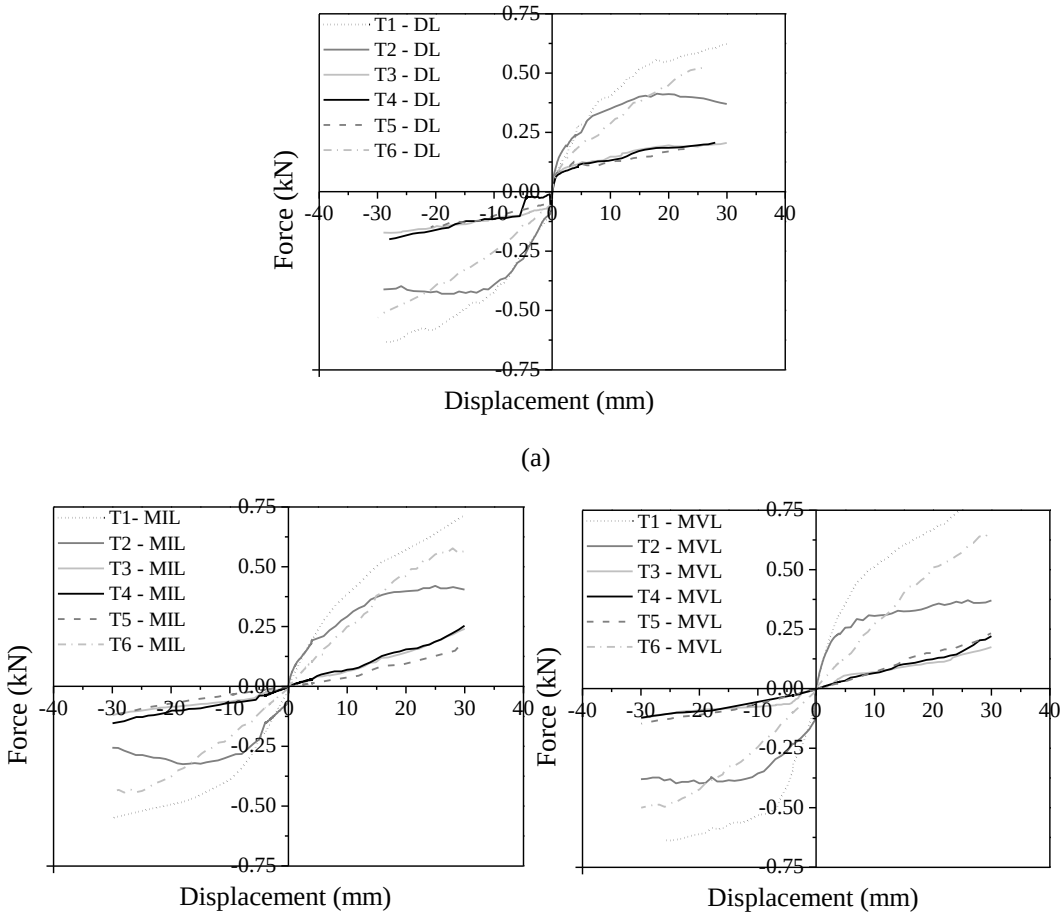

Figure 4.25 – Envelope curves from cyclic shear tests of (a) DL (b) MIL and (c) MVL specimens

The force-displacement envelops obtained for each tie in each different assemblage (DL; MIL and MVL) envelops shown in Figure 4.26, confirm that the tie features govern the shear behaviour of the connections. In fact, in all types of connections, the experimental envelops are very close for the different assemblages.

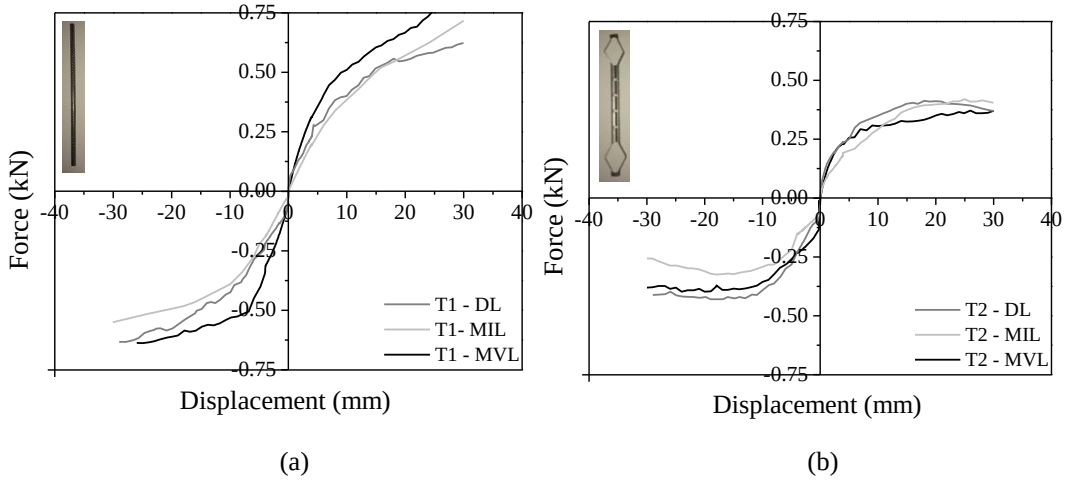

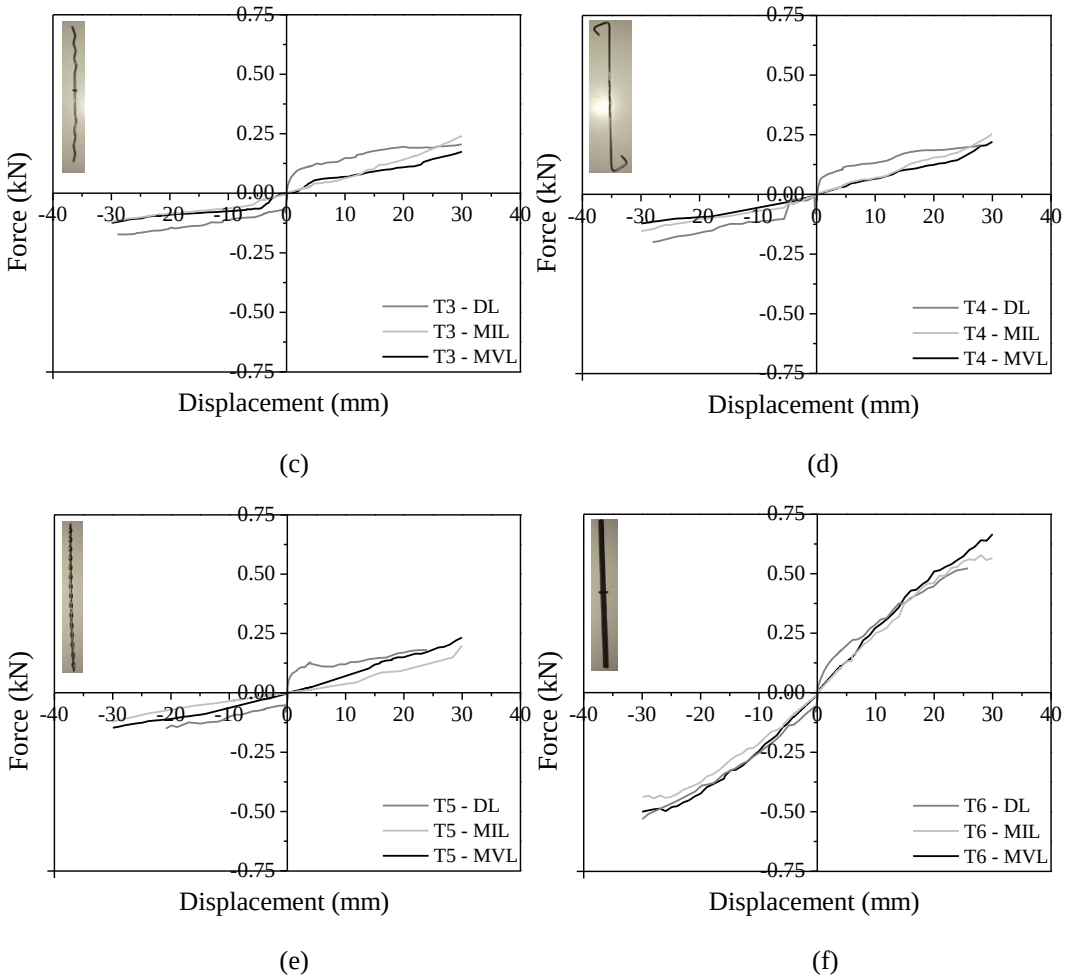

Figure 4.26 – Envelope curves from cyclic shear tests of (a) T1, (b) T2, (c) T3, (d) T4, (e) T5 and (f) T6 typologies of ties for each type of specimen

4.5.2. Damage patterns

The plastic deformation of ties governs the behaviour of the connections under shear loading. Besides, with increasing deformation, it was possible to observe a trend for the tie to pull-out from the mortar joint, see Figure 4.27 (a). This appears to be the result of the deterioration of the bond between the tie and mortar joint due to cyclic deformation of the tie. As mentioned before, this appears not to influence the overall shear response of the connections.

(a) (b) (c)

Figure 4.27 – Failure modes: (a) plastic deformation of T2, (b) pull-out of T5 tie e (c) degradation of surrounding mortar on T2 wall tie

In spite of damage is mainly controlled by plastic deformation of the tie, it should be stressed that in the deformation range imposed to the ties, the strength is still increasing in the majority of the connections.

In case of T5 wall tie, the chemical anchorage was detaching from the brick with horizontal perforations (MIL) leading to the cracking and crushing of the brick in the adjacent zone of the tie, as shown in Figure 4.27 (b). When the tie is connection to brick veneer units (MVL), it does not detach, resulting in the higher resistance. In DL specimens, the connections presented some damage on brick anchorage, but it is not so evident as in case of individual assemblage (MIL).

To sum up, it should be mentioned that the shear damage patterns is governed by tie deformation and the interaction between tie and mortar joints is less determinant. However, the type of fixation can influence the behaviour of connection, as could be seen in the connections with chemical anchorage (T5).

4.5.3. Mechanical parameters: stiffness

The initial shear stiffness (K_i) of the connections under study was obtained from the experimental cyclic results. The initial stiffness was calculated at the secant stiffness by measuring the slope of the line connecting the origin and the point corresponding to the force associated to the displacement of the first load cycle, i.e., 4 mm. The average values are presented in Table 4.4 and displayed also in Figure 4.28Figure 4.29. The initial stiffness values are only presented for one direction of shear load because there was not evident difference of the initial stiffness in other direction.

Table 4.4 - Average initial stiffness properties for each tie typologies of cyclic shear tests

		DL	MIL	MVL
T1	K_i (kN/mm)	0.057	0.049	0.078
	C.O.V (%)	20.49	18.01	12.49
T2	K_i (kN/mm)	0.058	0.048	0.057
	C.O.V (%)	25.88	25.88	26.77
T3	K_i (kN/mm)	0.028	0.006	0.01
	C.O.V (%)	29.70	9.89	6.71
T4	K_i (kN/mm)	0.028	0.008	0.007
	C.O.V (%)	30.32	16.38	15.93
T5	K_i (kN/mm)	0.030	0.003	0.006
	C.O.V (%)	28.23	22.81	20.67
T6	K_i (kN/mm)	0.044	0.026	0.028
	C.O.V (%)	21.90	10.05	11.44

From the analysis of results, it is observed that there is a great difference among the connections with differences types of ties, but it is possible to group the connections with ties T1, T2 and T6 and the connections with ties T3, T4 and T5 tie typologies. The stiffness of the connections is higher in case of stiff ties (T1, T2 and T6) compared to the connection with flexible ties (T3-T5). It is also observed that higher stiff is also associated to higher values of maximum shear force.

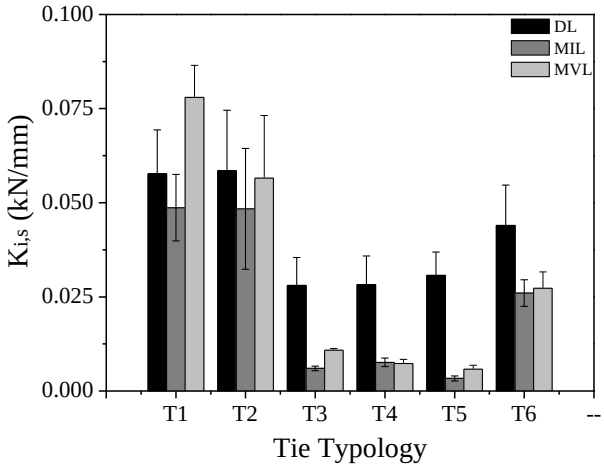

Figure 4.28 – Comparison of initial stiffness for each tie typology of shear tests

The degradation of stiffness during the cyclic shear loading was calculated from the cyclic shear force-displacement diagrams for each cycle as the slope of the line that connects the origin to the point of maximum displacement of the load cycle, see Figure 4.29. This was obtained only for some displacement levels to make the interpretation of the results easier

and for two directions of shear loading. The loss of stiffness is presented for each type of tie typology and for type of samples.

When the different assemblages are compared, it is seen that the stiffness is almost always higher in case of double leaf assemblages, representing the most realistic connections. This appears to be related to the boundary conditions in the extremity of the ties which also conditioned by the application of shear loading. This is particularly significant in case of flexible ties (T3, T4 and T5).

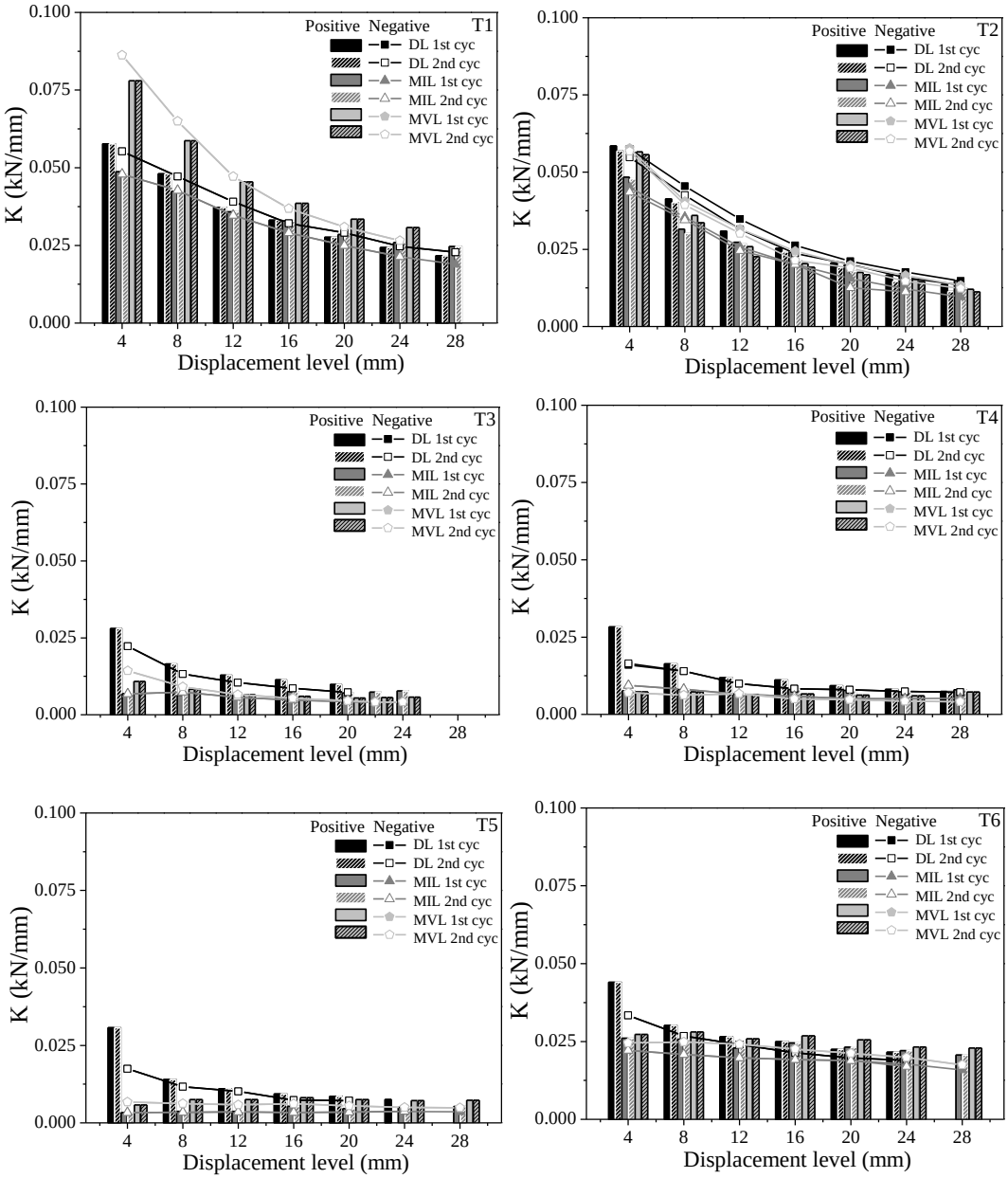

Figure 4.29 - Stiffness degradation under shear loading

The previous damage influence of stiffness degradation of wall tie behaviour. From the diagrams, it is possible to see that stiffness degradation in the connections with ties T1, T2

is more significant, which appears to be related to higher hysteresis of the shear loops of the connections. Note that from the cyclic shear force-displacement in the connections with ties T3 to T6 are characterized by very low hysteresis. The highest stiffness degradation is also the result of the higher damage level observed in stiffer and strength connections (higher abrasion).

Apart from the connections with tie T2, it is observed that no stiffness degradation occurs between the first and second cycles, resulting from the absence of accumulation of damage.

4.5.4. Seismic indicators: Energy of dissipation and Equivalent Viscous Damping Ratio (EVDR)

The energy dissipation for each cycle was determined through the area enclosed by a hysteretic cycle, obtained in the cyclic force-displacement curve (G_c). The cumulative energy dissipation was determined by summing the energy obtained for of each cycle (CG_c) until a certain level of displacement. The energy dissipated during the tests for each type of assemblages can be compared through the diagrams shown in Figure 4.30 and Figure 4.31.

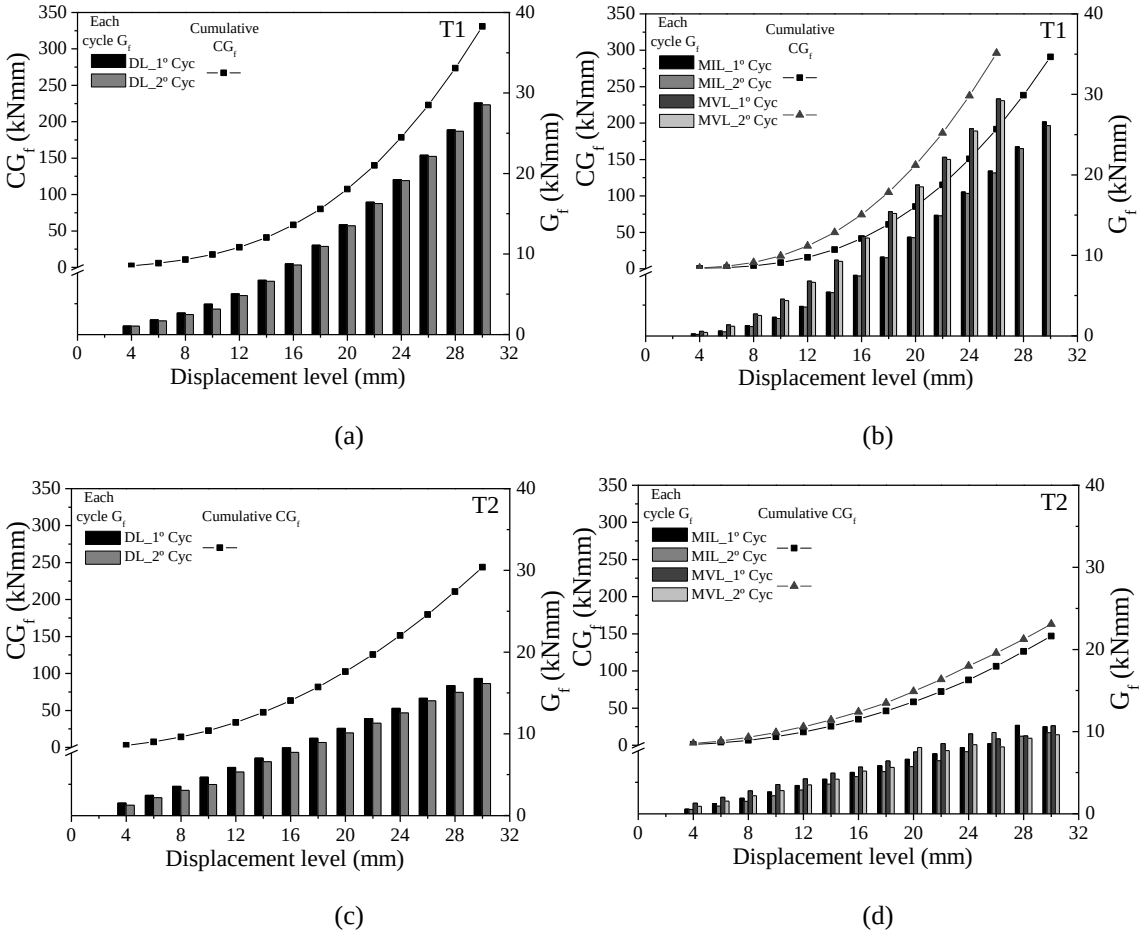

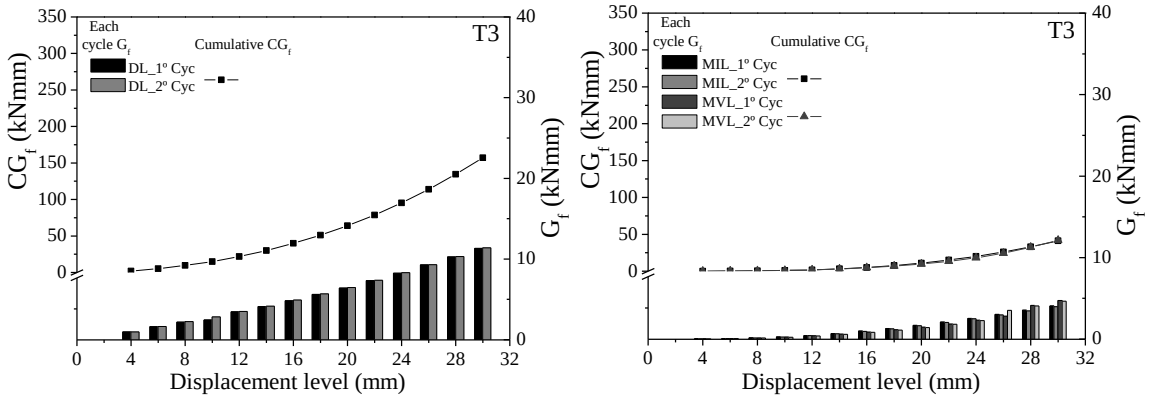

(e) (f)

Figure 4.30 – Cumulative dissipated energy for (a-b) T1, (c-d) T2 and (e-f) T3 tie typologies in each type of sample under shear loading

The diagrams are divided for each tie typology in (1) energy dissipated of each type of assemblage (DL, MIL MVL); (2) energy dissipated during first and second cycle at each displacement level (G_c) and (3) cumulative energy dissipation (CG_c).

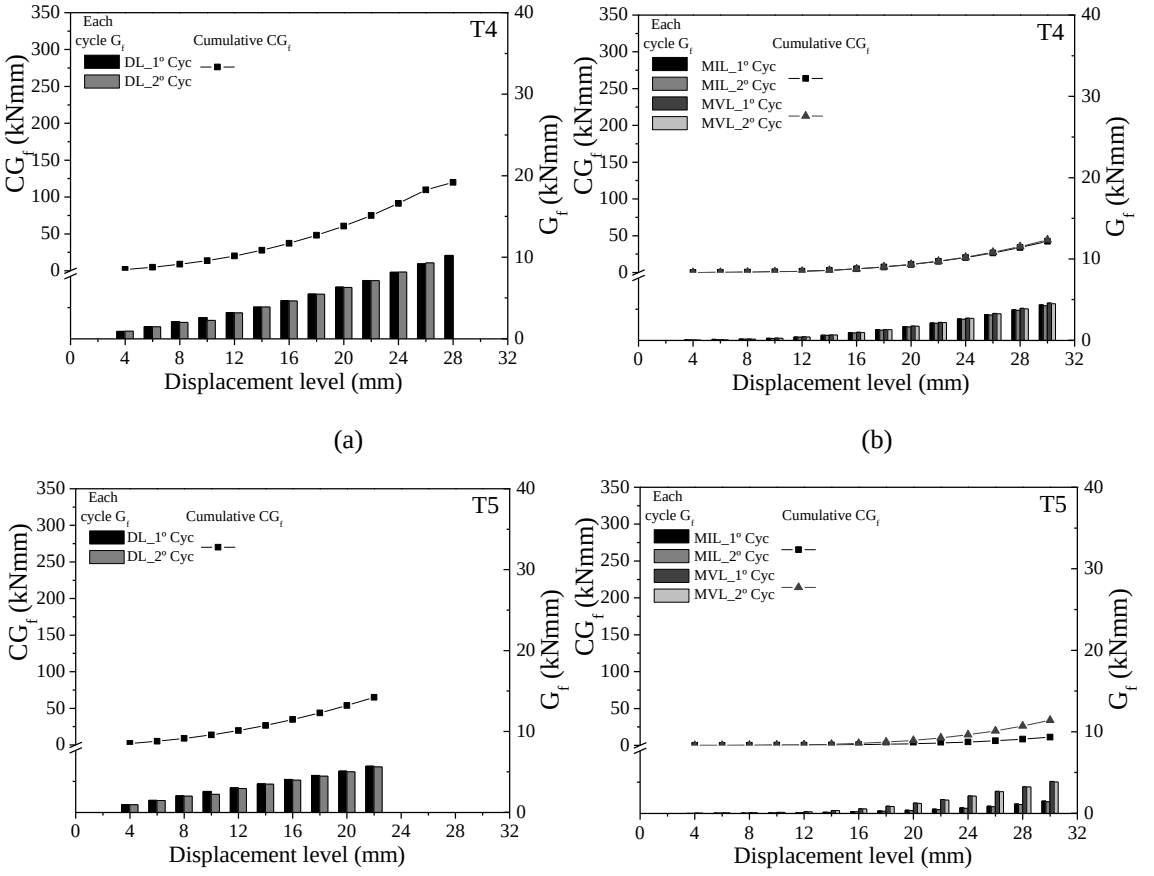

(a) (b)

(c) (d)

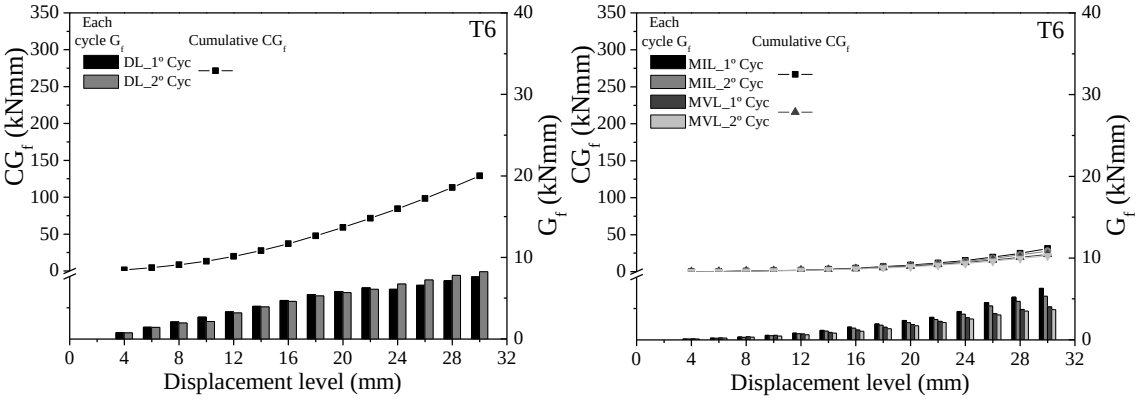

(e) (f)

Figure 4.31 – Cumulative dissipated energy for (a-b) T4, (c-d) T5 and (e-f) T6 tie typologies in each type of sample under shear loading

As expected, the different shear behaviour between the different assemblages from DL to MIL and MVL is also reflected by the ability to dissipate energy. It is seen that in all connections, the double leaf connections present always higher values of cumulative energy dissipation. It is also observed that the energy dissipated in the cycles for increasing displacements increases but the increasing rate is clearly different among the connection, resulting in different values of cumulative energy dissipation. One more time, it is possible to group the connection by the type of tie used in the assemblage. For the energy dissipation it is possible to observe that independently on the type of assemblage, the connections with ties T1 and T2 has considerable more dissipative than the connection with this T3 to T6. In spite of the connections with the rigid tie present reasonable resistance load, the hysteresis is low and is reflected by the low dissipation of energy.

The connections with ties T3, T4 and T5, the cumulative is considerably lower than the cumulative energy obtained in the connection with ties T1 and T2. The second cycle presented in majority of cases close values of dissipative capacity of first cycle. Nevertheless, the T2 response should be seen because the reduction of dissipative energy on second cycle was higher than other ties.

Following the calculation of the energy dissipation, it was also calculated the equivalent viscous damping ratio (EVDR), already described. The evolution of EVDR for increasing displacement in all connections are presented in Figure 4.32. According to the grouping mentioned before for the energy dissipation, also for the EVDR, it is possible to point out the clear different behaviour between the connections with ties T1 and T2 from the connections with ties T3 to T6. The values of EVDR from individual assemblage is always considerable lower than EVDR obtained in double leaf assemblages in case of ties T3 to T6.

In case of connections with ties T1 and T2, the difference is marginal. Due to crescent and very dissipative behaviour, the T1 typology presents an increase of EVDR values, whereas the T2-T5 typologies present a constant of EVDR values. The T6 present a decreasing trend due to low dissipative response.

The EVDR values of T3-T5 wall ties is very high comparing with other ties typologies. This means that, although these elements present lower values of resistance and stiffness comparing other wall ties, they have an interesting damping capacity.

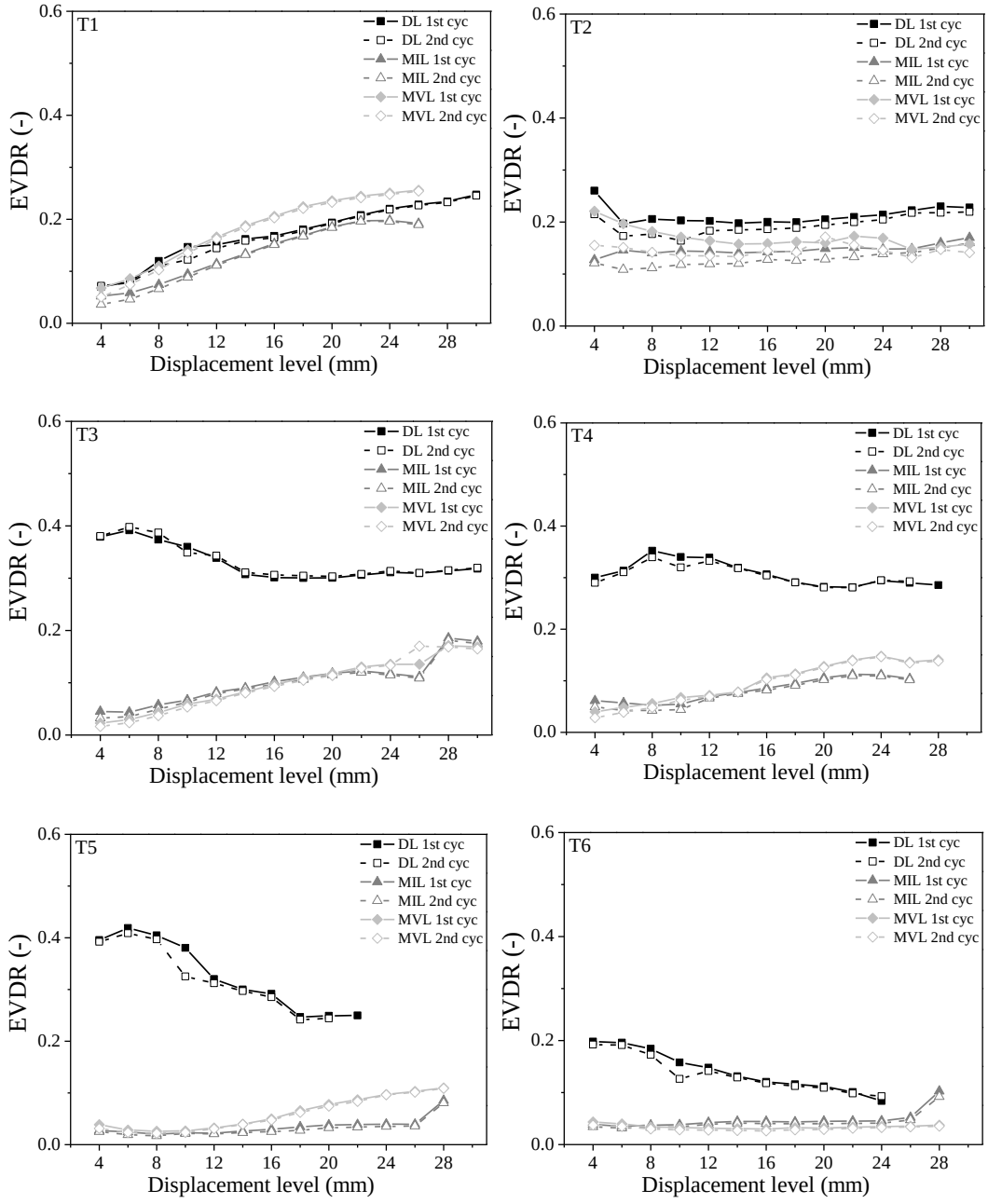

Figure 4.32 - EVDR values for all tie typologies in shear tests

4.6. Conclusion

This chapter presents and discusses the experimental results obtained in cyclic tension-compression and shear tests carried out on assemblies composed of brick masonry prisms connected by different types of ties. The experimental campaign was designed so that different specimens could be considered: (1) complete assemblage of brick veneer-tie-backing system; (2) assemblages involving the tie and brick infill masonry and (3) assemblages composed of the tie connected to the backing system. The tension-compression and shear loading configuration intended to simulate real loading conditions induced by earthquakes on ties connecting the backing system and the brick veneer walls. Taking into account the most common structural system for buildings in south European countries, it was decided to consider brick infill walls enclosed in reinforced concrete frames as the backing system to which the brick veneers are attached.

Based on the analysis of the results of the experimental campaign, the following conclusions can be drawn:

1. Nonlinear hysteretic behaviour could be seen even for small displacements. Hysteresis pinching and asymmetry became pronounced with an increase in displacements in tension-compression tests. In shear loading the curve was mostly symmetric and, in some cases, the pinching effect happen in more resistant ties. Strength and energy dissipation capacity reduction were recorded between the first and the second cycles in tension-compression loading. Under cyclic shear loading the reduction was insignificant.

2. Tensile-compression and shear behaviour of connections depend on the type of tie. Tie shape and geometry were the most important factors influencing strength of connections. Tie surface roughness and geometry at the ends influence the bond strength between the tie and mortar at bed joints and, thus, the tensile strength of the connection. Tie thickness influences in a great extent the compression and shear strength, stiffness and dissipative energy capacity.

3. The strength of assemblages where the tie is connected to bricks with horizontal perforations through chemical anchorages is influenced by the mechanical properties of the bricks mainly in the direction perpendicular to the horizontal perforations. This solution is very attractive and suitable to façade rehabilitation, but attention should be taken to the resistance of brick units in the perpendicular direction to perforations.

4. Tie pull-out, tie buckling or tie fracture, either at the mid length or at the end of the free length of the tie were the predominant failure modes in cyclic tension-compression and shear testing. The interaction between cyclic tension and compression loading results in the combination of different failure modes. In all double leaf assemblies, which are more representative of real conditions, the failure mode is mostly characterized by pull-out of the ties from the bed joint mortar of brick veneer leaf. This failure mode is attributed to lower compressive strength of mortar of the brick never prims, resulting in low bond strength between tie and mortar. In some cases, the fracture of wall tie was recorded, much associated to the fatigue of the ties promoted by the cyclic tension-compression loading. Regarding to compression behaviour, the cross section of ties determines if plastic deformation of the ties due to buckling develops (T2, T3, T4 and T5) or, instead, if penetration of wall tie on mortar bed joint occurs (T1 and T6). As concerning to shear behaviour, the shear damage is governed by tie deformation, and the interaction between tie and mortar is playing a minor role in the shear behaviour of the connections.

5. The analysis of behaviour presented by individual specimens revealed the role played by the compressive strength of mortar on tensile and compression strength of connections. This means also that the bond strength between ties and mortar influences the strength, stiffness and energy dissipation of individual connections. It was also seen that the behaviour of the double leaf assemblages is much close to the behaviour of ties embedded on brick veneer prims. This is explained by the role played by the bond strength of ties embedded in mortared joints of brick veneer prisms. The connections under shear revealed that its shear response is influenced by the tie properties, and not so much by adherence of tie to mortar.

6. Regarding to dissipative energy capacity, it can be possible to define the best ties to minimizing damage in constructive system: (1) the best energy dissipation is achieved for the connections with tie T2 under tension-compression and shear loading; (2) the compressive strength of mortar influences clearly the cyclic tension behaviour of the connections, resulting higher dissipative energy values for MIL. In DL specimens, the interaction of the tie with mortar joints occurs at both mortar extremities, MIL and MVL, and for that the results are very close to MVL dissipative energy values due to mortar lower mechanical properties; (3) the low energy dissipated in the connection with tie T5 is related with low compression and tensile strength obtained in the cyclic testing, which is instead attributed to the low strength of the horizontal perforated units commonly used in brick masonry infill walls; (4) in shear tests the maximum values of energy dissipation were

recorded on DL assemblages. Connections with ties T1 and T2 revealed to be the most dissipative.

7. The equivalent viscous damping ratio parameter is essentially influenced by type of tie and damage degradation between first and second cycle. The values of second cycle is mostly lower comparing with values of first cycle, taking into account that the second hysteresis is lesser dissipative and lower resistance than first cycle, happening in all type of loadings. In almost all cases, there is no variation of EVDR as the damage progresses with increasing of displacement levels, which it appears that there is an equilibrated system between resistance and dissipated energy. Although in tension-compression tests it was not evidenced, in shear loading there was a great difference between double and single specimen, result of higher values of accumulated dissipation energy in DL samples, mainly in ties with lower dissipative capacity (ties T3-T5). The T1 and T2 also present good values magnitude of these damping elements, which become interesting solutions to adopt in earthquakes resistant constructions.

8. It is considered that the most representative assemblage of the local behaviour of the tied connections is the complete assemblage composed of brick masonry prisms connected through ties. This testing assemblage is recommended for experimental and numerical characterization of the ties in brick veneer walls because it simulated with more accuracy the real boundary conditions. In addition, it is stressed that the results presented herein in terms of strength and stiffness of ties can be useful to (1) select the most appropriate tie, and (2) design tie spacing for out-of-plane design loads due to wind or earthquakes. For the continuity of this study, it was suggested that the T2 represent a good tension-compression and shear response and T4 give an excellent tension response for resisting the out-of-plane loading in earthquakes events.

Chapter 5

Analytical and Experimental Parametric Assessment of Tie Connections

Abstract:

The description of highly nonlinear hysteretic behaviour of the connections subjected to cyclic tension and compression loading can be very complex. Thus, simplified models were designed, giving equally good results and being able of accurately representing the real nonlinear behaviour of connections on simplified numerical analysis of a building. Besides that, an experimental parametric analysis was performed taking into account different constructive variables (mortar and tie typology, air cavity width and embedment length).The prior effect of shear loading on connections subjected under tension-compression behaviour was also evaluated. With the obtained results, it was concluded that: (1) the compressive behaviour is influenced mainly by tie typology and air cavity width; (2) the tensile behaviour is influenced mainly by tie typology and embedment length and (3) the prior shear damage reduces of strength and initial stiffness..

5.1. Introduction

This chapter intends to provide a more detailed analysis of the connections under tension and compression cyclic loading and cyclic shear loading. It can be divided in three parts: (1) analytical work to derive hysteretic models that simulate the mechanical behaviour of the connection under cyclic tension-compression and under cyclic shear loading. It should be stressed that an analytical model of the tie-masonry assemblages can be useful to simulate numerically masonry veneer walls attached to brick masonry veneer walls. For this, the analytical models are designed to accurately represent the real nonlinear behaviour of some connections with a reduced number of parameters and complex equations; (2) assessment of the influence of the in-plane damage of the connections on the cyclic tension-compression mechanical behaviour. In real earthquake events, the combination of in-plane and out-of-plane loading occurs mostly simultaneously. The goal is to evaluate the mechanical parameters in connections subjected to tension and compression cyclic loading with prior shear damage. In addition, a qualitative comparison between these connections with other ones without any type of damage is provided; (3) experimental parametric study for the assessment of the influence of different parameters in the cyclic tension-compression mechanical behaviour of the connections. Besides the typology of the ties, the parameters studied are: (a) resistance of the bed joint mortar; (b) embedment length of wall tie in mortar and (c) air cavity width of connections.

5.2.Background on existing hysteretic models

The numerical simulation of components and assemblages exhibiting a typical hysteretic behaviour can in certain cases be carried out through the use of more simplified elements (for examples macro-elements like shear walls and connections) with specific hysteretic nonlinear constitutive laws. There should be always a compromise between model complexity and necessary accuracy. The majority of analytical models intend to simulate in-plane behaviour of masonry and concrete shear walls and connections in timber structures. In Table 5.1, it is possible to consult a brief overview about difference between analytical models presented in literature with regard models' constitution and study application. Brief remarks are also presented in order to obtain an idea about model prescriptions.

Table 5.1 – Overview of analytical hysteretic models

Reference [REF]	Constitution of hysteretic loops	Study application	Model's observations
Polensek and Laursen (1984) [137]	Piecewise linear functions	Sheathing to wood connections	Models strength and stiffness degradation.
Stewart (1987) [138]	Piecewise linear functions	Sheathing to wood connections	Models strength and stiffness degradation, (Figure 5.1 (a)).
Dolan (1989) [139]	Piecewise exponential functions	Sheathing to wood connections	Models strength, pinching and stiffness degradation.
Ceccotti and Vignoli (1990) [140]	Piecewise linear functions	Semi rigid wood joints	Models pinching and stiffness degradation and incorporated it in the nonlinear dynamic analysis program DRAIN-2D.
Modena (1992) [141]	Piecewise linear functions	Masonry structures	Models with symmetrical envelope curve.
Foliente (1995) [142]	Piecewise linear functions	Wood structures	Based on the Bouc Wen Baber Noori (BWBN) hysteretic model for steel and concrete structures.
Krawinkler et al. (2000) [143]	Piecewise linear functions	Wood structures	Deterioration modes: basic strength deterioration, postcap strength deterioration, unloading stiffness degradation, and accelerated reloading stiffness degradation.
Folz and Filiatrault (2000, 2001) [144, 145]	Piecewise Exponential and linear functions	Wood structures	Based on Stewart (1987)'s model [135], the CASHEW program was includes a built-in shear wall parameter estimation module making it attractive as a simple-to-use analysis tool.
Pang et al. (2007) [146]	Piecewise Exponential functions	Wood structures	Based on CUREE model by Stewart (1987)'s model [135]. These evolutionary parameters are derived using multiple damage tracking indices used to model the cumulative damage of structures (Figure 5.1 (b)).
Belmouden, et. al (2007) [147]	Piecewise linear functions	Reinforced concrete structural walls	Deterioration modes: strength and stiffness degradation, pinching and slippage, bond slip effect, inelastic shear deformation mechanisms and confinement effects, (Figure 5.1 (c)).
da Porto et al., (2009) [148]	Piecewise linear functions	Masonry walls	Based on a symmetrical envelope curve on which the cycles are built, proposed by Modena (1992) (Figure 5.1(d)).
da Porto et al., (2012) [149]	Piecewise linear functions	Masonry walls	Based on Direct Displacement-Based Design (DDBD), proposed by Priestley et al., (2007): The equivalent elastic system was constructed by equivalent viscous damping. (Figure 5.1 (e)).

Many old and recent hysteretic models have been presented and discussed and revealed to be describe in a simpler way the nonlinear behaviour of the structural elements. Hysteretic models available were mostly based on experimental results. They are mostly described through linear and exponential functions with certain parameters that approaches the experimental cyclic behaviour, see Figure 5.1.

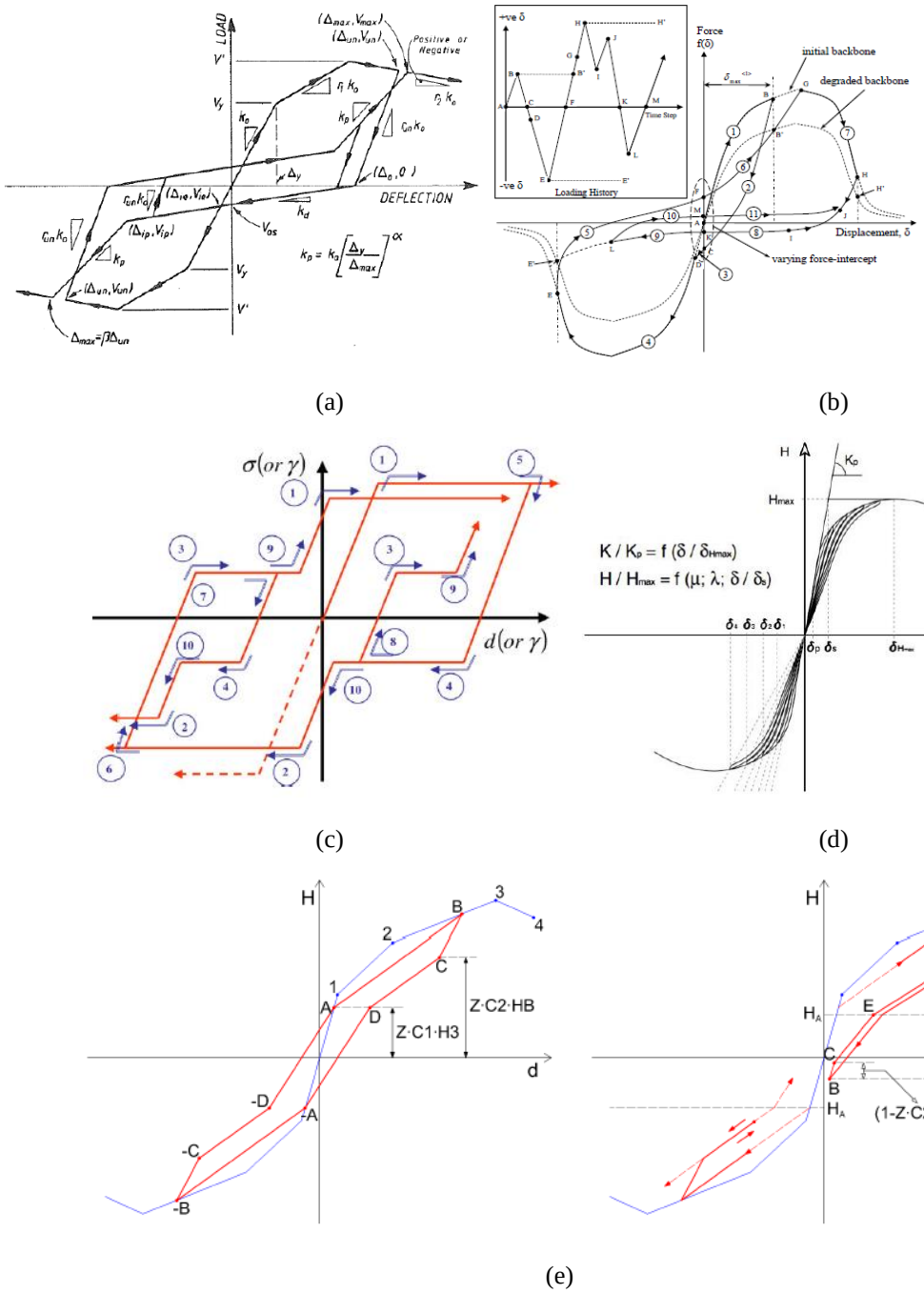

Figure 5.1 - Examples of existing hysteretic models: (a) hysteretic model developed by Stewart (1987) [138]; (b) evolutionary parameter hysteretic model developed by Pang et al. (2007) [146]; (c) hysteretic rules for nonlinear model by Belmouden, et. al (2007) [147], (d) masonry model developed by Modena (da Porto et al. (2009) [148]) and (e) hysteretic model developed by da Porto (2012) [149]

5.3. Analytical hysteretic model for tie connections

It is considered that the simulation of the veneer walls in a global structure should depend greatly on the connection that attach the masonry veneer to the backing system. Therefore, the analytical model presented herein can be useful for future numerical studies. Simplified analytical models can give good results without using much complex equations or parameters. The analytical models developed in this work are based on existing models and calibrated through the experimental cyclic hysteric response of the connections. The parameters that allow the construction of the hysteretic constitutive model should define key points of the nonlinear behaviour of tie connections and describe the strength degradation and stiffness degradation, being these greatly influenced by the pinching and dissipative response of tie connections.

For the development of the analytical models, it was decided to select two types of ties taking into account the best performance under tension-compression and shear loading. Therefore, ties T2 and T4 ties typologies were considered to calibrate the analytical models. Tie T2 presents a very good tension-compression and shear behaviour (strength, stiffness and dissipation energy) and tie T4 presents an excellent tension response.

5.3.1. Definition of backbone curves

An analytical model was designed in order to represent with accuracy the behaviour of tie connections under tension-compression and shear cyclic loadings. In a first phase, the backbone curve intending to describe the cyclic envelop experimental curve was designed. The backbone envelope is the curve that connects the points of maximum load for certain corresponding displacement for each load step in the hysteresis diagrams. The exponential function used to describe the ascending branch of the backbone curve for shear walls proposed by Foschi (1974) [150] and the ascending backbone envelope of the CUREE model [135] was selected to represent the pre-peak behaviour of tie connections. The Foschi (1974) [150] is widely recognized to representatively describe nonlinear connection behaviour, having been successfully implemented into several analytical studies in timber structures. The post-peak branch is described based on the evolutionary hysteretic model presented by Pang et. al (2007) [146]. These two exponential functions define the ascending and descending braches of the envelopes of the experimental force vs displacement hysteresis of diagrams obtained for the tie connections. Thus, the backbone curve (Figure 5.2) is defined

by seven static parameters, according to expressions (5.1) and (5.2) both for tension-compression and shear loadings:

$$\begin{cases} \left(1 - e^{-\frac{K_0}{F_o \delta}}\right)(K_d \delta + F_o) & for\ \delta \le \delta_{max}\ in\ all\ tests \\ f_x + (F_x - f_x)\left(1 - e^{-e^{K_x\left(\delta - \frac{\delta_x}{F_x} - f_x\right)e}}\right) & for\ \delta > \delta_{max}\ in\ tension - compression\ tests \\ F_{max} & for\ \delta > \delta_{max}\ in\ shear\ tests \end{cases} \quad (5.1)$$

$$\begin{cases} \left(1 - e^{-\frac{K_0{'}}{F_o{'} \delta}}\right)(K_d{'} \delta + F_o{'}) & for\ \delta \le \delta_{max}{'}\ in\ all\ tests \\ f_x{'} + (F_x{'} - f_x{'})\left(1 - e^{-e^{K_x{'}\left(\delta - \frac{\delta_x{'}}{F_x{'}} - f_x{'}\right)e}}\right) & for\ \delta > \delta_{max}{'}\ in\ tension - compression\ tests \\ F_{max}{'} & for\ \delta > \delta_{max}{'}\ in\ shear\ tests \end{cases} \quad (5.2)$$

The unique difference between expression (5.1) and (5.2) is related to the positive and negative branch of tension-compression and shear force vs displacement diagrams, respectively. The parameter K_0 or $K_0{'}$ is the tangent stiffness of the backbone curve for tension and compression loading, respectively. K_0 or $K_0{'}$ is also the tangent stiffness of the backbone curve for shear loading in positive and negative direction, respectively. The exponential loading of the envelope curve is defined through stiffness K_d or $K_d{'}$, which corresponds to the slope of the curve immediately before reaching the maximum load F_{max} or $F_{max}{'}$. F_0 or $F_0{'}$ is the load at which the line with slope K_d or $K_d{'}$, intersects the vertical axis. The curve also takes into account the softening behaviour by means of stiffness K_x or $K_x{'}$, corresponding to the slope of the curve after the displacement δ_{max} and $\delta_{max}{'}$, corresponding to the maximum load F_{max} or $F_{max}{'}$.

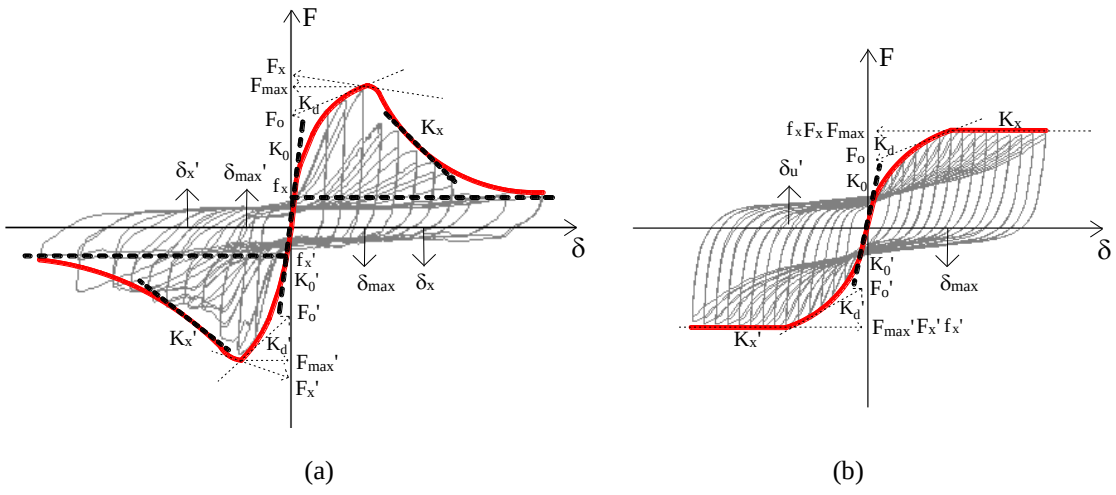

Figure 5.2 – Typical backbone curve of (a) tension-compression and (b) shear tests

F_x or F_x' is the load at which the line with slope K_x or K_x', intersects the vertical axis. For displacements larger than δ_{max}, the backbone curve is described by a four-parameter exponential decaying function (F_x or F_x', f_x or f_x', K_x or K_x' and δ_x or δ_x'). The force decays from an upper force asymptote, F_x or F_x', to a lower force asymptote, f_x or f_x'. The maximum decay rate occurs at the point of inflection located at deflection δ_x or δ_x', and it is drawn by stiffness K_x or K_x'. Note that F_x or F_x' is always equal or larger than F_{max} or F_{max}', when the post peak behaviour is known. When these values are equal, the slope or tangent stiffness of the descending backbone K_x or K_x' is always zero. Since there are physical interpretations associated with all backbone parameters, the backbone functions can be estimated using least-square regression or can be identified easily through visual analysis of the hysteresis loops.

Since this approach is used in tension-compression loading configuration, it was also decided to use it in shear loading, although in these cases the response is practically symmetric. Implementation of these equations to the negative displacement region of the hysteretic loops requires reversal of the sign convention used for force and displacement.

5.3.2. Definition unloading and reloading paths

To describe the cyclic response of the connections under tension-compression and shear loading, the unloading and reloading paths must be described. The constitutive law is considered to be the same for tension-compression and shear loading. Loading paths are identified as the branches where both the displacement and the gradient of the displacement have the same signs. Unloading paths need to be defined where displacement and the gradient of the displacement have opposite signs. The limits of these loading and unloading paths are modelled using simple parameters as strength, displacement and stiffness. In order to make the constitutive law more accurate with more consistent values, a percentage of maximum displacement was adopted to define the onset and the end of each linear segment. Thus, it was decided to divide the unloading and reloading path of cyclic tension-compression and shear force vs displacement hysteretic diagrams in three phases, being each one described through simple linear relations connecting the points characterizing each phase, see Figure 5.3.

Regarding unloading branch, the paths of the hysteresis loop are characterized by varying stiffness: (Figure 5.3):

(1) between δ_{max} and $\delta_{un,1}$ and $\delta_{max}{}'$ and $\delta_{un,1}{}'$ displacements at which the connections start to close, there is a great loss in strength for a small decrease of about 10% of maximum displacement. As the strength loss is very sudden, the values of unloading stiffness are high, $K_{un,1}$ and $K_{un,1}{}'$;

(2) From $\delta_{un,1}$ and $\delta_{un,1}{}'$, $K_{un,2}$ and $K_{un,2}{}'$ decrease until the load reversal that occurs at displacement $\delta_{un,F=0}$ and $\delta_{un,F=0}$;

(3) In order to take into account pinching, stiffness is described by the slope of the line defined between the points $(\delta_{un,F=0}, 0)$ and $(0;\ F_r')$, and $(\delta_{un,F=0}{}', 0)$ and $(0;\ F_r\ )$ where F_r' and F_r are the residual forces in the cycle when the displacement is 0.

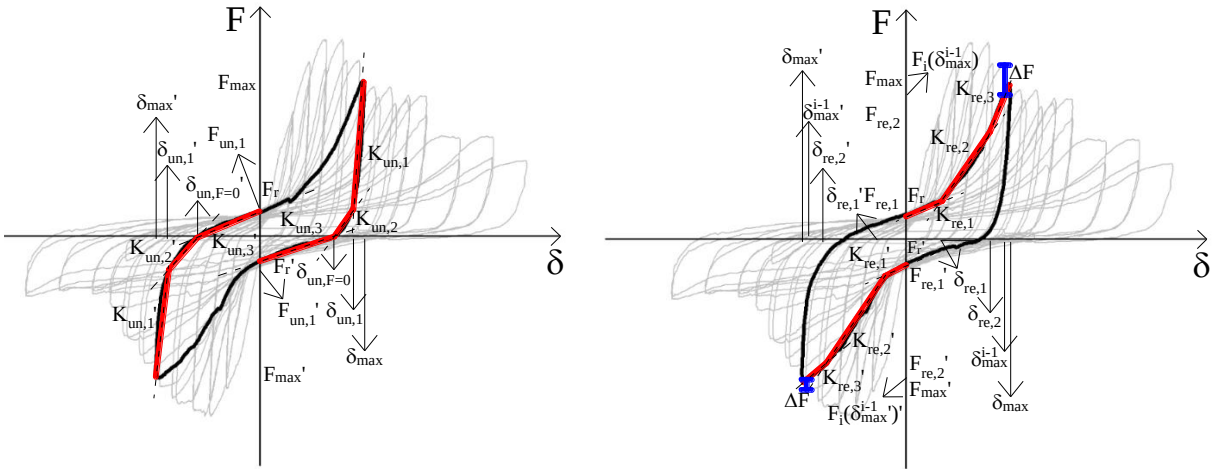

Figure 5.3 – General scheme of constitutive law of (a) unloading and (b) reloading path

Thus, the unloading branch is described according to the expressions given by expression (5.3) and expression (5.4), corresponding to positive and negative branches:

$$\begin{cases} F = F_{max} + K_{un,1}(\delta - \delta_{max}) & |\delta_{un,1}| < |\delta| \leq |\delta_{max}| \\ F = F_{un,1} + K_{un,2}(\delta - \delta_{un,1}) & |\delta_{un,F=0}| < |\delta| \leq |\delta_{un,1}| \\ F = F_{un,F=0} + K_{un,3}(\delta - \delta_{un,F=0}) & 0 < |\delta| \leq |\delta_{un,F=0}| \end{cases} \quad (5.3)$$

$$\begin{cases} F = F_{max}{}' + K_{un,1}{}'(\delta - \delta_{max}{}') & |\delta_{un,1}{}'| < |\delta| \leq |\delta_{max}{}'| \\ F = F_{un,1}{}' + K_{un,2}(\delta - \delta_{un,1}{}') & |\delta_{un,F=0}{}'| < |\delta| \leq |\delta_{un,1}{}'| \\ F = F_{un,F=0}{}' + K_{un,3}(\delta - \delta_{un,F=0}{}') & 0 < |\delta| \leq |\delta_{un,F=0}{}'| \end{cases} \quad (5.4)$$

Where:

F is the generalized force;

F_{max} and $F_{max}{}'$ are the maximum forces corresponding to displacement δ_{max} and $\delta_{max}{}'$, respectively;

$F_{un,1}$ and $F_{un,1}{}'$ are the forces corresponding to displacement $\delta_{un,1}$ and $\delta_{un,1}{}'$, respectively;

$F_{un,F=0}$ and $F_{un,F=0}{}'$ are the forces corresponding to displacement $\delta_{un,F=0}$ and $\delta_{un,F=0}{}'$, respectively.

The reloading branches are characterized following the same procedure, through smooth branches. A percentage of displacement correspondent to the maximum load was considered to define the start and end of each line segment, following the steps:

(1) The displacement limit of first segment, $\delta_{re,1}$ and $\delta_{re,1}{}'$, can be found at 30% of maximum displacement, corresponding to the force $F_{re,1}$ and $F_{re,1}{}'$, respectively. Because the hysteretic curves are characterized by pinching, this segment presents the same slope as the last unloading branch of the previous unloading cycle ($K_{un,3}{}' \cong K_{re,1}$ and $K_{un,3} \cong K_{re,1}{}'$).

(2) Subsequently, stiffness is restored in the wall and a linear branch is identified up to displacement corresponding to about 80% of maximum displacement, $\delta_{re,2}$ and $\delta_{re,2}{}'$, corresponding to the force $F_{re,2}$ and $F_{re,2}{}'$, respectively. The slope of this branch is given by $K_{re,2}$ and $K_{re,2}{}'$.

(3) After the displacement $\delta_{re,2}$ and $\delta_{re,2}{}'$, the wall behaves in the transition between linear and plastic regime and the stiffness is characterized by $K_{re,3}$ and $K_{re,3}{}'$, which describes the stiffness of the branch until the maximum load is reached.

Mathematically, the constitutive law is defined by expressions in positive (5.5) and negative (5.6) branches:

$$\begin{cases} F = F_r + K_{re,1}\delta & 0 < |\delta| \le |\delta_{re,1}| \\ F = F_{re,1} + K_{re,2}(\delta - \delta_{re,1}) & |\delta_{re,1}| < |\delta| \le |\delta_{re,2}| \\ F = F_{re,2} + K_{re,3}(\delta - \delta_{re,2}) & |\delta_{re,2}| < |\delta| \le |\delta_{max}| \end{cases} \quad (5.5)$$

$$\begin{cases} F = F_r{}' + K_{re,1}{}'\delta & 0 < |\delta| \le |\delta_{re,0.3max}{}'| \\ F = F_{re,1}{}' + K_{re,2}{}'(\delta - \delta_{re,1}{}') & |\delta_{re,1}{}'| < |\delta| \le |\delta_{re,1}{}'| \\ F = F_{re,2}{}' + K_{re,3}{}'(\delta - \delta_{re,2}{}') & |\delta_{re,2}{}'| < |\delta| \le |\delta_{max}{}'| \end{cases} \quad (5.6)$$

Where:

F is the generalized force;

F_r and $F_r{}'$ are the residual forces corresponding to zero displacement;

$F_{re,1}$ and $F_{re,1}{}'$ are the forces corresponding to displacements $\delta_{re,1}$ and $\delta_{re,1}{}'$, respectively;

$F_{re,2}$ and $F_{re,2}{}'$ are the forces corresponding to displacements $\delta_{re,2}$ and $\delta_{re,2}{}'$, respectively.

As expected, the degradation of strength is a parameter that characterizes the tension-compression cyclic behaviour. Thus, it is important to calculate the variation of strength between subsequent cycles, represented in Figure 5.3 by ΔF. In the cycle *i*, the variation can be calculated using the difference between F_{max} or $F_{max}{}'$ and F_{max}^{i-1} or $F_{max}^{i-1}{}'$. The last forces (F_{max}^{i-1} or $F_{max}^{i-1}{}'$) can be obtained considering the slope $K_{re,3}$ and $K_{re,3}{}'$ of the cycle *i*, and the displacement that correspondents to the maximum load in previous cycle (i-1), defined by $\delta_{max}^{i-1}{}'$ or $\delta_{max}^{i-1}{}'$.

5.4. Model validation based on cyclic tests

5.4.1. Tension and compression cyclic tests

According to constitutive laws presented above, the analytical hysteretic envelope was obtained for tested tie connections under tension-compression loading as shown in Figure 5.4. The model was constructed based on the average curve of each type of tie under tension-compression loading. The adequacy of hysteresis loops for ties T2 and T4 is very good, given the good fit between analytical and experimental diagrams. With this respect, it is stressed that it is possible to represent very well the pinching resulting from accumulated damage by the plateau observed in the unloading branch of the hysteretic response.

After the evaluation of the hysteresis loops, it should be mentioned that in the pre-peak regime at lower displacement levels because, the onset of the nonlinearity is not very well captured. However, the error is lower than 10%.

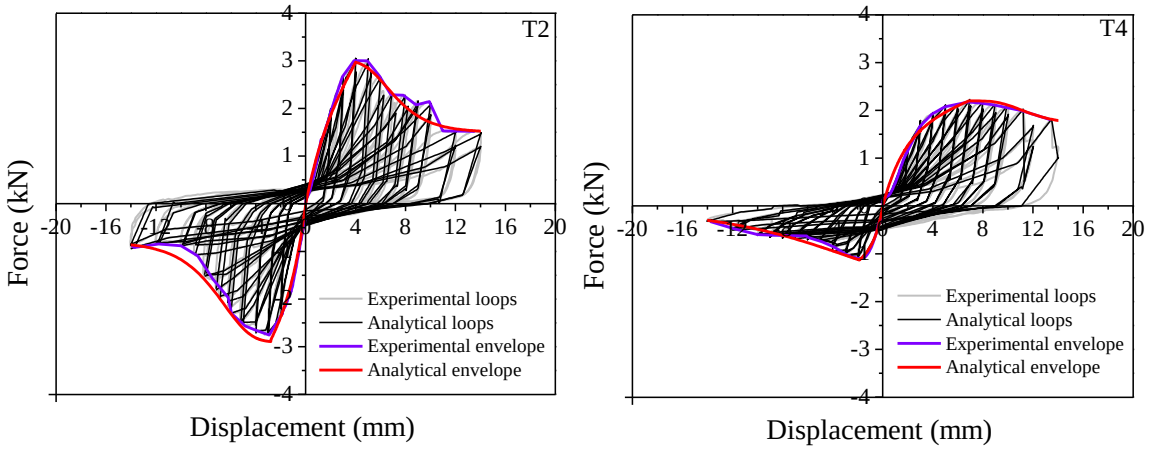

Figure 5.4 – Comparison between experimental results and analytical hysteresis for (a) T2 and (b) T4 tie typology under tension-compression loading

5.4.2. Shear cyclic tests

From Figure 5.5, it is possible to assess the performance of the analytical model to force vs displacement hysteric loops obtained under shear loading. It is observed that the analytical loops fits very well experimental hysteresis loops. Inclusively, the envelope curve is practically the same as the one obtained experimentally. Only on unloading path, between plastic and null deformations, the analytical law was not perfect because the experimental hysteresis presented nonlinearities not very well captured by the model. In case of connections with tie T4, only the pre-peak envelope curve was designed because the post peak behaviour is unknown.

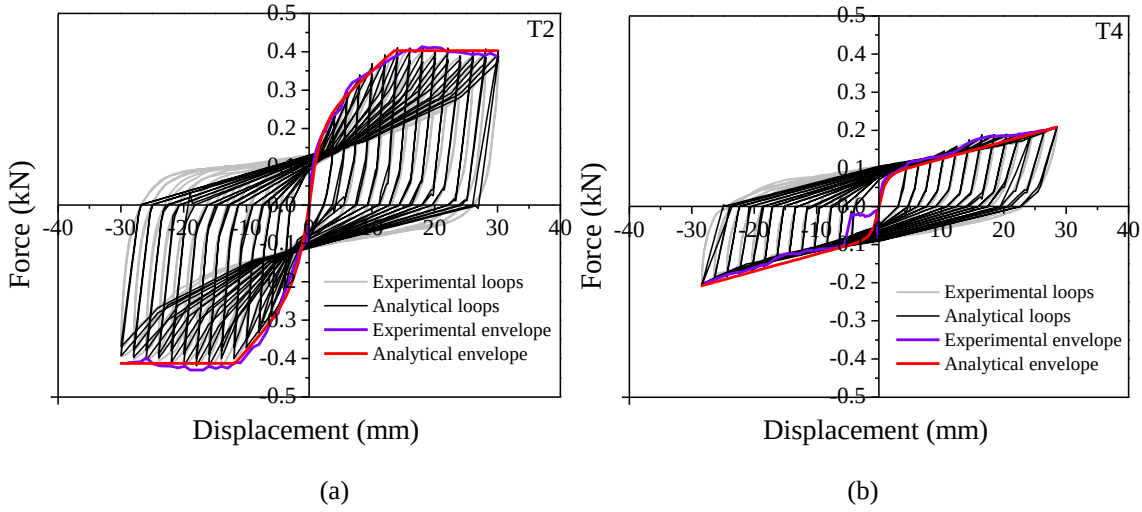

Figure 5.5 – Comparison between experimental results and analytical hysteresis for (a) T2 and (b) T4 tie typology under shear loading

5.5. Prior shear loading in tension and compression response

In order to understand the influence of shear damage in tension and compression response of tie-masonry connections, three of individual samples (MIL and MVL specimens) subjected to shear loading were further tested under tension-compression cyclic loading. The displacement protocol was the same as the one used for undamaged connections (Chapter 4), to make the comparison of results possible. With this comparison, it is possible to evaluate the influence of the extent of damage induced under shear loading in the tension-compression behaviour. This procedure enables also to take into account the combination of efforts: shear, tension and compression loadings. In practice, the goal is to reproduce the combination of in-plane and out-of-plane behaviour of local connections on a wall when submitted to seismic actions.

5.5.1. Force-displacements diagrams

An overview of the average force-displacement diagrams obtained for damaged and undamaged individual connections in presented in Figure 5.6 for specimens MIL and in Figure 5.7 for specimens MVL. It is seen that there is some difference between force-displacement diagrams with and without damage, regarding maximum tensile and compression resistance, initial stiffness and hysteresis behaviour.

In both types of specimens, the tensile resistance is essentially affected by prior shear damage in connections with stiff ties, T1 and T6, whereas the compression behaviour is more affected in connections with flexible ties, T3-T5 ties. Not always the previous damage causes decrease of resistance taking into account that in majority of cases, the hysteretic loops in samples with previous shear damage are almost overlapped with in original response (T1, T2 and T6 under compression loading, and T2-T5 under tension loading). The previous damage affected essentially the connections performance when the ties were not so good. Indeed, when the connections performances are compared, the undamaged connections with T1 and T6 exhibited a better compression behaviour and a weaker tensile behaviour and the connections with T3-T5 exhibited a weaker compression behaviour and a better tensile performance. The connections with wall tie T2 were not much affected by prior shear damage under tension and compression loading.

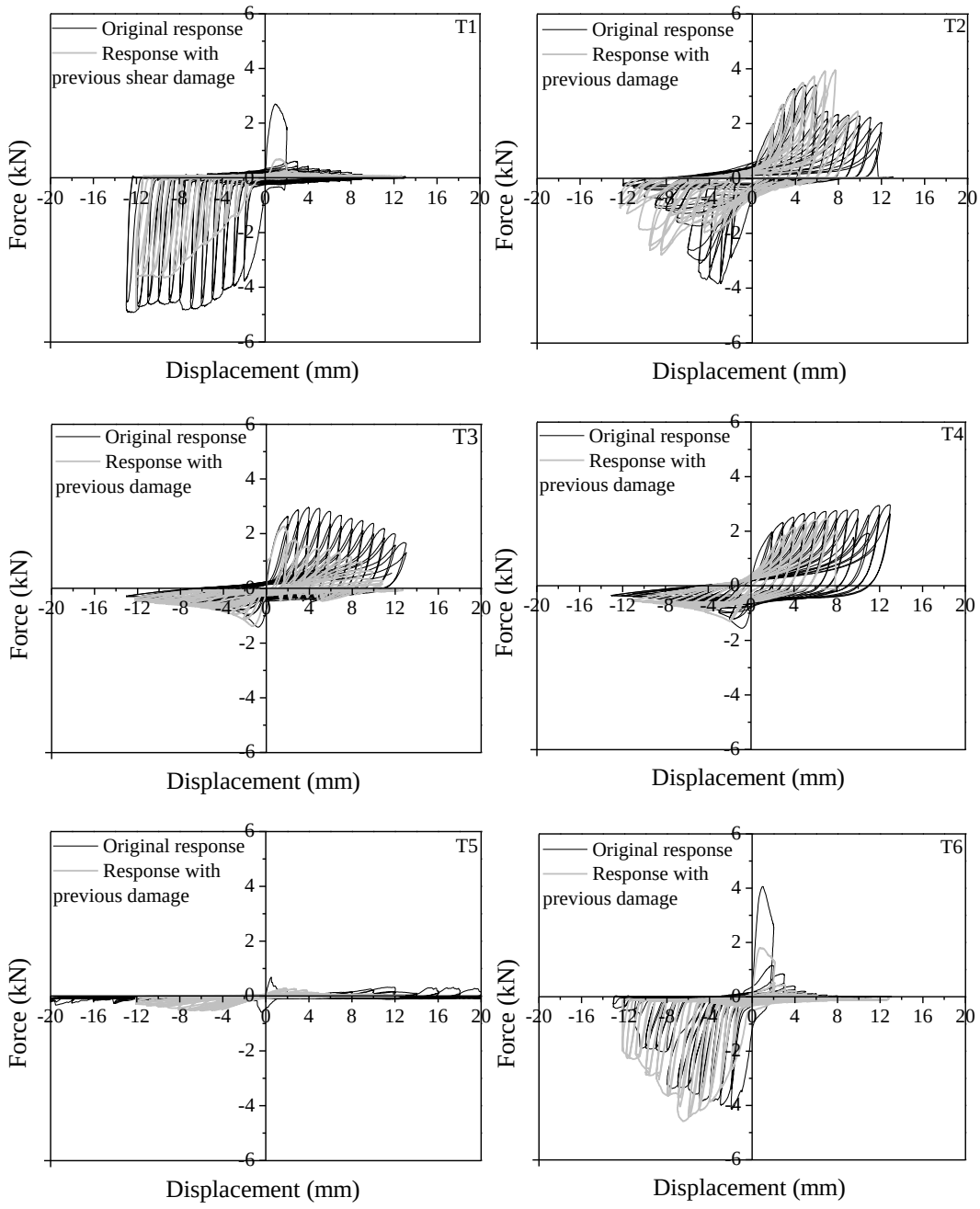

Figure 5.6 – Average force vs displacement curves for each tie typology on MIL under tension compression loading with previous shear damage

Besides that, the hysteretic loops are really modified in specimens with previous damage, essentially with regard to the dissipative capacity.

The pinching effect can be seen in the tension-compression force vs displacements, namely in the connections with ties T2, T3 and T4 wall ties. However, it should be mentioned that it is more severe in case of damaged connections with ties T3 and T4.

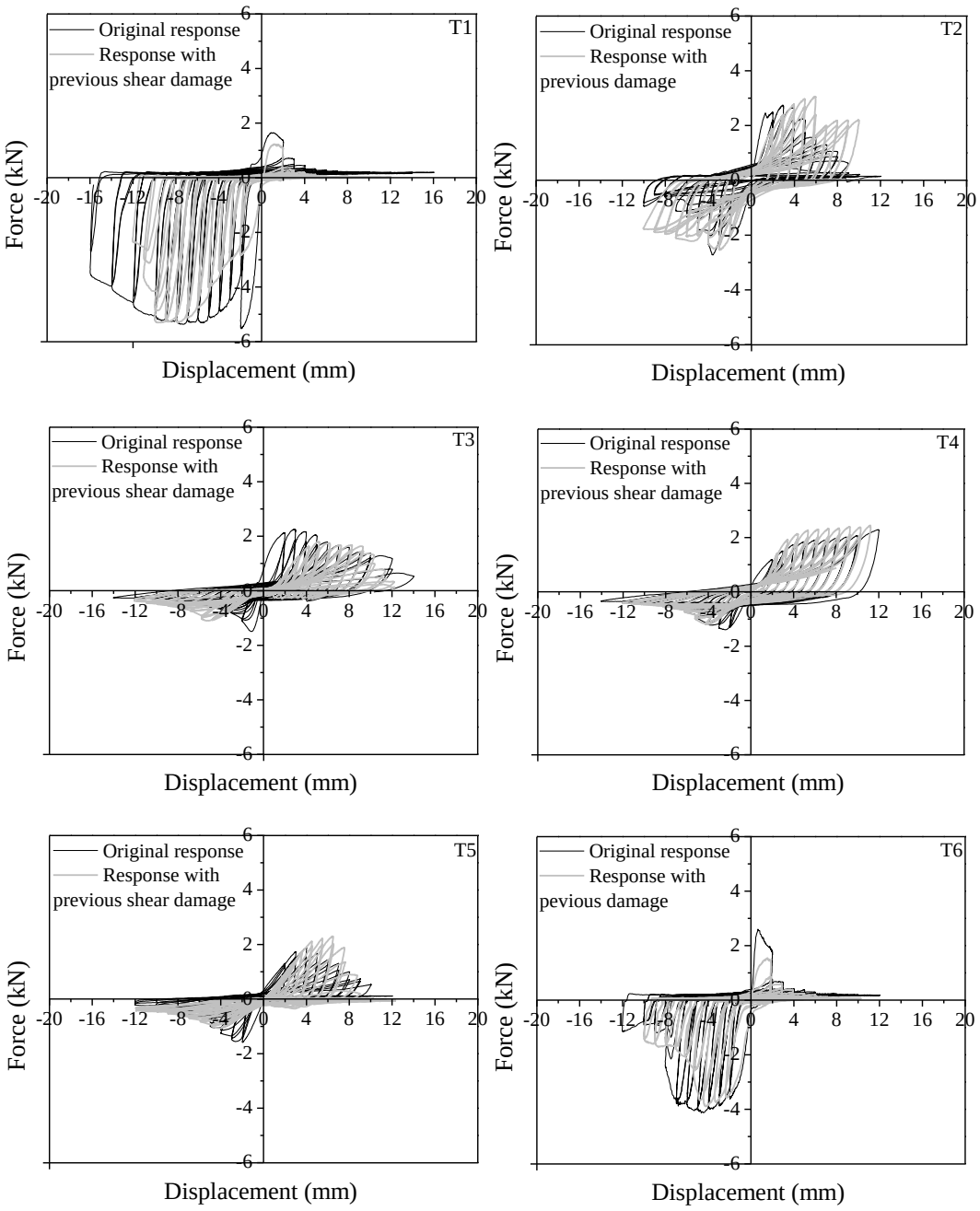

Figure 5.7 – Average force vs displacement curves for each tie typology on MVL under tension compression loading with previous shear damage

5.5.2. Comparison of mechanical parameters: strength and stiffness

The values of maximum strength and initial stiffness under cyclic tension and compression loading are presented in Table 5.2 and Table 5.3, respectively. Additionally, these values are also plotted in Figure 5.8 and Figure 5.9 for a better understanding of the variation between the specimens with and without previous shear damage.

These values confirm the analysis carried out previously to the force-displacement diagrams. It is seen that in case of tie-masonry infill connections (MIL) a decrease on the tensile strength of about 40% was recorded in case of tie T6 and a reduction of the about 25% was recorded in connections with ties T1 and T3. It is considered that almost no differences were found between damaged and undamaged conditions in case of ties T4 and T5 and in case of tie T2 there is an increase of about 16%. There is no a clear explanation for the increase of the strength, but it can be explained by the scatter found for the connections. For tie-masonry veneer connections (MVL), apart from connection with tie T2, all the other connections present a very significant decrease on the tensile strength, specially connections with ties T3-T5. In case of connection with ties T1 and T5, the decrease is about 70%, roughly 25% in connections with ties T3 and T4 of about 60% in case of connections with tie T6.

Table 5.2 - Mechanical parameters with and without prior shear damage under tension loading (coefficient of variation (%) is inside brackets)

		Tension behaviour					
		F_t (kN)	$F_{t\_shear\ damage}$ (kN)	$\frac{F_{t_{shear\ damage}}}{Ft}$ (%)	K_t (kN/mm)	$K_{t\_shear\ damage}$ (kN/mm)	$\frac{K_{t_{shear\ damage}}}{Kt}$ (%)
Masonry Veneer Leaf	T1	1.62 (22.89)	1.23 (14.52)	76.08	0.70	0.57 (15.23)	81.42
	T2	2.62 (13.14)	3.07 (17.96)	116.95	1.25	1.10 (14.63)	88.00
	T3	2.29 (6.6)	1.80 (22.69)	78.49	1.1	0.23 (18.65)	20.90
	T4	2.42 (10.37)	2.45 (25.63)	101.31	0.70	0.34 (17.52)	48.57
	T5	2.06 (14.28)	2.31 (23.61)	111.84	0.69	0.48 (21.36)	69.56
	T6	2.61 (17.95)	1.55 (14.52)	59.43	0.95	0.78 (25.64)	82.10
Masonry Infill Leaf	T1	2.52 (19.17)	0.75 (21.65)	29.72	1.41	0.24 (26.84)	17.04
	T2	3.59 (16.88)	3.95 (15.23)	110.20	1.23	1.02 (18.97)	83.11
	T3	3.07 (15.76)	2.27 (14.25)	73.99	1.33	1.02 (22.88)	76.89
	T4	3.13 (23.03)	2.46 (11.78)	78.50	1.01	0.81 (15.21)	80.50
	T5	0.91 (14.09)	0.28 (12.96)	30.69	0.13	0.11 (13.47)	82.74
	T6	4.30 (17.73)	1.81 (11.23)	42.09	1.30	0.61 (19.74)	46.79

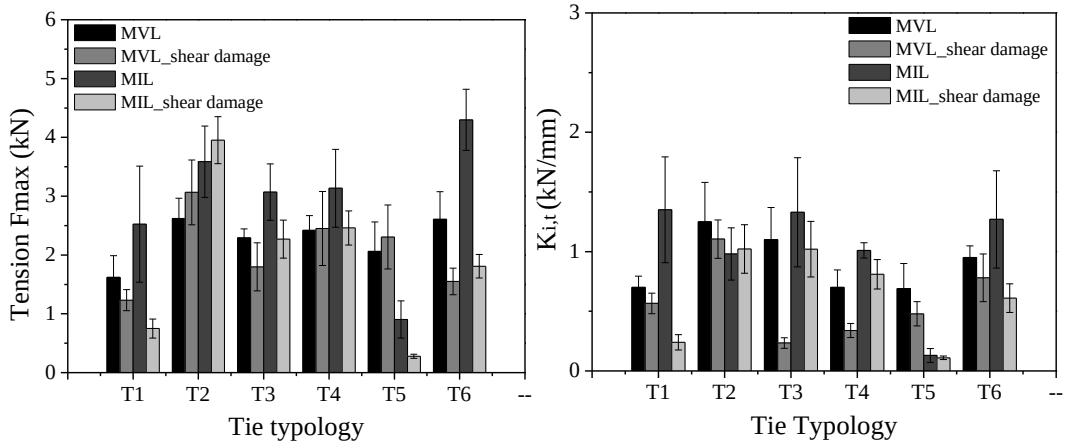

Figure 5.8 – Comparison of tension (a) maximum strength and (b) initial stiffness between MIL and MVL specimens with and without shear damage

On the other hand, under compression, all connection present lower compressive strength in case of connections with previous damage. The lowest decrease of compression strength is recorded in case of tie T1 and T6 (about 5%), whereas the highest decrease occurs in connections with tie T3 (about 25%) and tie T5 (about 42%). In case of individual tie-masonry veneer connections (MVL), apart from connection with tie T6, all the others damaged connections present also lower compression strength and a decrease in average higher when compared with MIL connections. In any case, the results appear to indicate that previous shear damage is important both in cyclic tension and compression behaviour, but the percentage of decrease depends on the type of tie.

Table 5.3 – Mechanical parameters with and without prior shear damage under compression loading

		Compression behaviour					
		F_c (kN)	$F_{c\_shear\ damage}$ (kN)	$\frac{F_{c_{shear\ damage}}}{Fc}$ (%)	K_c (kN/mm)	$K_{c\_shear\ damage}$ (kN/mm)	$\frac{K_{c_{shear\ damage}}}{Kc}$ (%)
Masonry Veneer Leaf	T1	5.54 (4.60)	5.31 (9.23)	95.88	2.81 (9.60)	2.43 (14.32)	86.48
	T2	2.82 (12.67)	2.54 (11.32)	90.10	1.82	1.30 (11.52)	71.43
	T3	1.46 (5.68)	1.10 (14.25)	75.35	0.62	0.21 (26.32)	33.87
	T4	1.50 (15.23)	1.20 (18.69)	80.09	0.65 (3.60)	0.29 (22.54)	44.62
	T5	1.82 (12.38)	1.07 (14.63)	58.68	0.77	0.20 (16.32)	25.97
	T6	4.13 (22.39)	3.90 (21.87)	94.31	1.76	1.55 (11.25)	88.07
Masonry Infill Leaf	T1	4.52 (12.21)	3.55 (16.23)	78.50	1.98	0.41 (14.89)	20.71
	T2	4.09 (13.28)	2.79 (21.11)	68.15	1.5 (29.07)	0.80 (16.78)	53.33
	T3	1.50 (9.37)	1.38 (18.63)	92.19	0.52 (8.84)	0.50 (18.95)	96.15
	T4	1.55 (6.75)	1.29 (14.52)	83.30	0.55	0.24 (21.33)	43.66
	T5	0.92 (19.01)	0.54 (17.65)	57.91	0.12	0.10 (17.58)	100
	T6	4.15 (18.22)	4.59 (18.96)	110.74	2.1 (26.86)	0.41 (19.65)	19.52

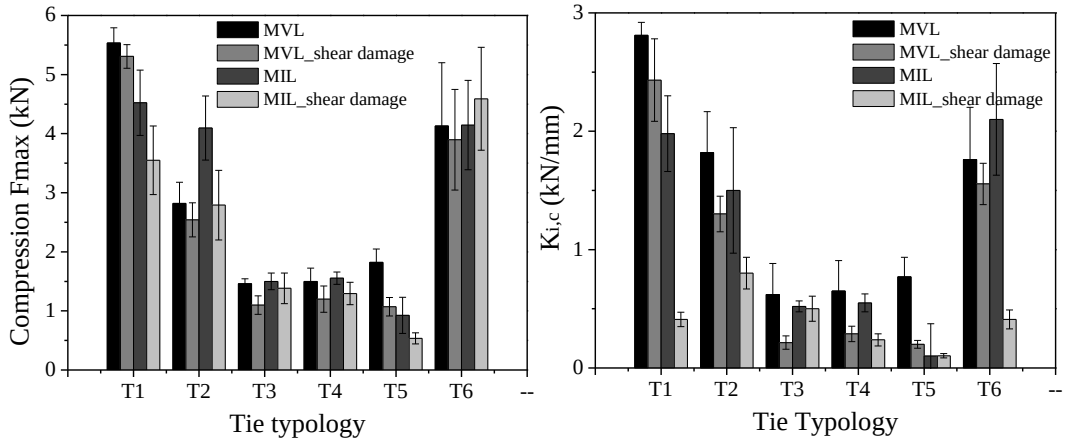

Figure 5.9 – Comparison of compression (a) maximum strength and (b) initial stiffness between MIL and MVL specimens with and without shear damage

The particular influence of previous shear damage in the tie-masonry veneer connections (MVL) under tension, can be associated to the higher deterioration of the tensile bend adherence and to the lower compressive strength of the mortar. Note that resistance of MVL undamaged connections is slightly lower than the resistance of MIL undamaged connections. It is stressed that the connections with tie T2 do not present any strength degradation under tensile loading, which confirm the considerable good performance of this tie.

It is clear also that the prior shear damage reduces the initial stiffness. The reduction level of initial stiffness depends on the tie and loading typologies. For instance, in case of tension and compression loading, the reduction can achieve 80% both in flexible and rigid ties. This means that the influence of prior shear damage on stiffness is rather high. Nevertheless, it would be necessary more number of samples for reduction the variability and to sustain the results.

The stiffness degradation was calculated and compared between specimens with and without damage for each type of tie and presented in Figure 5.10 and Figure 5.11. From the analysis of results, it is observed that the stiffness degradation of connections is greatly influenced by the previous shear damage. In most cases, the greater difference is seen for lower deformation levels. When deformation increase, the difference between samples with and without shear damage decreases, because the damage increase and the samples with previous damage and without any previous damage become very similar. In the majority of cases, the trend of stiffness loss is much smoother in samples with previous shear damage because the initial values are very low, when compared to the samples without damage.

The stiffness loss in the second cycle of each displacement level is higher in ties under compression loading, such as in ties T1 and T6 ties. In these cases, the reduction on the

stiffness in specimens with previous shear damage attains about 50% for low displacement levels.

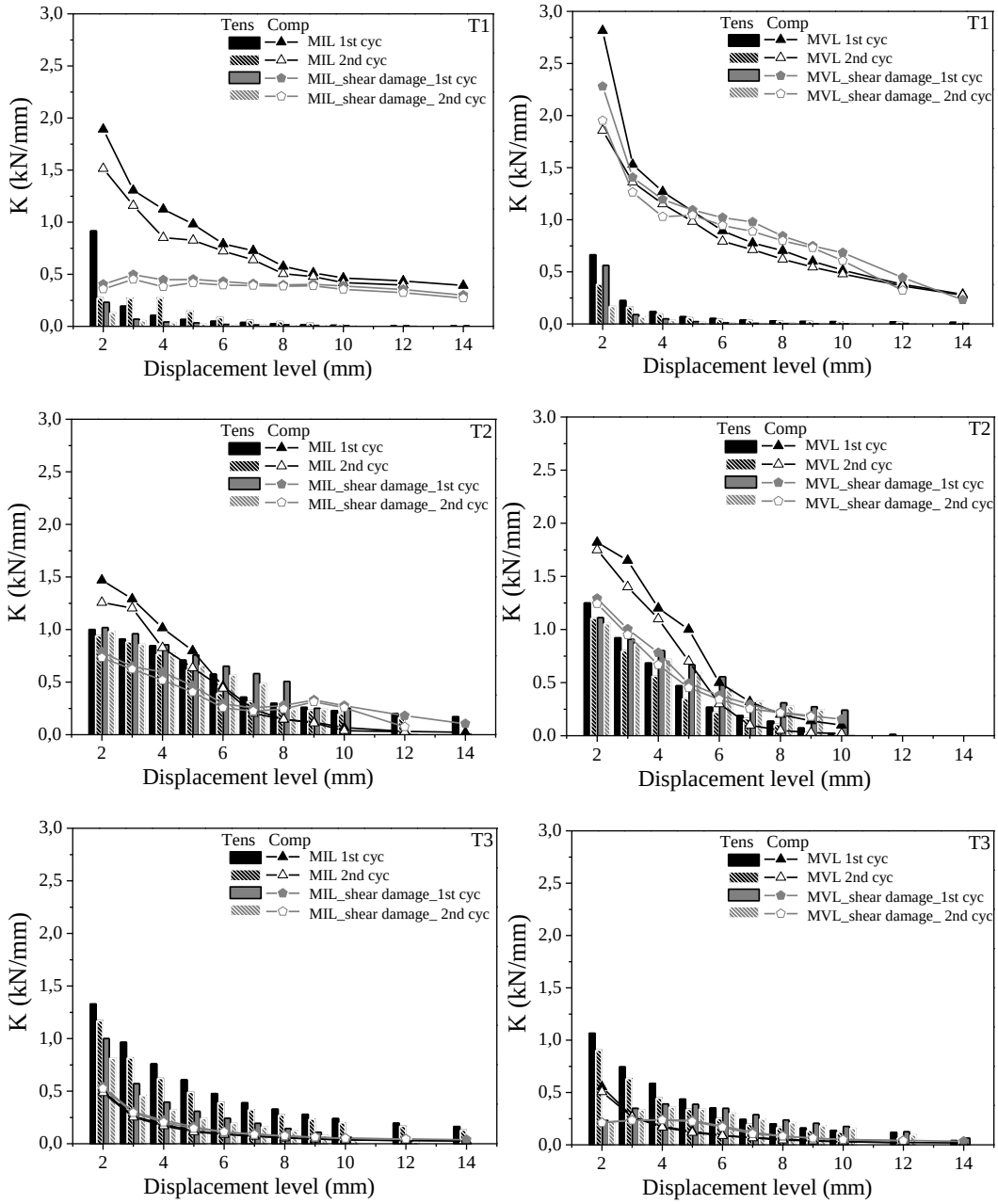

Figure 5.10 – Stiffness degradation of T1, T2 and T3 wall ties connections with and without shear damage in MIL and MVL connections

This is explained by the early loss contact of the tie from the mortar of masonry prims, resulting in non-recovery of the initial stiffness. In the remaining samples, the trend of loss of stiffness when increase the displacement level is not so severe, being at maximum about 20%. This means a positive feature because reveals that the connection is recovery yet through interlocking of tie on mortar caused by geometry of tie. In compression loading this effect is different and it is not so visible taking into account that the behaviour of connection

is very dependent on the individual behaviour of tie, which in turn is associated to the buckling resistance.

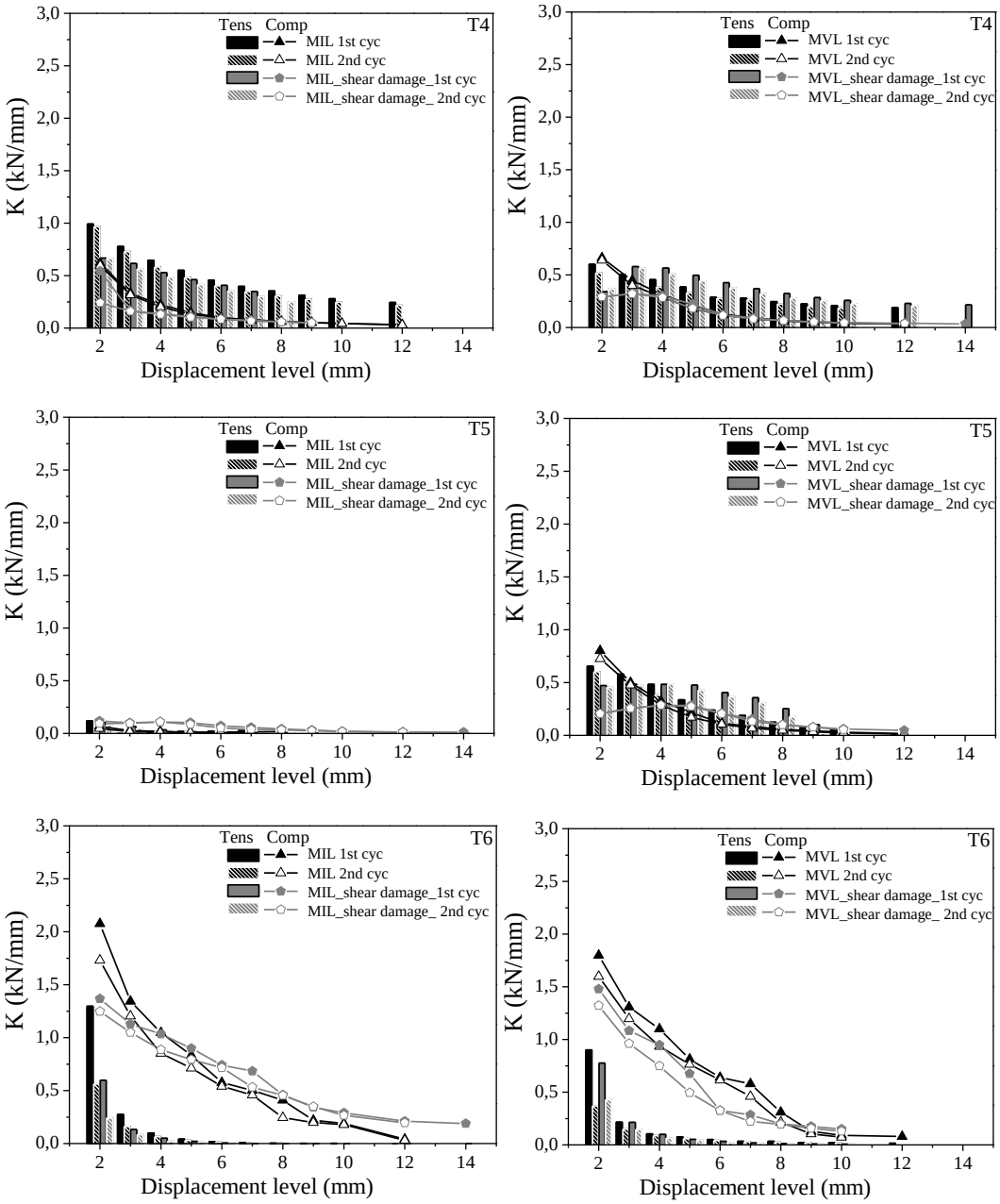

Figure 5.11 – Stiffness degradation of T4, T5 and T6 wall ties connections with and without shear damage in MIL and MVL connections

5.5.3. Dissipation of energy and Equivalent Viscous Damping Ratio (EVDR)

As far as the dissipation energy is concerned, a direct comparison between energy dissipation between damaged and undamaged connection can be carried out through Figure 5.12 and

Figure 5.13 for MIL and MVL connections. These diagrams show that the hysteresis of connections with damage are considerable different from the connection without damage.

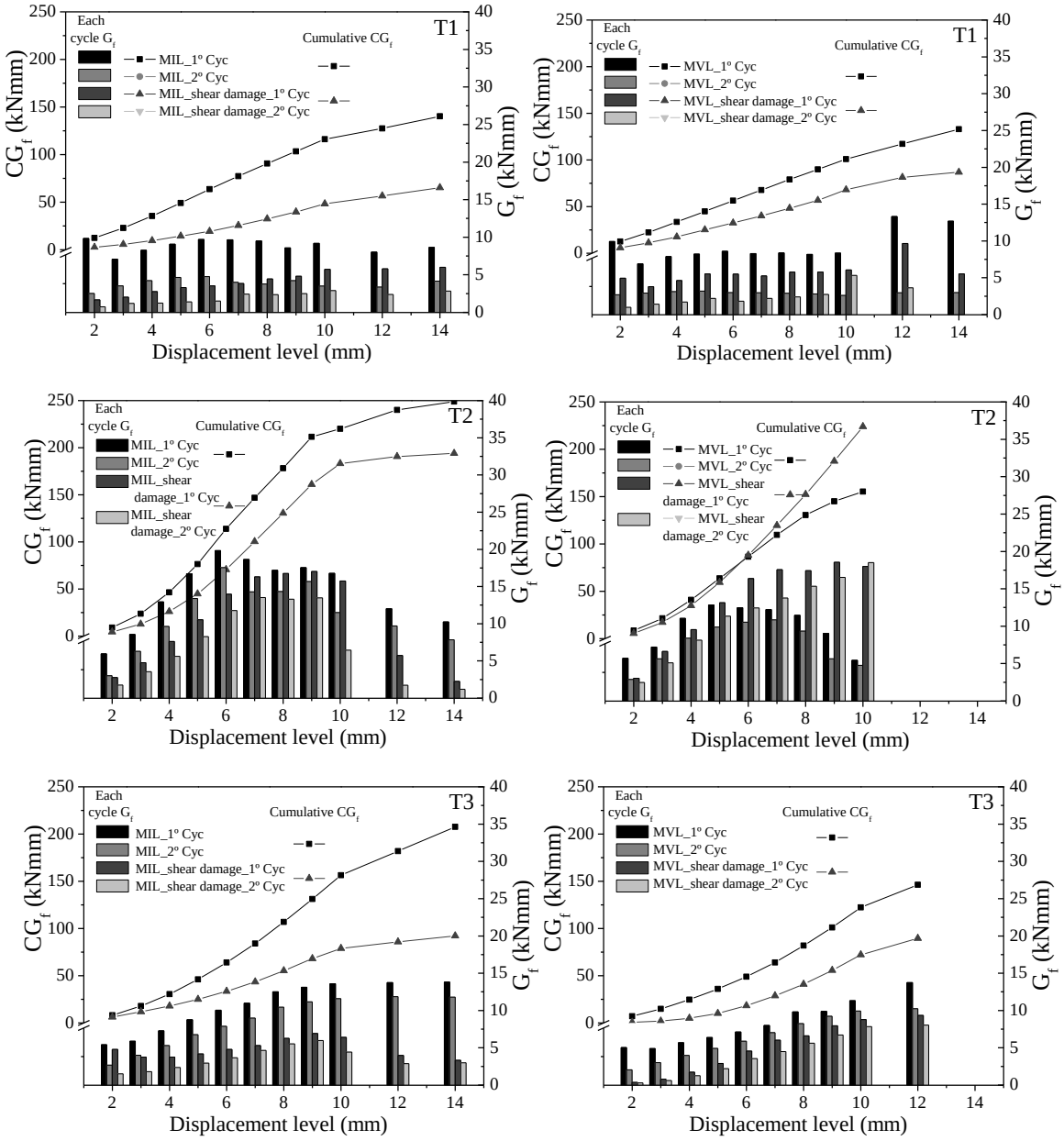

Figure 5.12 – Cumulative dissipated energy for T1, T2 and T3 tie typologies in each type of sample with and without shear damage

It is seen that all connections with prior shear damage exhibited lower capacity to dissipate energy during the cyclic tension-compression loading. In connections with tie T1 and T3 there is a considerable reduction of cumulative dissipation of energy if the comparison is made between the first and second cycles. In both assemblies (MIL and MVL), the reduction of the capacity to dissipate energy when submitted to previous shear loading is very clear (higher in connections MIL). Also in these connections, the reduction between the energy dissipation between the first and second cycles is lower in case of connections with prior

shear damage. This can be explained by the typology of tie and existing damage. In case of connection with tie T5, the values of energy dissipation are very low and despite there is a reduction of dissipation of energy in the damaged specimens, the difference is much lower. In spite of a reduction of energy dissipation in the damaged connections, it should be stressed that connections T1-T4 keep a very reasonable ability to dissipate energy, which is very important in earthquakes events to keeps the functional connections. In addition, it is seen that the trend and evolution of dissipative response follow the trend recorded in the undamaged connections. This appears to indicate that the robustness of the seismic response of brick veneer walls can be assured by the adequate behaviour of ties, as they seem to keep the ability to work under out-of-plane loading, even after shear damage.

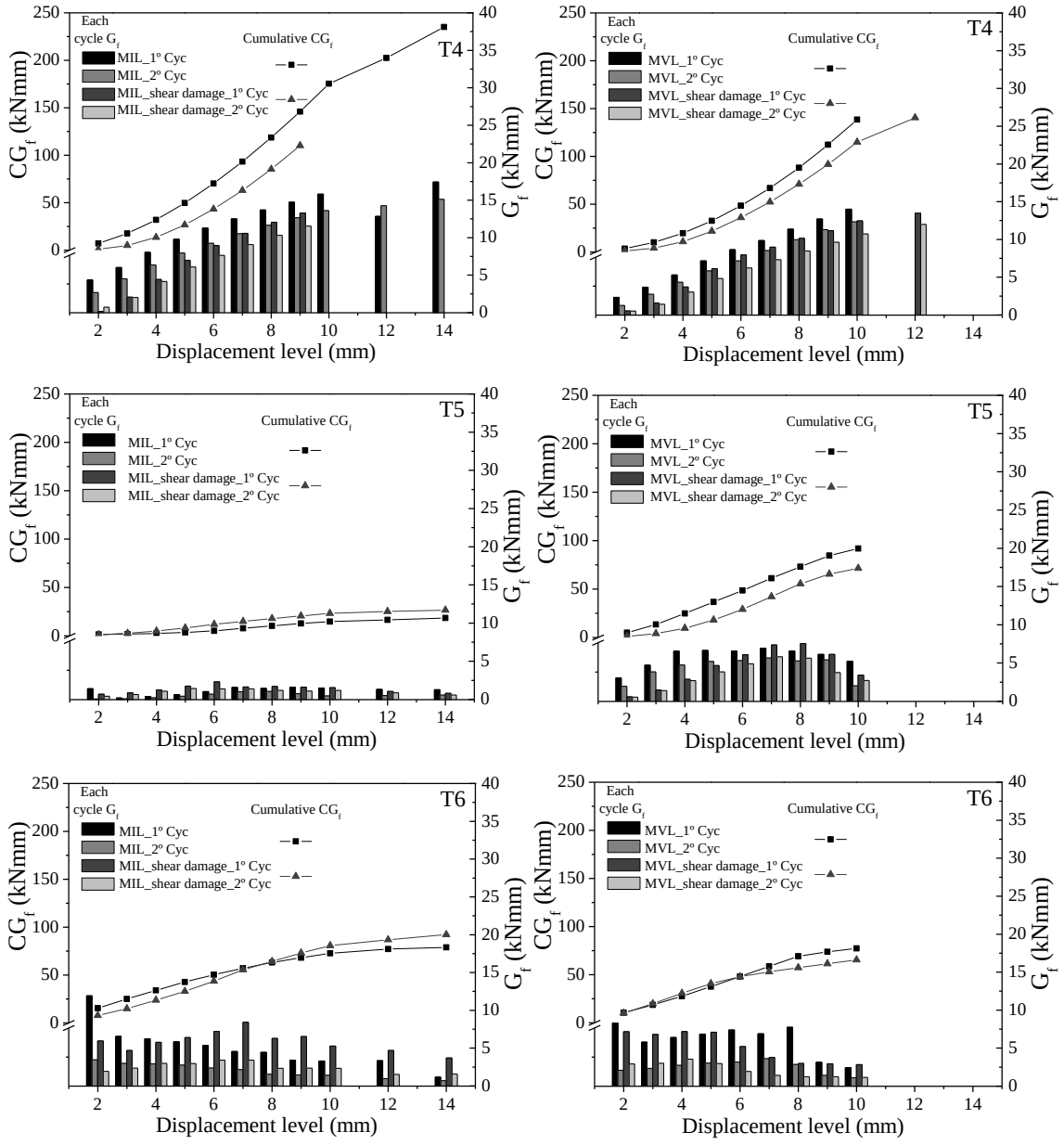

Figure 5.13 – Cumulative dissipated energy for T4, T5 and T6 tie typologies in each type of sample with and without shear damage

Similar conclusions can be drawn in relation to the equivalent viscous damping ratio measured for the connections (Figure 5.14 and Figure 5.15). Values of damping of connections are influenced by pinching. In fact, damaged connections presented lower values of damping. This can be explained by the existing damage and by the consequent more severe pinching observed in damaged specimens, even if the input energy is the same. In any case, despite in a lower extent, it is seen that the damaged connections keep ability to dissipate energy when submitted to tension-compression loading. The trend observed in EVDR values of damaged connections is the same of the undamaged connections trend.

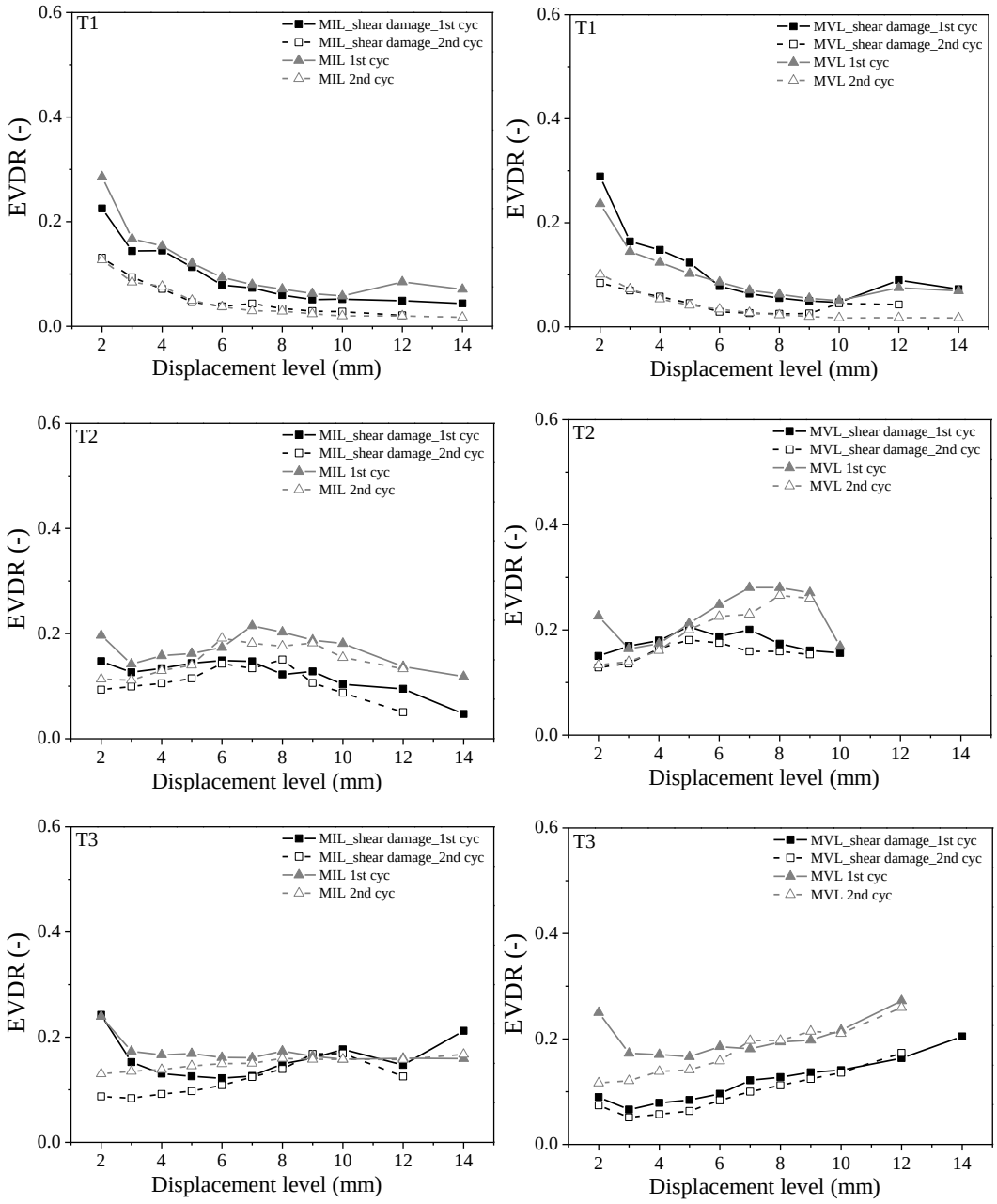

Figure 5.14 – Equivalent viscous damping ratio for T1, T2 and T3 wall ties in connections with and without shear damage

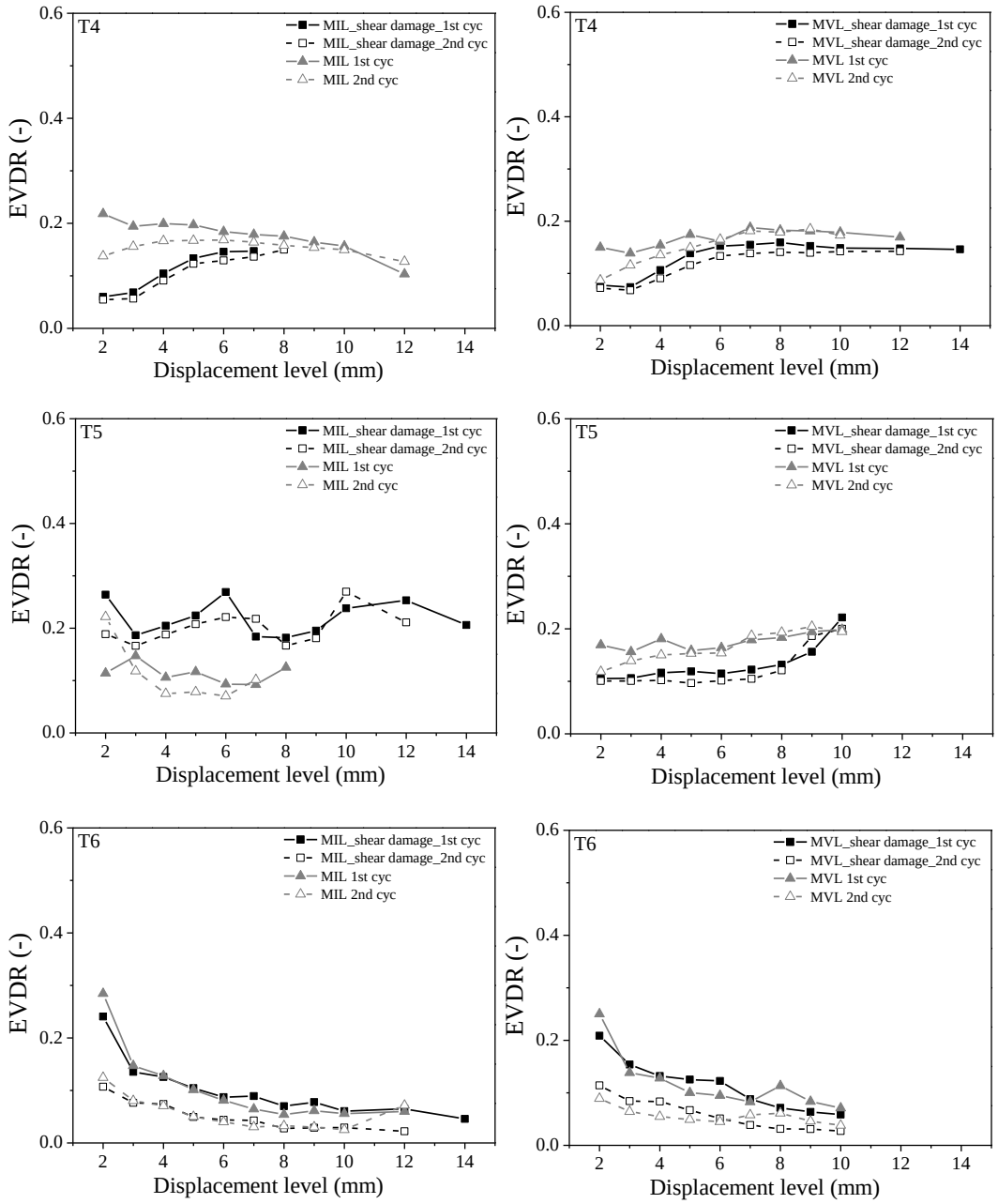

Figure 5.15 – Equivalent viscous damping ratio for T4, T5 and T6 wall ties in connections with and without shear damage

5.6. Experimental parametric study

As mentioned in the beginning, a complementary experimental study was carried out in order to understand the influence of different parameters in the response under compression and tension cyclic loading. For this, double leaf assemblies were considered and four specimens were constructed for each variable.

The construction methodology used in previous study, namely workmanship, was exactly the same used in this campaign. The connections under study were built with ties T1, T2, T3 and T4 typologies, see Table 5.4. In these connections different parameters were varied, according to what is indicated in Table 5.4, namely: (a) mortar strength of masonry infill prism according to different classes of mortar (M5 and M10); (b) air cavity width (75mm and 100mm); (c) embedment length on masonry veneer and infill prims. The variation of the embedment length in both veneer and infill masonry prims is indicated in Table 5.4 and varies according to the length of the tie.

The nomenclature of the specimens describes the different features of connections: "tie typology_air cavity_tie length_mortar class". The results of previous tie-masonry connections "Tie typology_100_225_M10*" are also presented herein as they are considered as the reference for the comparison of results.

Table 5.4 – Different properties of connections for each tie assembly in this study

Samples	Mortar typology	Air cavity width	Tie length	Embedment length on masonry veneer	Embedment length on masonry infill
T1_100_225_M10*	M10*	100	225	60	65
T2_100_225_M10*				60	65
T3_100_225_M10*				60	65
T4_100_225_M10*				60	65
T1_100_225_M5	M5	100	225	60	65
T2_100_225_M5				60	65
T3_100_225_M5				60	65
T4_100_225_M5				60	65
T1_100_200_M10	M10	100	200	60	45
T3_100_200_M10				60	45
T4_100_200_M10				60	45
T1_75_200_ M10	M10	75	200	60	65
T3_75_200_ M10				60	65
T4_75_200_ M10				60	65
T1_75_225_ M10	M10	75	225	85	65
T2_75_225_ M10				85	65
T3_75_225_ M10				85	65
T4_75_225_ M10				85	65

The mortar used on the veneer masonry prims was the same as the one used in previous experimental campaign (Chapter 4) and the average compressive strength is presented in Chapter 3. In infill the brick infill prisms, two mortars were considered: general purpose M5 with an expected compressive strength of 5MPa and a mortar of class M10, with an expected

compression strength of 10MPa. The mortar M5 was used to vary mechanical properties regarding to previous study mortar and M10 mortar was used theoretically to keep the same properties that previous study. Unexpectedly, the mechanical flexural and compressive strength were higher than the prescribed strength at 28 days (Chapter 3). The mortar M5 presented an average compressive strength of 5.5 MPa (COV of 4%) and a flexural resistance of 3.2 MPa (COV of 12%). These properties are very close to obtained in M10* mortar used in previous study, which presented an average compressive strength of 6 MPa (COV of 3%) and an average flexural strength of 2.5 MPa (COV of 6%). The new assemblies have been built with a mortar M10 that presents an average compressive strength of 12 MPa (COV of 4%) and an average flexural strength of 8 MPa (COV of 3%). These values are greater than the values presented by mortar M10*.

The setup configuration was the same as the one used in Chapter 4 in order to keep the same testing conditions between the different specimens. Only for time reasons the time-history was changed and it is presented in Figure 5.16. The cycle amplitude of cycle i is the amplitude of cycle i-1 more 2mm, instead of previous tests that was the amplitude of cycle i-1 more 1mm.

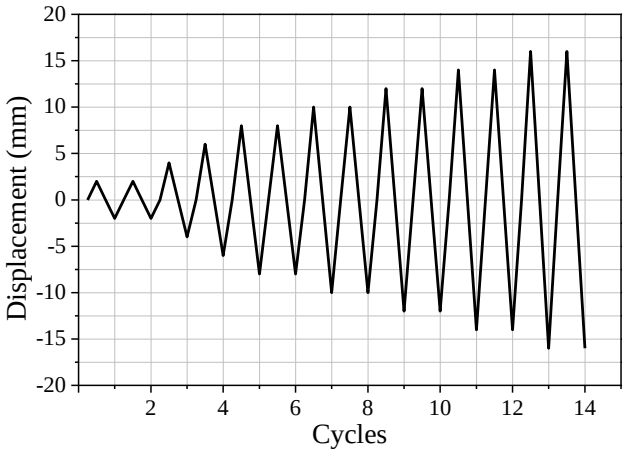

Figure 5.16 – Time-history used in second campaign of experimental evaluation of wall ties.

The results obtained in the experimental campaign to be presented and discussed are based on the force-displacement diagrams. From these diagrams, the main key parameters, such as strength, stiffness and energy dissipation, can be calculated to characterize the cyclic tension-compression behaviour. The failure modes are also analysed to understand behaviour of connections in detail.

5.6.1. Force-displacement diagrams

The behaviour of the double leaf tie-masonry connections under cyclic tension-compression loading was evaluated for each type tie considered and is presented from Figure 5.17 to Figure 5.20.

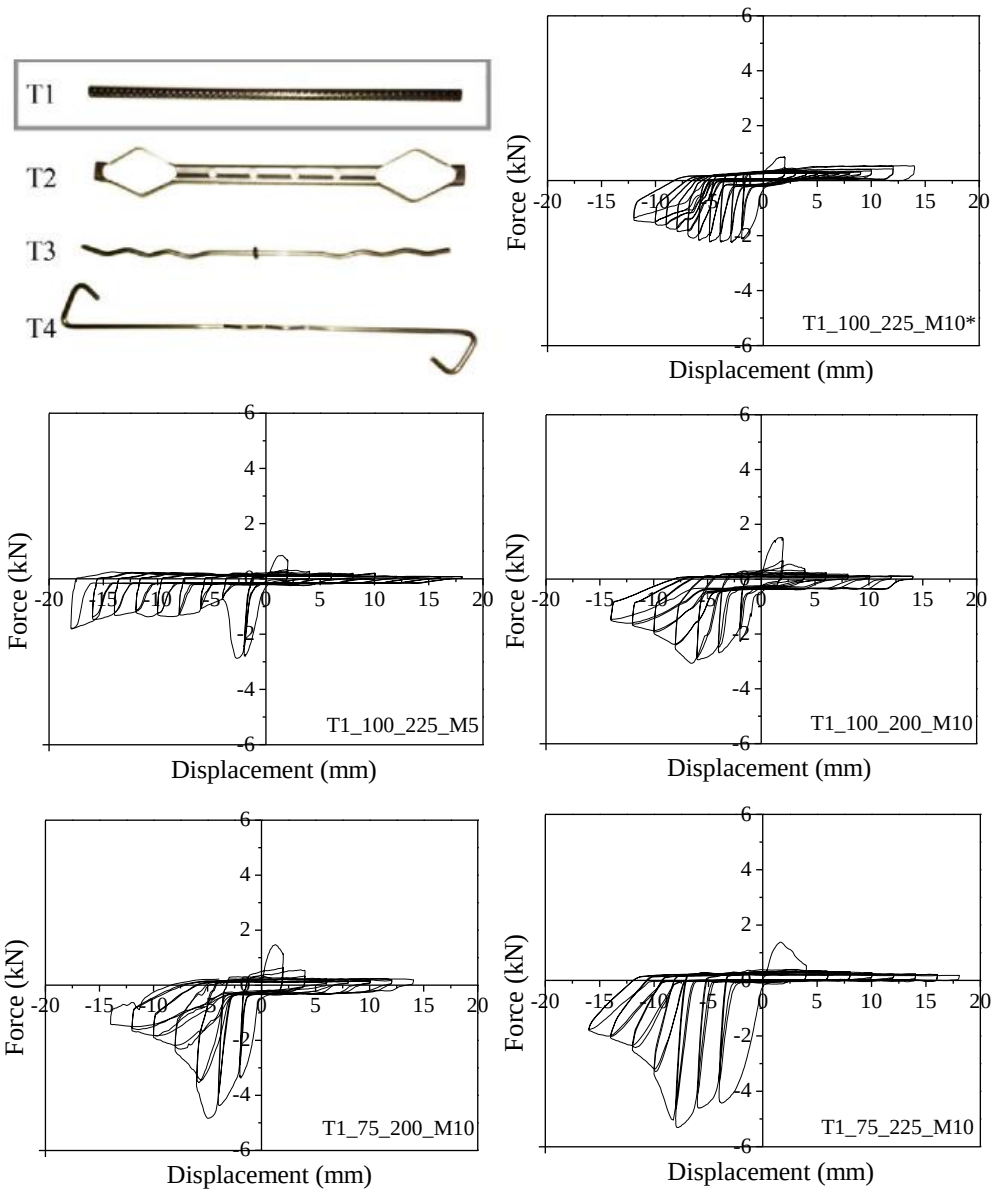

Figure 5.17 – Average force vs displacement curves for T1 tie typology on each parameters combination

The cyclic tensile-compression behaviour obtained for the different types of connections is similar the hysteresis behaviour of the reference specimens. The nonlinear hysteretic behaviour starts at early stages of displacements. Independent on the parameters under analysis, the tensile-compression behaviour is characterized by an asymmetric response in tension and compression, particularly in connection with ties T1, T3 and T4, which is attributed to the different geometry of the ties. In case of the connections with tie T2, the

reference specimens present an almost symmetric behaviour, but the use of a mortar with lower strength in the masonry brick infill prims and the air cavity width appears to contribute for the different behaviour of the connection under cyclic tension-compression. Pinching effects is less pronounced in subassemblies that presented higher tensile and compression resistances, taking into account their more resistance and dissipative behaviour. Even so, with the increase in displacements in all samples, the pinching effect becomes more pronounced.

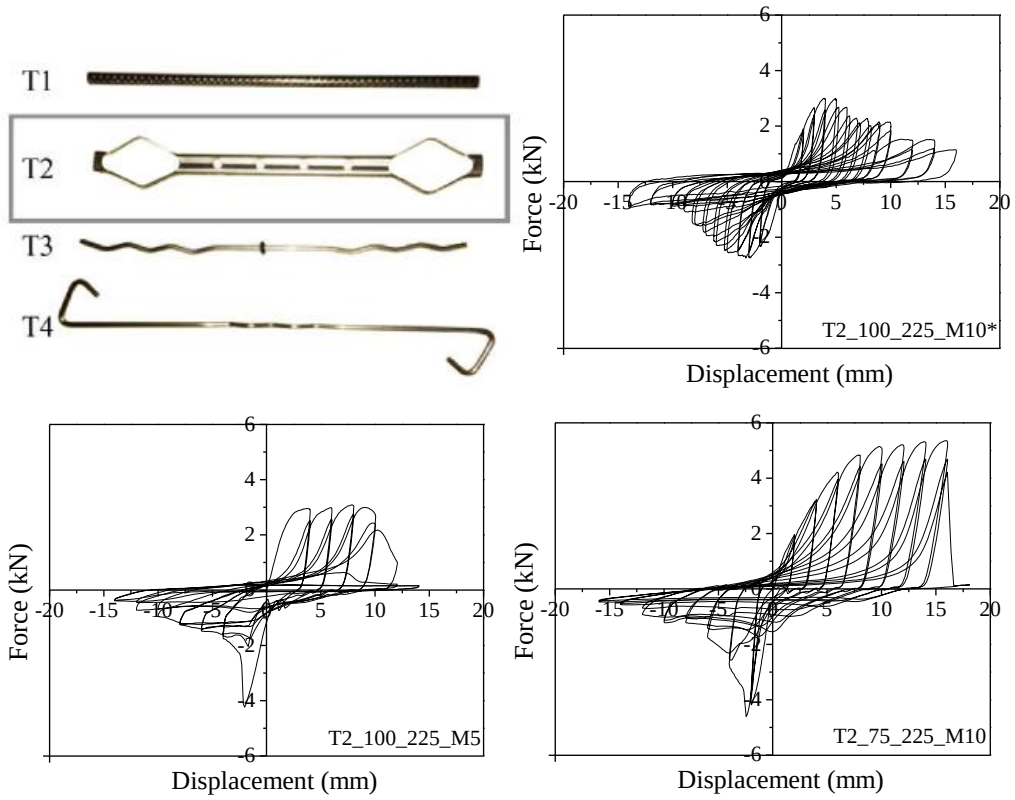

Figure 5.18 - Average force vs displacement curves for T2 tie typology on each parameters combination

It is also observed that, even when all parameters are considered, the connections with tie T3 and tie T4 exhibit a very interesting tensile behaviour, due to reasonable anchorage given by the geometry of the extremity of the ties. This justify that the use a thin tie can provide a good bond adherence under tension and adequate to out-of-plane behaviour. However, under compression loading, these connections (T3 and T4) present a poorer performance. The reduced diameter of the cross section of ties T3 and T4 justifies the difference in the tensile and compression maximum forces attained in connection assemblies with these ties.

Connections with tie T1 present low resistance under tensile loading but a good behaviour in compression loading due to higher cross section. This is valid for all parameters under analysis, namely variation of the mortar strength, air cavity width and embedment length of the tie. In these case, the compression strength is considerably higher than the tensile

strength, which is attributed to the distinct resisting mechanisms involved in the tensile and compression loading. The tensile resistance is controlled by the bond adherence of the ties to the bed joint mortar, whereas the compression strength is much more attributed to the behaviour of the ties under compression, which is dependent on the geometry of the cross section at the lower trend to buckle. The plane surface of tie T1 result in the reduced bond adherence to the bed joint mortar and thus reduced tensile strength of the connection.

In spite of some asymmetry introduced by the variation of the mortar strength and embedment length, the connection with tie T2 present the more equilibrated behaviour under tension and compression, following the same trend of the reference specimens.

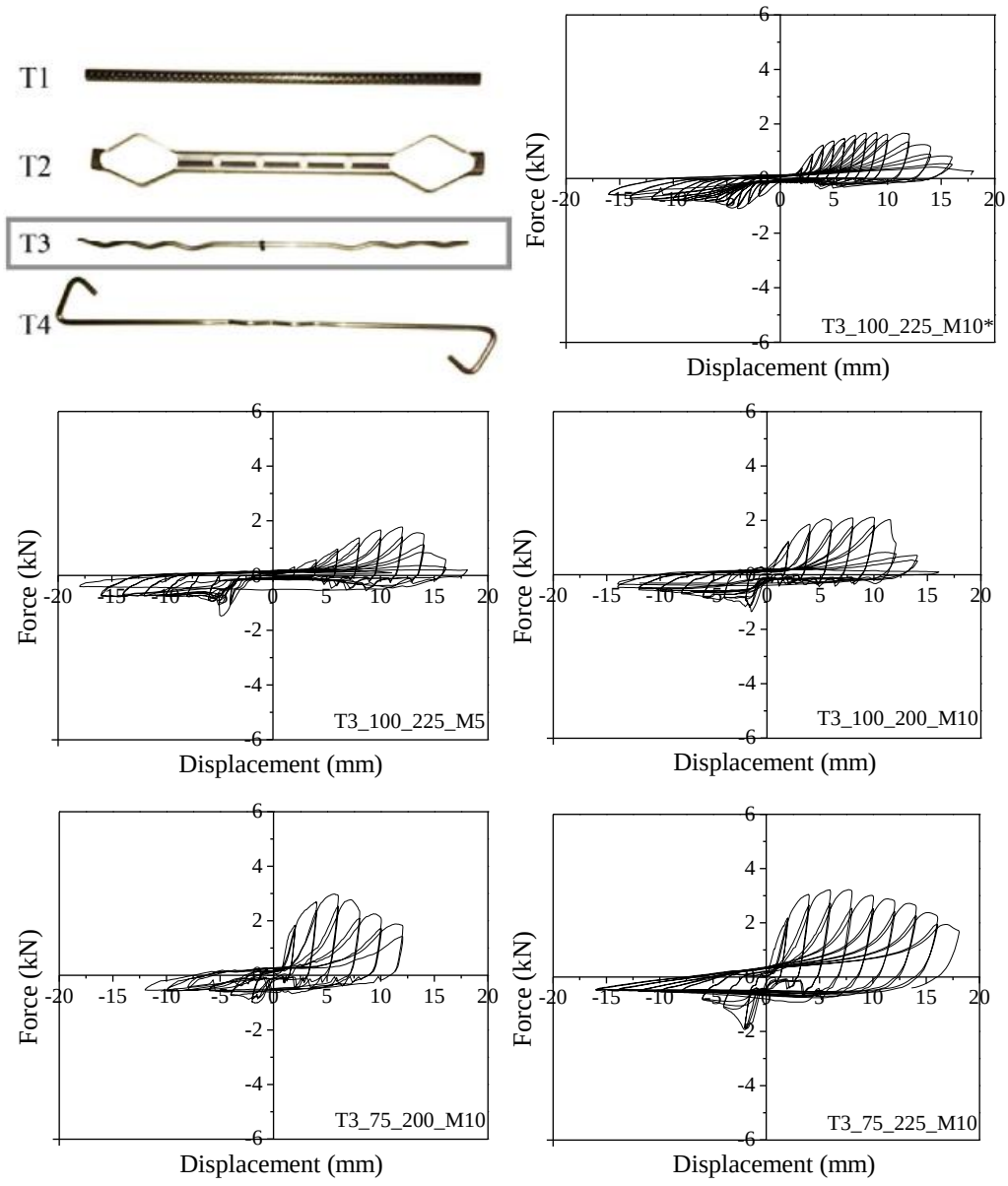

Figure 5.19 - Average force vs displacement curves for T3 tie typology on each parameters combination

As already discussed in Chapter 4, the geometry of this tie became it robust both under tension and compression: (a) the geometry results in a good interlocking at the mortar joints resulting in high tensile bond adherence; (b) the cross section and the shape of the tie lead to reasonable resistance to bucking, leading to considerable resistance under compression.

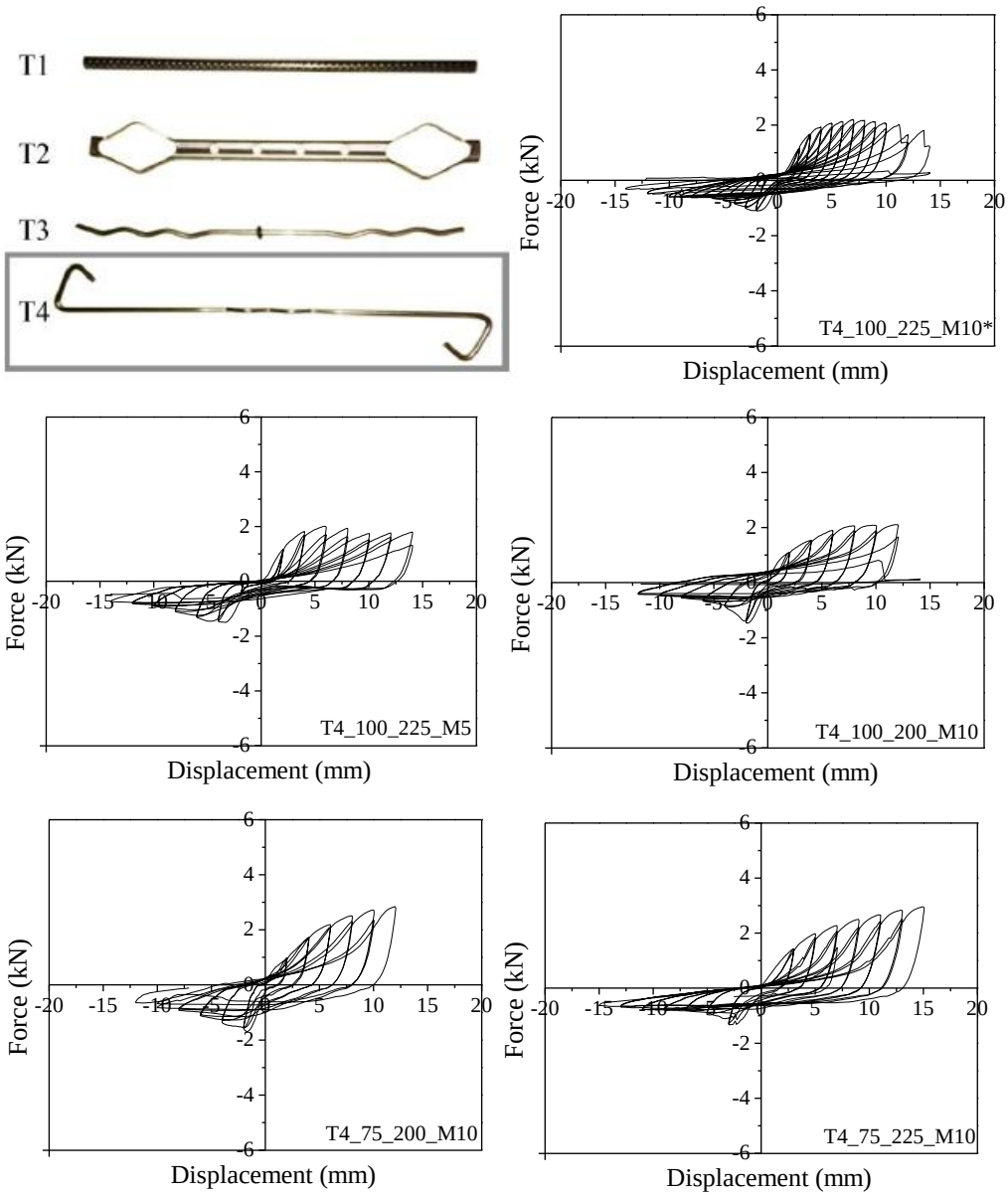

Figure 5.20 - Average force vs displacement curves for T4 tie typology on each parameters combination

The brief analysis of the influence of the different parameters under study enable to observed that: (a) the increase of compressive strength of mortar appears to play a positive role in the tensile and compression resistance of connections with Tie T1; (2) the reduction of the air cavity result in the increase of the tensile strength and in particular in the compressive strength of the connections with tie T1. This is attributed to the decrease of the free length and to the trend to buckle under compression; (c) the increase of the embedment length

results in the increase of the tensile strength, particularly in connections with tie T2, T3 and T4. It has almost no influence in case of the connection with tie T1 because it is not enough to overcome the negative influence of the smooth surface in the tensile bond adherence of the tie to the mortar joint.

5.6.2. Mechanical parameters

From the force-displacement diagrams some key parameters were derived in order to better analyse and compare the different variations defined for the connection, namely: (1) maximum tensile force *(F_t)* and (2) maximum compression force *(F_c)* and (3) initial tensile stiffness *($K_{i,t}$);* (4) initial compression stiffness *($K_{i,c}$).* A summary of the average of the key parameters for each specimen is presented in Table 5.5.

Table 5.5 – Summary of key parameters for each connection

	F_c (kN)	**COV (%)**	**$K_{i,c}$ (kN/mm)**	**COV (%)**	**F_t (kN)**	**COV (%)**	**$K_{i,c}$ (kN/mm)**	**COV (%)**
T1_100_225_M10*	2.61	2.38	1.25	23.53	0.98	13.16	0.47	10.13
T2_100_225_M10*	2.76	25.09	1.24	20.91	3.00	24.00	0.97	18.32
T3_100_225_M10*	1.24	17.6	0.7	20.00	1.66	25.00	0.98	25.00
T4_100_225_M10*	1.11	14.89	0.6	8.92	2.17	4.22	0.58	17.27
T1_100_225_M5	2.88	18.78	1.43	24.36	0.85	14.99	0.56	16.52
T2_100_225_M5	4.24	11.31	2.16	15.36	3.08	17.58	1.27	15.23
T3_100_225_M5	1.48	13.62	0.25	9.58	1.78	15.69	0.13	14.25
T4_100_225_M5	1.50	7.56	0.27	14.87	2.01	8.88	0.58	8.99
T1_100_200_M10	3.07	8.97	1.15	8.47	1.53	9.57	0.82	9.84
T3_100_200_M10	1.35	16.35	0.92	17.84	2.12	15.00	0.60	15.32
T4_100_200_M10	1.47	9.67	0.75	5.48	2.11	17.32	0.56	16.34
T1_75_200_M10	4.84	21.54	2.37	21.59	1.47	16.14	1.40	17.96
T3_75_200_M10	1.01	19.84	0.62	22.69	2.98	20.47	0.93	17.65
T4_75_200_M10	1.69	15.66	0.84	30.45	2.84	9.31	0.49	18.64
T1_75_225_M10	5.32	15.01	1.73	17.56	1.39	6.32	0.61	15.32
T2_75_225_M10	4.60	16.35	2.13	17.25	5.36	11.62	0.99	20.41
T3_75_225_M10	1.94	8.65	0.97	8.65	3.23	15.32	1.10	16.74
T4_75_225_M10	1.33	8.36	0.61	26.32	2.96	9.65	0.54	19.32

The initial stiffness is defined as the secant stiffness calculated as the slope of the line connecting the origin and the point of the force-displacement diagrams corresponding to the displacement of 2 mm. These values are also plotted in Figure 5.21 and Figure 5.22 to help the comparison among the distinct type of connections.

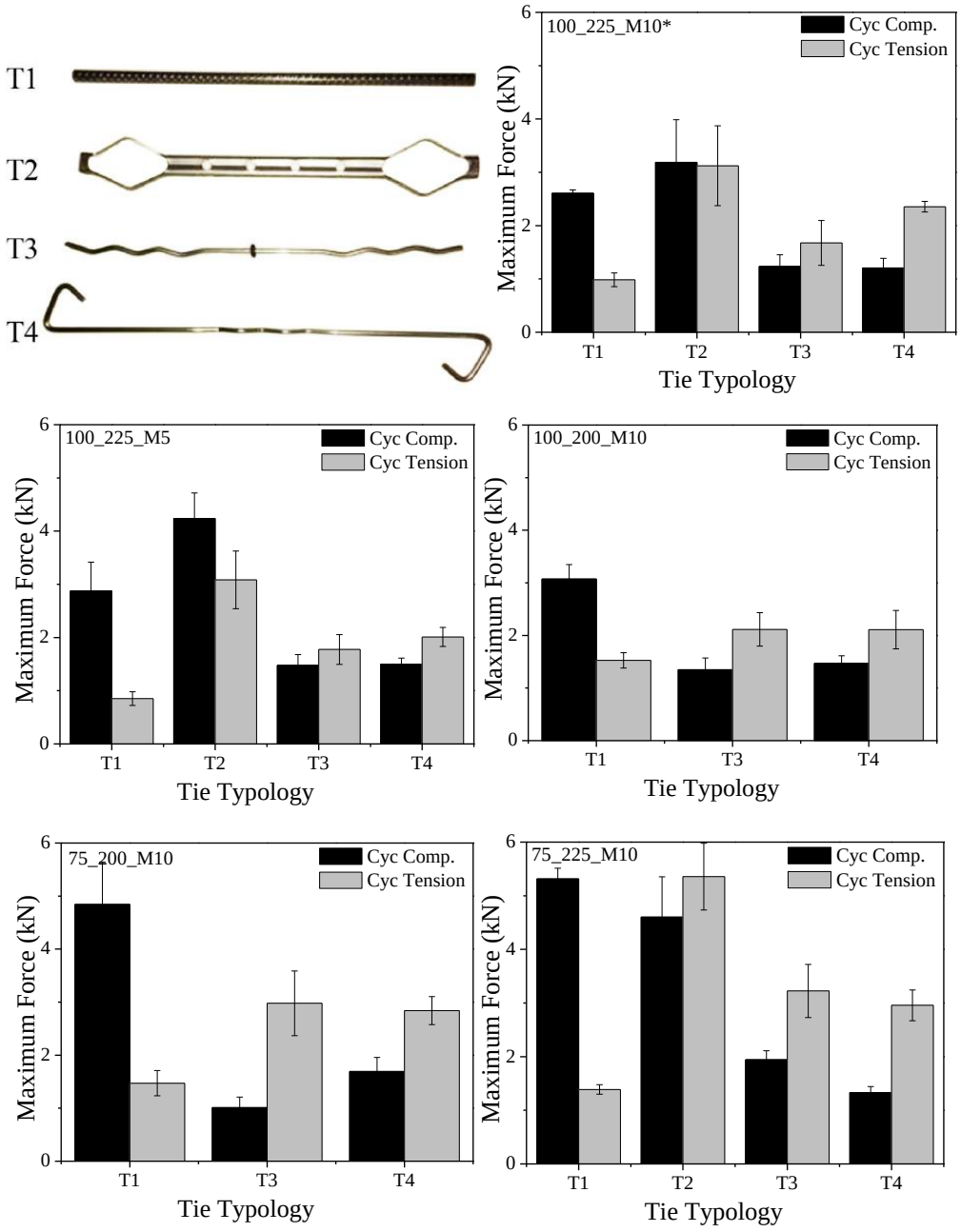

Figure 5.21 – Maximum forces values for each tie typology on each parameter combination

As seen before, the tie typology that present higher compressive and tensile resistance is tie T2. Connection with tie T3 and tie T4 present a considerable higher resistance in tension than in compression loading. Connections with tie T1 present much better compression resistance. This is even more evident in case of mortar strength variation (T1_100_225_M5) and in particular when the air cavity width decreases and embedment length increases

(T1_75_200_M10), see Figure 5.21. For the ties T3 and T4, the increase on the tensile bond adherence occurs in connections with reduced air cavity width (T3_75_200_M10 and T4_75_200_M10) and higher length of the ties (T3_75_225_M10 and T4_75_225_M10). In case of connections with tie T2, the higher mortar strength and the increase on the length of ties resulting in high embedment length result in the increase on the compressive and tensile strength.

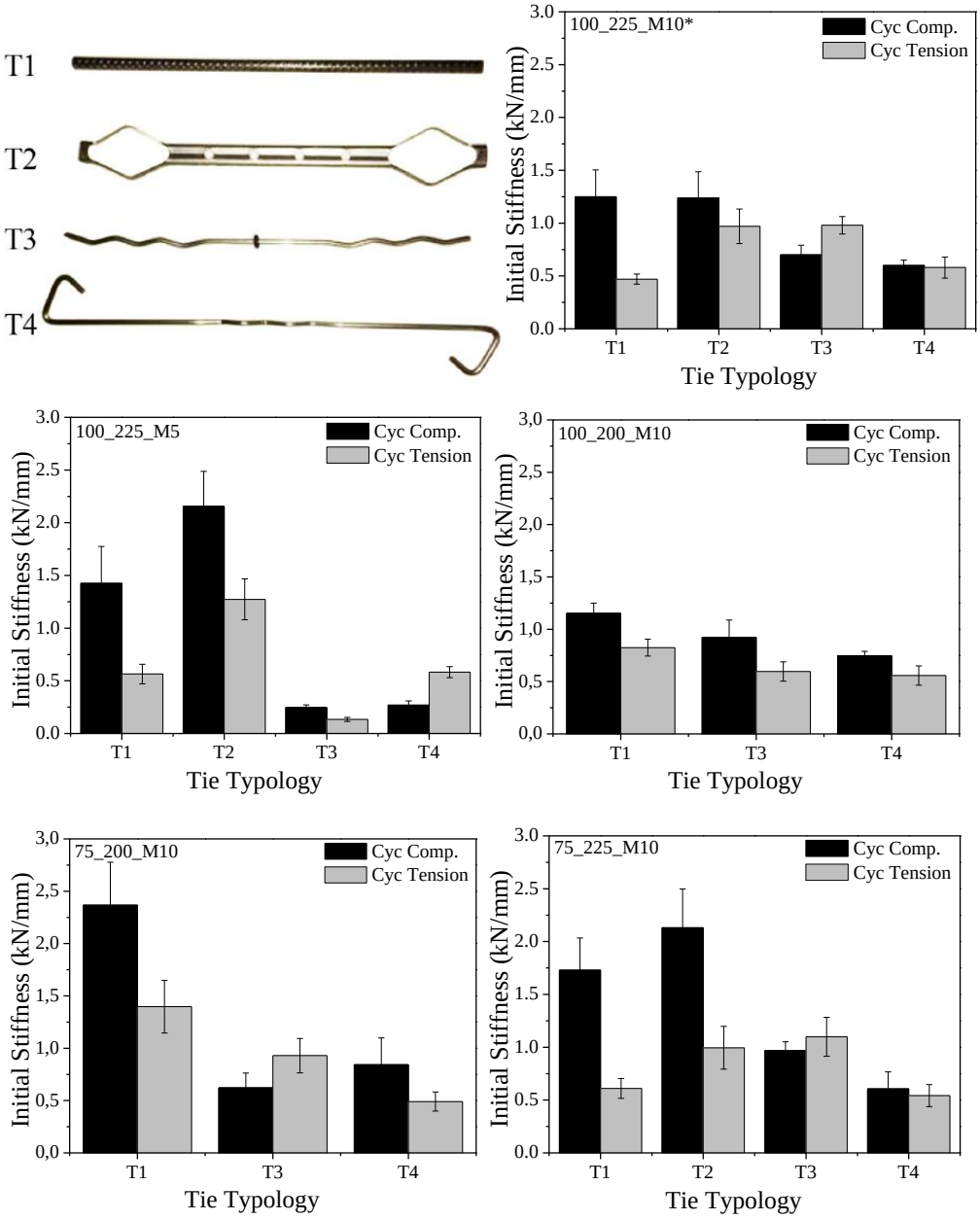

Figure 5.22 – Initial stiffness values for each tie typology on each parameter combination

In terms of initial stiffness in compression, it is observed that for all variation of parameters under consideration, the stiffness on connections with ties T1 and T2 present the higher stiffness values. This is explained mainly by the cross section are of these ties. Lower length

of the cavity space contributes also for the increase on the difference of the compressive stiffness of the connections with tie T1 and T2 in relation to the connections with tie T3 and T4. This is again explained by the lower free length of the tie. Under tension, there is higher equilibrium among the different connections, being the connection with tie T2 close to the stiffness of tie T4 when the strength of mortar is varied and when the length of the ties increases. This is justified by the fact that the initial stiffness is controlled more by the stiffness provided by the bond between the tie and mortar joints

5.6.3. Energy dissipation capacity

The energy dissipated by the connections during the tension-compression tests was calculated from the cyclic force-displacements diagrams as the area enclosed under the cyclic loop. The cumulative dissipation of energy for a reference displacement level was calculated as the sum of the energy until that displacement, see Figure 5.23.

From the analysis of results obtained in the complete assemblies, it is observed that the ties that enables a considerable better dissipation of energy of connection is tie T2, when compared to the other ties. When the compressive strength of mortar in the veneer prism is used (M5), the dissipation of energy of the ties reduces and in particular of tie T2. This appears to reveal that the compressive strength of mortar is important to ensure an adequate bond behaviour of the ties to the mortar joints.

In majority of cases, connections with T1 and T3 tie typologies exhibited lower dissipation energy capacity. However, when the air cavity width reduction (from 100mm to 75mm) is combined with higher length of the ties, resulting in higher embedment length (75_225_M10), it is observed that all ties present good dissipative behaviour. It is also possible to observe that the loss of dissipative capacity observed in the second cycle of each displacement level is higher in case of more resistance combinations maybe due to more severe degradation of system.

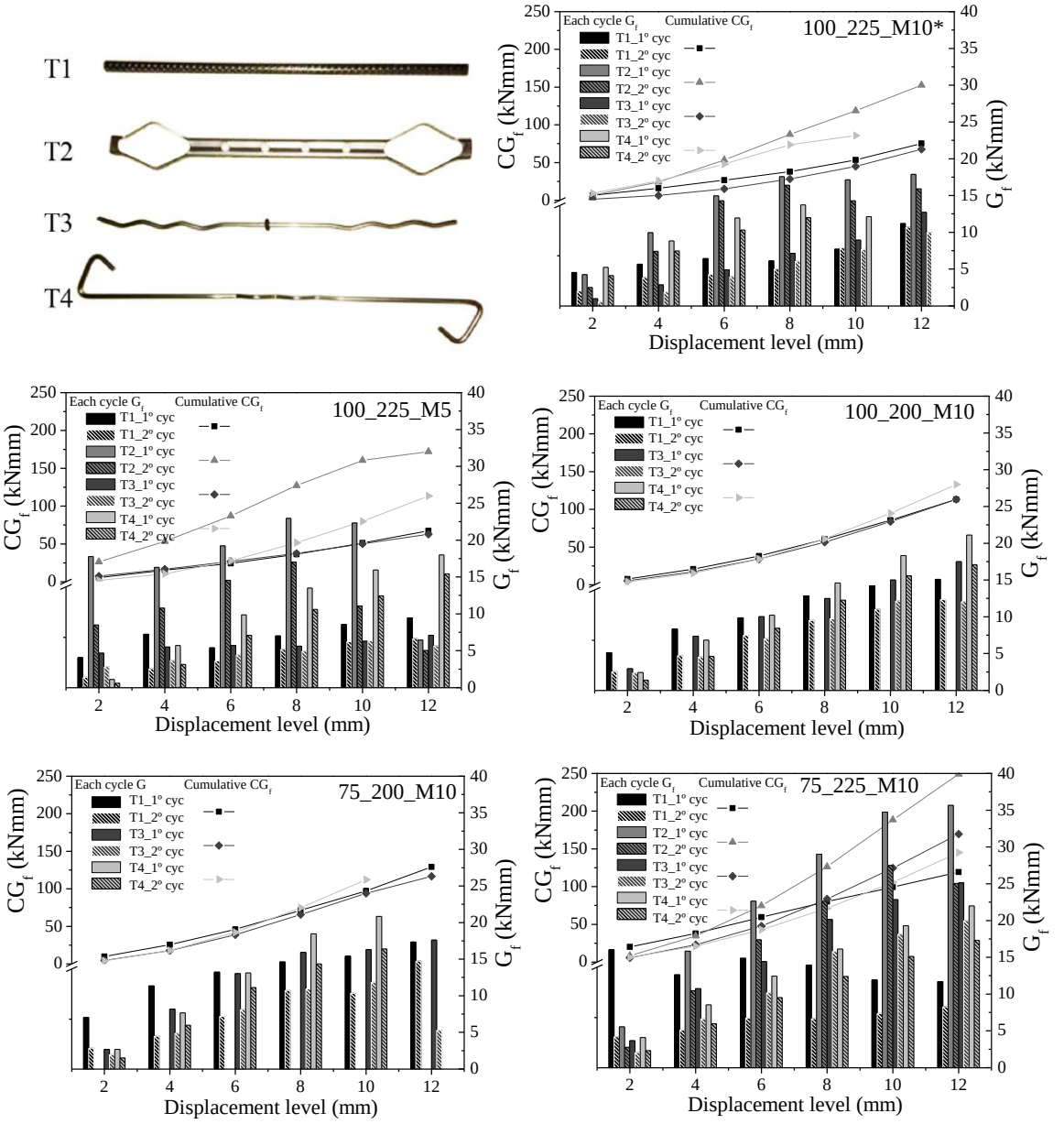

Figure 5.23 - Dissipated energy for each connection combination

5.6.4. Failure modes

During the cyclic tension-compression testing, various failure modes have been observed, including tie pull-out, tie buckling, tie fracture at middle length and tie fracture at interface of mortar joint, as shown in Table 5.6 and Figure 5.24. In case of tensile loading, the majority of connections presented a pull-out of the tie from the mortar bed joint of bricks veneer leaf, namely assemblages T1_75_200_M10 and T1_100_225_M5. In these connections, the ties have normal embedment length and mortar used in the masonry infill prism is of class M10, with higher mechanical properties than the mortar used on the masonry veneer prism.

Complementary, in connections *75_225_M10* and *100_200_M10*, slippage of the wall tie on from masonry infill block was observed in many cases, given that in these samples the ties have a higher embedment length on the masonry veneer prism. This type of failure has occurred also in some specimens of the group *100_225_M5* due to the lower compressive strength of the mortar used in the construction of the brick infill prim, regarding to the mortar used in the brick veneer prism. Under compression load, all samples have exhibited buckling of the tie. In few situations, tie fractures at interface of mortar joint or at mid length have occurred, which should be associated to the fatigue from the cyclic loading.

Table 5.6 – Summarize of obtained failure modes for each combination

Tie	**100_225_M5**	**75_225_M10**	**100_200_M10**	**75_200_M10**
T1	Pull-out from MVL/MIL; Push-out into MVL/MIL	Pull-out from MIL: Push-out into MIL.	Pull-out from MIL; Push-out into MIL.	Pull-out from MVL Push-out into MVL.
T2	Pull-out from MVL; Tie buckling; Tie fracture.	Pull-out from MIL; Tie buckling and push-out into mortar; Tie fracture.		
T3	Pull-out from MVL; Tie buckling; Tie fracture.	Pull-out from MIL; Tie buckling; Tie fracture.	Pull-out from MIL; Tie buckling; Tie fracture.	Pull-out from MVL; Tie buckling; Tie fracture.
T4	Pull-out from MVL; Tie buckling; Tie fracture.	Pull-out from MIL; Tie buckling; Tie fracture.	Pull-out from MIL; Tie buckling; Tie fracture.	Pull-out from MVL; Tie buckling; Tie fracture.

An interesting aspect to be mentioned is regarding to the connections with tie T2 tie in lower air cavity width (T2_75_225_M10). In air cavity width of 100mm, when the T2 wall tie starts its buckling, the follow cycles exhibit permanent deformations. In the lower air cavity width (75 mm), the wall tie buckles, but is also pushed into mortar when the compression cycle is stated. This is due to the lower free length of buckling, resulting in lower lateral instability of the tie. In this case, compression loading causes more damage into mortar ate the bed joints.

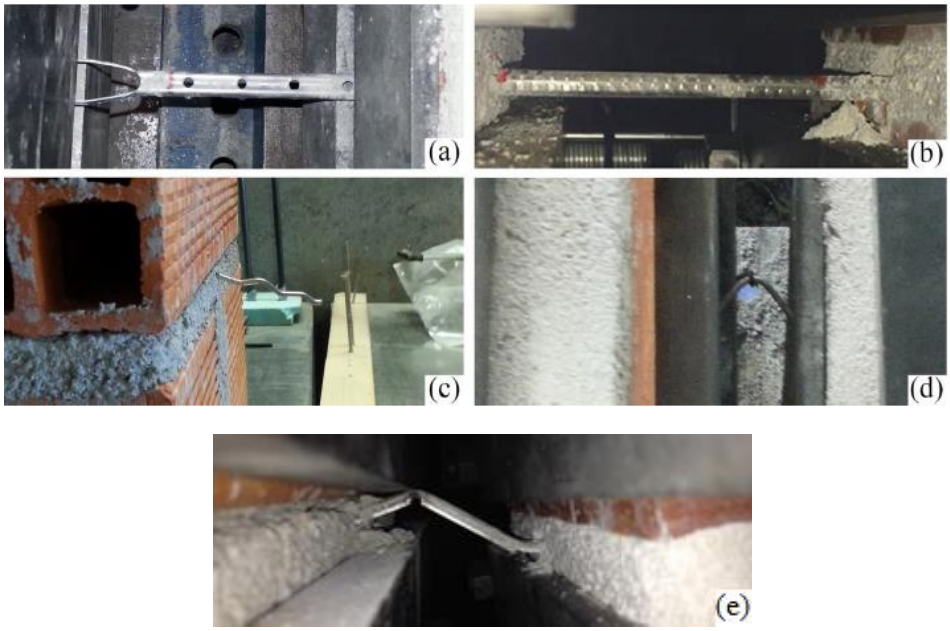

Figure 5.24- Failure modes: pull-out on (a) infill bed joint of T2 tie and (b) veneer bed joint of T1 tie; (c) fracture at middle length of T3 tie; buckling (d) on 100mm air cavity width of T4 tie and (e) with pushing into mortar joint of T2

5.6.5. Parametric analysis

In order to understand the influence of different parameters, namely (1) mortar properties, (2) embedment length, (3) air cavity width, together with the tie typology, a comparison between variables is presented for each tie typology. Average envelope load-displacement curves have been prepared and plotted according to the variable effect in order to provide an easier comparison for each different parameter. In addition, the comparison is carried out based on strength, stiffness and energy dissipation.

e) Influence of the mortar class

Regarding to the influence of mortar properties on the cyclic tensile-compression behaviour of connections, it was decided to compare the specimens with masonry infill prims having different classes of mortar (M10 and M5). To analyse only this variable, the reference connections (*tie typology_100_225_M10**) were used for comparison with connections in which the infill prims was built with mortar M5 (*tie typology_100_225_M5*). As mentioned before, the direct comparison is not so easy, as the compressive strength of the mortar M10* used in the reference specimens presented lower values than the ones expected (6 MPa under compression and 2.5MPa under flexure). The compressive strength of mortar M5 was

5.5MPa and the flexural strength was 3.2MPa. For this reason, the effect of the compressive strength of mortar is not so noticed on the average curves. Under tension, the experimental envelops are rather close, which means that the difference on the compressive strength is not relevant enough to change the tensile bond adherence. Under compression, the connections in which the brick infill prism was built with mortar M5 present higher resistance, particularly in case of tie T2 and tie T1, see Figure 5.25 (a) and Figure 5.26. This fact can be only caused by scatter of results.

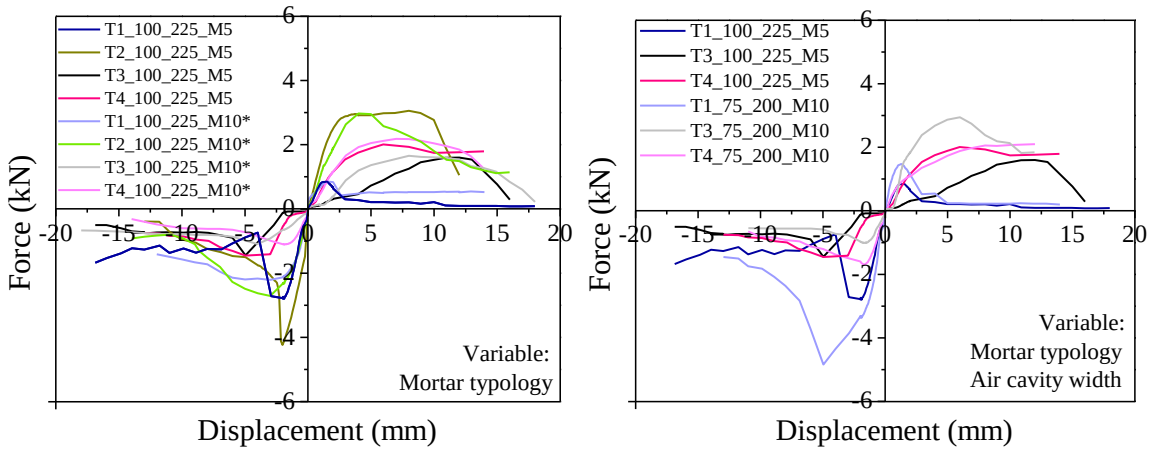

Figure 5.25 – Average envelope load-displacement curves for analysing the direct effect of (a) mortar properties, and the (b) mortar influence combined with air cavity width

On the other hand, comparing the connections, in which the brick infill prims were built with mortar M5 (*tie typology_75_200_M5*) and with mortar M10 presenting a compressive strength of 12MPa and flexural strength of 8MPa (*typology_100_225_M10*), it is possible to compare easier the effect of the compressive strength of mortar in the behaviour of the connections. However, it should be noticed that the air cavity width is different but the length embedment is maintained (Figure 5.25 (b) and Figure 5.26).

The combined effect of the higher compressive strength of mortar and the reduction of the air cavity width, resulted in the improvement of tensile strength of the connection, being the maximum increase of about 50% in the connection with tie T1 tie typology. It is considered that under tension, the main influencing parameters is the compressive strength of mortar because it enables to increase the bond adherence of the ties to mortar joints. This aspect has been already pointed out by Negro et al. (2016) [151]. Under compression load, it is considered that in spite of the compressive behaviour of mortar can be important, the major influence in the connections is regarding to the reduction of the air cavity width. An improvement of strength of the connections of at least 25% was obtained in connection with

tie T1 wall tie and an increase of about 45% was obtained in the connection with tie T3. The positive influence of the reduction of the air cavity width is justified by the reduction of the free length of the tie. This is also the main justification for the increase on the initial stiffness of about 40% in all connections. Notice that the ties work mainly as an element working under tension and compression and thus its stiffness is proportional to the free length. In tensile regime, the initial stiffness presented also an important gain of 30%.

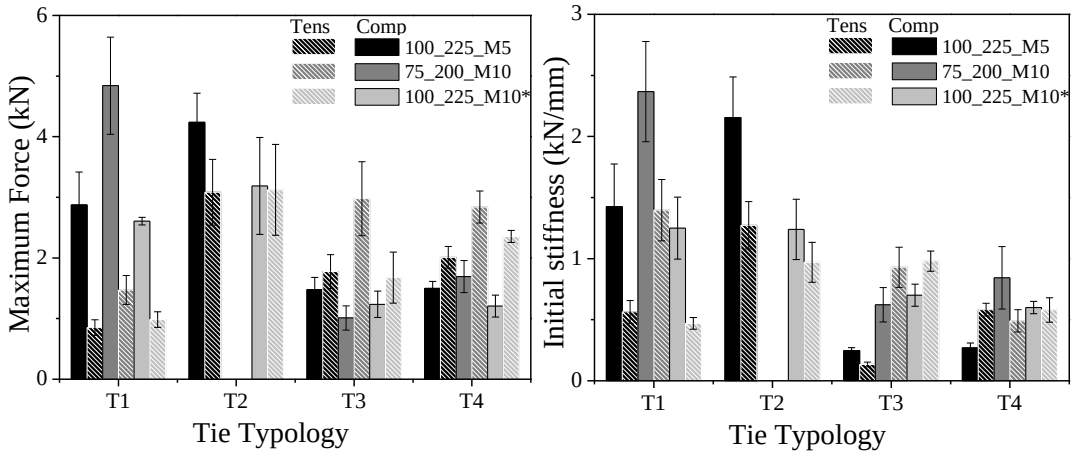

(a) (b)

Figure 5.26 – Comparison of (a) maximum strength and (b) initial stiffness between combination to study the mortar influence

f) Influence of the embedment length of ties

The influence of embedment length of ties in the cyclic tension-compression behaviour of connections can be evaluated through the comparison between samples with 75mm of air cavity width and variable length of ties (*typology_75_225_M10* and *tie typology_75_200_M10*) (Figure 5.27 (a) and Figure 5.28). In this case the increase of the of the embedment length in the brick masonry veneer prisms is about 25mm.

It is seen that the increase of the embedment length has a marginal influence in the tensile behaviour of the connection with tie T1, but an unexpected increase of the compression resistance was obtained. The increase of the embedment length led to the increase of tensile strength both in the connections with tie T3 (11%) and Tie T4 (4%). The increase on the embedment length appears to be a negligible effect in the connection with tie T4 under compression

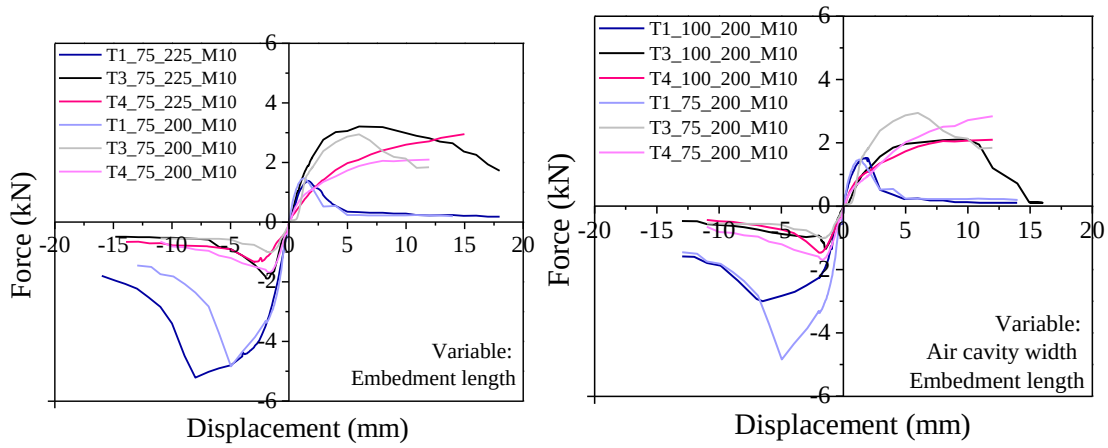

(a) (b)

Figure 5.27 - Envelope average load-displacement curves for analysing the direct effect of (a) embedment length, and the (b) length embedment influence combined with air cavity width

When the embedment length is increased though the reduction of the air cavity width, the improvement on the tensile strength of connection with tie T3 and T4 is more evident, particularly in connections with tie T3, see Figure 5.27 (b) and Figure 5.28. In this case, the improvement of the compressive behaviour of all connections is very visible. To sum up, it can have pointed out that the lower air cavity width and higher embedment length of ties in mortar joints improved the compression maximum force in rigid wall tie (T1) about 60% and about 30% in flexible wall ties under tension loading. The increase on the stiffness is more evident in the connections with tie T1, presenting an increase of about of double stiffness under compression loading and 60% under tension loading.

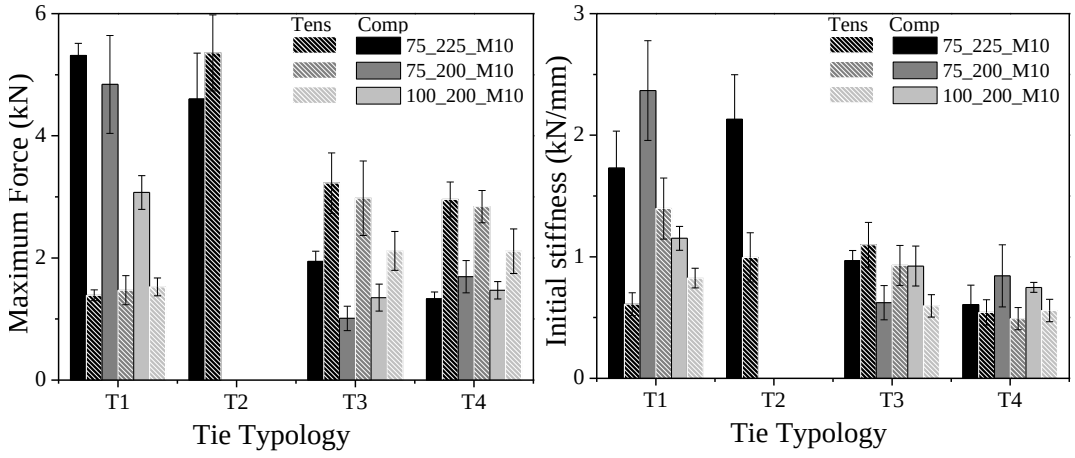

(a) (b)

Figure 5.28 – Comparison of (a) maximum strength and (b) initial stiffness between combination to study the embedment length influence

For both variations of the variables, the connections with tie T3 and T4 present a clear higher performance under tension when compared to the connections with tie T1. The contrary occurs in compression regime.

g) Influence of the air cavity width

The influence of the air cavity width can be evaluated in the samples with same the embedment length and mortar class: *tie typology_75_200_M10* and *tie typology_100_225_M10** (Figure 5.29 and Figure 5.30). However, it should be noticed that the mortar used in the reference specimens (*tie typology_100_225_M10**) presented an expected poor performance under compression, as mentioned above. This means that by comparing these two types of connections, both air cavity width and compression strength of mortar are evaluated.

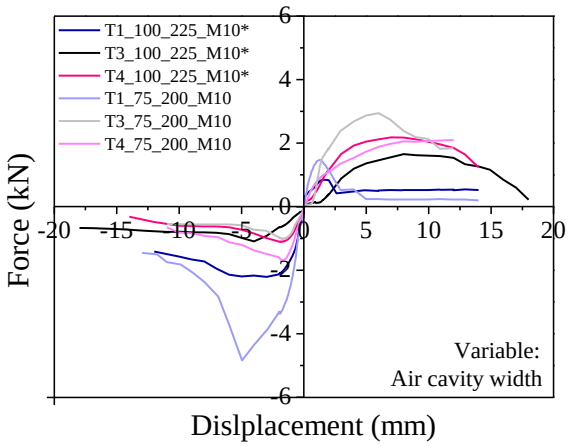

Figure 5.29 - Envelope average load-displacement curves for analysing the direct effect of air cavity width

By analysing the experimental envelops shown in Figure 5.29, it is seen that the positive influence of lower air cavity width and higher resistance mortar is clear either under tension or compression loading. Under compression loading, the connections with rigid wall ties (T1) that have lower air cavity width presented almost the double of resistance. As aforementioned, the air cavity width is more important when the tie T1 is used given its better behaviour under compression when comped to the flexibles ties T3 and T4. On the other hand, under tension load the connections with flexible ties present a more significant improvement of the tensile strength (about 30%) given that the tensile bond adherence is enhanced by the increase on the compression strength of mortar. The initial stiffness did not show evident differences among the connections, with exception of connections with tie T1 that presented more than double in compression and tension loading.

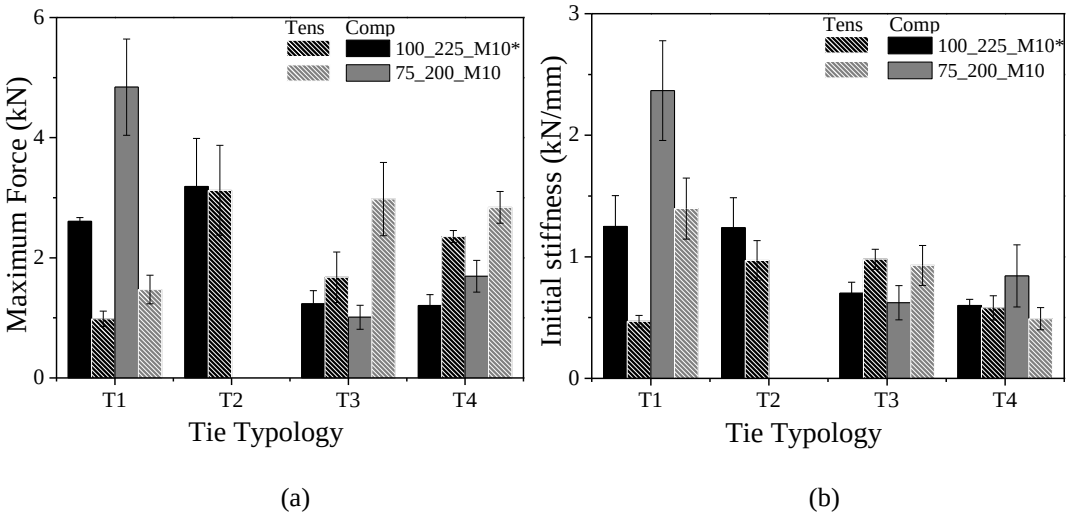

Figure 5.30 – Comparison of (a) maximum strength and (b) initial stiffness between combination to study the air cavity width influence

To sum up, a comparison between the connections *tie typology_75_225_M10 and tie typology_75_225_M5* can be made in order to evaluate the simultaneous influence of the variation of the compression strength of mortar, embedment length and air cavity width in the cyclic tensile-compression behaviour, see Figure 5.31 and Figure 5.32.

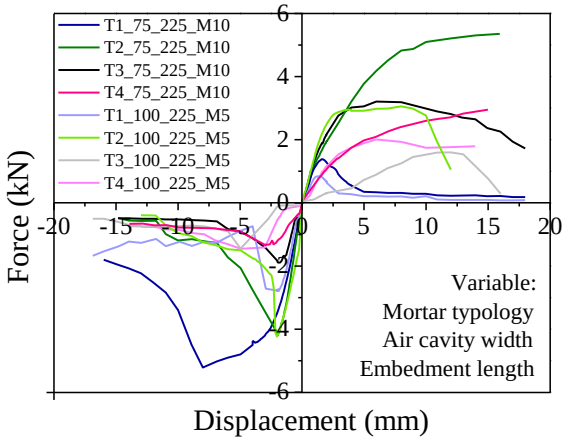

Figure 5.31 - Envelope average load-displacement curves for analysing the air cavity width effect combined with embedment length and mortar variation

It should be mentioned that connections *tie typology_75_225_M10* present higher compressive strength of mortar, higher embedment length and lower air cavity width when compared to the connections *tie typology_75_225_M5*. In this way, it is possible to evaluated the positive effect of all of them both in tensile and compression behaviour of the ties. As expected, the connections *tie typology_75_225_M10* exhibit better performance than *tie typology_100_225_M5* both under tension and compression. Under tension loading, the connections can achieve almost the double of resistance in almost all ties typologies. Under

tension, the higher embedment length is combined with the higher compression strength of mortar, promoting an improvement of tensile bond adherence of the ties. Under compression, the enhancement of the behaviour is obtained mainly in the connections with tie T1 and tie T2. These results are attributed to the fact that under compression, the connection behaviour is more dependent on the tie buckling capacity, which affect particularly tie T1 and tie T2.

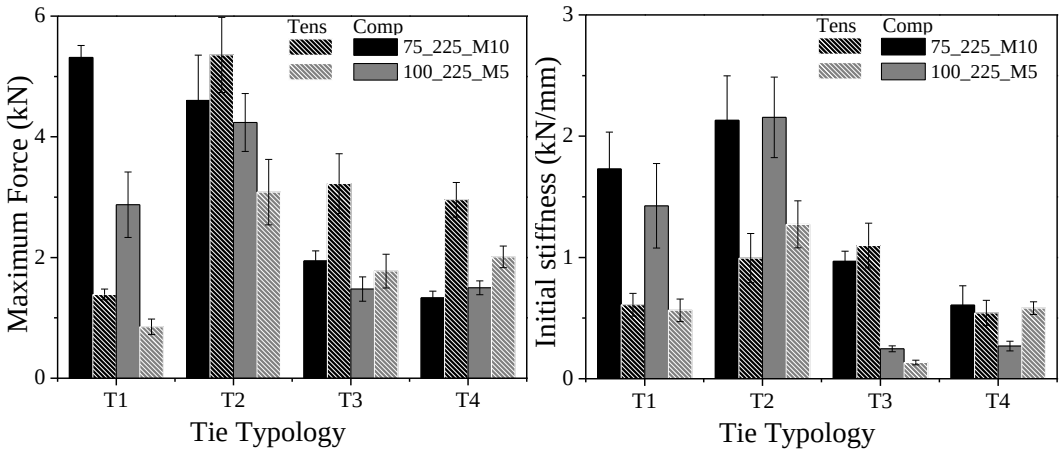

(a) (b)

Figure 5.32 – Comparison of (a) maximum strength and (b) initial stiffness between combination to study the air cavity influence, embedment length and mortar typology

As far as to initial stiffness is concerned, it can possible to see a great difference between compression and tension stiffness in the connections with rigid ties (T1 and T2), being the compression stiffness much higher.

Finally, it is possible verify that the compressive behaviour is mainly influenced by tie typology and air cavity width, whereas the, tie typology, embedment length and mortar capacities influences more positively the tensile strength of the connections.

5.7. Conclusions

This chapter intended to provide an analytical model to simulate the cyclic tension-compression and shear behaviour of connection of different types of ties to brick masonry. This analytical model can be used in further numerical analysis where brick veneer intends to be simulated together with the backing system. Based on previous available hysteretic models, it was possible to obtain an analytical model that fitted very reasonably to the

experimental cyclic tension-compression and shear behaviour of the connections with ties T1 and T4.

In order to understand the influence of previous shear damage in the cyclic tension and compression response, some samples subjected previously to shear cyclic loading were further tested to tension and compression cyclic loading. Based on comparison of the behaviour of damaged and undamaged connections, it was possible to conclude that:

1. The reduction of strength in damaged samples is associated to the higher deterioration of the adherence tie-mortar and to the lower compressive strength of the mortar. The maximum reduction is about 70%.

2. The prior shear damage reduces substantially of the initial stiffness. The reduction level of initial stiffness depends on the tie and loading typologies. For instance, the reduction can achieve until 80%.

3. The connections with rigid ties (T1 and T2) exhibited higher reduction on the energy dissipation capacity. However, all of the connections followed the same cumulative energy trend as the undamaged connections.

4. The damaged connections presented lower values of damping, as the effect of pinching was more severe than that observed in undamaged samples. In these cases, the energy dissipation was diminished by pinching, decreasing its ratio with input energy.

Finally, a parametric experimental study was carried out in order to understand the influence of different parameters in cyclic tension-compression behaviour of the connections, namely mortar class (compression strength of mortar), air cavity width and embedment length of the ties. Based on the results obtained, it was possible to conclude that:

1. The more resistant mortar capacity with lesser air cavity width can positively influence the strength and stiffness under tension and compression loading. The higher strength of mortar contributes to the better performance under tension loading and the lesser cavity air width contributes to the improvement of the compression behaviour.

2. The lower air width and higher embedment length of the ties in mortar joints increased the compression maximum force in rigid wall ties (T1) by 60% and the tensile resistance by 30% in flexible wall ties. Regarding to the stiffness, the more evident positive influence can be seen in the connections with tie T1 tie typology, where an increase of about the double was observed under compression loading and an increase of about 60% was recorded under tension loading.

3. The effect of the simultaneous increase of mortar strength, reduction of the air cavity width and the increase on the embedment length, resulted in almost double of the tensile resistance in the connection with ties T1, T2, T3 and T4. Under compression, the positive influence could be observed mainly in the connections with rigid ties (T1 and T2). In compression regime the connection behaviour is more dependent on the tie buckling capacity than the tie-mortar bond, and therefore, the improvement of the compression behaviour is more evident in the connections that perform better under compression loading.

To sum up, the compressive behaviour is probably influenced mainly by tie typology and air cavity width, whereas the embedment length and mortar capacities effect is not too evident. The tensile behaviour is influenced mainly by tie typology and embedment length, being the air cavity width and mortar properties not obvious effects. There are many reasons that can influence the behaviour of connections, for example the installation method of the tie is applied on mortar bed joint that depends of workmanship essentially, its alignment, as well as the mortar properties. These can be probably the reasons what not always the results do not reveal the unequivocal trends and comparisons.

Chapter 6

Experimental Characterization of Brick Veneer Walls

Abstract:

In order to contribute to increasing of knowledge about the seismic behaviour of masonry veneer walls, an experimental campaign was developed testing quasi-statically full-scale systems under in-plane and out-of-plane actions. Thus, this chapter describes in detail the out-of-plane performance of more typical constructive systems of Portugal and South of Europe, composed by masonry veneer façade connected to infill wall inserted in a RC frame. In this study, it was also done a parametric analysis based on seismic parameters of walls with different tie typology, tie spacing, air cavity width and embedment length of wall ties and presence of flashing. It is also evaluated the influence of in-plane damage on out-of-plane performance of system, in order to approximate to a real seismic action. These results provide important experimental data to calibrate analytical models and to contribute for better understanding of behaviour of walls under out-of-plane actions.

6.1. Introduction

Horizontal loads induced by earthquakes can cause severe in-plane and out-of-plane damages on masonry walls in buildings. Normally, masonry walls present particular vulnerability if pushed horizontally in a direction perpendicular to its plane (out-of-plane loading) but offers higher resistance if pushed along its length (in-plane loading). This is not only valid for loadbearing walls but also for non-structural walls that are forced to behave in a structural way in case of seismic actions. Among the non-structural walls, masonry infills and masonry veneers are well known to be used in more modern construction, where reinforced concrete frames as a structural system predominate. As it was shown in Chapter 2, masonry veneers are particularly vulnerable to lateral actions under out-of-plane loading, being observed in recent seismic events the detachment and rupture of masonry veneer panels.

Therefore, detailed investigation on the seismic behaviour of masonry veneer walls becomes necessary, specially taking into account the connection of the masonry veneers to the backing infill masonry walls. The primary gap identified through literature review was the lack of experimental research that addressed the response of masonry veneer walls, whose backing is composed by masonry infill wall inserted in a concrete frame. This represented the major motivation for conducting this research based on experimental characterization of the mechanical behaviour of brick veneer walls attached to brick masonry infills with different types of wall ties and different arrangement for the ties under in-plane and out-of-plane loading.

Thus, the main objectives of the experimental work are: (1) obtainment of the static cyclic in-plane behaviour of masonry veneer walls and (2) assessment of the static cyclic out-of-plane behaviour of masonry veneer system in different walls configurations.

The main results of the experimental campaign intended to be obtained are: (1) hysteretic force-displacement diagrams under in-plane and out-of-plane loading; (2) deformation features of the walls and (3) damage patterns and failure mechanism of the masonry veneers and connections under in-plane and out-of-plane loading. In order to complement this analysis, a parametric analysis was carried out aiming at assessing the influence of different parameters related to constructive practices, namely: (1) tie typology, (2) tie spacing, (3) air cavity width and embedment length and (4) flashing. An additional comparison was also

performed to assess the influence of prior in-plane damage on out-of-plane performance, aiming at reproducing closer real conditions in seismic events. The performance of masonry veneer walls and comparative analysis among the different cases are based on defined seismic indicators such as: (a) the backbone of hysteretic curves and evolution of strength during cyclic loading and the initial stiffness, (b) stiffness degradation, (c) plastic or residual deformation, (d) energy of dissipation and (e) equivalent viscous damping ratio (EVDR). These test results can help to calibrate finite element models of masonry veneer systems, enabling additional parametric studies to explore the effects of different features of this system, contributing for suggesting recommendations for the design of the masonry veneer systems.

6.2. Characterization of specimens

The experimental models of masonry veneer walls were designed taking into account real features of typical brick masonry veneer walls and laboratory conditions. The experimental model was defined based on the constructive system presented in Chapter 2 composed of a reinforced concrete (RC) frame with brick masonry infills having attached brick veneer walls. This constructive system is not only very common in Portugal but also in south of European countries. The experimental program on brick veneer walls was defined in order to get the maximum information about the in-plane and out-of-plane performance of these constructive elements, varying ties typology, ties spacing layout, air cavity width/embedment length and friction conditions at the veneer base. Nine specimens were subjected to out-of-plane static cyclic loading, being one of them subjected previously to an in-plane cyclic test in order to characterize in-plane performance and to assess the influence of a determined prior in-plane damage level on the out-of-plane behaviour. The test specimens and its features are presented in Table 6.1. The nomenclature of the experimental models describes all features of the masonry veneer system: “tie typology,_type of loading, air cavity width and number of ties per square meter”. Thus, regarding the type of loading, “O” refers to out-of-plane loading, “I” refers to in-plane loading and “IO” refers to previous in-plane test to induce prior in-plane damage with a sequential out-of-plane test. The air cavity width is 100mm or 75mm, and the number of ties per meter square is 1.4, 2.5 or 5. The influence of the type of interface at the base of the brick veneer with the steel profile is analysed by considering a specimen where flashing was added at the base. This was analysed for the tie T2 and by considering 2.5 ties per square meter (T2_O_100_2.5_No flashing).

The results obtained in this specimen can be directly compared with the results obtained in specimen T2_O_100_2.5, where no flashing is added.

Table 6.1 - Specimens for in-plane and out-of-plane static cyclic tests

Models' name	Tie typology		Tie spacing			Air cavity width		Flashing material on shelf angle
	T4	T2	Normal spacing (2.5ties/m^2)	Small spacing (5ties/m^2)	Large spacing (1.4ties/m^2)	100mm	75mm	
T2_O_100_2.5_No flashing		x	x			x		
T2_O_100_2.5		x	x			x		x
T2_O_100_5		x		x		x		x
T2_O_100_1.4		x			x	x		x
T2_I_75_2.5		x	x				x	x
T2_O_75_2.5		x	x				x	x
T2_IO_75_2.5		x	x				x	x
T4_O_100_2.5	x		x			x		x
T4_O_100_5	x			x		x		x
T4_O_75_2.5	x		x				x	x

6.2.1. Details of RC Frames

The reinforced concrete frames used in the experimental campaign had been previously used in other experimental campaign on the analysis of the out-of-plane behaviour of masonry infill walls [152]. The RC frame could be re-used because the damage previously induced was minor given that the out-of-plane loading was directly applied in the brick masonry infill walls. In addition, fixed bottom and upper beams were considered as the boundary condition, resulting in the low damage observed. The RC frames are considered as typical construction of South European countries in 1980s [153]. Given the limitation of the laboratory facilities, it was decided to define a reduced scale experimental model from the representative prototype. For this, a geometrical scale factor of 0.54 was used in the definition of the experimental model. The design of the reinforcing elements of the frame was carried out taken into account the Cauchy's similitude law and the maximum allowable forces and flexural moments of real scale sections obtained according to ACI 318-08 [154] guidelines. With these guidelines, it was possible to calculate the maximum allowable forces and bending moments of reduced scale cross sections [152]. Thus, the cross-sections and reinforcement details of the reduced safe RC frame are presented in Figure 6.1. A concrete of class B20 with a maximum aggregate of 9mm was considered in the casting of the frames.

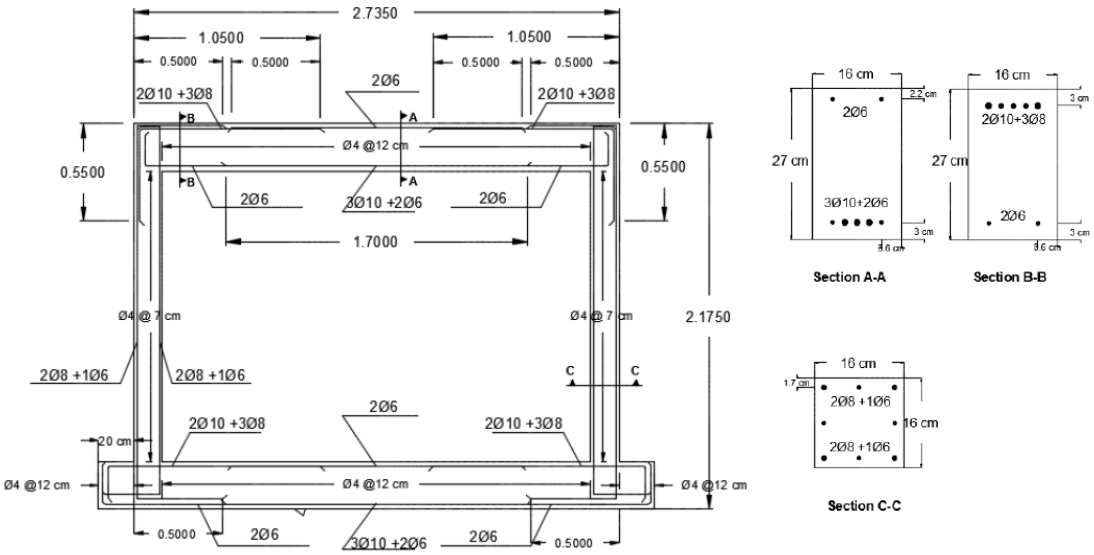

Figure 6.1 - Geometry and reinforcement scheme of the reduced scale RC frame (dimensions in meters) [152]

6.2.2. Constructive elements: bricks, mortar and wall ties

As mentioned before, the system under evaluation is composed of an RC frame with brick infills with a brick veneer attached by wall ties. The brick veneer wall is constituted by ceramic bricks with vertical holes with approximately 237mm x 115mm x 70mm (length x thickness x height). The brick masonry infill walls were built with ceramic brick units perforated horizontally with approximately 300mm x 150mm x 200mm (length x thickness x height). Notice that, even if the RC frame is built at reduced scale, it was decided to build the brick infill and brick veneer walls with full scale brick units to have better representativeness. The brick veneer walls assemblage was carried out by using a pre-mixed water-repellent cement mortar, usually recommended by the brick unit producer. For the backup pre-mixed M5 general purpose mortar was used, following what was used in the previous experimental work on brick infill walls. The thickness adopted for the mortar bed joints was 15mm to enable the perfect levelling of the tie. The mechanical properties of the bricks and mortar have been already presented in Chapter 3.

The wall ties considered in this study were T2 and T4 typologies with 225mm, whose details were already provided in Chapter 3. The selection of these ties took into account the performance of the tie-brick assemblages under tension, compression and shear loading thoroughly explored in Chapter 4. Effectively, the assemblages with tie T2 exhibited the best behaviour under tension and compression loading and assemblages with tie T4 exhibited a very reasonable tension response. The wall ties used in construction of each wall (with

exception of T2_O_100_2.5_No flashing sample) were instrumented with strain gauges in order to control the real deformations of these elements in different parts of the wall and to monitor the level of contribution for global performance of the veneer walls.

6.2.3. Construction and ties layout detailing

The construction of the masonry walls systems is a complex task because it has to be made by phases. In a first phase, the brick infill enclosed in the RC frame is built. In this phase, the positioning of the ties is of major importance to ensure adequate alignment between masonry and brick veneer walls (Figure 6.2 (a) and (b)).

After this, a shelf angle is bolted to the bottom RC beam just above the foundation, and a flashing is placed on the shelf angle, as shown in Figure 6 (c and d). This was made in all specimens with exception of the "T2_O_100_2.5_No flashing" model to evaluate its role in the friction level developed at the base between the shelf angle and the brick veneer. Finally, the brick veneer walls were built parallel to the masonry infill with similar dimensions of the concrete frame (2.32 length x 1.80 height), see Figure 6.2 (e).

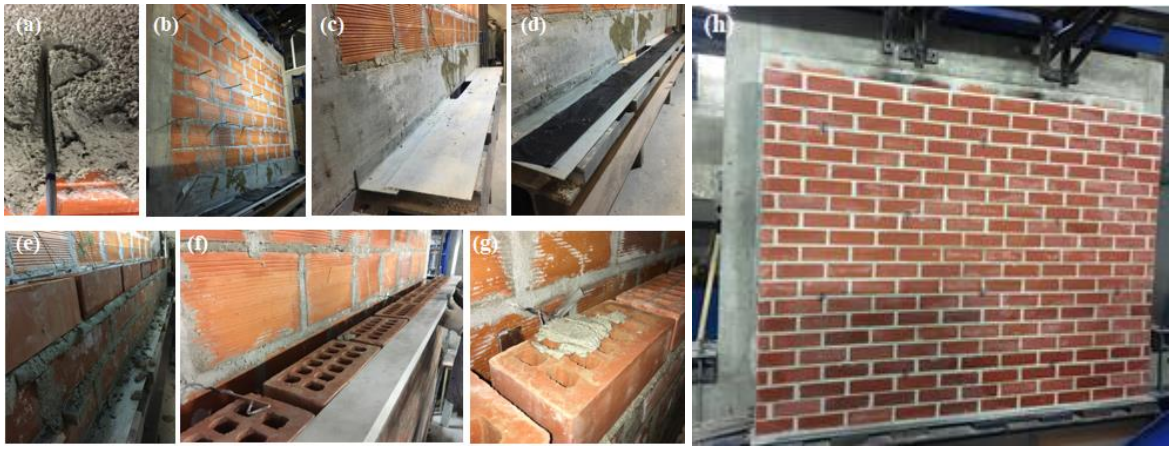

Figure 6.2 – Specimen construction detailing: (a) wall tie embedment on infill leaf; (b) previous construction of infill wall; (c) shelf angle without and (d) with flashing; (e) construction of veneer wall; (f) alignment of the connectors and (g) wall tie embedment on veneer leaf (h) global view of specimen

In order to understand the importance of the free length of wall ties in the global performance of the constructive system, especially when they are compressed, two air cavity width were selected, namely 100mm and 75mm. On the other hand, it was also intended to analyse the influence of embedment length of the wall ties in mortar bed joint under tension. For air cavity width with 100mm, the embedment length of the wall ties on masonry veneer mortar bed joint is 60mm, and in the masonry infill mortar bed joint it is 65mm. For the air cavity

with 75mm, the embedment length of the wall ties on masonry veneer mortar bed joint was 85mm, and on masonry infill mortar bed joint is 65mm.

Other aspect to be described in detail is the spacing and configuration of wall ties in the brick veneer wall. Three wall ties configurations were designed with the aim of understanding the advantage and disadvantages of them in the mechanical behaviour of brick veneers, mainly when submitted to out-of-plane loading. As aforementioned, the location of wall ties in the infill wall was planned so that there was no misalignment of the connectors in relation to the veneer leaf, see Figure 6.2 (f) and (g). In this study, the insulation material in air cavity was not considered. However, this aspect should be considered in further investigation because it is assumed that it can influence the response of the system, particularly in case of the wall ties are submitted to compression loading. The ties were applied in the traditional pattern, a quincunx, at an approximately density of 1.4, 2.5 and 5 ties per square meter. The wall ties configuration are in accordance with the standard that specify this type of element [26, 34-36], with exception of greater spacing (1.4ties/m^2). This spacing was used with the purpose of knowing the performance of possible current constructive applications, given that it is believed that in practice larger ties spacing should be used. The specimens dimensions and the wall ties layouts are presented in Figure 6.3.

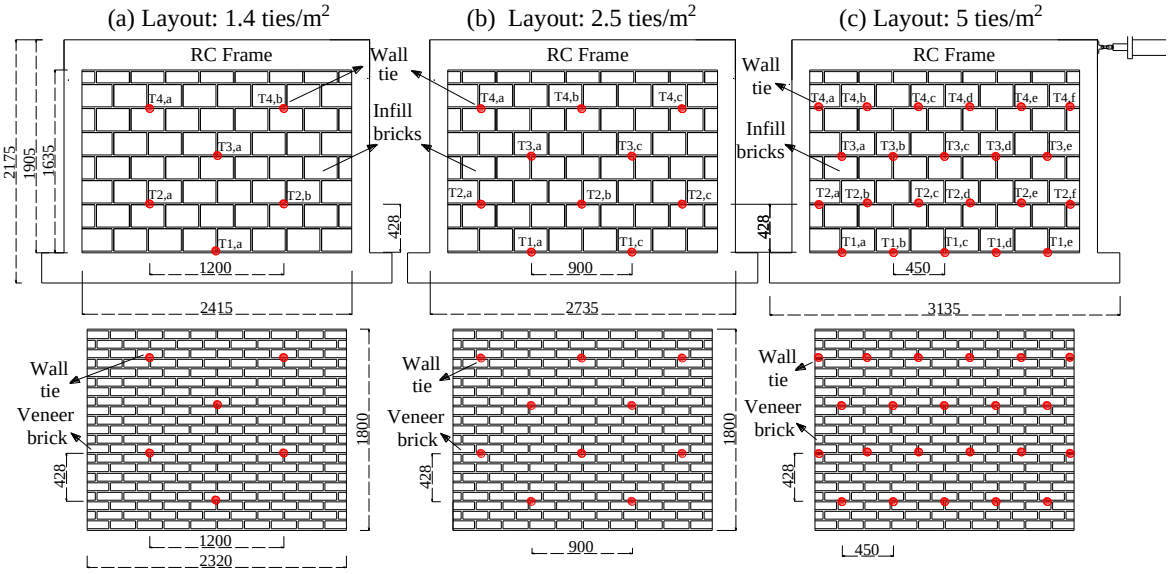

Figure 6.3 – Layout of wall ties on masonry infill and veneer wythes (dimensions in millimetres)

The scheme presented in Figure 6.4 summarizes the features of each veneer wall system tested at laboratory.

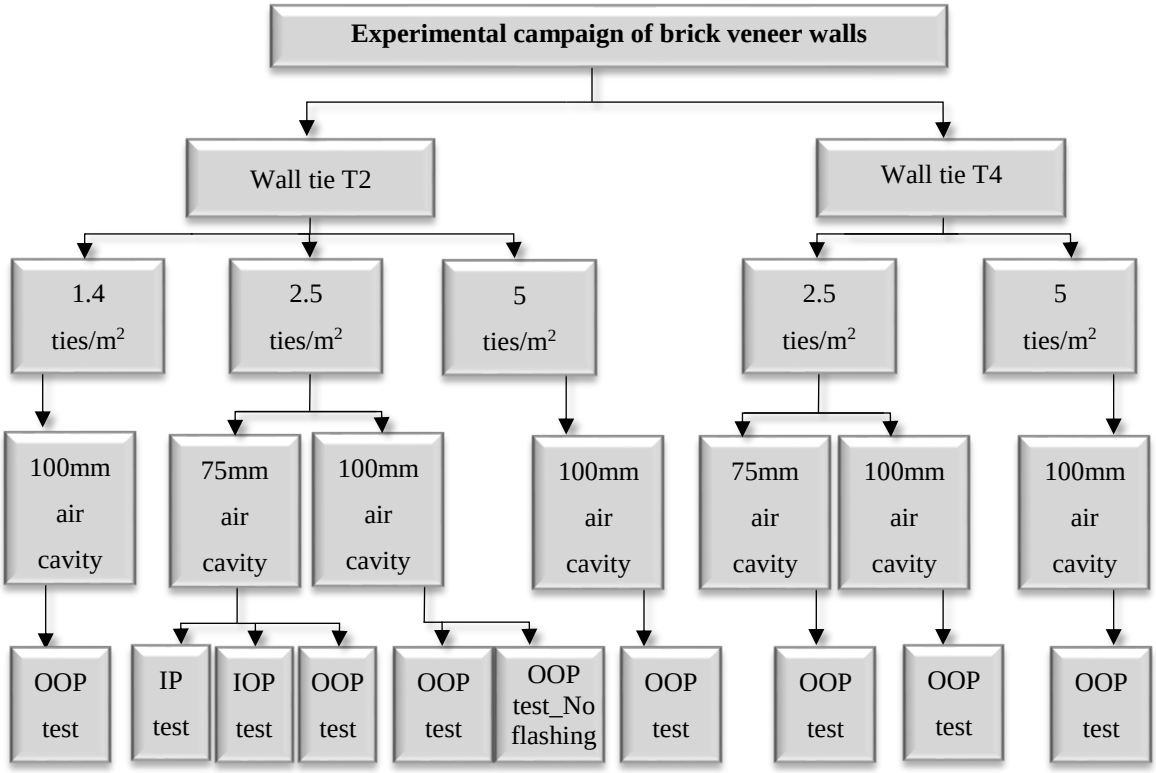

Figure 6.4 – Research methodology for brick veneer walls characterization

6.3. Experimental setup, instrumentation and loading pattern

The experimental setup for in-plane and out-of-plane testing was based on recommendations of standard [155] and decided according to the laboratory conditions described below.

6.3.1. In-plane tests

For the in-plane test, the RC frame with masonry infill wall was attached to two steel beams (HEA 300), which in turn were attached firmly to the strong floor to avoid sliding and uplifting. A L-shape steel profile of L200x200x20mm was bolted at each side of the steel beam to prevent the sliding of the RC frame. In turn, the uplifting was additionally prevented by bolting two tubular steel profiles (UNP140) to the steel beams (Figure 6.5). In addition, the out-of-plane movements of the RC frame were constrained by bolting a L-shaped steel profile of L100x100x10mm to an external steel frame at each side of the upper concrete beam (Figure 6.5). Three rollers were placed on upper L-shaped profiles to completely minimize or even eliminate the friction between them and the upper reinforced concrete beam during in-plane loading. The veneer wall was supported at the base by a steel beam

(HEA 200) welded to RC frame (Figure 6.5). This wall was also connected to the masonry walls through wall tie, with the purpose of making a wide panel applied in large facades of buildings realist.

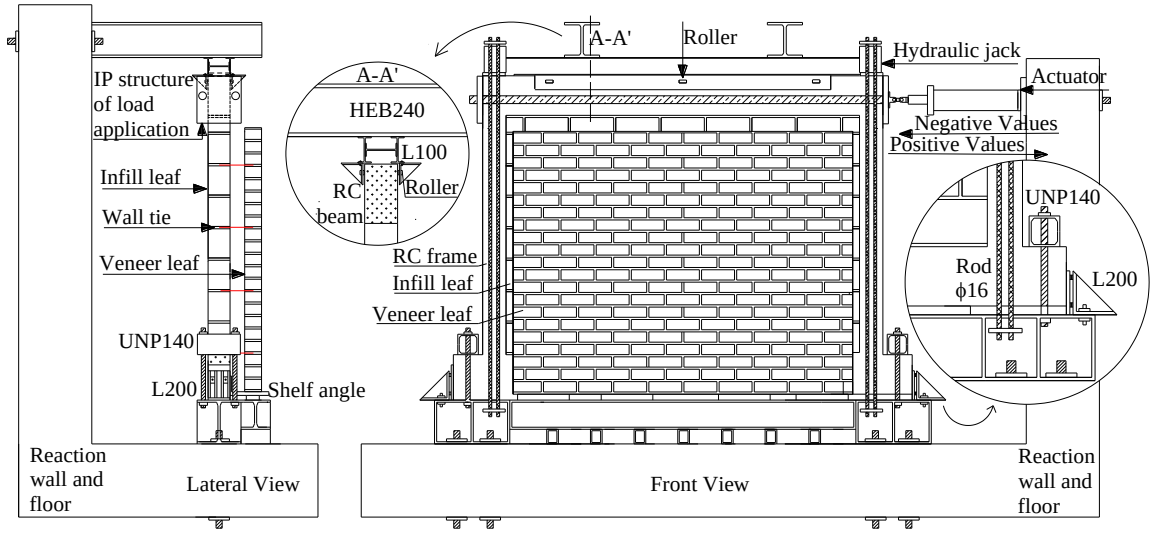

Figure 6.5 – Setup scheme for in-plane cyclic loading

A hydraulic actuator with a capacity of 250kN was attached to the reaction wall and connected at mid height of the top concrete beam of the RC frame, see Figure 6.5 (b). Two steel plates (400x300x30mm^3) were connected by two 2ϕ50 steel rods, one at each side, confining the top RC beam and enabling the application of reversed cyclic loading. One of them is coupled to the horizontal actuator by means of a hinge. A vertical load of 100 kN was applied at the top of the columns of RC frame through of two vertical jacks, corresponding to 25% of the column's axial force capacity. Each jack was pinned to the lower steel beam by means of two vertical rods at each side of the RC frame.

(a) (b) (c)

Figure 6.6 – In-plane test setup: (a) lateral view setup; (b) actuator, out-of-plane constraints and vertical loading; (c) in-plane instrumentation

The measurement of the main deformations of the walls during the static cyclic in-plane testing was carried out by 26 LVDTs distributed according to the layout presented in Figure 6.6 and Figure 6.7. As far as concerned to infill leaf, two LVDTS were considered to measure the horizontal displacement of the upper beam of the reinforced concrete frame (L1 and L26). Eight LVDTs were used to measure the relative displacement of the infill with respect to the surrounding frame in the corners (L6-L13). The control of possible undesirable displacements at the base of the walls due to regarding to gaps and clearances was also performed. The sliding and uplifting of the infilled frame with respect to the steel profile and of the steel profile with respect to the strong floor was recorded by LVDTs L14-L17.

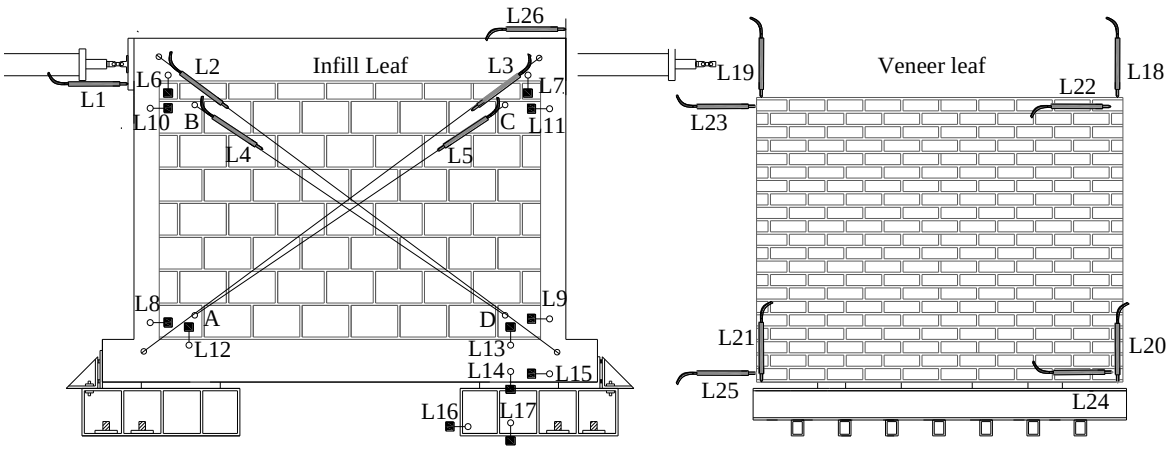

Figure 6.7 – Instrumentation scheme for in-plane cyclic loading

Two LVDTs were applied on the masonry infill to measure the main diagonal deformation on the free side (L4 and L5), and 2 LVDTs were mounted on the reinforced concrete frame to measure the diagonal deformation of the surrounding frame (L2 and L3). The deformations measured by these LVDTs enable to calculate the shear distortion of the masonry infill through the following expression:

$$\gamma = \frac{(\Delta d_1 - \Delta d_2) L_d}{2 L_h L_v} \tag{6.1}$$

Where γ is the shear distortion (rad); Δd_1 and Δd_2 are the length variation of diagonals length AC (measured through L5 for infill and L3 for RC frame) and BD (measured through L4 for infill and L2 for RC frame) respectively; the length L_d is the initial length of the diagonals (AC and BD); L_h is the initial horizontal length between points A and D and L_v the initial vertical length between A and B.

Regarding to the masonry veneer leaf, 8 LVDTS were mounted on corners of the panel to measure the vertical (L18-L21) and horizontal (L22-L25) displacement.

The in-plane cyclic test was performed by imposing different pre-defined levels of displacements through a control LVDT connected to the horizontal hydraulic actuator (L1). The displacement law adopted for in-plane quasi static cyclic testing is shown in Figure 6.8, which is based on guidelines provided by FEMA 461[156] with some adjustments: the displacement amplitude a_{i+1} of step i+1 is 1.2 times the amplitude a_i of step i. The loading protocol starts with a displacement of 0.9mm, representing 0.04% drift, calculated as the ratio between the top lateral displacement and the height at which the horizontal load is applied from the base of the RC frame. The maximum lateral displacement applied to the specimen was about 10mm, corresponding to a lateral drift of 0.5% drift, in order induce considerable damage in the masonry infill but avoid its collapse to enable to proceed with out-of-plane testing. Each step was repeated two times, except the first step that was repeated six times.

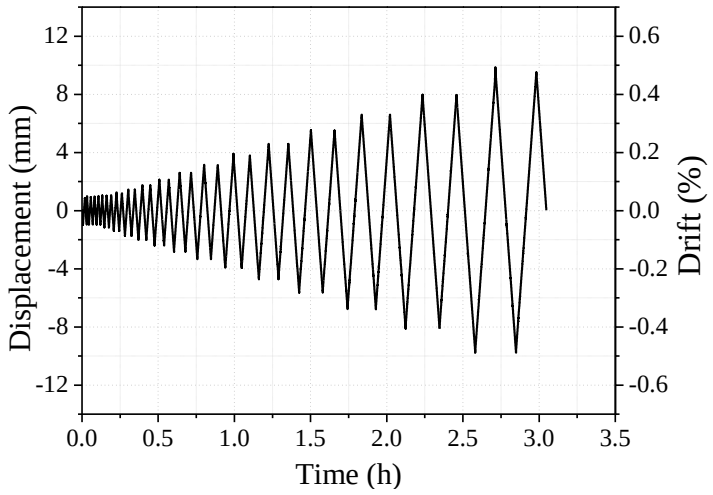

Figure 6.8 – Displacement protocol for in-plane testing

6.3.2. Out-of-plane tests

For the out-of-plane cyclic test, a complex solution was designed in order to promote the ideal boundaries conditions for the brick veneer walls. The out-of-plane loading system consisted in three parts: (1) a braced loading frame, (2) a structure to simulate distributed loading and (3) a braced reaction frame (Figure 6.9 and Figure 6.10).

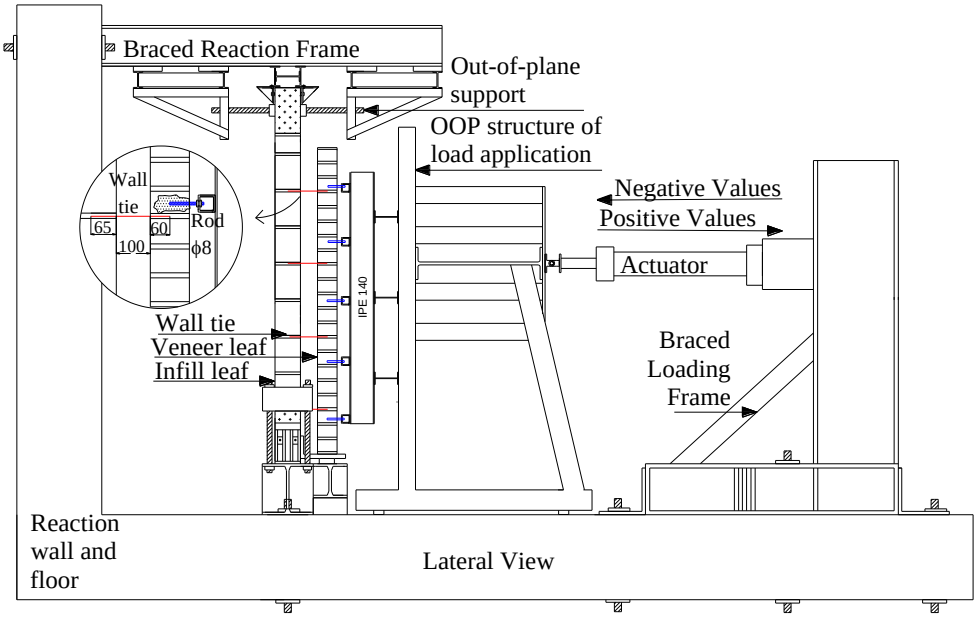

Figure 6.9 – Setup scheme for out-of-plane cyclic loading

(a) (b)

Figure 6.10 – Out-of-plane setup: (a) global view of test setup and (b) instrumentation of infill leaf

The top steel frame was reinforced to ensure that the top beam of RC frame was adequately constrained to out-of-plane movements. The restraint was carried out by using four steel rods M40 attached to a steel triangular structure, connected to two HEB 240 steel profiles that were fixed to the lateral reinforced concrete reaction wall. The out-of-plane loading was applied by a structure composed by a welded stiff L-shape profile with a horizontal HEB220 steel profile, an inclined HEB160 steel profile, two perpendicular HEB140 steel profiles and finally a set of tubular elements UNP50. Four rollers were added at the base of the steel frame to enable its free movement along the horizontal direction without developing friction

and thus to induce additional force recorded by the horizontal actuator. This framed structure distributes the load from hydraulic actuator into 30 load points (5 rows and 6 columns). Each load point covers an area of about 0.14m^2, as shown in Figure 6.11 and Figure 6.12. The framed structure is connected to the veneer wall trough of threaded rods HIT – V 5.8 anchored to the clay masonry veneer using the Hilti HIT – HY 270 adhesive anchoring system in each load point (Figure 6.11). This structure is a steel rigid HEB360 steel profile fixed adequately to reaction floor to completely prevent its uplifting and sliding during the test.

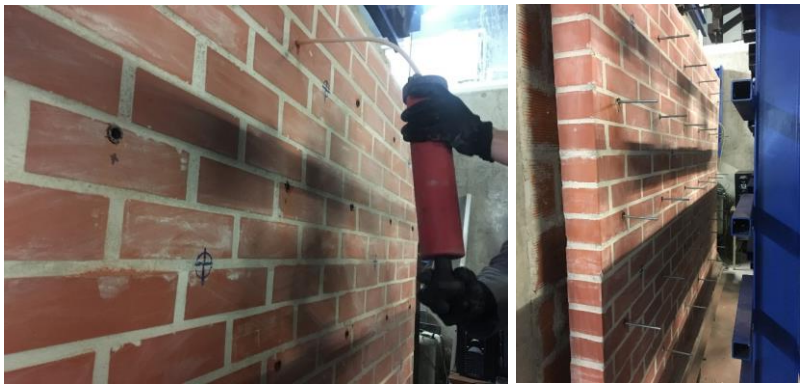

Figure 6.11 – Preparation and previous application of HIT – V 5.8 rods on veneer leaf

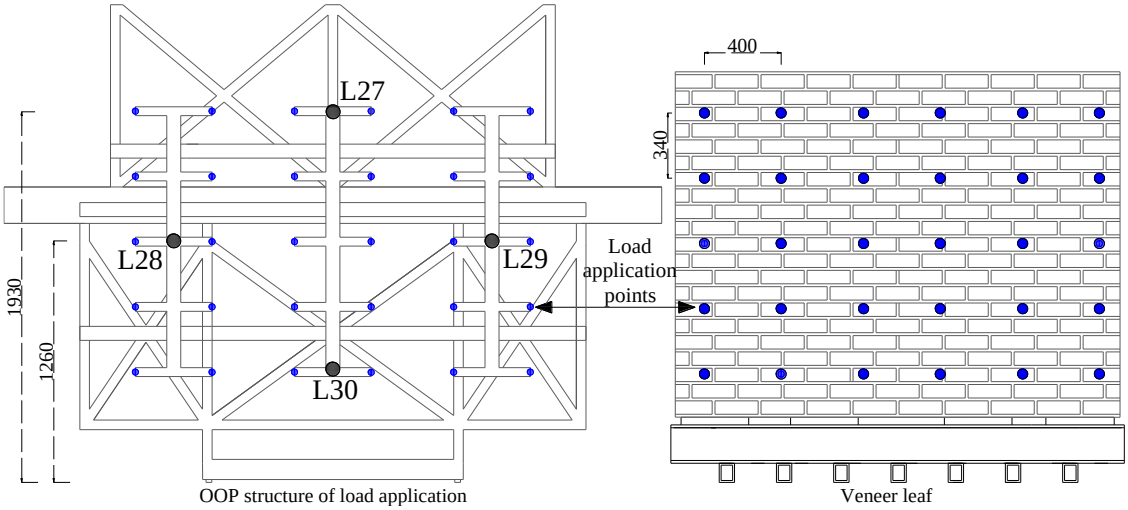

Figure 6.12 – Load application points layout scheme on structure and veneer leaf

The instrumentation of the infill and veneer brick walls was designed to measure the main deformations was based on 31 LVDTs as shown in Figure 6.10, Figure 6.12 and Figure 6.13. The out-of-plane deformation of the brick infill was monitored in the back side through 11 LVDTs. LVDTs L1 to L4 were applied to measure the relative displacement between masonry infill from the surrounding RC frame. LVDTs L5 to L11 measured the out-of-plane deformation of the infill panel during loading. Two additional LVDTs were placed to control

de out-of-plane movement of the boundaries, namely at the bottom and top RC beams (L0 and L12). In the brick veneer walls, 12 LVDTs were placed according to the layout presented in Figure 6.13 to measure the main deformations. An additional LVDT was placed on the connection between actuator and structure of load application to compare the internal displacement of the actuator and the real displacement that is imposed to the veneer wall.

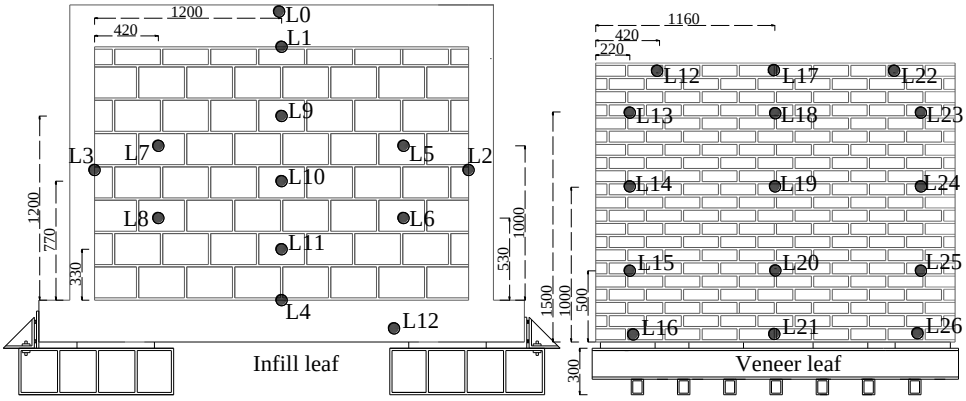

Figure 6.13 – Instrumentation scheme for out-of-plane cyclic loading

Four LVDTs were placed at the external borders of the load application structure to measure the real displacement imposed during test and its distribution on veneer leaf, as indicated in Figure 6.12 (L27-L30). The loading protocol was based on FEMA 419 [156] described previously for the in-plane test: the displacement amplitude a_{i+1} in step i+1 is about 1.2 times the amplitude a_i in step i. All levels are repeated twice, with exception of the first cycle that is repeated 6 times. Only the first wall "T2_O_100_2.5_No flashing" was tested with a different law, which is presented in Figure 6.14 (a). The measured displacement law applied at a middle of the remaining brick veneer walls is presented in Figure 6.14 (b). This law was adapted from the first law in order to have more progressive displacements during the test.

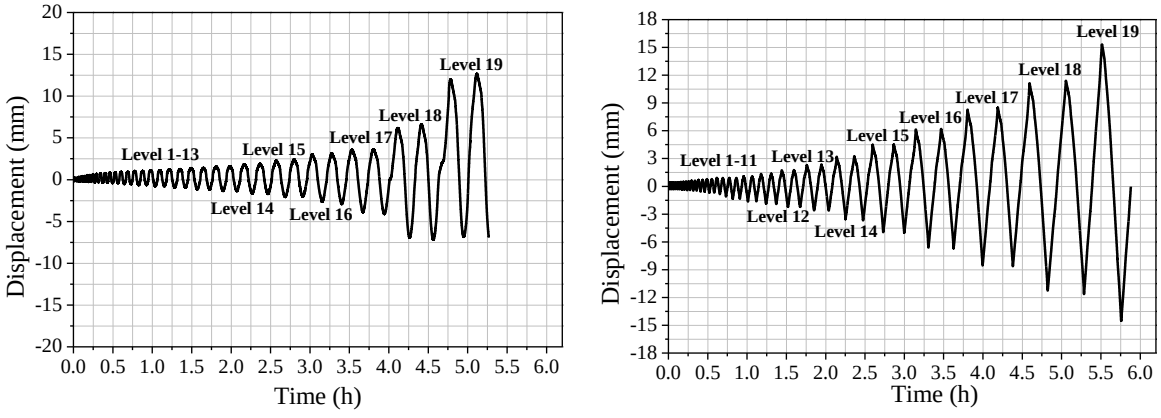

(a) (b)

Figure 6.14 – Displacement protocol for out-of-plane testing of (a) specimen T2_O_100_2.5_No flashing wall; (b) all walls with flashing

6.4.Experimental in-plane results

Only one wall was tested under in-plane cyclic loading, and its detailed characterization is here presented. This topic includes: (1) a brief characterization of the hysteretic force displacement diagram; (2) a discussion of the seismic indicators (stiffness degradation, plastic residual deformation, dissipation energy and equivalent viscous damping ratio); (3) a discussion of the main deformation features and (4) typical failure modes.

6.4.1. Lateral force-displacement diagram

The positive direction is considered to be the direction in which the hydraulic actuator pushes the specimen, whereas the negative direction is the direction in which the actuator pulls the specimen through two plates that were connected with two thick steel rods. The load-displacement cyclic diagrams shown in Figure 6.15 (a) relate the displacement measured at mid height of the of RC beam by LVDT L1 and by L26 placed in the opposite side of frame. The force-displacement backbone curves are also presented in Figure 6.15 both for the first and second cycles and for negative and positive directions. The backbone curves result from connecting the points of maximum force per cycle with linear segments, following the suggestion pointed out by Frumento et al. (2009) [157].

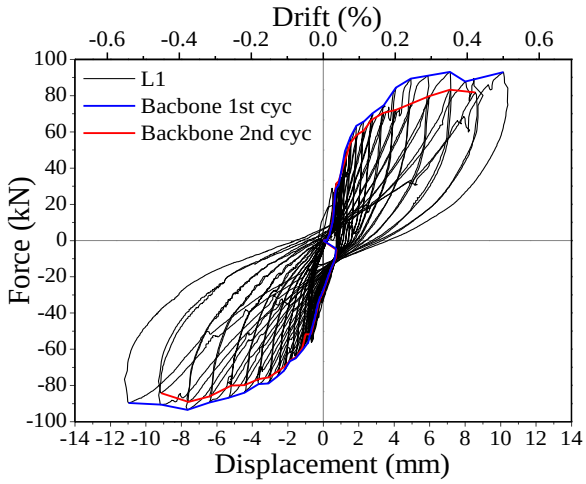

Figure 6.15 – In-plane force-displacement diagram: cyclic response with backbones corresponding to first and second cycles

Figure 6.16 (a) summarizes the maximum in-plane strength (F_{max}) and correspondent drift (in percentage). Figure 6.16 (b) indicates the values of the maximum resistance obtained for the first and second cycles and for both positive and negative directions.

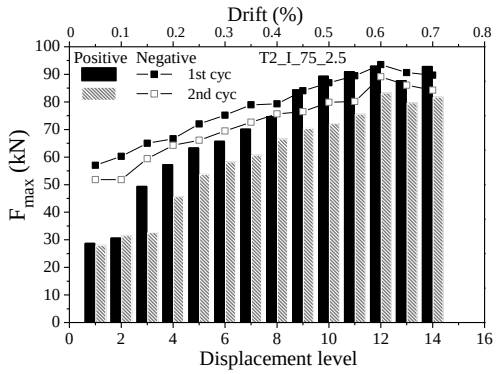

(a)

Negative direction	1st cyc	$\boldsymbol{F_{max}}$ (kN)	93.55
		δ_{Fmax} (mm)	7.65
	2nd cyc	F_{max} (kN)	89.13
		δ_{Fmax} (mm)	7.59
Positive direction	1st cyc	F_{max} (kN)	93.01
		δ_{Fmax} (mm)	7.15
	2nd cyc	F_{max} (kN)	83.21
		δ_{Fmax} (mm)	7.14

(b)

Figure 6.16 – Maximum strength: (a) obtained in each level displacement in positive and negative direction of load application and (b) obtained in in-plane test and correspondent displacement

Based on the backbone curves and the of maximum lateral load obtained for first and second cycles (Figure 6.15 (a) and Figure 6.16 (a)), it is possible to observe that the strength degrades from first to the second cycle. The strength maximum loss of about 30%, occurs after 3rd, which corresponds to the onset of nonlinear response due to accumulated damage and development of cracks. At maximum resistance, the difference is lesser, being the first cycle resistance higher 12% and 6% for positive and negative load records, respectively.

It appears that the specimen shows almost symmetric behaviour in the positive and negative direction. The higher asymmetry for low levels of lateral imposed displacement is associated to initial clearances on setup conditions, initial adjustments and the asymmetry in the lateral load application, as only one horizontal actuator is used.

6.4.2. Discussion of seismic performance

The discussion of in-plane behaviour of the RC frame with brick infill walls attached to the brick veneer wall is based on some seismic indicators, namely: (a) initial stiffness and stiffness degradation, (b) plastic or residual deformation, (c) energy of dissipation and (d) equivalent viscous damping ratio. These indicators were calculated based on the cyclic force-displacement diagrams presented in Figure 6.15.

a) Initial stiffness and stiffness degradation

The initial stiffness, *K*, was defined as the secant stiffness measured for the maximum displacement calculated for each cycle. Due to asymmetric behaviour abovementioned, the initial stiffness differs slightly for both directions, see Figure 6.17. The wall exhibits a

progressive loss of stiffness in both directions, before and after the peak of strength. The stiffness loss varied between 67% and 80% since the initial stiffness until the maximum resistance.

As expected, once again there is a little difference between first and second cycle, associated to strength degradation between cycles. This is related to the accumulation of damage when the loading path is repeated for the second time.

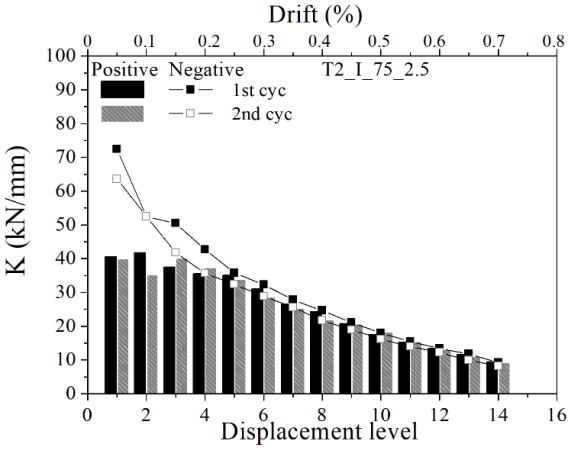

Figure 6.17 - Stiffness degradation of specimen test in-plane loading

b) Plastic residual deformation

The plastic deformations were determined in the unloading branch of the force-displacement diagrams for positive and negative loading when the force is zero, and they are presented in Figure 6.18 for first and second cycles. It is seen that the plastic deformations in the positive direction are always positive and present an increasing trend. In the negative direction, the plastic deformation is very close to zero until the lateral drift of 0.23%, after which present negative values. This asymmetry should be in certain extend associated the existence of only one actuator, and to the fact that it present different performance when it pull or push the wall. It is observed that in the first cycles (until 3rd level) the plastic deformations are constant and very low for both directions of load, which is attributed to the linear behaviour of the wall. After the 10th displacement level (lateral drift of 0.23%) the increasing of residual deformations is considerable, which results from the nonlinear behaviour of the wall.

At the end of the test, the values of residual deformations are different, being the negative plastic deformation about 30% of values of residual deformations from positive plastic deformations in the first cycle. In the negative direction, there is a higher increase of the plastic deformation in the second cycle of loading in the nonlinear regime.

The maximum displacement at ultimate cycle is about 10mm and the maximum plastic residual deformations is almost 4mm, in positive direction, which represents about 25% of total deformation.

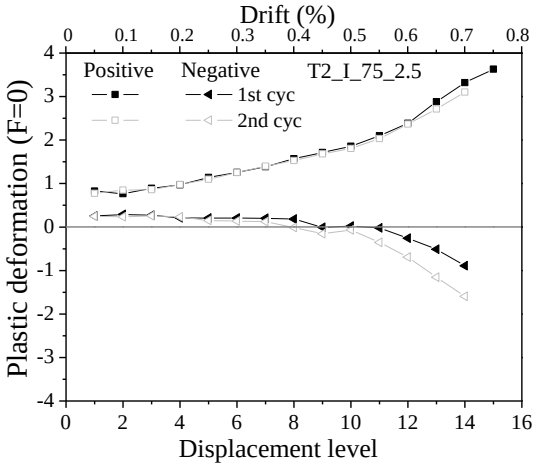

Figure 6.18 - Plastic residual deformations during in-plane cyclic test

c) Energy of dissipation and equivalent viscous damping ratio

The cumulative dissipation of energy, CG_f, was calculated as the sum of the energy dissipated at each cycle until a certain displacement, G_f, and it represents the amount of energy dissipated during the cyclic loading.

As expected, the energy is increasing for increasing displacements. The onset of the nonlinear behaviour of the wall occurs for the 3rd level of displacement (1.2mm of displacement and 0.6% of drift), associated to the formation of cracks. After this displacement level, the increase on the dissipation energy increases markedly, as shown in Figure 6.19 (a), achieving a value of about 1700kNmm at the level of maximum resistance. The values of energy recorded during the second cycle are lesser than values of first cycle, which appears to indicate that no significant new damage develops during the second cycle.

Another parameter correlated with dissipation of energy is the Equivalent Viscous Damping Ratio (EVDR), whose definition has been already presented in Chapter 4. Figure 6.19 shows the values of EVDR for the specimen tested under in-plane loading for each displacement level. It is clear that there is trend for the EVDR decreases as the lateral displacement increases. This trend is justified by the increasing plastic deformations and pinching in the reloading branch. Besides, it is seen that the second cycle presents lesser damping capacity confirmed by lesser energy of dissipation. It is observed also that after the 3rd displacement level (1.2mm of displacement and 0.6% drift), corresponding to the onset of nonlinear behaviour, the decrease evolves to a lower rate, which is associated to the nonlinear.

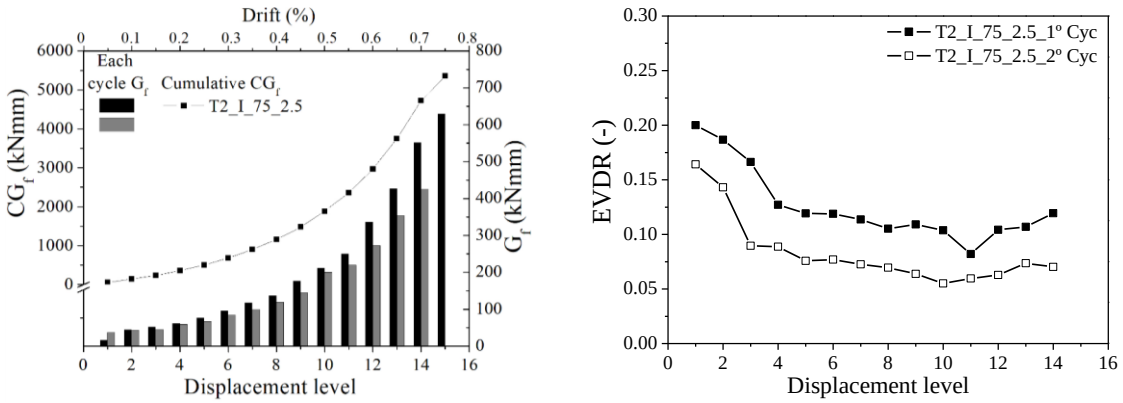

(a) (b)

Figure 6.19 – Evolution of (a) energy of dissipation and (b) EVDR during in-plane cyclic test

6.4.3. Deformational features of the infill and veneer leaf

The cyclic in-plane test of the infilled frame was performed until the lateral drift of 0.5% both in the positive and negative directions, which based on existing results, it was assumed to lead to substantial damage. During the cyclic in-plane loading, it was observed that two diagonal cracks opened at a displacement of 1.2mm. This event could be recorded through the lecture recorded by diagonal LVDTs (Figure 6.20) that enables also to calculate the shear distortion of the masonry infill wall and RC frame. The diagrams relating the lateral force and shear distortion for RC Frame and masonry infill wall are presented in Figure 6.21 (a) and Figure 6.21 (b), respectively.

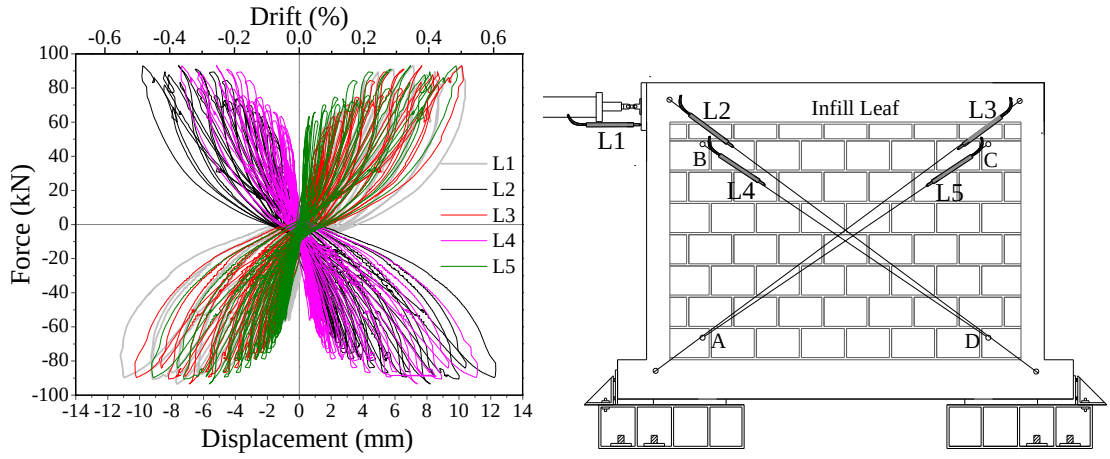

Figure 6.20 - Diagonal openings responses of RC frame and infill wall during in-plane cyclic test

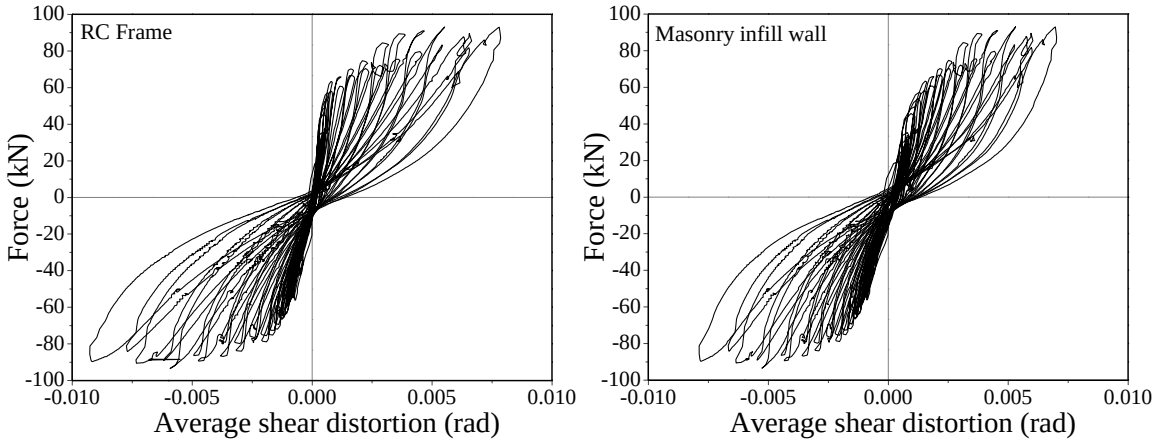

(a) (b)

Figure 6.21 - Average shear distortion of the (a) RC frame and (b) masonry infill wall

It is observed that the nonlinear trend found in the shear distortion of the reinforced concrete frame and masonry infill wall started at the lateral force about 50kN, corresponding to the lateral drift of 0.06% (1.2mm). This resulted from initial separation of masonry infill from RC frame and the formation of the first diagonal cracks in the infill in both directions. At this stage, the average shear distortion of the RC frame reached 0.0004 rad, whereas the shear distortion of masonry infill leaf was 0.001 rad. After this point, the stress redistribution is evident and the deformation of masonry infill increased. At maximum resistance, the average shear distortion of the masonry infill leaf reached 0.0053 rad and the shear distortion of RC frame achieved a shear distortion of about 0.0055 rad. In the post peak regime, the difference is even more important. In the last cycle of displacement, the shear distortion of the RC frame was about 0.0079 rad, being 13% higher than the shear distortion recorded in the masonry infill leaf, due essentially to evident separation of the infill from the RC frame and consequent development of the shear strut connecting the upper and bottom corners.

The horizontal and vertical separation of the infill wall from its surrounding frame at different levels of imposed displacement is represented in Figure 6.23 (a) and (b), respectively. At the lower corner, the first signals of separation of the masonry infill from the RC frame is recorded since the staring of the test, but it was increasing during the test. However, the final values of the separation are very low, lesser than 0.5mm at final of the test. At the upper corners, higher values of separation of infill wall from the RC frame were recorded. The width of the horizontal separation at the boundaries of the infill wall is lesser than 2mm and the vertical separation is lesser than 1.5mm for the maximum drift applied of 0.5%.

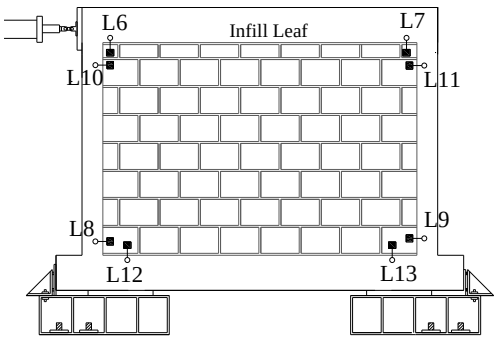

Figure 6.22 – Position of LVDTs in RC frame and masonry infill leaf

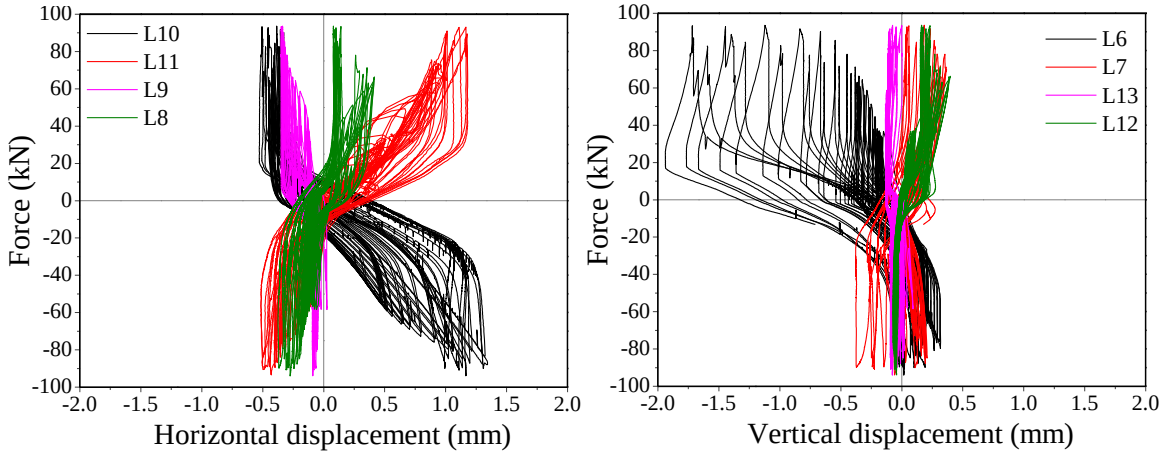

(a) (b)

Figure 6.23 – Relative displacement of masonry infill in relation to the RC frame: (a) horizontal and (b) vertical separation

Figure 6.25 shows the relation between vertical and horizontal displacements measured at corners of veneer masonry wall (L18 to L21) with the control displacement (L1) and correspondent drift. The load vs displacement/drift is also presented in order to correlate the de responses of infill and veneer leaf.

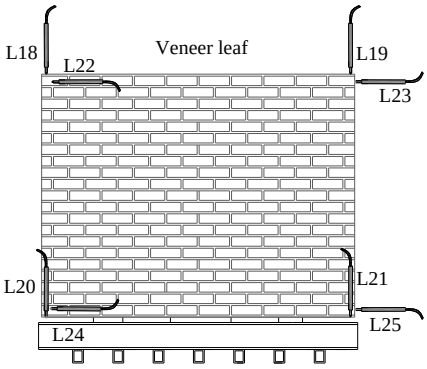

Figure 6.24 – Position of LVDTs in veneer leaf

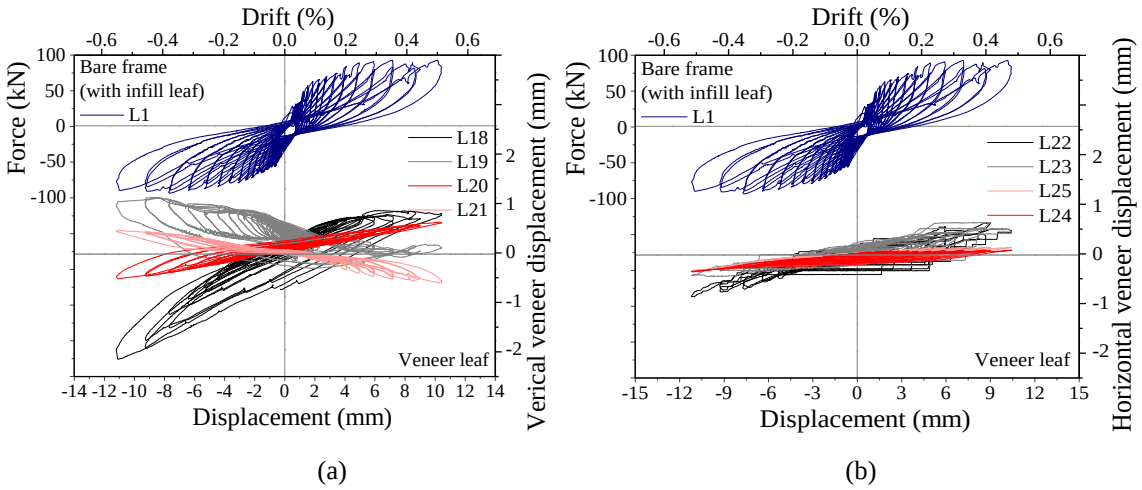

Figure 6.25 – In-plane force vs displacement diagrams of the infill wall and displacement of infill wall vs. (a) vertical displacement (b) horizontal displacements at each corner of veneer leaf

The maximum vertical displacement observed at the opposite corner to the load application point, measured by L18 was about 2 mm for an imposed lateral displacement of 10mm. In the corner of load application side, a displacement of about 1mm was measured by LVTD 19. Although the deformation of the veneer is very low comparing with infill deformation, it is seen that it exhibited a flexural rocking deformation due to lateral load application.

The deformation was lower in lower corner of veneer leaf, as expected taking into account higher restriction at bottom side compared to the upper free boundary of veneer leaf.

Another indicator of load transfer to and masonry veneer wall was also captured by strain gages of wall ties. The strains measured in each wall tie are presented in Figure 6.27. It is clear that the level of strain was very low, and for this reason the damage on wall ties was not visible at naked eye. This result appears to be in accordance to the results from the study presented in Chapter 4 on wall ties-masonry assemblages under shear loading, from which it was possible to observe that the ties presented a very reduced damage. Nonetheless, it is possible to compare the values between bottom and upper rows. The strains gauges of wall ties distributed in upper row, T4a-c, show higher values of strain than the strain gauges of wall ties distributed in lower row, T1a-b. The values of strain gauges increased with the height of veneer leaf, resulting from the deformation of the wall, which is higher in the upper part of the walls.

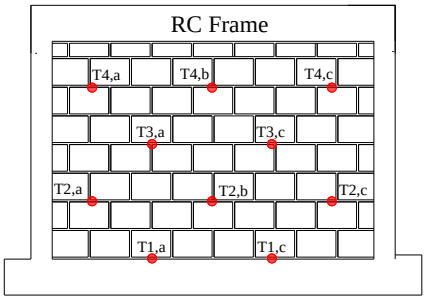

Figure 6.26 – Position of wall ties

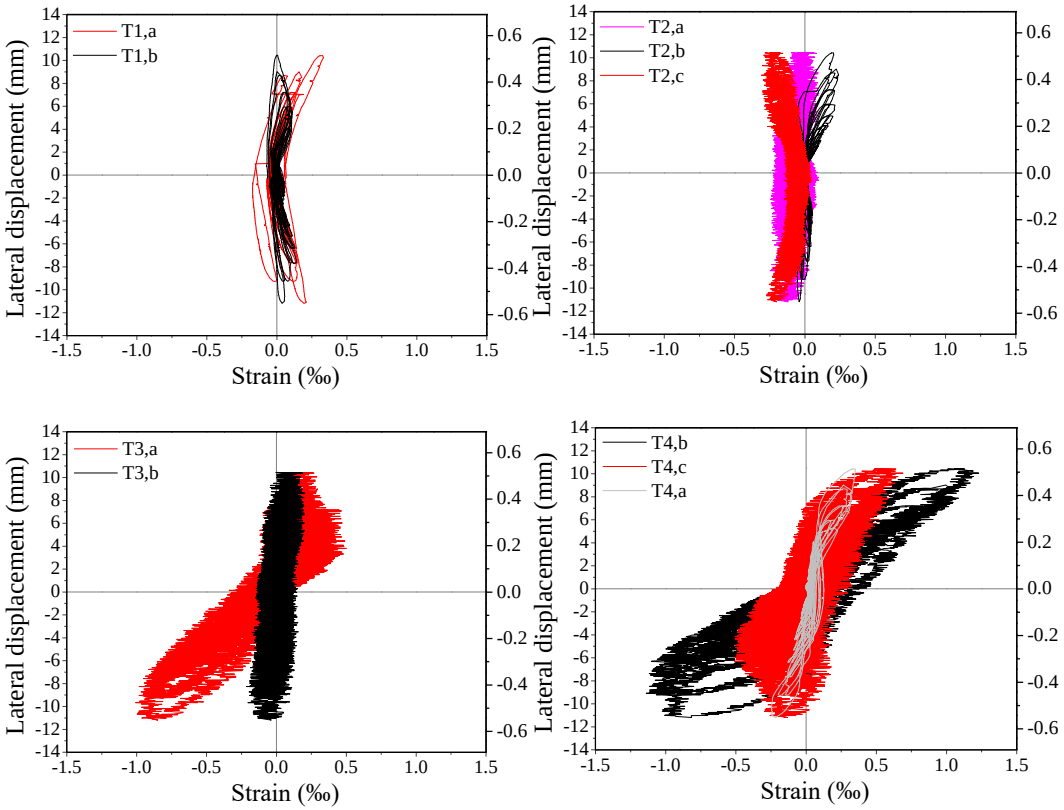

Figure 6.27 – Strain gauges of wall ties distributed in each row and in each position

6.4.4. Typical damage patterns

The first crack developed at the lateral drift was equal to 0.06%, corresponding to the onset of nonlinear behaviour of masonry infill wall. By increasing the lateral displacement, the cracks propagate along the diagonals of the masonry infill as stair step cracks passing through head and bed mortar joints, as shown in Figure 6.28 and in Figure 6.29 (a).

The separation of the infill wall from its bounding frame appears to start at the lateral drift of 0.13%, especially at the corner adjacent to the applied load. This was extended in the subsequent cycles as seen in Figure 6.29 (b). The crushing at upper mortar-beam interface shown in Figure 6.29 (c) was also identified due to friction accumulated stress. The most

serious crushing of the bricks was observed at the last imposed lateral drift of 0.5% (Figure 6.29 (d)), and localized along the "compression strut diagonal".

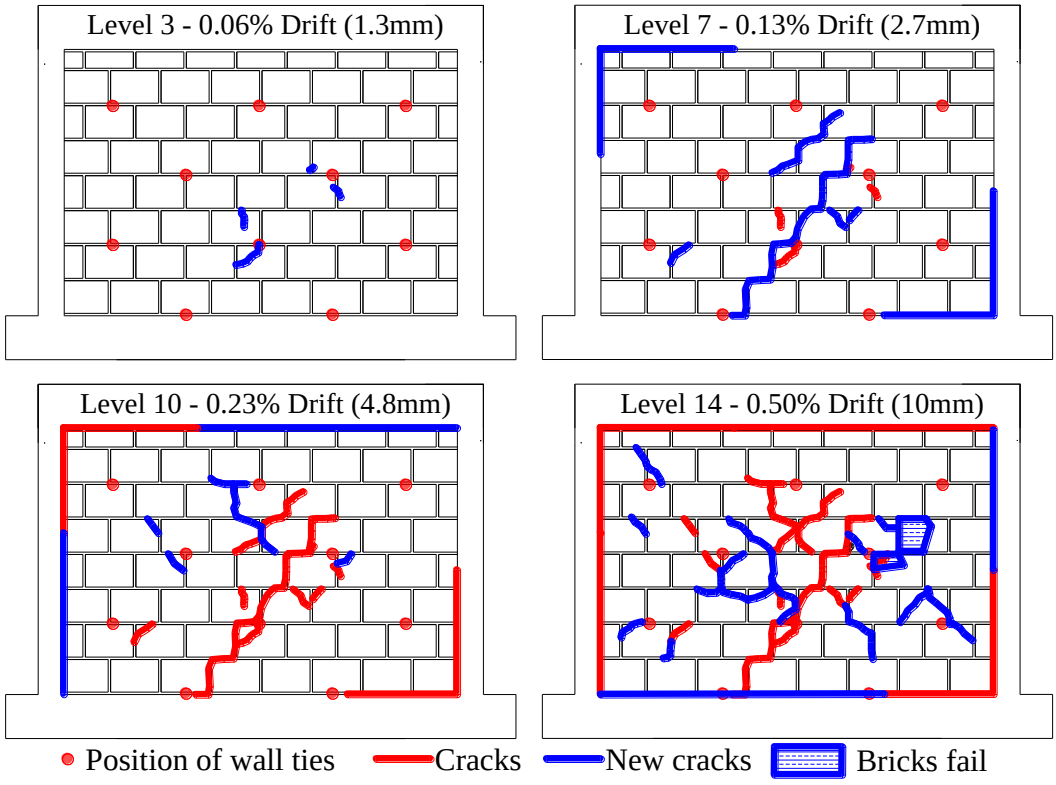

Figure 6.28 - Crack propagation in the specimen at lateral drift of 0.06%, 0.13%, 0.23% and 0.5%

The masonry veneer leaf did not exhibit any visible signal of damage during the cyclic test. In order to obtain a more clear idea about the deformation of the brick veneer walls, it was decided to multiply the real displacements at the final of the test (0.5% drift) by 100 times, see Figure 6.30. This exercise enables to amplify the real deformations measured at the corners under negative loadings, that could be used as reference in the symmetric behaviour obtained under positive loadings. The amplification of real deformations shows the potential development of a flexural rocking mechanism, see Figure 6.30. Consequently, crushing on compressive areas and cracks on tension area could be possible damage patterns that would be found in the masonry veneer wall. Based on deformations of the masonry veneer leaf, it is possible to see that the right upper corner is the point with higher deformations.

Figure 6.29 – Typical failure modes reported in infill leaf at 0.5% of drift

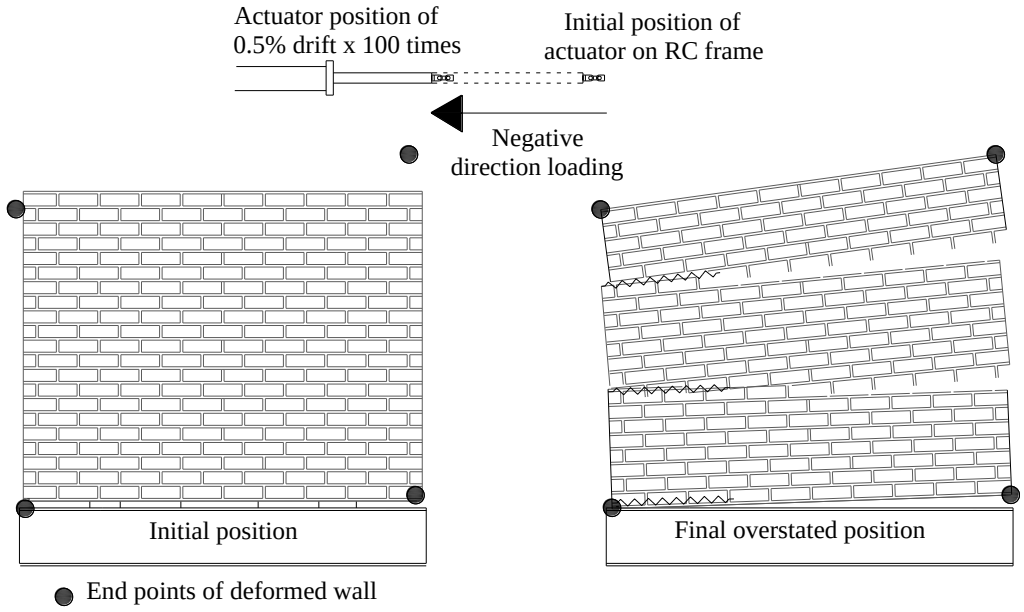

Figure 6.30 - Possible behaviour of veneer exaggerated 100 times from real deformations

6.5. Results of the out-of-plane tests

The analysis of results of the out-of-plane static cyclic tests is carried out considering different response indicators: (1) force-displacements hysteresis diagrams; (2) deformation features and (3) failure modes. In this section, these parameters are presented and a discussion of their general behaviour is provided.

6.5.1. Hysteretic diagrams

The cyclic force-displacement responses for each masonry veneer wall are presented in Figure 6.31 and Figure 6.32. For the masonry veneer walls, two force-displacement diagrams are provided, namely considering the out-of-plane displacement measured at the top (L17) and the out-of-plane displacement measured at mid height of the wall (L19). Together these diagrams, it was decided also to add the force-displacement diagrams of the masonry infill wall (backing wall) considering the displacement measured at the centre of the walls. The idea of representing these different diagrams consisted of: (1) making the comparison of the deformations at masonry veneer and masonry infill easier; (2) enabling the comparison between the displacement at the top and centre of the masonry veneer. It should be mentioned that the positive and negative values of force induce tension and compression stresses on ties respectively. Due to these different types of loading, the nonlinear hysteretic response was not symmetrical in majority of cases because the wall ties have different behaviour under compression and tension loading as already seen in Chapter 4. Nevertheless, it is highlighted that in some types of walls, whose compression behaviour is comparable with tension behaviour, namely T2_O_100_2.5 and T2_O_75_2.5, an almost symmetric behaviour is obtained.

The hysteretic curves of walls T2_O_100_1.4/2.5 and T2/T4_O_75_2.5 are slightly flat at the origin, when there is the load inversion, which is associated to the pinching effect. This effect is correlated to the accumulated damage and clearances created, promoted by the contact loss between tie-mortar due to degradation of the connection in successive cycles.

For a better assessment of the performance among the different masonry veneer walls, a comparison between obtained and expected maximum forces (F_{max}) was carried out, see Figure 6.33. The expected force is an estimation based on previous results from the cyclic tensile-compression tests (Chapter 4 and chapter 5) The expected force was, thus, calculated by multiplying the obtained tensile/compression maximum force obtained in single tie-

masonry prims assemblages by the number of connection presented in each wall, see Table 6.2.

It is seen that the maximum capacity was recorded in walls with lesser spacing of ties either constructed with T2 or T4 wall ties. Meanwhile, the tension maximum capacity of the walls built with T2 is similar with T4 wall ties. In compression, the resisting capacity of the veneer walls is different when wall ties T2 and T4 are used, as recorded in individual assemblages. The walls built with wall tie T2 was able to achieve a similar tension and compression maximum capacity.

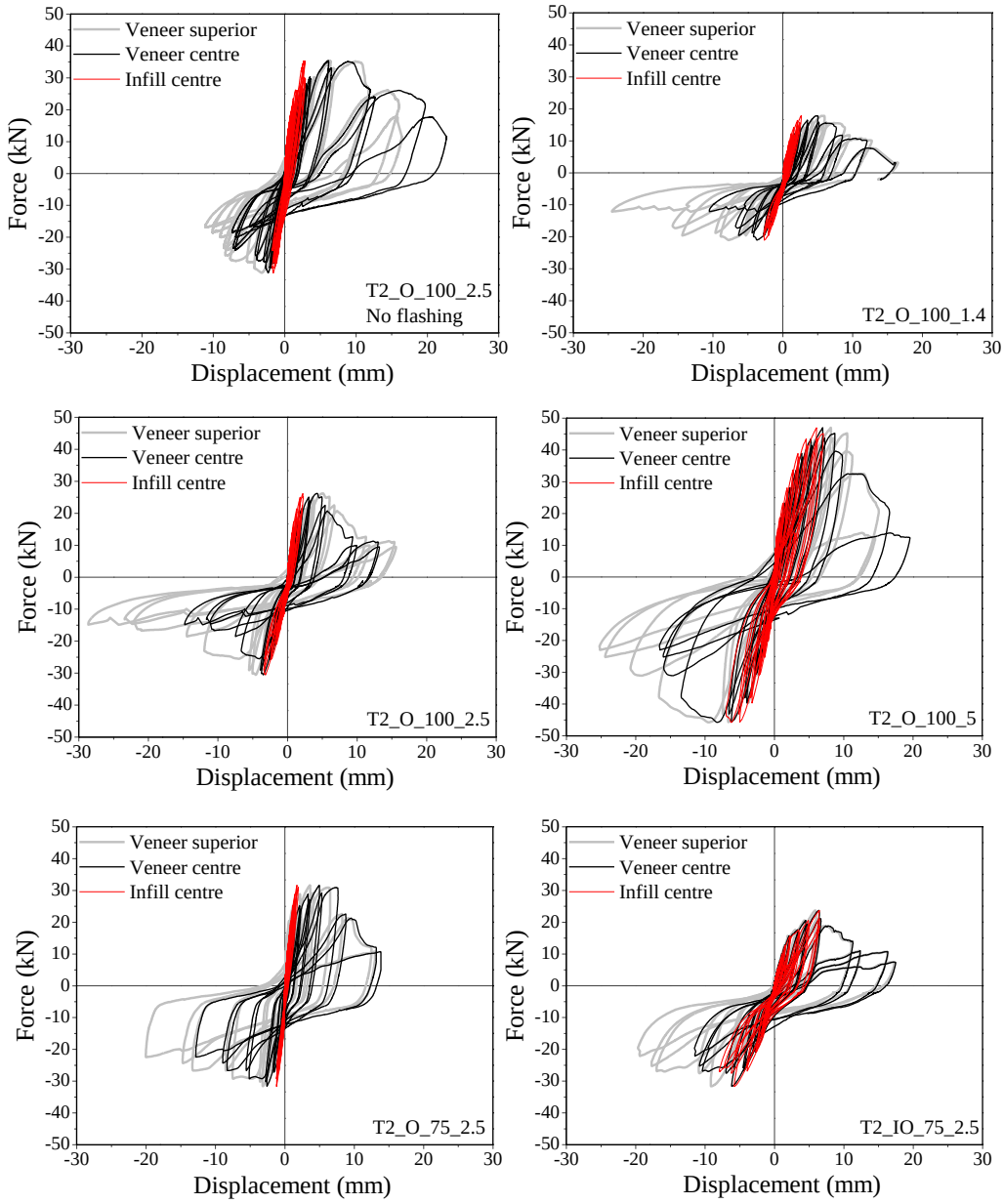

Figure 6.31 – Hysteretic diagrams for walls constructed with T2 tie typology

Based on this estimation it is possible to understand in which extent the resistance of the individual tie-brick connection can be reproduced in the masonry veneer wall.

In compression behaviour, some walls built with wall tie T2 presented a lower resistance than the theoretical and other walls presented a maximum capacity higher than the estimated value. The reduction of resistance in the masonry veneer walls ranged from 30% to 46%, being the highest difference recorded in wall T2_IO_75_2.5. On the other hand, the resistance of the walls built with T4 is always higher than the estimated value, being the differences in the range ranges from 23% and 69%.

Under tension, the walls presented almost always an experimental capacity lower than the estimated value. The difference varied between 0 and 126%, being the maximum difference observed in wall T2_IO_75_2.5, which was submitted to previous in-plane damage.

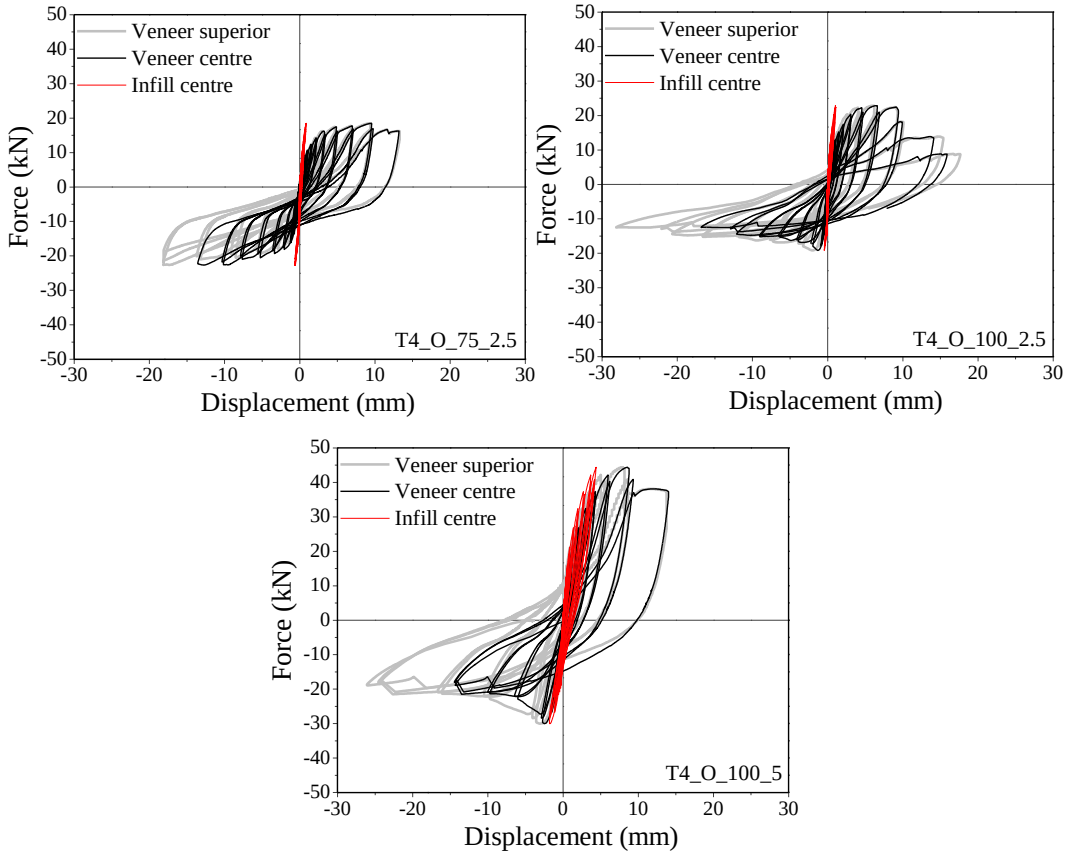

Figure 6.32 – Hysteretic diagrams for walls constructed with T4 tie typology

Based on the analysis of results on the experimental and estimated load capacity of the masonry veneer walls, it is seen that under compression, there is a clear trend but under tension, there is a trend for the experimental value is lower than the estimated load capacity. The discrepancy between experimental and estimated values can be explained by the workmanship in the application of the wall ties (misalignment in wall ties), differences on boundary conditions of single connections and walls, load application mode and a combination of them.

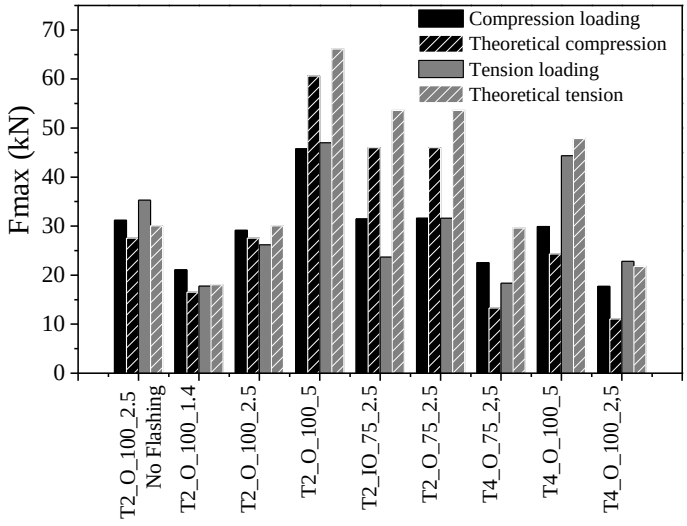

Figure 6.33 – Comparison between estimative and obtained maximum resistances.

Table 6.2 – Summary of maximum forces and displacements obtained in individual assemblages and walls

		Compression Loading				Tension loading			
		F_{max} 1º cyc (kN)	F_{max} 2º cyc (kN)	δ_{Fmax} 1º cyc (mm)	δ_{Fmax} 2º cyc (mm)	F_{max} 1ºcyc (kN)	F_{max} 2º cyc (kN)	δ_{Fmax} 1º cyc (mm)	δ_{Fmax} 2º cyc (mm)
Single conecti ons [1]	T2_100_225_M10	2.75	2.53	2.92	2.98	3.01	2.68	3.87	5.18
	T2_75_225_M10	4.60	3.60	2.44	3.94	5.36	4.40	16.00	16.00
Walls with T2 wall tie	T2_O_100_2.5 No flashing	31.18	29.42	2.31	2.00	35.28	32.93	6.12	6.53
	T2_O_100_1.4	21.07	19.16	3.68	2.70	17.76	15.84	4.82	5.19
	T2_O_100_2.5	29.12	30.60	3.86	3.45	26.19	23.28	4.22	3.12
	T2_O_100_5	45.78	43.19	5.76	4.58	47.00	43.70	6.04	6.31
	T2_IO_75_2.5	31.49	27.57	5.98	6.97	23.70	21.09	6.37	6.66
	T2_O_75_2.5	31.60	30.24	2.58	2.74	31.61	29.15	4.98	5.33
Single conecti ons [1]	T4_100_225_M10	1.11	1.07	2.93	1.97	2.18	1.98	6.83	6.87
	T4_75_225_M10	1.33	1.28	2.88	3.00	2.96	2.47	13.00	13.20
Walls with T4	T4_O_75_2.5	22.56	21.73	9.89	10.25	18.35	16.77	9.22	9.64
	T4_O_100_2.5	17.7	19.19	0.86	1.27	22.83	20.96	6.49	6.88
	T4_O_100_5	29.93	28.30	2.57	2.72	44.35	40.83	8.53	9.31

[1] – Results obtained in experimental campaign of connections, chapter 4 and 5.

As far as concerned to strength degradation between maximum resistance of first and second cycles, it was observed that there was in majority of cases a slight loss of resistance. The highest loss was about 12% for wall T2_IO_75_2.5 under compression loading. The average loss of resisting load in tension is higher than in compression loading, being about 8.8% compared with 6% of strength loss in compression.

In all walls, a considerable difference between response at middle and top of veneer is noticeable, which is related to the different displacement measured at mid height. Taking into account that the veneer wall is simply supported at base and anchored through wall ties in its perpendicular direction, being the other three sides free to move out-of-plane, there is trend for the out-of-plane rotation of the wall, particularly in case of the wall ties are

compressed. In both cases the wall rotates, being the base of the veneer working as an "hinge". Therefore, it presents the highest out-of-plane displacement at the top of the wall and the lowest at the base. However, this difference is much more significative when the ties are compressed. This can be explained by the different behaviour of the ties under tension and compression. It was observed that when the veneer wall is pulled and the wall ties are submitted to tension, the veneer wall presents an initial sliding parallel to the masonry infill wall and the wall ties are pulled out across mortar joints of veneer and/or infill leaves. When the brick veneer walls are pushed towards the backing system, the wall ties are submitted to compression and due to constrains caused by compression buckling resistance of wall ties, the veneer walls present an evident rotation around the veneer base, being the maximum rotation observed at the top of wall. Practically all the walls experienced pinching phenomenon, being explored in more detailing in after section with regard to seismic indicators.

As far as force-displacement diagrams of infill walls are concerned, it is noticed that there is a significant difference with respect to veneer wall. The deformation of infill wall is dependent on the capacity that the wall ties have to transfer the out-of-plane loading to the backing system, taking into account that the load is applied directly in veneer wall. This is a very important aspect to take into account regarding the seismic behaviour because it shows the interaction between leaves and can provide some indications for a suitable structural design for resisting the loading. More deformation of the infill wall means that the wall ties accomplish its function of transferring the load, resulting in the increase of the seismic demand for the masonry infill walls. It is highlighted that the detailing of wall construction and correct application of wall ties is crucial for its adequate performance. Indeed, the deformation of infill leaf varied much according to type of wall. The higher the resisting capacity of the system, more communication exists between leaves and in turn, more deformation in the infill wall is observed. This feature can be seen in walls T2_O_100_5 in compression and tension loading and T4_O_100_5 under tension loading. In the specimen T2_IO_75_2.5 the infill wall deforms also simultaneously with the brick veneer wall. In this case, the previous in-plane damage corresponding to a lateral drift of 0.5%, namely the separation of the infill from its enclosing frame especially at upper boundary, results in higher out-of-plane deformation during the out-of-plane test. The deformations at the centre of veneer and infill leaves corresponding to the maximum capacity are given in Table 6.3. In addition, it was possible to define the ratio between both deformations in percentage ($\Delta = \delta_{Fmax}^{Infill} / \delta_{Fmax}^{Veneer} \times 100$). It is easily concluded that the walls showing lesser capacity to transfer

the out-of-plane load are constructed with the wall type T4 and with wall tie T2 without flashing. This is because the composite behaviour is much more controlled by the tensile bond of the wall ties to the mortar joints, being the load transfer jeopardized. In the walls with more number of wall ties (lower tie spacing) the load transfer is also improved, especially in case of wall tie T2. It means that in case of seismic events, these configurations should work better than other layouts, given they are able to mobilize the composite behaviour between brick veneer and backing masonry infill wall.

Table 6.3 – Summary of maximum force and correspondent displacement in out-of-plane tests

		T2_O_ 100_2.5_ No flash	**T2_O_ 100_1.4**	**T2_O_ 100_2.5**	**T2_O_ 100_5**	**T2_IO_ 75_2.5**	**T2_O_ 75_2.5**	**T4_O_ 75_2.5**	**T4_O_ 100_2.5**	**T4_O_ 100_5**
Compression	F_{max} (kN)	31.18	21.07	30.60	45.78	31.49	31.60	22.56	19.19	29.93
	δ_{Fmax}^{Veneer} (mm)	2.31	3.68	3.45	5.76	5.98	2.58	9.89	1.27	2.57
	δ_{Fmax}^{Infill} (mm)	1.61	2.64	3.40	6.24	5.66	1.20	0.66	0.35	1.79
	$\Delta_{\delta}^{Inf/ven}$ (%)	69.77	71.77	98.55	108.42	94.73	46.59	6.72	27.50	69.56
Tension	F_{max} (kN)	35.28	17.76	26.19	47.00	23.70	31.61	18.35	22.83	44.35
	δ_{Fmax}^{Veneer} (mm)	6.12	4.82	4.22	6.04	6.37	4.98	9.22	6.49	8.53
	δ_{Fmax}^{Infill} (mm)	2.71	2.62	2.20	6.08	6.46	1.74	0.83	1.03	4.38
	$\Delta_{\delta}^{Inf/ven}$ (%)	44.36	54.27	52.07	100.61	101.40	34.89	8.99	15.94	51.37

Other important aspect to highlight is the post peak behaviour of the infill wall. In the infill wall the maximum displacement was recorded at the displacement corresponding to the maximum resistance of system. This happens because after the maximum resistance have been achieved, the wall ties are not able to transfer loading anymore, being the deformation of infill wall very low or even absent.

6.5.2. Deformational features of the walls

The deformation of the brick veneer and masonry infill walls is analysed in detail herein. The lateral deformation profile measured at the centre of wall is provided in order to understand the differences in the deformation pattern among the different walls and understand considering the influence of the type of wall tie and its layout. The complete overview of the deformation patterns find for the walls is presented in Figure A.1 – Figure A.10 in Appendix A. The sequential deformations of the walls following the cyclic loading are presented in Figure 6.34 and Figure 6.35. The deformation profiles are shows the

displacements of masonry infill walls and veneer walls under tension (OOP tensile displacement) and compression (OOP compression displacement).

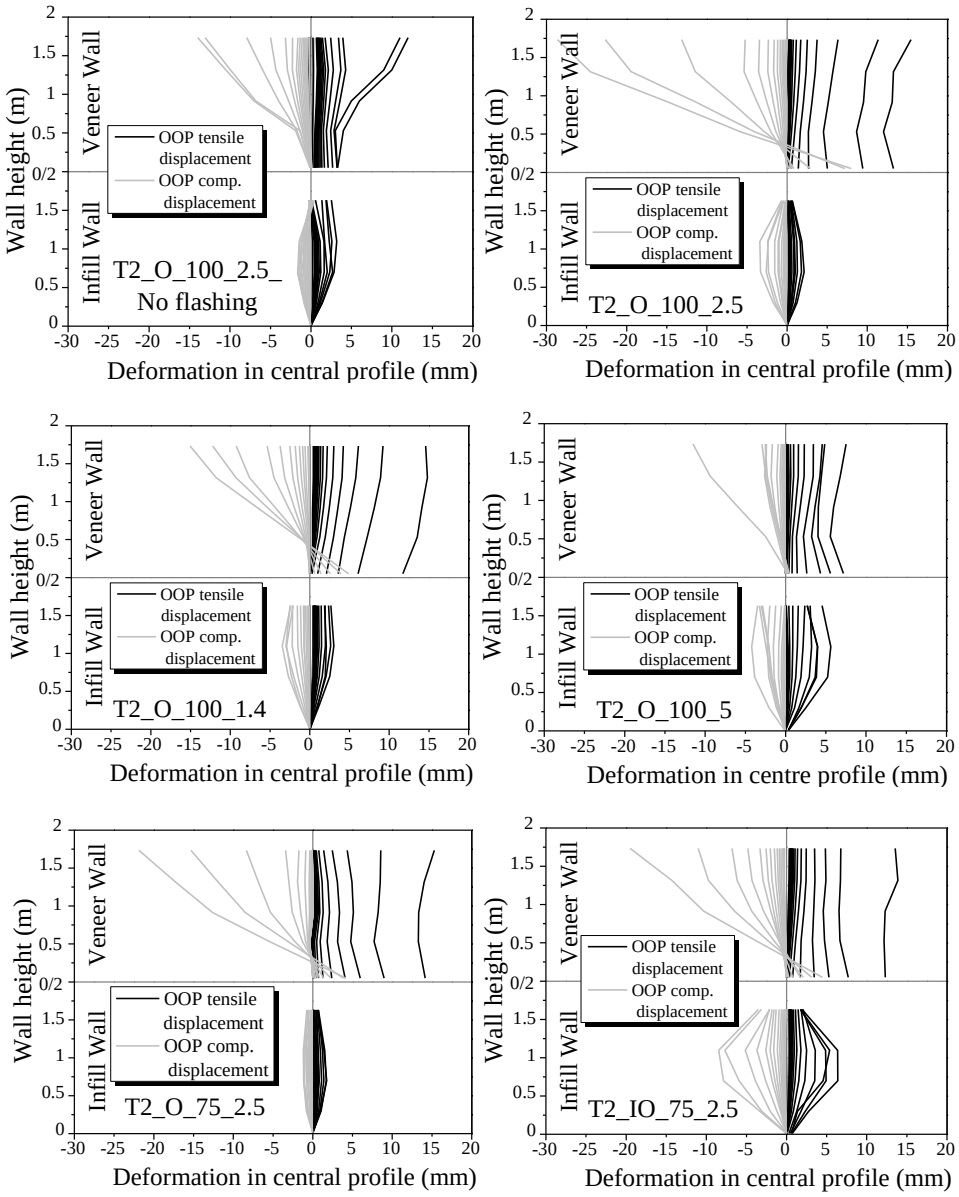

Figure 6.34 – Deformation of central profile of veneer and infill wall for specimens built with wall tie T2

Each deformation profile corresponds to the average displacements recorded in the first and second cycle of each imposed displacement level. Figure 6.36 and Figure 6.37 show the typical displacement field on the area of the walls to complement the information of lateral deformation profiles. It is seen that the central profiles of the infill and veneer wall leaves show higher lateral deformation, being represented in the deformation profiles. It should be mentioned that it is common that the displacements of the veneer walls measured by the LVDTs L12-L16 and LVDTS L22 to L26, measure different displacements, meaning that the veneer walls experiment rotation around the central vertical axis.

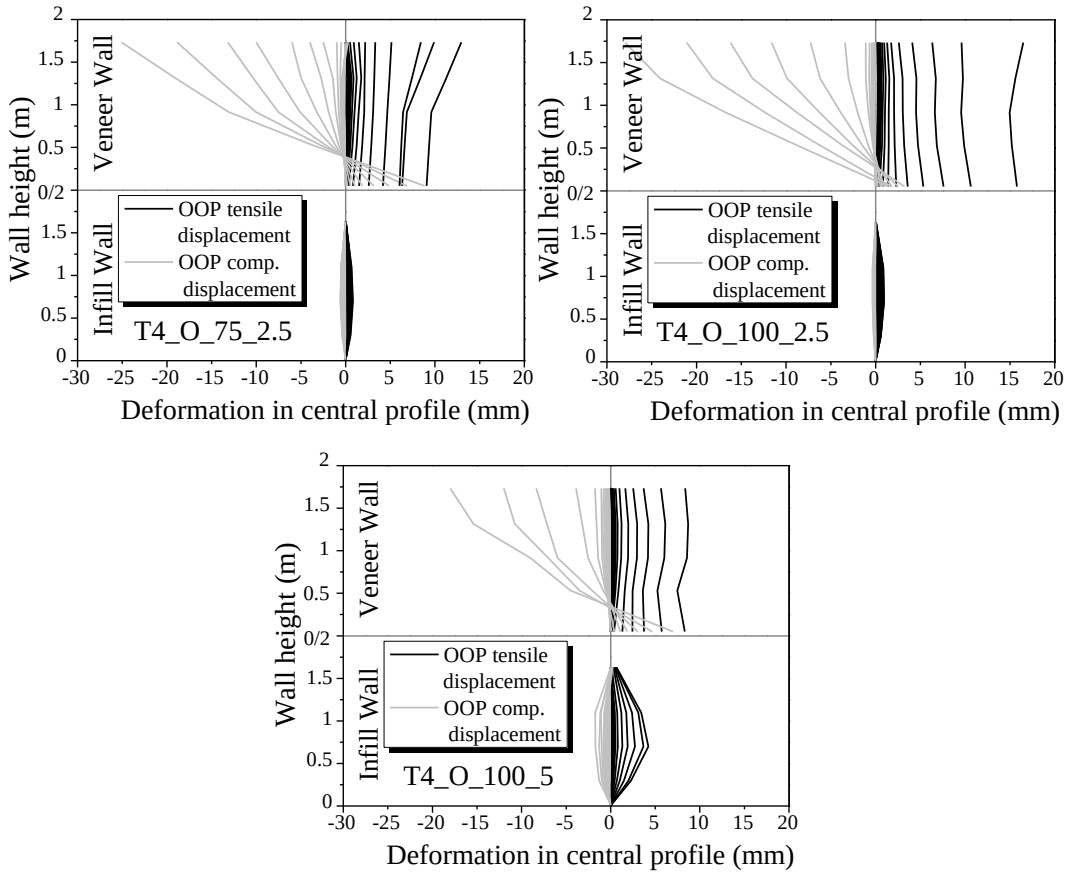

Figure 6.35 – Deformation of central profile of veneer and infill wall for specimens constructed with T4 tie

The displacement profiles along the vertical central line of the masonry walls are clearly different when the walls are submitted to tensile and compression loading. In a first phase, until the attainment of the peak load, the veneer wall did not exhibit great deformations, similarly to what happened in the infill wall. This should be attributed to the composite behaviour associated to the assemblage composed by both masonry walls. After failure of the connections, the stiffness of the system decreases substantially, resulting in the significant increase of the deformation of the walls. In case of the walls are submitted to compression loads, it is seen that horizontal rotation of the walls is more significant when compared to the rotation experienced when the walls are under tensile loading.

When submitted to tensile loading, it is seen that the out-of-plane displacement profiles show an almost parallel sliding of the veneer walls, resulting from the progressive pull-out of wall ties along the pull of the veneer wall. For this reason, the displacements measured at the surface of the veneer walls are more uniform. They are equal or lower than the displacement observed in top of veneer wall under same level of compression loading because practically there is no rotation. The effect of rotation causes an increase of displacement at the top of wall regarding to its centre. The different displacement profiles are justified mainly by the

boundary conditions and the different behaviour of the wall ties under tension and compression.

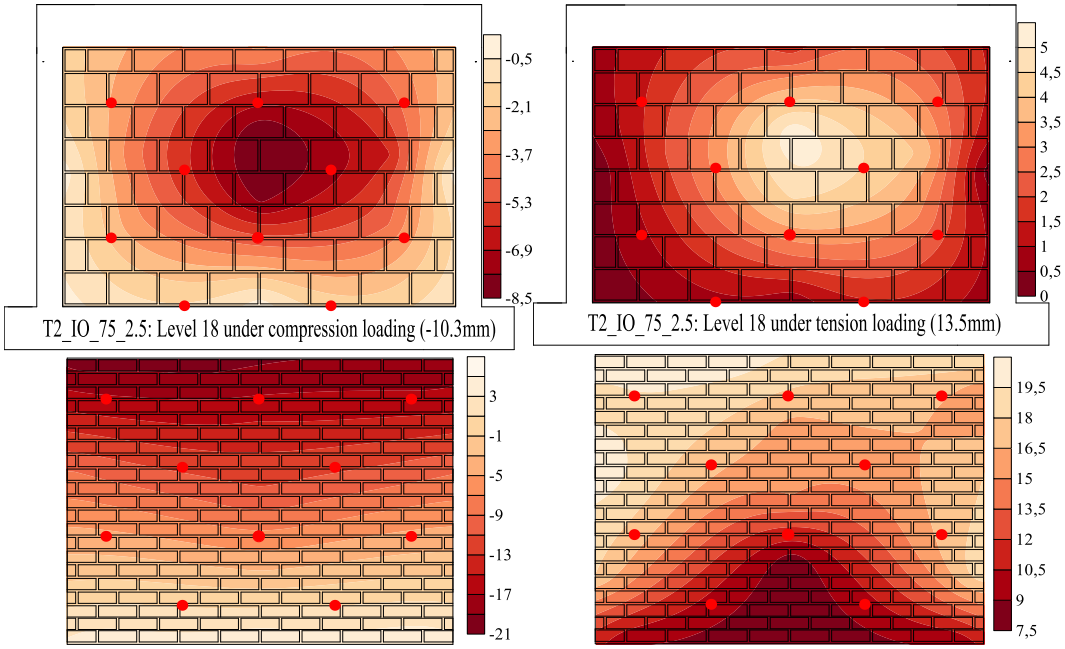

Figure 6.36 – Deformation of T2_IO_75_2.5 specimen under compression and tension loading at last cycle (displacement in millimetres)

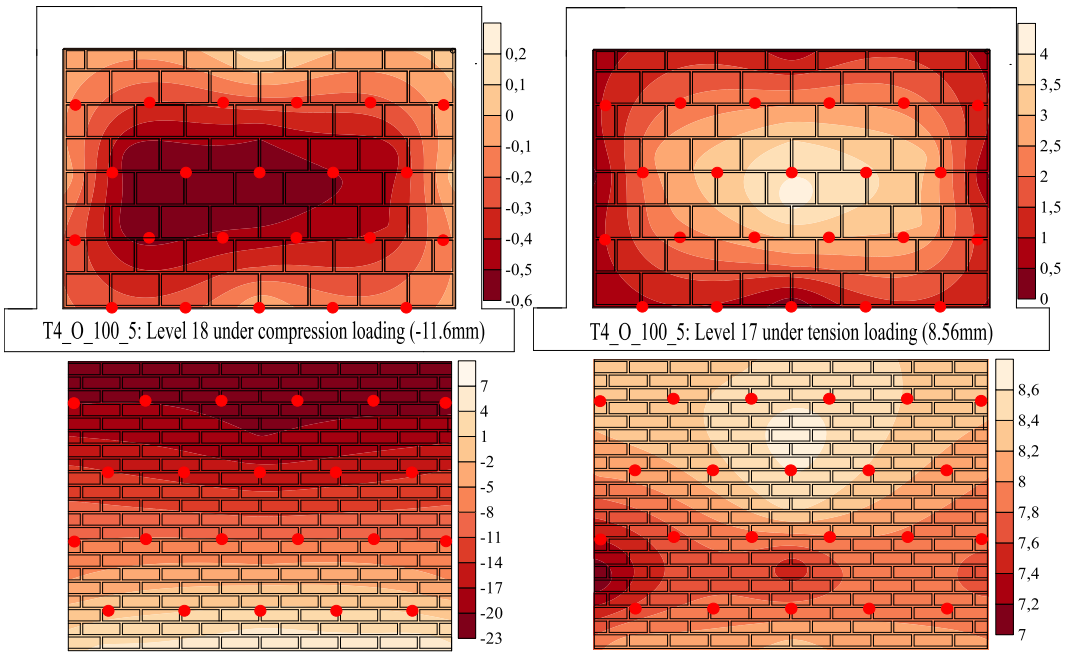

Figure 6.37 – Deformation of T4_O_100_5 specimen under compression and tension loading at last cycle (displacement in millimetres)

It should be underlined that the wall T2_O_100_2.5_No flashing with no flashing at the base and wall T2_O_100_5 with flashing at the base present also differences on the displacement profiles. In case of the walls with no flashing, the displacement profiles in compression and tension are very similar, given the absence of horizontal rotation of the wall due to high

friction at the interface between the masonry veneer walls and the bottom steel beam. Taking into account that the unique difference between both walls is the bottom boundary out-of-plane, the higher resistance of the walls with no flashing is attributed to the develop of the friction at the base activated during the out-of-plane loading.

The displacement profile showed by the infill walls is very different from the ones exhibited by the veneer walls, which should be attributed to: (1) the load transfer is from the veneer walls is not completely effective because the wall ties do not behave as completely rigid, being deformable; (2) the different boundary conditions. The masonry infill is considered to be rigidly attached to the RC frame through general purpose mortar. Therefore, the masonry infill walls present a typical displacement profile characterized by almost null displacement at top and bottom masonry infill-RC frame interfaces and maximum displacement at mid height of the wall. This deformation pattern in compatible with the two-way resisting arching mechanism. In some cases, for example walls T2_O_100_1.4 and T2_O_100_5, it is observed that the upper interface cracks and sliding occurs along the top interface. The sliding of the masonry infill wall is particularly evident in case of this is submitted to prior in-plane damage (T2_IO_75_2.5). In fact, as seen in section 6.5.3, the masonry infill detaches from the RC frame along the wall perimeter. Notice that the different displacement profile of the infill walls in specimens T2_O_75_2.5 and walls T2_IO_75_2.5 is fully justified by the prior in-plane damage of the infill walls, given that the other features are kept constant.

Comparing the different types of walls, it is possible to carry out a simple parametric analysis, according to different available variables. The deformation pattern of the veneer walls is very similar among the specimens built with wall tie T4 and T2. Apart from the magnitude, the shape of the deformation profile is very close. However, the type of wall tie appears to have an important influence on the deformation of the masonry infills, both regarding the magnitude and the shape profile. In the specimens built with wall tie T4, the masonry infill walls present very low values of displacements, especially in cases of higher spacing and lesser air cavity width (T4_O_75_2.5 and T4_O_100_2.5). This is the result of the low capacity of the wall ties to transfer the out-of-plane load from the brick veneer to the backing masonry wall. This appears also to influence of the upper interface that presents almost no sliding in the infill walls in specimens T4_O_75_2.5 and T4_O_100_2.5. In case of the infill walls of the specimen T4_O_75_5, with higher spacing, the sliding occurs due to the higher load transfer. This is also responsible for the greater magnitude of the displacements measured in the masonry infill wall. The tie spacing is also relevant in case

of wall tie T2. The deformation of the veneer walls decreases as the tie spacing increase, particularly in case of the lower spacing (number of steel per meter square equal to 5). On the other hand, the deformation of the masonry infill increases as the tie spacing decreases, as the loading transfer is greater. In case of specimen T2_O_100_5, the displacement of masonry infill tends to approximate the displacement of the masonry This appears to indicate that when the tie spacing is lower, the composite behaviour is improved loading to a higher stiffness of the system and thus to lower displacements of the veneer wall.

The influence of the air cavity thickness and consequently of the embedment length in the out-of-plane behaviour of the masonry infill walls appears not to be relevant in case of the veneer walls are attached to the backing masonry infill through wall ties T4 (T4_O_100/75_2.5). The wall ties in the specimens T2_100_75_2.5, with lower thickness of the air cavity width, show a lower capacity to transfer the out-of-plane load from the veneer to the masonry infill, given that the displacements measured in the masonry infill are lower.

As already mentioned, the prior in-plane damage has a great influence in the deformation profiles of the masonry infill wall. The out-of-plane displacements obtained in the masonry infill walls of the specimens T2_IO_75_2.5 are markedly higher than the ones observed in the masonry infill wall of the specimen T2_O_75_2.5 without prior in-plane damage. In particular, the higher deformations of the upper zone of infill wall results from the cracking of the upper interface and separation of the masonry infill from the enclosing frame. It should be mentioned that the composite behaviour and the adequate attachment of the masonry veneer to the backing walls is fundamental to ensure its stability under seismic loads, avoiding its collapse. The out-of-plane collapse of the veneer walls is very dangerous, which emphasizes the importance of construction and application of connections.

For each veneer wall, the strain gauges glued at each wall ties was analysed to assess the evolution of strains during the out-of-plane loading. The strains recorded in the wall ties along the central vertical line are provided in Figure 6.38 for all specimens, with the exception of the specimen where no flashing was considered (T2_O_100_2.5_No flashing). In general, it is observed that the strain gauges did not record very high deformations, being usually lower than 2.0‰ but close to the yielding. The highest values of strains were recorded in specimen T4_O_100_2.5, which were beyond the yielding strain. This is mainly justified by the higher ability of the wall ties T4 transfer the out-of-plane load from the brick veneer to the masonry infill wall. In addition, the strains in compression are higher than the strain measured in tension, which is associated to the failure mode of the tie/connection.

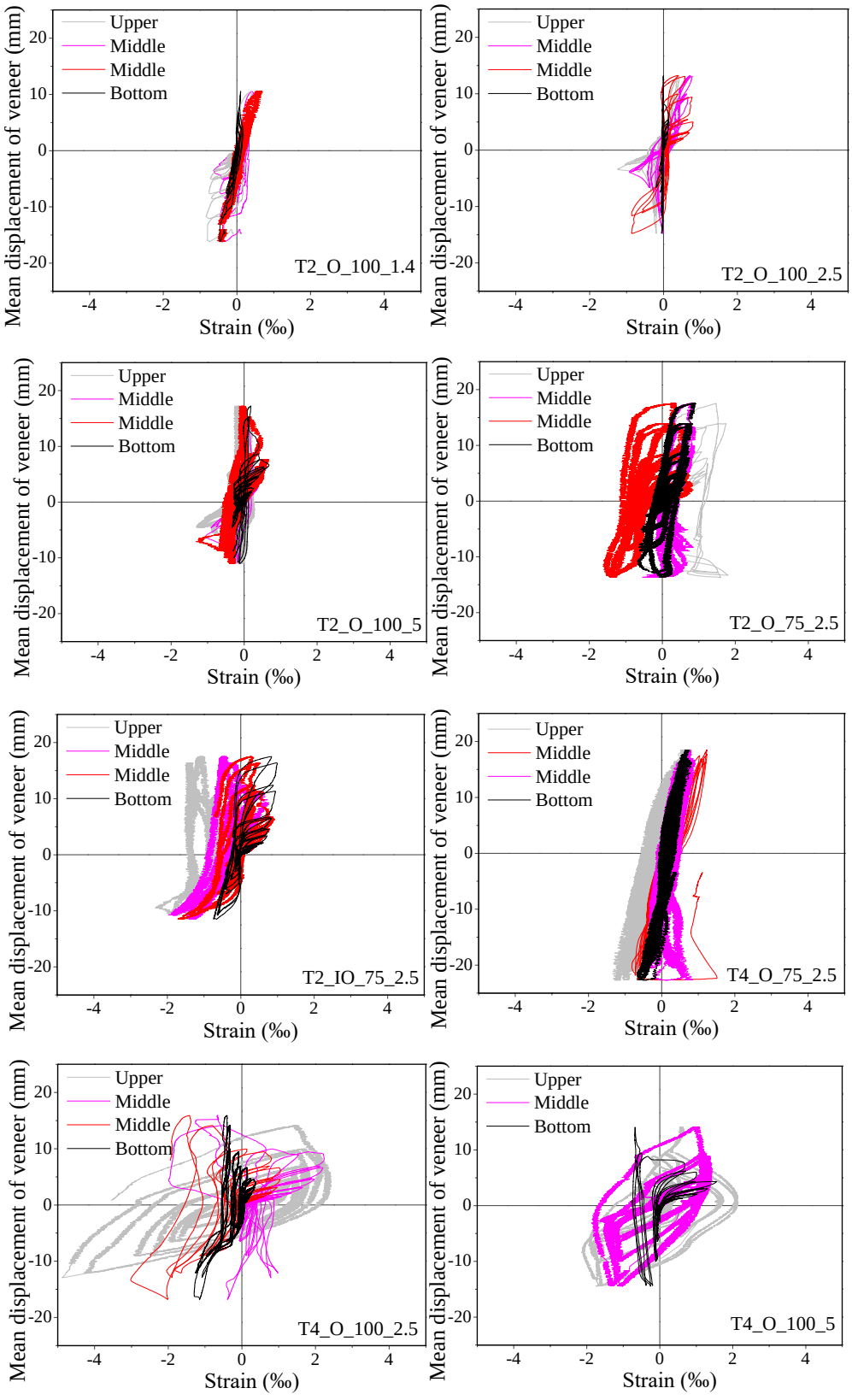

Figure 6.38 – Strain gauges of wall ties distributed in upper, middle and bottom of each wall type

Under compression, the wall ties mostly bend and buckle. Under tension, in spite of tensile strains develop due to the load transfer from the veneer walls to the masonry infill wall, the

most common failure mechanism occurs at the connection between the wall tie and masonry wall at the mortar joints. Hence, the tensile strains are usually low.

Another important aspect that appears to be relevant is the difference in strains at top and bottom rows of the wall. In all specimens, the strain values are gradually increasing with the height of wall, being more evident in compression loading. This is mainly related to the higher out-of-plane displacements experienced by the veneer wall, which are mainly controlled by the different boundary conditions at top and bottom borders of the wall.

6.5.3. Typical damage patterns

The distinct deformational features of the walls discussed previously resulted from the different behaviour of the wall ties, namely as regarding the damage patterns both under compression and tension. As above mentioned, when the wall ties are under compression (veneer walls are pushed), the veneer walls exhibit a deformation mostly characterized by the rotation along a horizontal axis close to the base (rocking). When the wall ties are under tension (veneer walls are pulled), the veneer walls also rotate but at much lower grade and mostly slides along the base, as seen in Figure 6.40. When a veneer wall rocks or slides, it can achieve significant displacements without a visible damage.

The damage is mainly concentrated at the wall ties and at the connection of the wall tie to the masonry infill and veneer walls, which justifies the importance these elements in structural safety of buildings with brick veneer walls.

With this respect, the brick veneer wall in the specimen T2_O_100_5 presented cracking along bricks and mortar as shown in Figure 6.40. The cracks were located mainly at the adjacent region to the connections, near to the boundaries of the wall. Similarly, the damages on the masonry infill walls are also very reduced, resulting from the low displacements induced by the out-of-plane loads.

The main failure modes observed in ties and wall ties connections to the brick masonry walls (infill and veneer) are shown in Figure 6.41. The ties experienced severe damages but, in most cases, they were still able guarantee an adequate resistance of the wall at the end of the test. The damages observed in the ties were similar for all specimens and consisted in: (1) pull-out of the tie from embedment bed joint; (2) tie fracture when under tensile loading and (3) buckling of the tie when the veneer wall is subjected to out-of-plane compression loading. The visible damages start on the ties located at uppermost rows of the wall when its

maximum capacity was achieved in various connections. This means that the maximum capacity of the walls is controlled by the capacity of the ties.

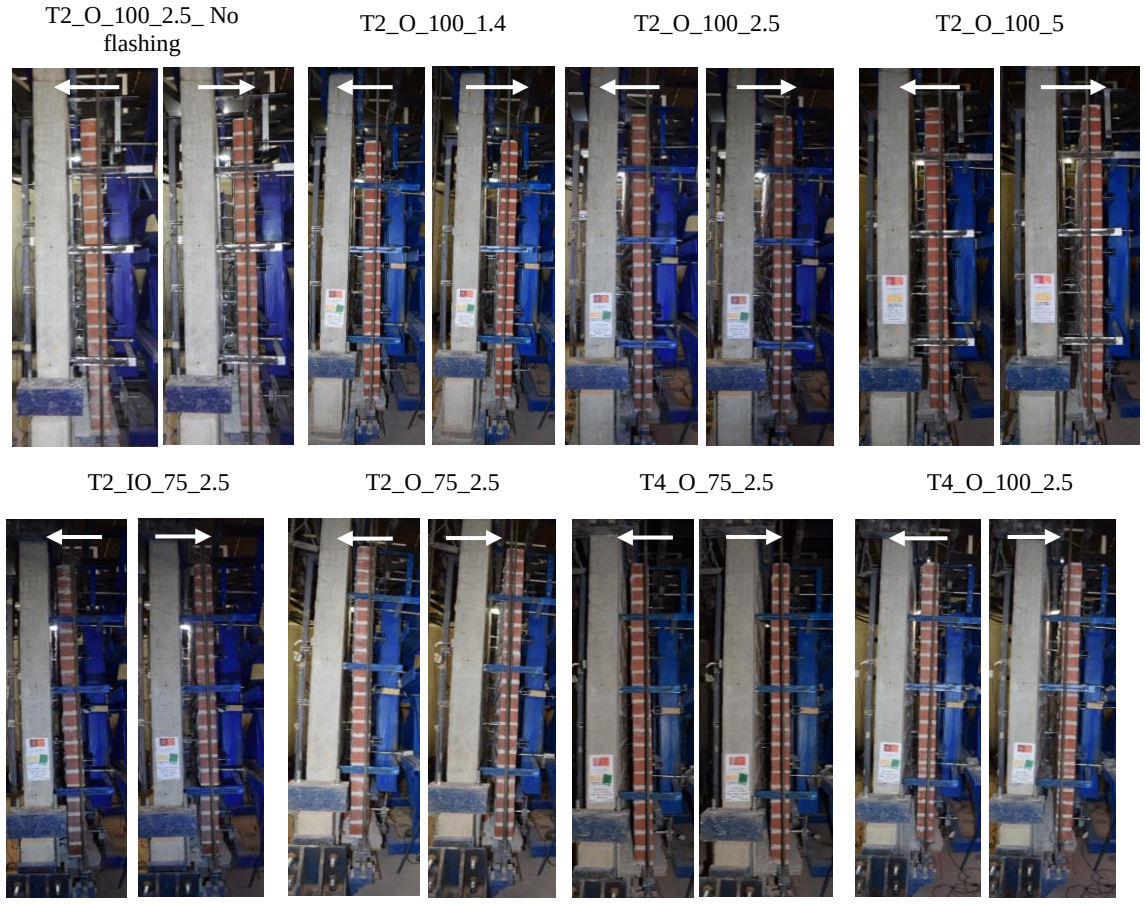

Figure 6.39 – Lateral view of each wall under out-of-plane actions in compression and tension directions

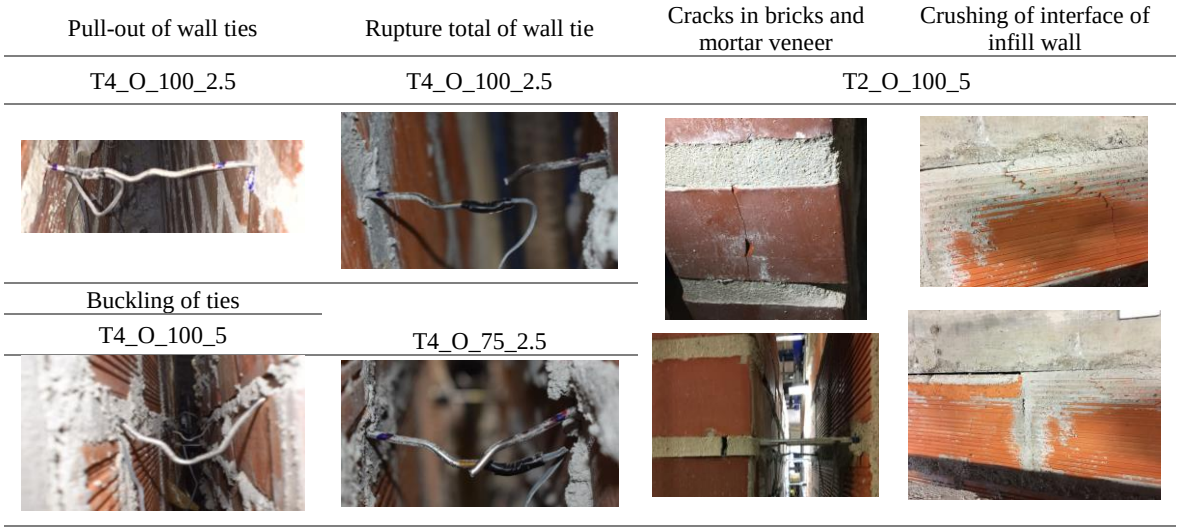

Figure 6.40 – Different types of failure modes in veneer and infill wall in different walls

When the load transfer between the brick veneer and masonry infill walls is effective, it is possible to observe a significant degradation of mortar and bricks around the connection, as shown in Figure 6.41.

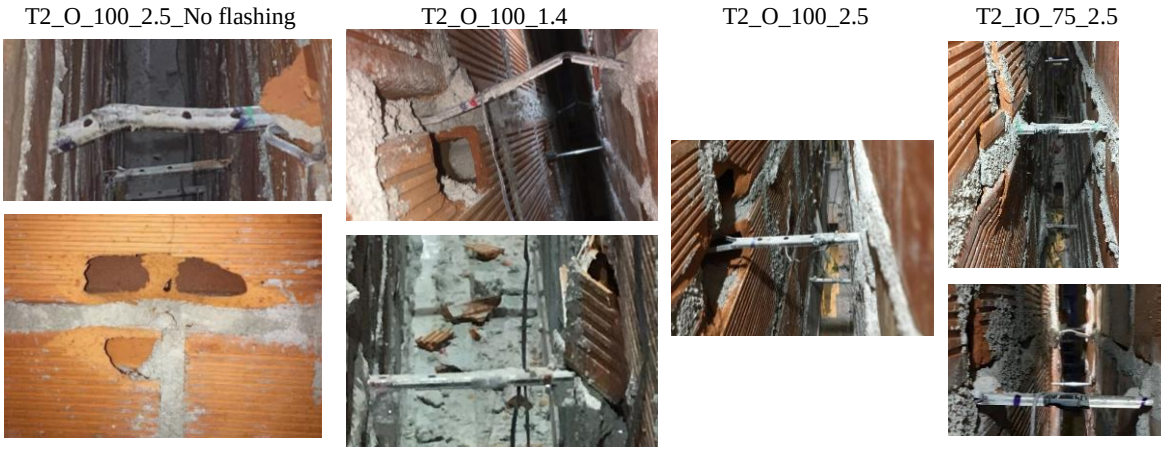

Figure 6.41 – Local stress concentration on connections – Local damage of bricks and mortar infill

the crushing of mortar and bricks around the more stressed wall tie connections is common in the specimens built with tie T2. This shall be attributed to the geometry of the extremity of this tie, which improve the anchorage of the ties to the masonry walls. In case of the masonry infill walls, built with horizontal perforation, the tensile strength of the brick is lower, and the damage is higher than in the brick veneer, which present bricks with vertical holes. The anchorage achieved with the wall tie T2 is much lower effective, leading to minor local damage of the masonry infill walls, resulting also from the lower ability to transfer the out-of-plane loads from the brick veneer to the masonry infill walls.

Another important information provided in Table 6.4 concerns the displacement levels corresponding to the achievement of the maximum resistance of wall system, in order to organize chronologically the sequential events. As expected, the damage signals occur immediately after the maximum resistant capacity of system is attained. It is noticed that the adequate number of ties improves the redundancy, resulting in the adequate robustness of the walls system in avowing the complete failure of the system, which should be mandatory to prevent severe economic and human losses under earthquake events.

Table 6.4 – Summary of failure modes observed in walls tested to out-of-plane actions

Specimen	Displ. level	Damaged connections	Observations
T2_O_100_2.5 No flashing	Level 15		Maximum compression resistance achieved
		T4,a-c; T3, a-b; T2,c	Buckling of ties
	Level 17		Maximum tension resistance achieved
		T1,a; T1,b; T2,a	Sliding and pull-out of wall tie from veneer leaf
	Level 18	T4,b	Degradation of infill mortar bed joint and brick
T2_O_100_1.4	Level 14	T4,a and T4, b	Buckling of ties
	Level 15		Maximum compression and tension resistance achieved
		T1,a; T2,a; T3,a and T4,a	Sliding and pull-out of wall tie from infill leaf Degradation of infill mortar bed joint and brick
	Level 16		Crushing in upper interface of infill wall
T2_O_100_2.5	Level 13	T2,c;T3,b and T4,c	Signals of buckling of ties
	Level 16	T2,c; T3,a; T3b; T4,a and T4,c	Sliding and pull-out of ties from infill leaf
		T4, a	Degradation of infill mortar and infill bricks
			Maximum tension resistance achieved
	Level 15		Maximum compression resistance achieved
T2_O_100_5	Level 16	All ties	Buckling, sliding and pull-out of ties
			Crushing in upper interface of infill wall
		Near of T4,a and T4,f	Cracks in veneer mortar
		Near of T2,a and T2,f	Cracks in veneer bricks
	Level 17		Maximum compression and tension resistance achieved
T2_IO_75_2.5	Level 17		Maximum compression and tension resistance achieved
	Level 16	T1,a; T2,a; T3,a and T4,a	Severe buckling and pull-out of ties from infill mortar bed joint
		T2,b and T4,b	Reasonable buckling and pull-out of ties from infill mortar bed joint
		T2,a and T3,a	Failure of infill bricks and infill mortar
T2_O_75_2.5	Level 15		Maximum compression resistance achieved
	Level 16		Maximum tension resistance achieved
		T1,a; T2,a and T4,a	Sliding and pull-out of wall ties from veneer mortar
		T2,a; T4,a and T4, b	No buckling – the wall ties has been introduced on veneer mortar
T4_O_75_2.5	Level 17		Maximum tension resistance achieved
	Level 18		Maximum compression resistance achieved
		T4,a-c	Slight sliding of ties from veneer leaf
		T3,a and T4,a-c	Buckling of ties
	Level 17	T4,a and T4,c	Complete rupture of wall ties
T4_O_100_2.5	Level 12		Maximum compression resistance achieved
	Level 13	T3,b; T4,b and T4,c	Buckling of wall ties
	Level 17		Maximum tension resistance achieved
		T2,a; T3,a and T4,a	Sliding and pull-out of wall ties from veneer wall
		T3,a; T4,a and T4,c	Rupture of wall ties
T4_O_100_5	Level 15		Maximum compression resistance achieved
	Level 19		Maximum tension resistance achieved
	Level 14	T3,a-f and T4, a-e	Buckling of ties
	Level 17	T3,a-f and T4, a-e	Sliding and pull-out of wall ties from veneer mortar
	Level 19	T4,e	Rupture of wall tie

6.6. Evaluation of seismic performance and parametric analysis

The assessing of seismic performance of structures is a paramount importance for adequate design of new structures or rehabilitation of existing structures. Therefore, a better understating of the hysteretic factors that govern their seismic performance is important for a safe and economical seismic design or for the adoption of the most adequate strengthening measures.

A discussion of seismic indicators found for the tested specimens under analysis is presented herein in order to assess their performance under cyclic loading. In addition, a comparison among the results obtained for the different specimens is provided aiming at gathering a better insight on the influence of different variables in the seismic performance of brick veneer walls. The variables under analysis are: (1) of tie typology, (2) influence of tie spacing, (3) influence of air cavity width and embedment length, (4) influence of flashing and (5) influence of prior in-plane damage of masonry in the out-of-plane behaviour of the system. To discuss the influence of tie typology, 3 combinations of specimens were considered: (1) walls built with an air cavity of 100mm of thickness and with 2.5 ties per square meter (T2_O_100_2.5 and T4_O_100_2.5); (2) walls built an air cavity of 100mm of thickness and 5 ties per square meter (T2_O_100_5 and T4_O_100_5) and (3) walls built with an air cavity with 75 mm thickness and 2.5 ties per square meter (T2_O_75_2.5 and T4_O_75_2.5). The tie spacing is analysed in walls built with tie T2, considering 3 layouts of ties (T2_O_100_1.4/2.5/5) and built with T4 distributed according 2 layouts (T4_O_100_2.5/5), both with an air cavity of 100mm thickness. The influence of the air cavity width and consequently the embedment length of the wall ties on the mortar joints is analysed by comparing wall T2_O_100_2.5 with wall T2_O_75_2.5 and wall T4_O_100_2.5 with wall T4_O_75_2.5. To analyse the effect of flashing on behaviour of the walls, a comparison between wall T2_O_100_2.5_No flashing and wall T2_O_100_2.5 is carried out. The influence of prior in-plane damage of the masonry infill walls in the out-of-plane behaviour of the system is analysed though the comparison between the specimen in which the RC frame with masonry infill was submitted to in-plane damage (about 0.5% of drift) T2_IO_75_2.5 with specimen T2_O_75_2.5.

This discussion is based on several performance indicators: (a) backbone curves, (b) initial stiffness and stiffness degradation, (c) plastic or residual deformations in out-of-plane behaviour, (d) energy of dissipation and (e) equivalent viscous damping ratio. These

performance indicators were calculated based on the load versus displacement diagram presented.

6.6.1. Backbone curves

The backbone curves were determined as the monotonic envelop of the hysteretic force-displacement diagrams. The original hysteretic curves are grouped in Figure A.11 – Figure A.15 in Appendix A for each type of variable in order to get a better idea about the difference of hysteretic behaviours. For obtaining the backbone curves, the method suggested by Frumento et al. (2009) [157] was considered. The backbone curves result from connecting, with linear segments, the points of maximum force obtained in each cycle. In this case, two backbones were drawn based on veneer and infill wall responses as the same level of displacement was applied twice.

a) Influence of tie typology

From the backbone curves presented in Figure 6.42, it is possible to confirm that the deformation of the masonry infill is much lower than the deformation of the brick veneer walls and that there is only deformation until the maximum resistance of the system is achieved. The maximum resistance is followed by the damage on the wall ties/tie-wall connections, which makes the load transfer from the brick veneer to the masonry infill wall inefficient.

It is also possible to see that the typology of the wall ties has a great influence in the out-of-plane behaviour of the walls when the veneer walls in pushed, imposing compression stresses on the wall ties. This is valid for the air cavity of a thickness of 100mm and for the number of ties of 2.5/m^2 and 5/m^2. The results provided in Chapter 4 in single connections, demonstrated a considerable weaker performance under compression loading of wall ties T4 regarding wall ties T2 due its low buckling resistance. The compression resistance of the system T2_O_100_2.5 and T2_O_100_5 is 40% and 53% greater than the resistance of the systems T4_O_100_2.5 and T4_O_100_2.5 respectively.

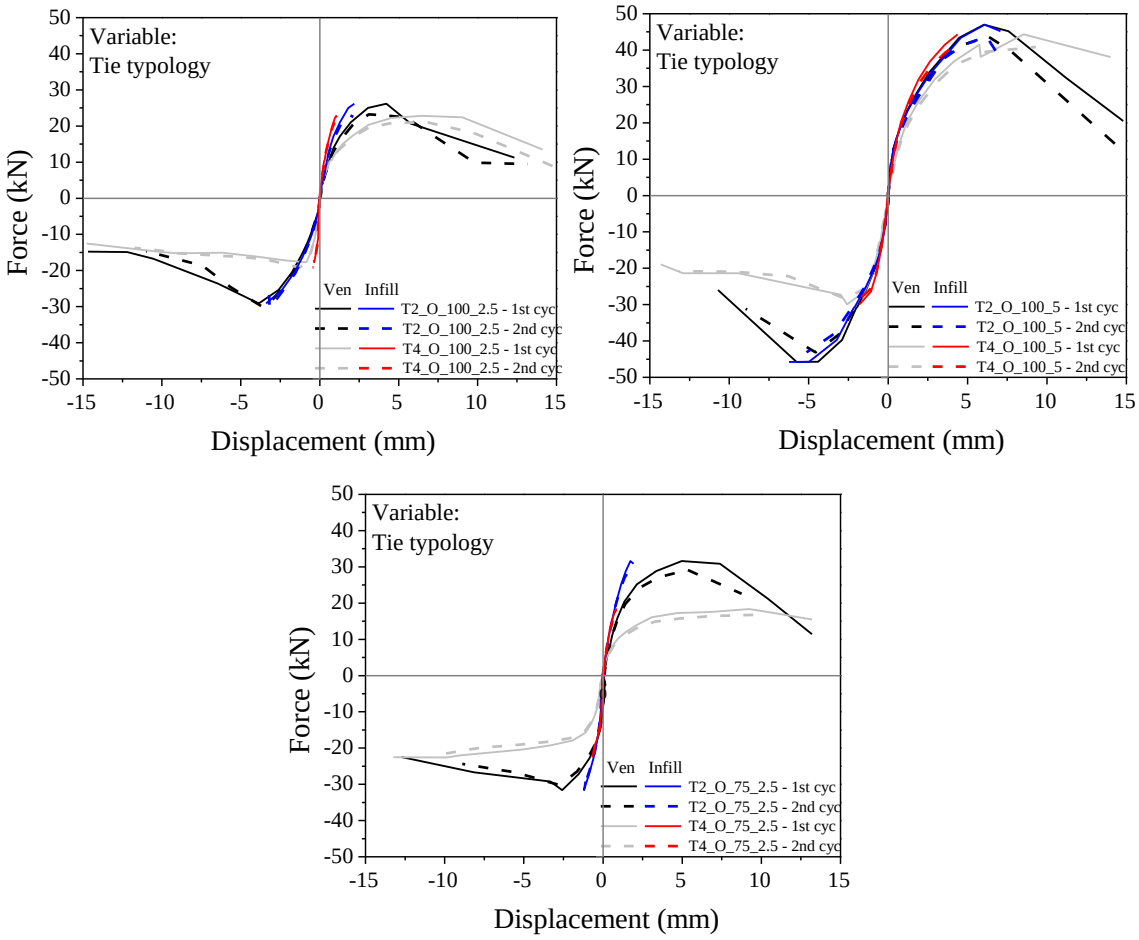

Figure 6.42 – Backbone curves of hysteretic cyclic behaviour in specimens with different tie typology

For the cavity of 75mm thickness, the difference on the behaviour between both typologies of wall ties is also important when the brick veneer is pulled out. In this case, the tensile capacity of the wall T2_O_75_2.5 is 72% greater than the capacity of wall T4_O_75_2.5. Under compression loading, the difference in the capacity between T2_O_75_2.5 and T4_O_75_2.5 is about 40%.

It should be mentioned that the systems built with both types of wall ties presented an important deformation capacity after the attainment of the maximum resistance, which is considered to be in preventing very brittle ruptures. Particularly, the wall T4_O_75_2.5 did not exhaust the compression resistance, considering that the resistance was always growing in tested displacements. This may be justified by lesser air cavity width, which increase indirectly its compression resistance due to lesser width of free length to buckling. It would be necessary more displacement levels to know the maximum resistance of wall.

Figure 6.43 enables to compare the differences on the compression and tensile strength in walls built with the different type of tie along to the out-of-plane test. It is observed that the walls built with tie T2 have almost the same strength under tension and compression actions

(at maximum a difference of 10%). The walls built with tie T4 present a compression strength about 50% lower when compared to the walls built with tie T2. Taking into account the behaviour under tension and compression, the walls built with tie T2 are considerably more resistant than walls built with tie T4.

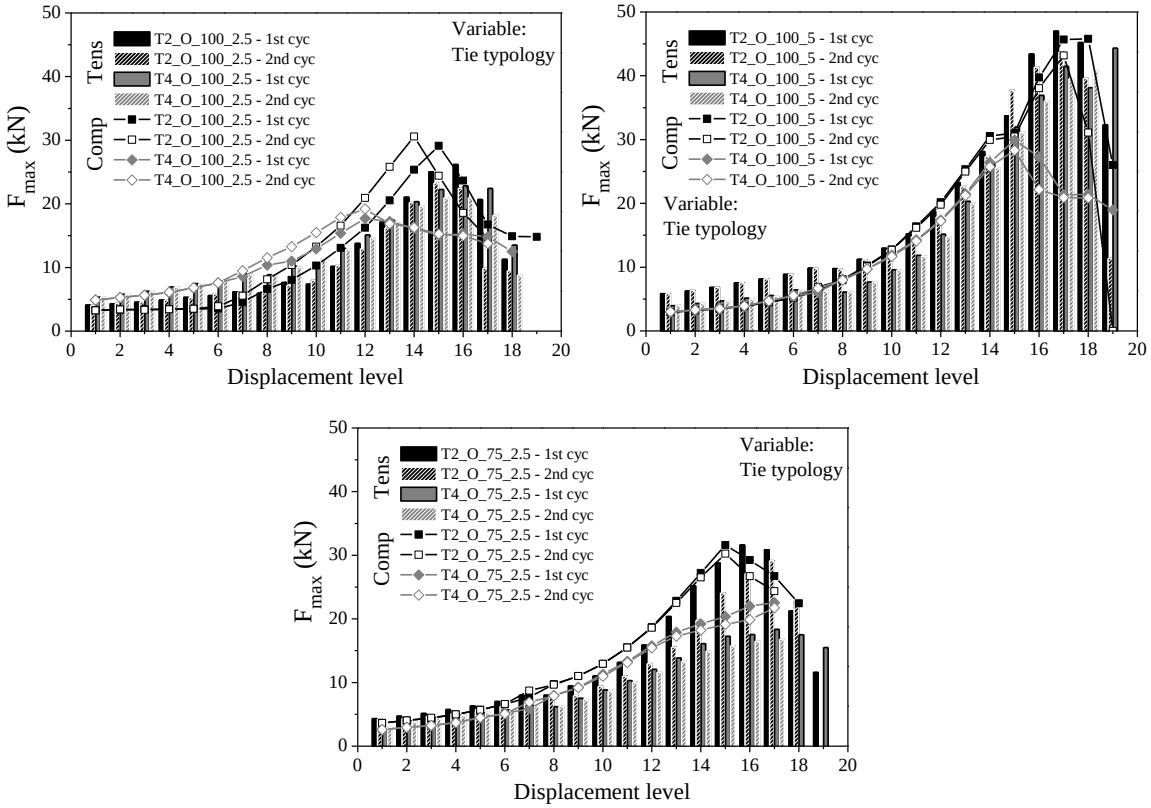

Figure 6.43 – Evolution of tensile and compression strength in specimens with different tie typology

It is also possible to see that the second cycle in the backbone curve is normally under the first cycle backbone, but differences between the lateral resistance obtained in the first and second cycles of loading is similar in all specimens. This means that the strength degradation was not significant and initiates especially after failure of connections.

b) Influence of tie spacing

Comparing the backbones shown in Figure 6.44 and the values of lateral strength (Figure 6.45), obtained in the specimens built with the same of tie but with different spacing, it is possible to conclude that the lower spacing and, thus, the increase on the number of ties per meter square influences greatly the out-of-plane behaviour of the system, both regarding the brick and masonry infill walls. It is observed that the specimen T2_O_100_5 exhibits the best performance, being the resistance under compression loading 58% higher than the resistance obtained in specimen T2_100_2.5 and 80% under tensile loading.

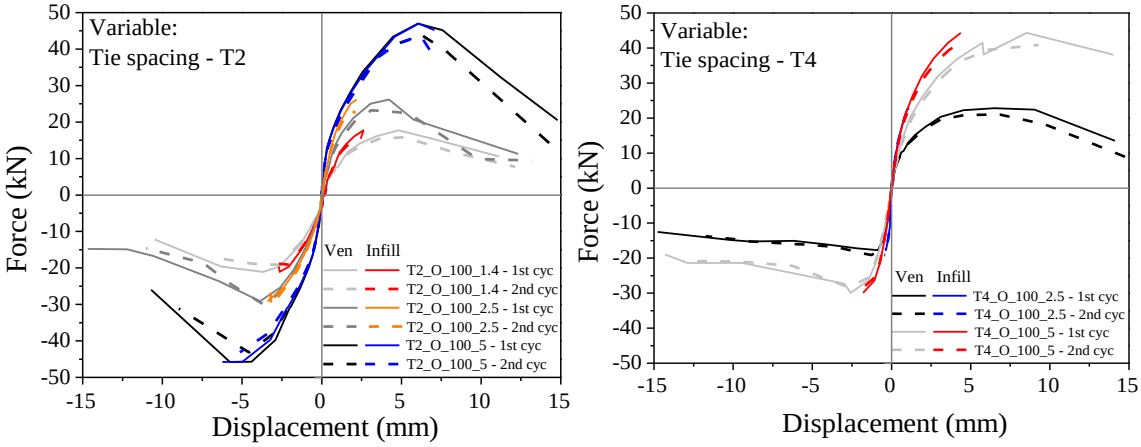

Figure 6.44 – Backbone curves of hysteretic cyclic behaviour in specimens with different tie spacing

There is also an improvement on the resistance of specimen T2_O_100_2.5 when compared to specimen T2_O_100_1.4, of 40% under compression loading and 50% under tensile loading. In case of walls constructed with tie T4, it is concluded that increasing the number of tie to the double (T4_O_100_5), results in an enhancement of resistance both under compression (70%) and tensile loading (95%).

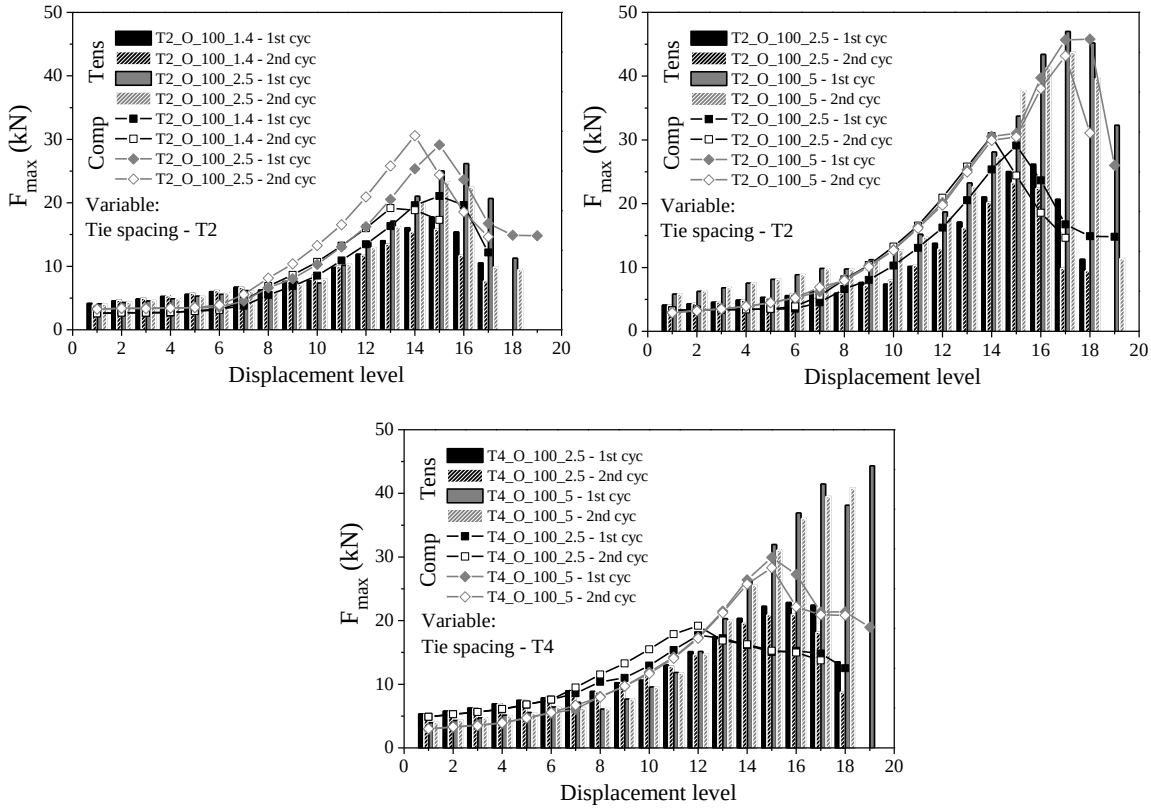

Figure 6.45 – Evolution of tensile and compression strength in specimens with different tie spacing

c) Influence of air cavity width and embedment length

As aforementioned, the decrease of the air cavity space results in the decrease of the embedment length of the wall ties in the mortar joints of masonry. The reduction of 25mm in the air cavity spacing results in the increase of embedment length on mortar bed joint of veneer leaf of the 25mm. By analysis the backbone curves (Figure 6.46) and evolution of the lateral strength (Figure 6.47) is observed that the change on air cavity and reduction of embedment length has moderate influence in the out-of-plane resistance of the system. Under compression loading, there is an increase of resistance from 7% and 22% in walls built with ties T2 and T4 respectively when the air cavity decreases from 100mm to 75mm. This result is mostly attributed to the reduction of the free length of the wall ties, which contributes to prevent lateral bucking of the ties, particularly of tie T2, which is very susceptible to buckle. Under tensile loading, the out-of-plane resistance is 17% higher in T2_O_75_2.5 when compared with T2_O_100_2.5. In case of the walls are built with tie T4, the decrease of the embedment length does not contribute for the lowering in the tensile resistance. In fact, unexpectedly, the specimen T4_O_75_2.5 presents an out-of-plane resistance under tension of 20% higher than specimen T4_O_100_2.5. A similar behaviour was also observed in single connections under tension and compression. The increase of the embedment length should not be relevant in case of wall tie T4, assuming that the adherence is mostly achieved though the hook at the extremities, which remain unchangeable for the different air cavity space.

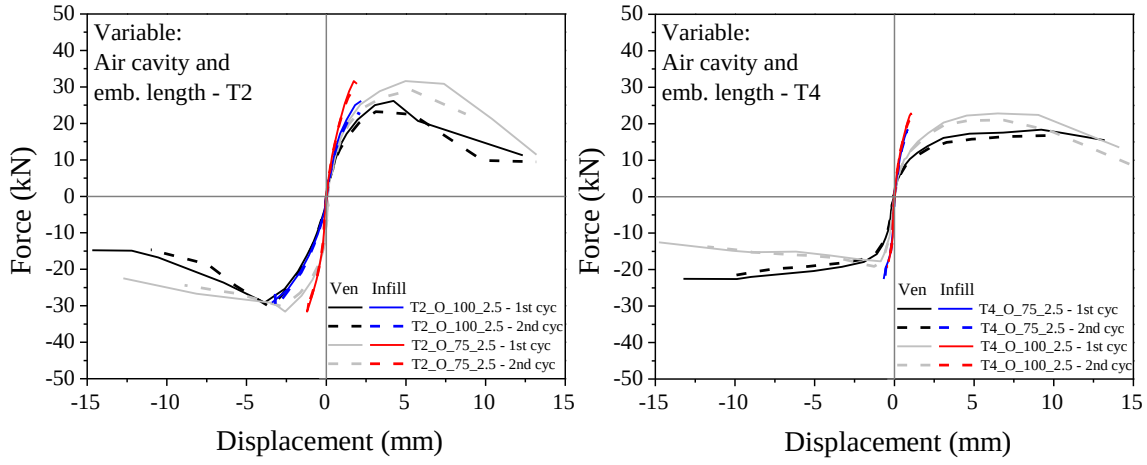

Figure 6.46 – Backbone curves of hysteretic cyclic behaviour in specimens with different air cavity width and embedment length

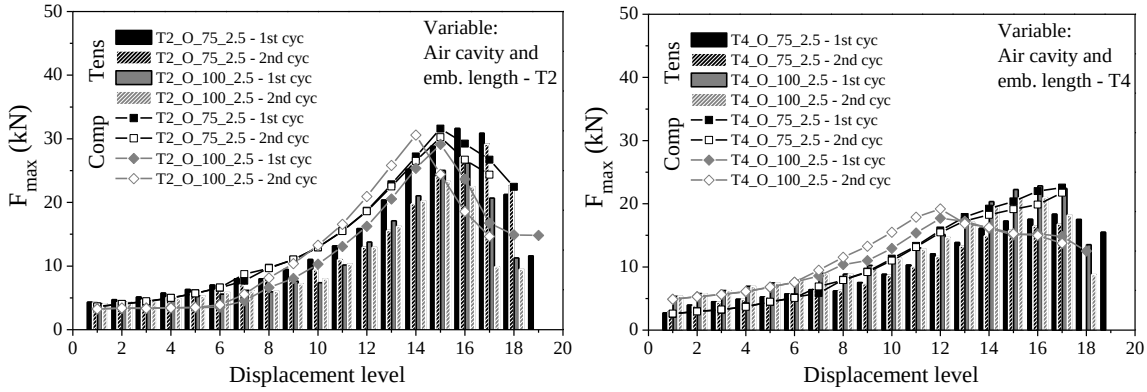

Figure 6.47 – Evolution of tensile and compression strength in specimens with different air cavity width and embedment length

d) Influence of flashing

The flashing at the base of the brick veneer walls that reduces the friction at the bottom interface influences significantly the behaviour of the system composed by the RC frame with the masonry infill ant the with the brick veneer attached to it. This influence is particular relevant in case of the brick veneer walls is pulled out, according to what can be seen from the backbone curves and evolution of the lateral strength in Figure 6.48. The increase of strength at in the early cycles of displacement is much higher in the specimen with no flashing (T2_O_100_2.5_No flashing) than the specimen without flashing (T2_O_100_2.5). The resistance is practically the double in specimen T2_O_100_2.5_No flashing) both when the walls is pushed and pulled until the tenth displacement level. In addition, the maximum resistance in the specimen without flashing was 7% higher under compression and 35% higher under tensile loading.

This difference is the consequence of the friction developed at the base and of the which requires higher load for the same displacement. The difference in wall resistance under tensile and compression loading is associated to the different deformation profiles of the walls. Under tensile loading, the deformation is mostly governed by the parallel sliding of the brick veneer walls along allowed by the flashing. In compression, the veneer walls are mostly characterized by the rotation deformation along a horizontal axial close to the base. Therefore, the absence of the flashing is much more important for the deformation profile under tension than in compression.

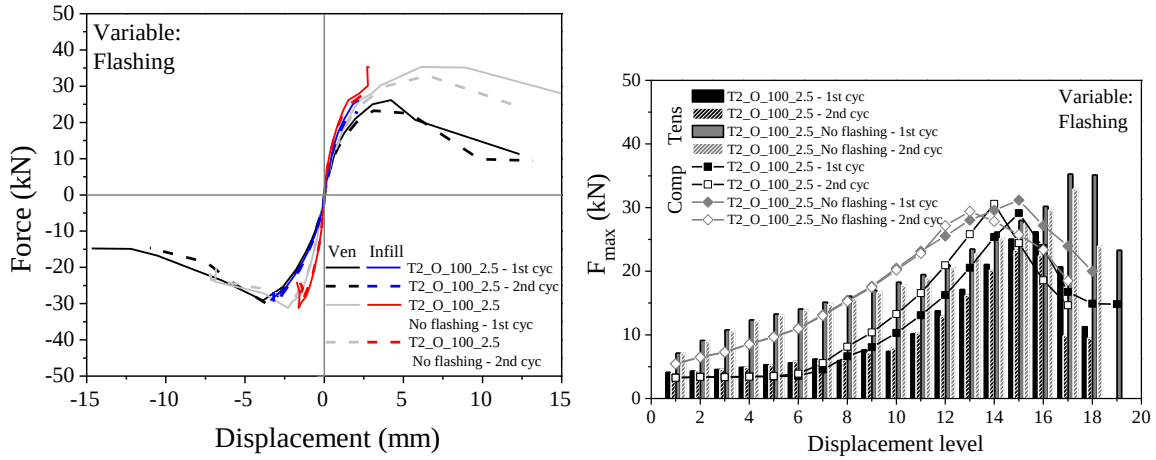

(a) (b)

Figure 6.48 – Specimens with and without flashing: (a) backbone curves of hysteretic cyclic behaviour and (b) evolution of tensile and compression strength

e) Influence of prior in-plane damage on out-of-plane response

According to the backbones presented in Figure 6.49 (a), the in-plane damage of the masonry infill walls influences considerably the initial stiffness of the system, both in tension and compression. It is observed that a considerable decrease on the stiffness is found in case of the masonry infill is damaged. However, it influences in a different manner the out-of-plane resistance of the system. When the system is pushed and the wall ties are submitted to compression loading, there is almost no change on the out-of-plane resistance. Under tensile loading, the resistance of the specimen with damaged masonry infill decrease 25% in relation to the specimens without damage.

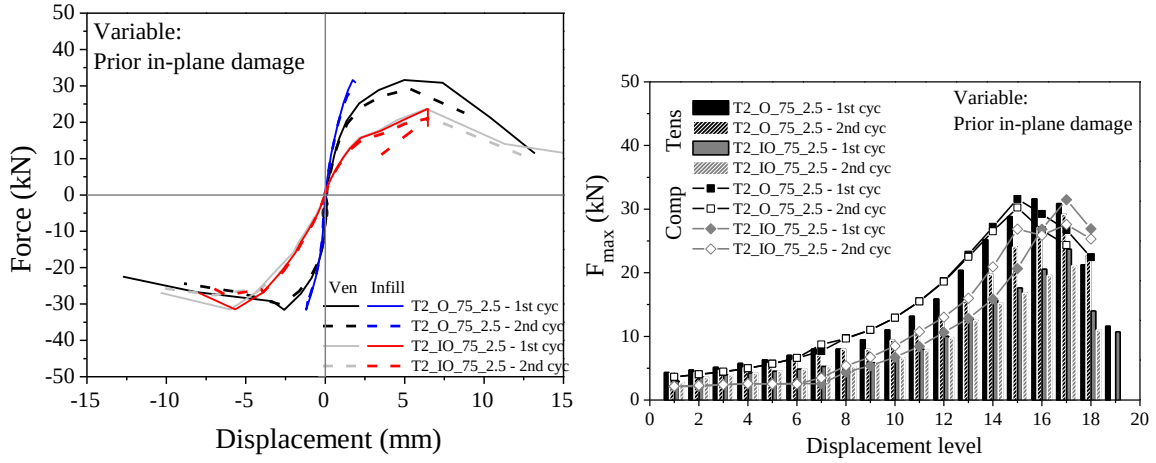

(a) (b)

Figure 6.49 – Specimens with and without in-plane damage: (a) backbone curves of hysteretic cyclic behaviour and (b) evolution of tensile and compression strength

The specimen with masonry infill previous damage exhibits half of the resistance obtained in the specimen without damage practically in all cycles of displacement, even if the residual resistance in both systems is the same. The reason that contribute for the decrease of the tensile strength can be associated to the previous cracking of the infill wall and separation to its surrounding, which make the masonry joints and infill wall weaker and thus can degrade the tensile bond adherence of the wall ties to the mortar joints.

6.6.2. Evaluation of initial stiffness and stiffness degradation

The stiffness, *K*, is defined as the secant stiffness measured for the maximum displacement corresponding to each cycle. The stiffness calculated for the first level corresponds to the initial stiffness because the linear elastic response of the walls was guaranteed for very low displacements. It should be mentioned that the elastic stiffness should be seen as a measure of the composite behaviour of the system composed by the RC frame with masonry infill with attached brick veneer walls thought the wall ties. After the linear range, the stiffness does not represent the perfect behaviour of system due to the different damage and failure patterns of the wall ties. On the other hand, it should be mentioned that the behaviour of system depends much on the ability of the wall ties have to transfer the load from the veneer to the masonry infill wall. Therefore, the stiffness decrease along the out-of-plane tests should be seen indicative of the damage of the system, much concentrated at the wall ties. The stiffness for first and second cycle was calculated for veneer and infill wall based on displacement measured at centre of each leaf and force recorded by actuator. The stiffness of veneer leaf cannot be compared with stiffness of infill leaf directly because of the very different boundary conditions. However, the idea of representing the infill stiffness is to compare the variation of the stiffness of each leaf according to the different variable under analysis.

a) Influence of tie typology

Analysing individually each specimen, it is possible to observe that the compression stiffness is in the majority of cases higher than tensile stiffness, see Figure 6.50. Another feature is the stiffness loss in second cycle of each displacement level, achieving at maximum 20%. However, the loss decreased with increasing deformation.

There is a clear trend for the secant stiffness decrease as the load displacement level increases. In addition, it is seen that the decrease on the secant stiffness is much more significant in case of higher strength walls, i.e., the walls having 5 wall ties per square meter.

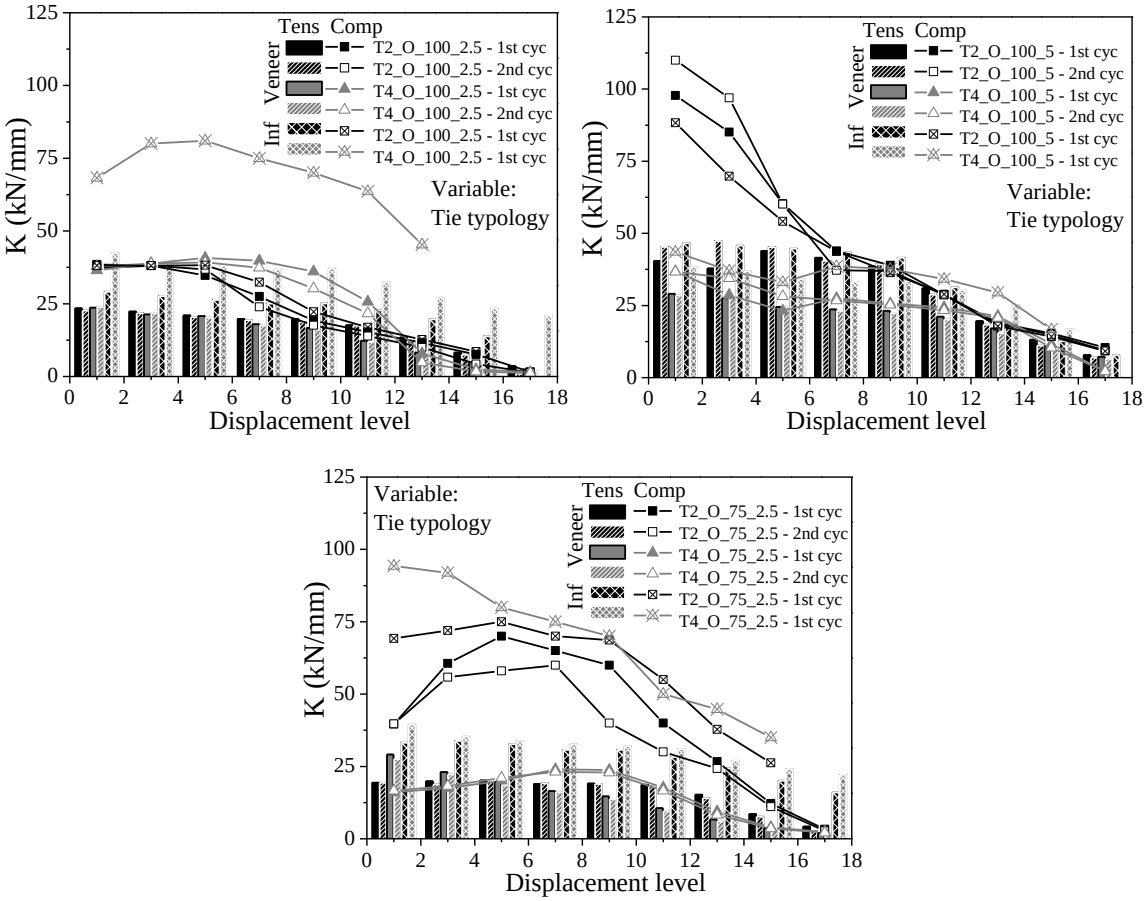

Figure 6.50 – Initial stiffness and its evolution in specimens with different tie typology

The effect of type of wall tie is more relevant in the higher resistant specimens, being the specimen T2_O_100_5 about 30% stiffer under tension loading and 170% stiffer under compression loading than specimen T4_O_100_5. The difference in compression loading decreases during the test, but in tension, the difference is kept until the end of the test. For higher spacing of ties, the typology is not so important.

From the results it can be concluded that the influence of tie typology in tension is not so significant because the failure mechanism that controls the tensile behaviour is related to the tie-mortar adherence. In compression the tie T2 lead to higher stiffness of the brick veneer when compared to the specimen built with tie T4. This behaviour is justified by the different shape and geometry of the wall ties that controls the behaviour under compression. In compression, the overall behaviour of the system depends mainly on the behaviour of the tie under compression. Under tensile loading, the stiffness depends much more on the adherence of tie-mortar.

b) Influence of tie spacing

The effect of tie spacing was found to be relevant in specimens constructed with wall tie T2 by varying the number of ties from 2.5 to 5 ties per square meter. The initial stiffness of the system built with wall ties T2 when submitted to compression loading is the double in case of the number of ties is 5/m^2 compared to the case of 2.5 wall ties per meter square. When the system is submitted to tensile loafing, the stiffness is 70% higher in case of the number of ties is 5/m^2. In case of walls built with wall tie T2, the initial stiffness is higher 30% under compression loading and 130% under tension loading when the number of ties per meter square layout from 1.4 per square meter to 2.5 ties per square meter. The differences observed in the system with tie T4 wall tie were not so significant, although an increasing of stiffness in walls with more ties was identified. The influence of the tie spacing was not so pronounced because the wall with higher number of ties T4 is not so stiff when compared to the system built with ties T2. As mentioned before, when under tension, the adherence area of tie T4 wall tie is much lower than the adherence area of T2 wall tie, resulting in lower stiffness of the system.

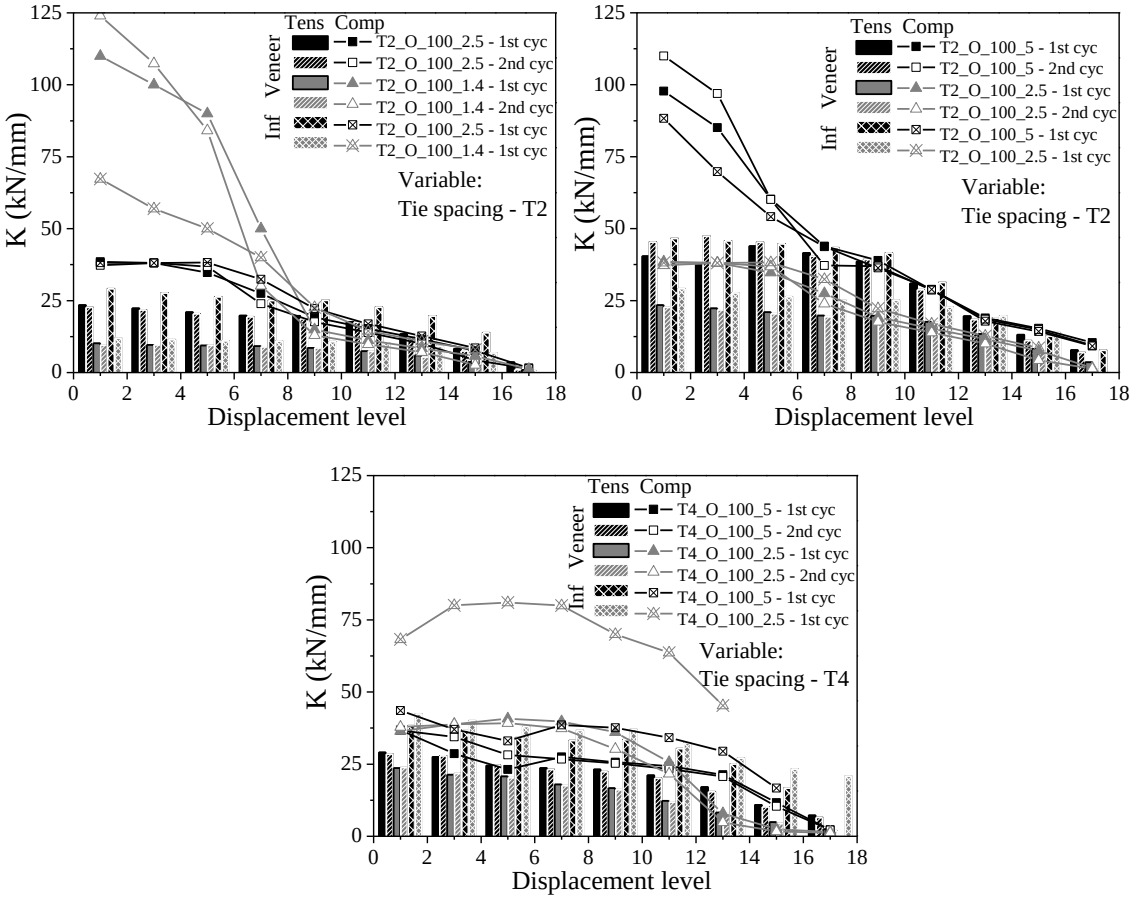

Figure 6.51 – Initial stiffness and its evolution in specimens with different tie spacing

As the reduced number of ties caused lesser stress transference to infill leaf, the deformation of infill was reduced and consequently the results of stiffness were higher than walls with higher number of ties. As conclusion, it can be suggested that the increase o number of ties affect much more the walls constructed with T2 than T4 and, on the other hand, the out-of-plane performance in compression direction.

c) Influence of air cavity width and embedment length

From the results shown in Figure 6.52, it is seen that the stiffness of the system is influenced by the width of the air cavity. Lower width of the air cavity leads to an increase of the stiffness by 2.4 times higher under compression loading. Under tension loading, the increase is only 30%. The main reason that justify this variation if the different stiffness behaviour of the wall tie and wall ties-masonry connections under compression and tensile loading.

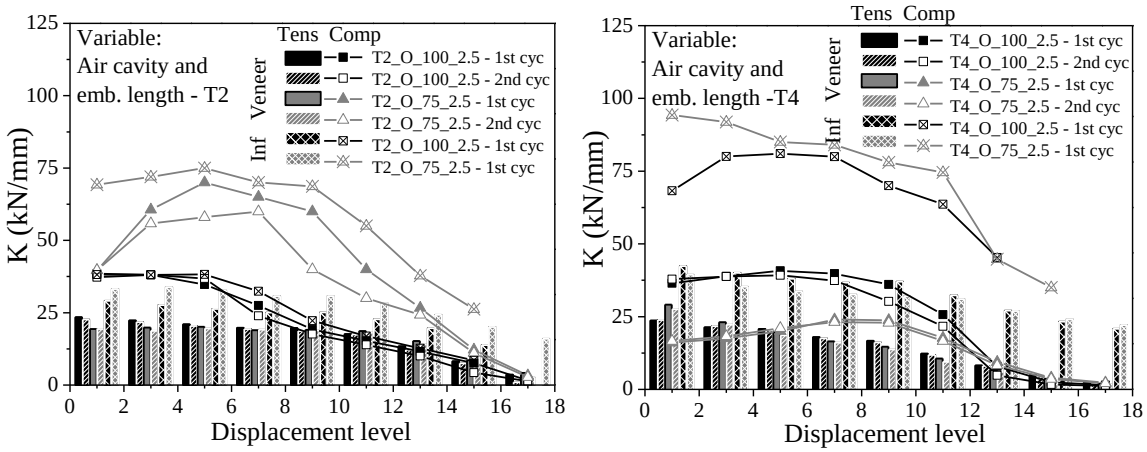

Figure 6.52 – Initial stiffness and its evolution in specimens with different air cavity width and embedment length

As previously mentioned, the lower width of the air cavity results in the reduction of the free length of connection, which consequently increase the stiffness of the wall ties. Taking into account that the wall tie behaves mainly in the axial direction, the stiffness in inversely proportional of the free length. Under tension loading the difference found is more related to the embedment length because the stiffness is much more controlled by the stiffness of the connection of the wall tie to the mortar joints of masonry walls.

d) Influence of flashing

As can be observed in Figure 6.53, the presence of flashing at the base of the veneer wall base did not influence substantially the initial stiffness and stiffness degradation. In compression loading, the presence of flashing contributed to a slight increase of stiffness,

contrarily to what is observed in tension behaviour. However, the results should be seen with caution and it considered that additional tests are needed to obtain more sound consecutions about the influence of the friction at the base in the system.

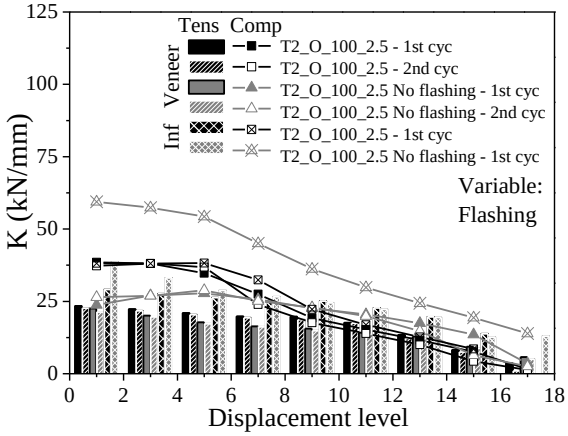

Figure 6.53 - Initial stiffness and its evolution in specimens with and without flashing

e) Influence of prior in-plane damage on out-of-plane response

In the Figure 6.54 it is possible to compare the stiffness evolution of the system with and without prior in-plane damage of the masonry infill wall. Although it was seen previously that the resistance was not be always clearly influenced by prior damage, the stiffness varies considerably if the masonry infill walls in previously damaged. In compression loading, it is possible to see that the system with masonry infill wall without previous damage presents a stiffness by 5.5 times greater that the system with the masonry wall with prior in-plane damage. Under tension, the difference is not so high, even so the stiffness of wall T2_O_75_2.5 is about the double of T2_IO_75_2.5. In the latter case, it is interesting to notice that the degradation of stiffness is considerably lower, which should be justified by the damaged state of the masonry infill, which already result in a very low value of the initial stiffness.

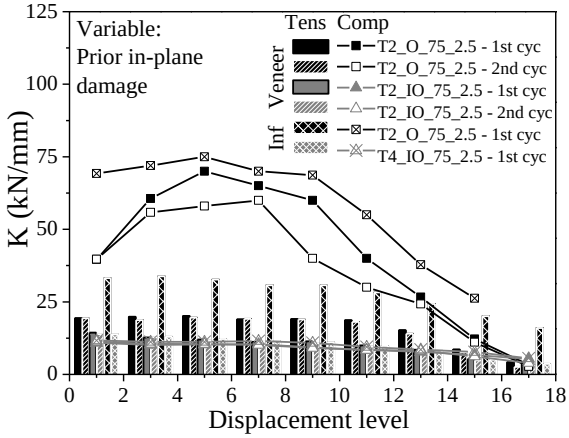

Figure 6.54 - Initial stiffness and its evolution in specimens with and without prior in-plane damage

This result seems to indicate the importance of the masonry infill walls for the stiffness of the system composed of the RC frame with the masonry infill with the attached brick veneer wall. This confirms that the interpretation on the variation of the stiffness should be discussed on the system and not in the individual masonry walls.

6.6.3. Residual plastic deformations

The plastic or residual deformations were determined based on the hysteretic diagrams of the masonry walls and are measured at middle height of the veneer wall. The plastic deformations were determined on the unloading branch in tension and compression and correspond to the displacement at zero force.

a) Influence of tie typology

According to what can be seen in Figure 6.55, the plastic deformations are practically zero at early stages of deformation, which correspond to the initial elastic behaviour of the system. It is seen that until 12th displacement level, corresponding to an average displacement of 1.5mm, very low values of plastic deformation were observed. This means that a great percentage of the out-of-plane deformation was recovered before the nonlinear behaviour characterizes the system, which is mainly associated to damage and failure of tie connections. After this displacement level, the first signs of damage at the connection and wall tie-mortar joint connections, result in the development of plastic deformations. These considerably increase by increasing imposed displacement, particularly after the attainment of the maximum resistance. This behaviour results naturally from the progress of damage of wall ties and connections.

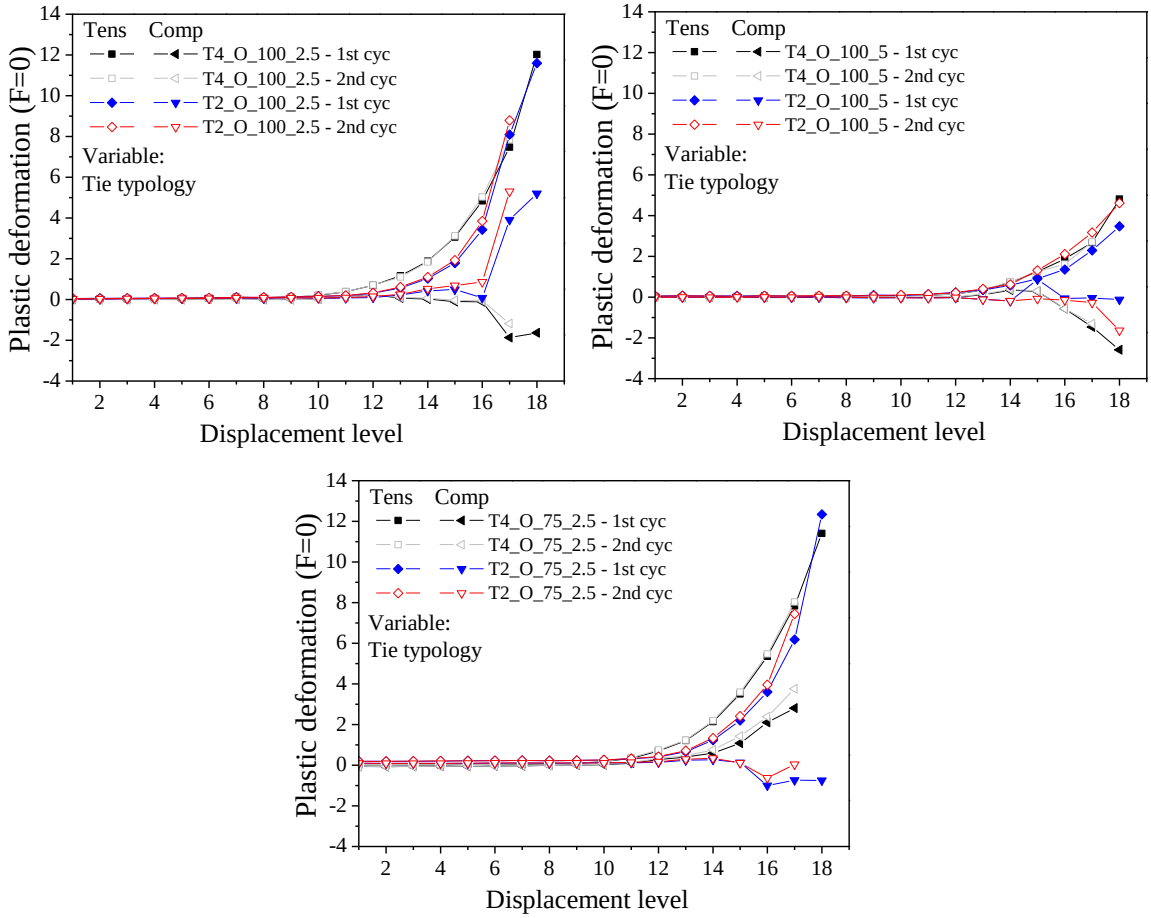

Figure 6.55 – Evolution of plastic deformation during cyclic loading in specimens with different tie typologies

A particular feature was identified in the plastic deformations in majority of walls. In most cases, the plastic deformations in compression stages have positive values, which means that the unloading branch intersects the positive x-axis (F=0). Under compression, the deformation of the wall ties is cumulative and it is not possible of recovering it. The force-displacement diagrams in the compression unloading range present a high amount of pinching, associated to the buckling of the wall tie. The pinching was observed in the cyclic behaviour in the majority of cases. However, the specimens T4_O_100_2.5, T2/4_O_100_5 and T2_O_75_2.5 exhibited the lowest pinching and for that the values of residual deformation of compression stage are negatives.

The values of residual deformations recorded in the second cycle of each displacement level is similar or higher than the correspondent first cycle, resulting from the accumulated damage.

The walls constructed with tie T4 exhibited higher values of tensile plastic deformation between 12th and 16th. This trend is attributed to the uniaxial behaviour of the ties because tie T4 presents higher plastic deformation than tie T2. As far as concerned to the compression

plastic deformation, when comparing the most resistant walls, T2_O_100_5 with T4_O_100_5, it is seen also that the use of tie T4 contributes to higher plastic deformation.

b) Influence of tie spacing

Regarding to tie spacing, it is possible to observe that the decreasing of number of ties lead to the increase of tensile plastic deformation as shown in Figure 6.56. In specimens constructed with tie T2, the plastic deformation recorded in wall T2_O_100_5 is about 30% of the plastic deformations recorded in specimen T2_O_100_1.4. In walls with tie T4, the trend is similar, but the plastic deformation in specimen T4_O_100_2.5 is about 2.5 higher than the tensile plastic deformation recorded in specimen T4_O_100_5. Thus, the influence of tie spacing in the plastic deformation is more pronounced in specimens built with tie T4 in comparison to the specimens built with tie T2. This behaviour is attributed to the different behaviour of the ties under compression as tie T4 buckles easier than tie resistant than T2. The pinching effect was more detected in lesser resistant combinations in walls constructed with T2, which caused positive residual compression deformations.

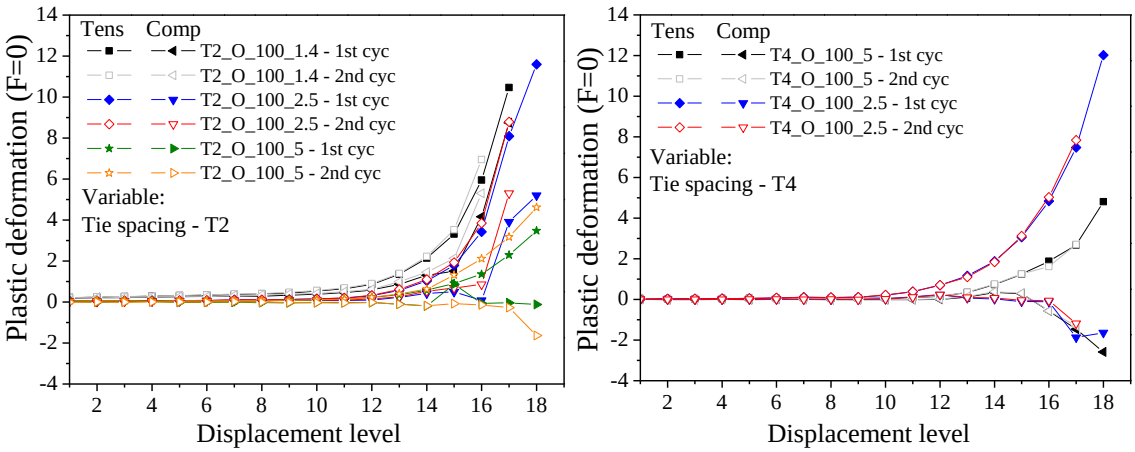

Figure 6.56 – Evolution of plastic deformation during cyclic loading in specimens with different tie spacing

In the specimens constructed with tie T4, the tie spacing appears not to have much influence in the plastic deformation as for both tie spacing as similar values of plastic deformations under compression were recorded. This is justified by the deformation of the ties under compression, which is similar in both cases, given that this deformation controls the plastic deformation measured in the specimens.

c) Influence of air cavity width and embedment length

The influence of the width of the air cavity in the plastic deformation under tension and compression can be analysed based on the results presented in Figure 6.57 for both types of

wall tie. As seen already for other parameters, the influence of the width of the air cavity is very reduced in tensile loading, because the values of plastic residual deformations are associated to the adherence of the tie to the mortar joint, which is not influence by the width of the air cavity. This trend is very similar in both types of tie. In case of compression loading, it is seen that the differences on the plastic deformation according to the tie spacing are more evident in tie T4. This should be attributed to the higher distribution of the compression loads by the wall ties when the spacing is higher, resulting in lower compressive forces and, hence in lower plastic deformations.

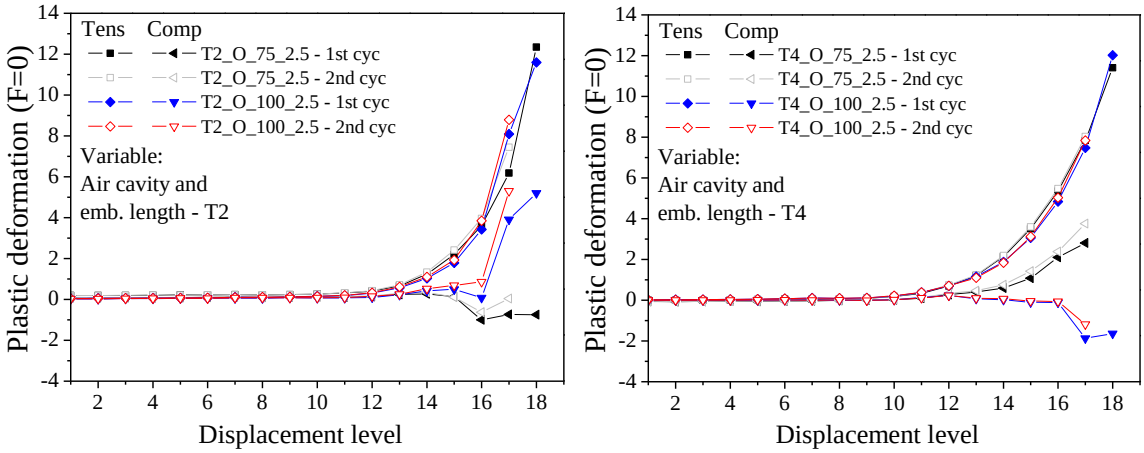

Figure 6.57 – Evolution of plastic deformation during cyclic loading in specimens with different air cavity width and embedment length

d) Influence of flashing

The influence of flashing in the plastic deformations can be analysed though Figure 6.58. The plastic deformation developed in tensile loading in walls with flashing was 8 times lesser than the plastic deformations developed in the specimens without flashing at the base of the brick veneer wall. Under compression loading, the plastic deformation in the specimen with flashing is slight higher than the plastic deformation in the specimen without flashing. The wall with flashing until 17th imposed displacement level deforms very little under tension due to friction caused at veneer base and consequently the plastic deformations are also low. Under compression, as the flashing did not influence very much the deformation mode (rotation as seen before), the plastic damage is similar in both specimens.

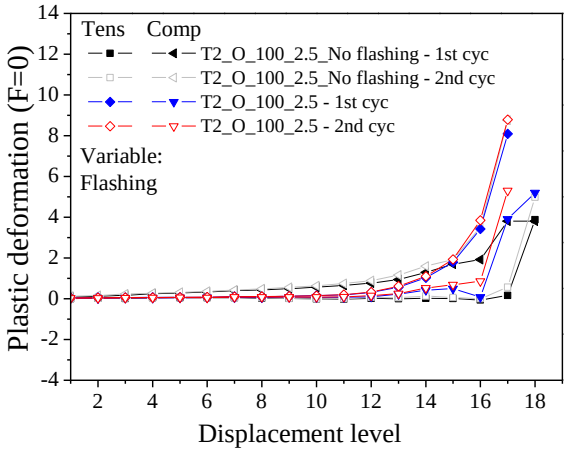

Figure 6.58 – Evolution of plastic deformation during cyclic loading in specimens with and without flashing

e) Influence of prior in-plane damage on out-of-plane response

The plastic deformation in the specimen where the infill wall was induced with prior in-plane damage was slightly higher than the plastic deformation measured in the specimen without in-plane damage of the infill wall, see Figure 6.59. The effect of prior damage did not cause difference on trend of plastic deformations because this parameter is essentially dependent by connections performance, and the prior in-plane damage on infill did not affect directly the connections, but mainly the stiffness of infill leaf.

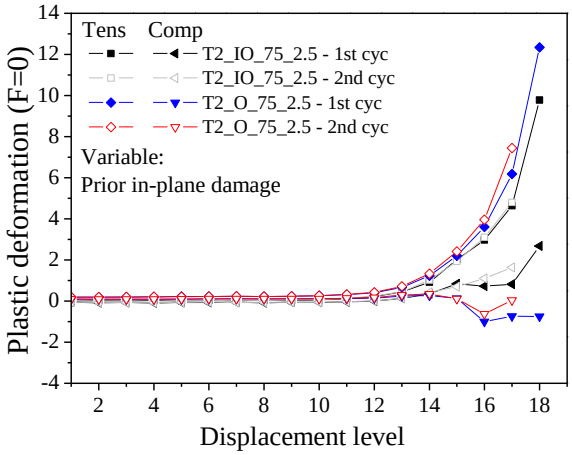

Figure 6.59 – Evolution of plastic deformation during cyclic loading in specimens with and without prior in-plane damage

6.6.4. Energy dissipation capacity and Equivalent Viscous Damping Ratio (EVDR)

The energy dissipation capacity and equivalent viscous damping ratio are common parameters to assess the seismic performance of structural elements and are used herein to

assess the performance of the system composed of the RC frame with attached brick veneer walls. In general, higher dissipative structures present a better seismic behaviour because these are able to develop damage without collapse. In the system under analysis, the energy dissipation should be the result on the damage developed in the walls but mainly due to the local damage at the tie and tie connections.

The energy dissipated by the system at each tension-compression loading cycle was calculated as the area enclosed in the cyclic loops of the force-displacement diagrams at middle of veneer wall. The cumulative dissipation of energy, CG_f, was calculated as the sum of the energy dissipated until a certain displacement, G_f, and it represents the amount of energy dissipated during the cyclic loading. Another parameter correlated with dissipation of energy is Equivalent Viscous Damping Ratio (EVDR) as explained in detail in Chapter 4. In this scope, this parameter enables to understand the damping of the walls.

a) Influence of tie typology

The dissipated energy during cyclic tests is very dependent on the damage accumulation in the wall ties and in the tie-mortar joint connections. According to Figure 6.60, until the 12th displacement level, the values of dissipated energy are very reduced because the predominant linear behaviour, being the loading and unloading branches practically coincident.

After this displacement level, it is observed that the cumulative dissipated energy presents an exponential increasing trend. Considering the tie typology, it is possible to see that all walls with tie T2 present higher energy dissipation than walls with tie T4. This result is in line with others revealing that the system built with tie T2 is more efficient than the system built with tie T4, due to the better performance of the tie under tension and compression loading (Chapter 4). The better performance of each tie is reflected in the better performance of the walls. It should be underlined that the ties used in the construction of the veneer walls lead to a good dissipative behaviour, which also contribute to avoid the brittle failure of the system.

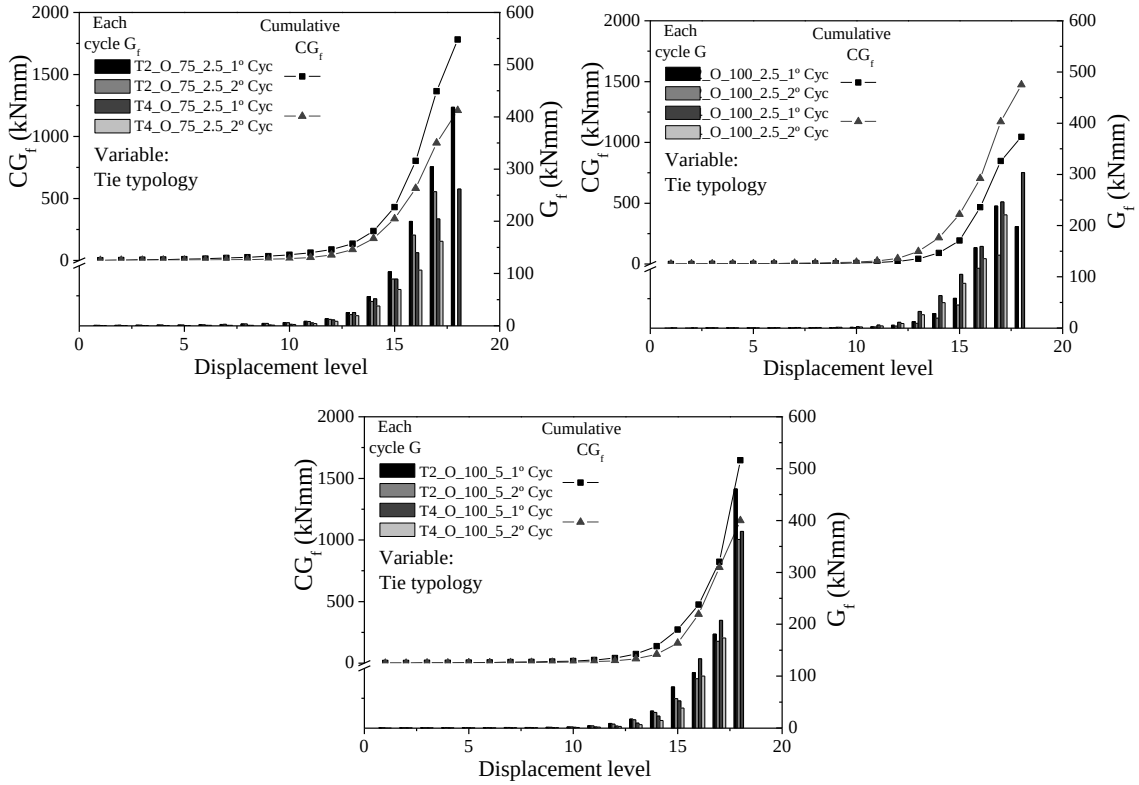

Figure 6.60 – Evolution of energy of dissipation during cyclic loading in specimens with different tie typologies

The evolution of EVDR for all systems under analysis is show in Figure 6.61. The values of the equivalent viscous damping are influenced by the pinching observed in the force-displacement diagrams plays also an important role. In general, high pinching result in lower values of damping. This is the consequence of the lowering of the energy dissipation due to pinching. The EVDR presents a nonlinear evolution with an initial lowering until the 10th displacement level (1.0mm), after which a significant increase is observed due to the dissipative mechanisms associated to the development of damage at the wall ties and at the wall tie connections. The systems with higher EVDR are built with tie T2 with air cavity width of 100mm and 5 ties per square meter and with 75mm of air cavity width, being the lowest ratios belongs to walls with more pinching and plastic residual deformation, walls built with T4 wall tie.

The comparison of the EVDR obtained for the system through the global response measured at the veneer and the EVDR calculated for the masonry infill walls, it is seen that the masonry infill contributes in a lower extent for the equivalent viscous damping of the system and the major contribution is achieved through the behaviour of wall ties. Notice that this was expected because the damage of the infill wall was quite reduced because it is dependent on the capacity of the load transfer from the veneer through the ties.

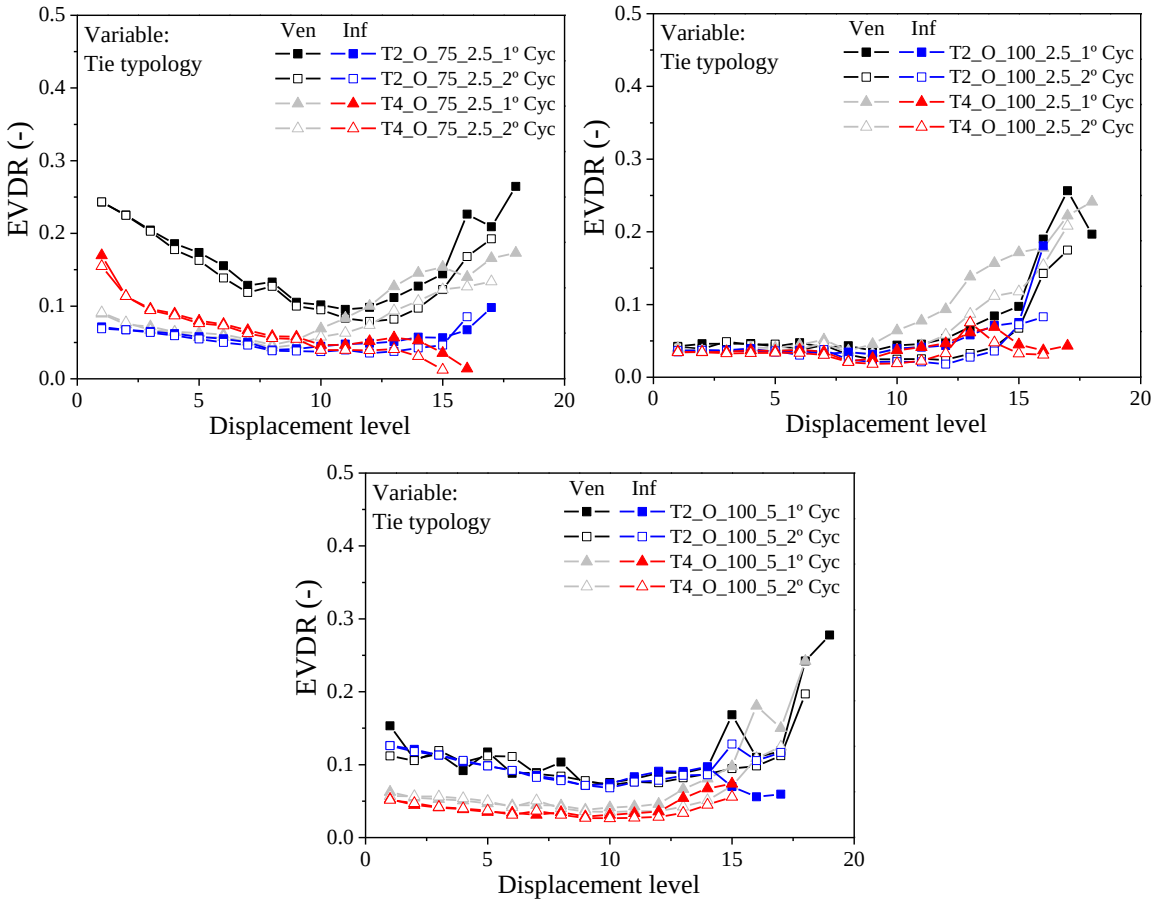

Figure 6.61 – Evolution of EVDR during cyclic loading in specimens with different tie typologies

b) Influence of tie spacing

The influence of tie spacing in the capacity of the system to dissipate energy can be analysed in Figure 6.62. It is seen that the walls with higher number of ties present better capacity to dissipate energy. This should be attributed to the possibility of better distribution of the out-of-plane forces, which result in the better distribution of damage among the wall ties. This trend is very clear in energy dissipation when the brick veneer is attached to the masonry infill walls with 1.4, 2.5 and 5 ties per square meter. The same trend is also seen in the systems built with tie T4 for layouts with 2.5 and 5 ties per square meter. The energy dissipation of the system built with 5 ties per square meter of type T2 is about 2.5 times the energy of the system built with 2.5 ties per square meter. This is attributed to the worse distribution of damage among the ties when the number is low, which is reflected by a higher trend to exhibit a pinching behaviour. In case of the system built with tie T4 the difference of energy dissipation when 2.5 and 5 ties per square meter are used is about 25%. Thus, tie

spacing of tie T2 has more influence than in case of tie T4 because the system with ties T2 have higher amount of energy.

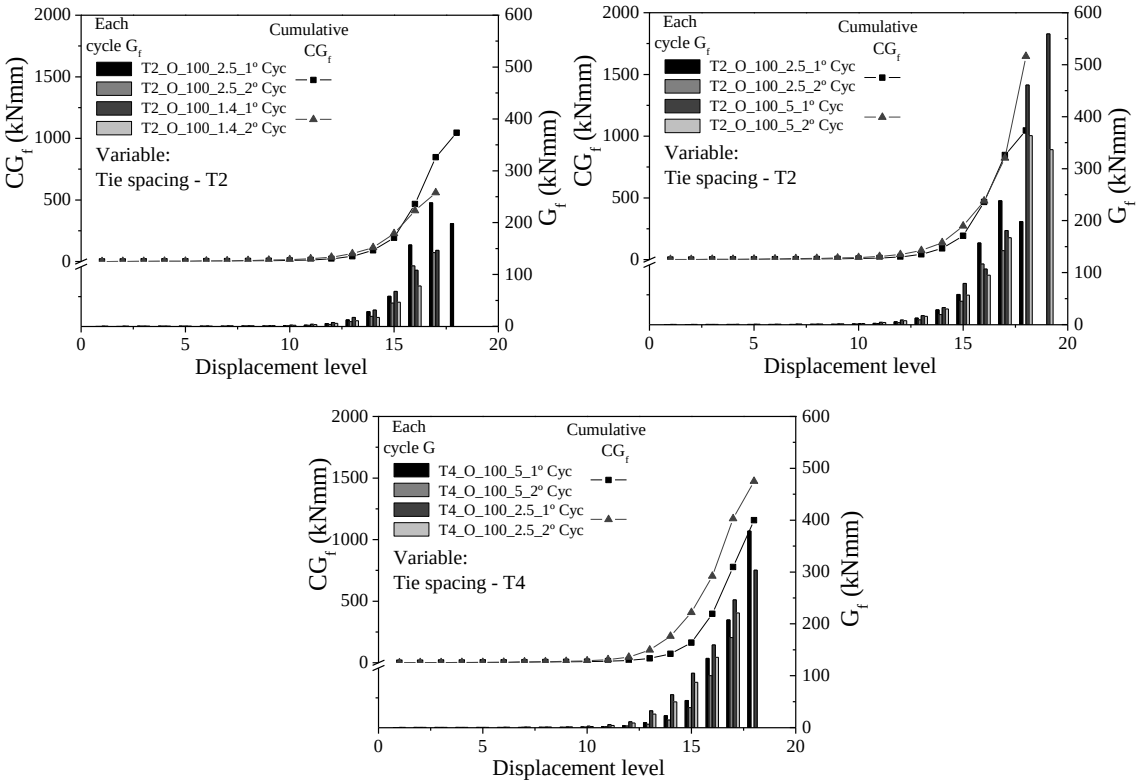

Figure 6.62 – Evolution of energy of dissipation during cyclic loading in specimens with different tie spacing

The evolution of the equivalent damping ratio (EVDR) for the systems with different tie spacing presented in Figure 6.63. It is observed that EVDR is higher in case of higher number of ties, either the system is built with tie T2 or tie T4. This was expected, taking into account the trend previously dissuaded for the dissipation of energy. The differences are more relevant in case of tie T2, in which the decrease on the tie spacing (5 ties per square meter) result in the double of EVDR when compared to the system with 2.5 5 ties per square meter.

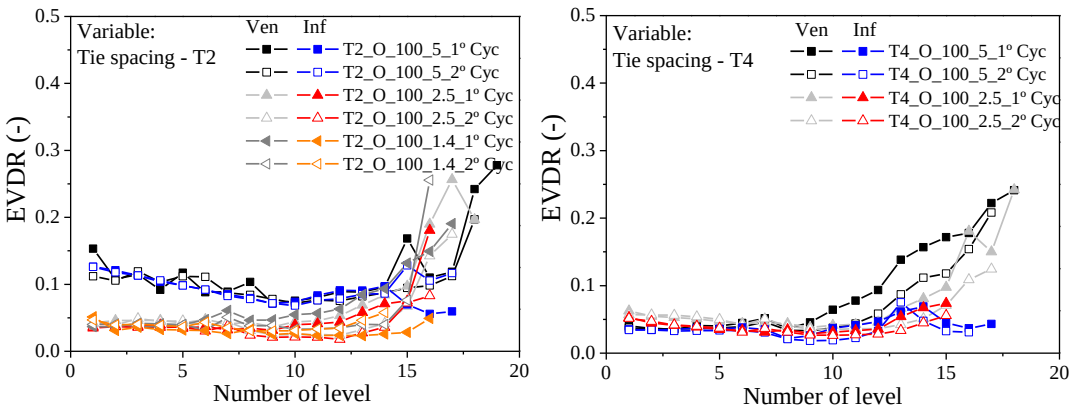

Figure 6.63 – Evolution of EVDR during cyclic loading in specimens with different tie spacing

c) Influence of air cavity width and embedment length

According to what can be seen in Figure 6.64, the thickness of the air cavity influences the dissipation of energy in systems built with tie T2, despite there are no very important differences between the system with thickness of air cavity of 100 mm and 75mm. In addition, in system built with tie T4, there is no a clear trend of increasing the energy dissipated by changing the thickness of the air cavity. Taking into account that the major damage mechanisms that contribute for the dissipation energy develops at the ties and tie-mortar joints connections, the difference in the energy dissipation by varying the thickness of the air cavity should be attributed to the better performance of the ties under compression. As discussed before, the change on the thickness of the air cavity does not a major role in the damage mechanism of the systems in tension but influences the behaviour under compression due to the change on the free length of the ties and to the lower feasibility to buckle. Therefore, it is considered that the more dissipative behaviour in case of the system in case of using tie T2 comes from its better performance under compression.

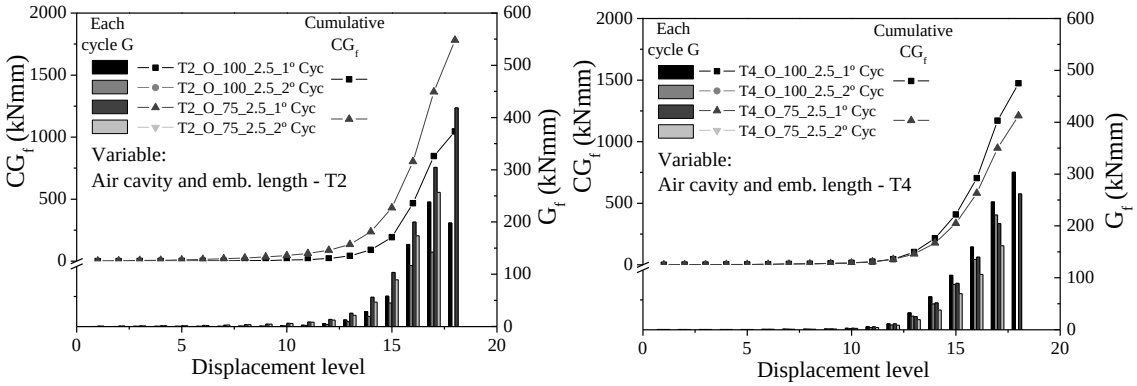

Figure 6.64 – Evolution of energy of dissipation during cyclic loading in specimens with different air cavity width and embedment length

Regarding to the equivalent viscous damping ratio, it is clear that the thickness of the air cavity plays an important role in the EVDR for the systems built with tie T2 when the thickness of the air cavity is varied, see Figure 6.65.

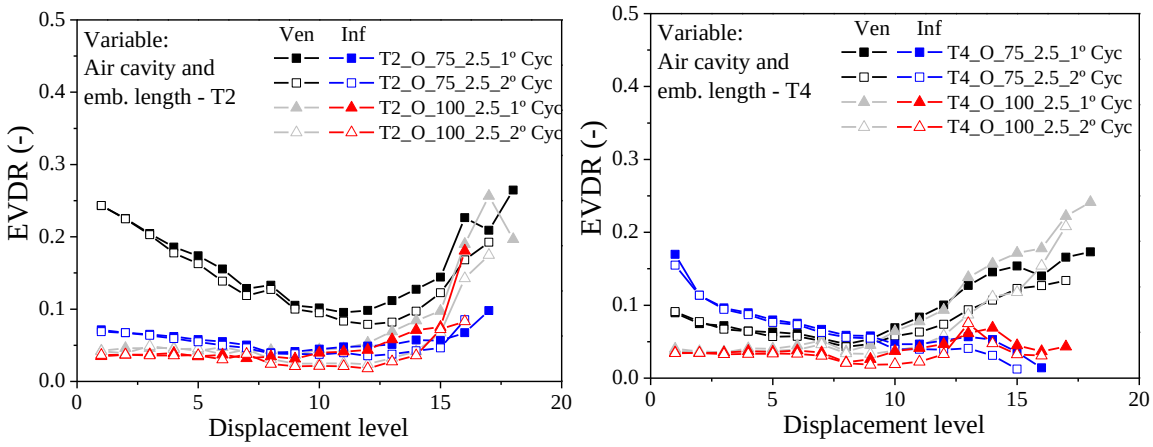

Figure 6.65 – Evolution of EVDR during cyclic loading in specimens with different air cavity width and embedment length

Lower thickness of the cavity (75 mm) leads almost always to higher values of EVDR during the out-of-plane test when the tie T2 is used. In case of the system consider the veneer walls attached to the masonry infill walls with tie T4, there are no significant differences in the values of the EVDR and, thus, it is considered that from the results obtained the influence of the air cavity can be neglected. Again, this behaviour can be attributed to the poor performance of tie T4 under compression loading.

d) Influence of flashing

As can be seen from Figure 6.66 (a), the energy dissipation in the system in which there is no flashing at the base of the brick veneer walls is 100% higher (achieving 100%) than the energy dissipated in the system with flashing. In addition, the EVDR in wall without flashing is slightly higher than in wall with flashing as seen in Figure 6.66 (b).

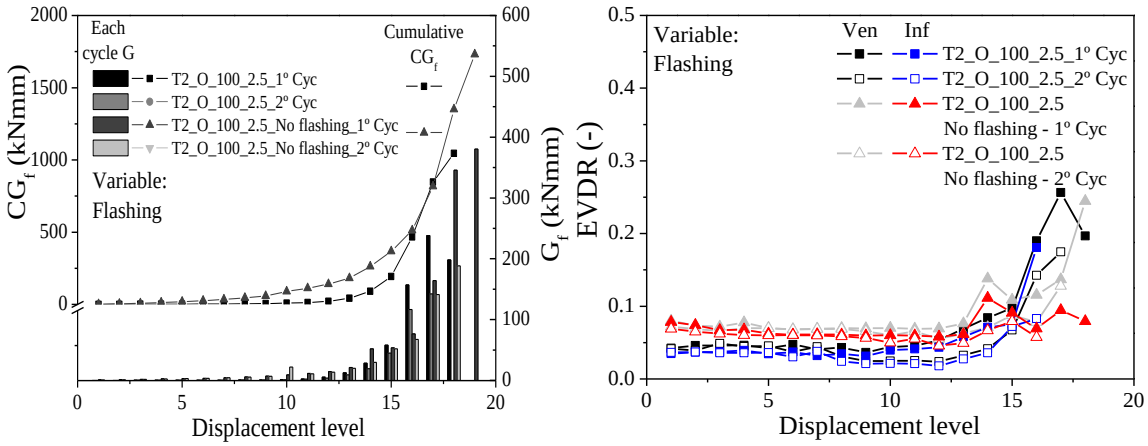

Figure 6.66 – Specimens with and without flashing: evolution of (a) energy of dissipation and (b) EVDR

The unloading branches of wall without flashing are smoother, providing a greater dissipative capacity to the walls, which consequently cause lower pinching effect than walls with flashing and consequently higher EVDR values.

e) Influence of prior in-plane damage on out-of-plane response

The energy dissipation of walls with and without prior in-plane damage is presented in Figure 6.67. The in-plane damage of the masonry infill walls takes a major role in the energy dissipated by the system when submitted t out-of-plane loading. The capacity to dissipate energy is about 2 times higher in the system without previous damage when compared to the

system in which the masonry infill was induced prior in-plane damage. As aforementioned, the prior in-plane damage caused many cracks and discontinuities on the infill wall mainly. The previous damage affects significantly the out-of-plane behaviour of the system because the load transfer from the brick veneer to the masonry infill is much less effective and the masonry infill has, thus, a lower contribution for the global behaviour of the system. This contributes also for the low values of the equivalent viscous damping ratio obtained in the system with prior damage, see Figure 6.67(b). It should be underlined that the prior in-plane damage takes a major role on the mechanical behaviour of the system and thus on the seismic performance of the brick masonry infills. As the masonry infill walls are rather susceptible to suffer in-plane cracking during seismic events, it is considered that the influence of the previous damage on the safety of the brick veneer walls ned to be better addressed in future research.

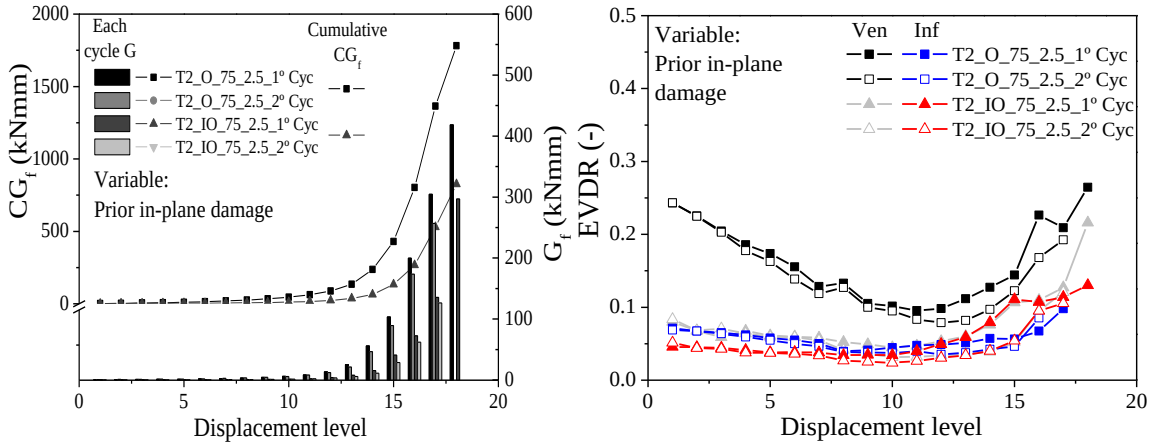

(a) (b)

Figure 6.67 – Specimens with and without prior in-plane damage: evolution of (a) energy of dissipation and (b) EVDR

6.7. Conclusions

This chapter presents and discusses the experimental results obtained on quasi-static cyclic in-plane and out-of-plane tests carried out on systems composed on an RC frame with brick masonry infill to which a brick veneer walls is attached through different types of wall ties. The adoption of the RC frame with the masonry infill as the backing system of the brick veneer walls derived from the common use of this structural system in residential buildings in Portugal and in other south European countries. Nine samples were subjected to out-of-plane cyclic loads and one was loading under in-plane direction. The loading configuration

was intended to simulate as close as possible the loading conditions induced by earthquakes on the brick veneer wall.

Based on the analysis of the results of the experimental campaign, the following conclusions can be drawn for in-plane tests:

1. Nonlinear hysteretic behaviour characterizes the composite system composed by the RC frame with masonry infill having the brick veneer wall attached with wall ties. It is considered that the response is typical of an RC frame with masonry infill, meaning that for the loading conditions considered in the experimental testing, the contribution of the brick veneer can be neglected.

2. The wall exhibited a progressive loss of stiffness, being the variation of stiffness between 67% and 80% since the initial stiffness until the maximum resistance point. The most notorious change in stiffness was identified after 0.06% of drift, corresponding to the onset of the nonlinearity of the system.

3. The higher strength loss between first and second cycle occurs between 0.06% and 0.23% of lateral drift, which corresponds to the onset of the of nonlinear response before of resistance peak, achieving about 30%. This results from the accumulation of damage by opening or increase on the crack opening;

4. The maximum displacement at ultimate cycle is about 0.5% of drift (10mm) and the maximum plastic residual deformations is almost 0.2% of drift (4mm), which means representing only 25% of residual deformation;

5. The ratio was decreasing with the increase of displacement due to more plastic deformations and pinching effect. An important characteristic from the trend of damping ratio is recorded in 0.06% of drift, that present a severe declining of ratio value, which is associated to nonlinear behaviour starting of specimen and consequently the lesser damping capacity;

6. After 0.06%, first cracks are formed and the loops of hysteresis cumulate more energy and the energy dissipative capacity increased exponentially;

7. By increasing the lateral displacement, the cracks in the masonry infill wall propagate in the diagonal direction as stair stepped cracks passing through vertical and horizontal mortar joints. The separation of the infill masonry wall from its bounding frame and crushing at upper boundary was identified from early stages of loading. The most serious crushing of the bricks was observed at the drift of 0.5%, localized along the compression diagonal strut;

8. The veneer wall and wall ties did not exhibit any visible signal of damage during cyclic test.

From the out-of-plane tests, it is possible to conclude that:

1. Nonlinear hysteretic behaviour begins for very early stages of deformation. The hysteretic response is not symmetric in majority of cases because the wall ties play a central role on the out-of-plane performance of the system. As they exhibit different behaviour under compression and tension loading, as seen in individual study previously presented, they influence also in the same way the out-of-plane behaviour when tensile and compression loading is induced.

2. The maximum out-of-plane resistance was recorded in system with higher number of ties (lower spacing) both in case of tie T2 and tie T4. The tensile resistance of the system built with tie T2 is similar to the resistance of the system built with ties T4. Under compression loading, the system built with tie T2 presents a lateral resistance clearly higher than the one obtained in the system built with tie T2 and it is very similar with tensile resistance;

3. In majority of cases, there is slight loss of resistance between first and second cycle, being achieved the highest loss about 12% due to cumulative damage;

4. The initial stiffness of the system depends greatly on the type and spacing of ties and the decreasing of stiffness due to the progressive damage at the ties and tie-mortar joint connections. Thus, the system with tie T2 is stiffer than the system built with tie, which is associated to the stiffness of the ties and to the ability of transferring he out-of-plane loading to from the brick veneer to the masonry infill wall. In addition, the stiffness has been influenced greatly by prior in-plane damage because the stiffness decreased substantially due to previous cracks localized mainly at the unit-mortar interfaces.

5. The system with tie T2 is dissipative because these ties lead to higher resistance under compression loading, comparing to the ties T4 that exhibit poor performance under compression loading due to premature lateral instability. Nevertheless, it is underlined that both types of ties seem enable the system to have an important deformation capacity beyond the peak resistance, leading to ductile responses by avowing brittle failure.

6. Damping values of walls are influenced by connection performance. The walls with lower values of damping showed more severe pinching effect. This effect is correlated to the accumulated damage of connections and clearances created, promoted by the contact loss between tie-mortar. Consequently, the energy of dissipation decreases, which influences directly the damping behaviour of system.

7. The deformation of infill wall is dependent on the ability of the ties to transfer the out-of-plane loading from the brick veneer walls to the masonry infill wall. More deformation of infill wall means that the wall ties accomplish the loading transfer, resulting in a more dissipative response and improving the performance of the system under cyclic loading. With this respect, it should be stresses that tie T2 is more efficient in transferring the out-of-plane loading than tie T4. In addition, when the number of ties increase, the load transfer is also improved. It means that in these cases, the stress distribution of stresses among the ties in enhanced, leading to more resistance and higher redistribution capacity. After maximum resistance of the system is achieved, the ties loose the capacity to transfer loading and the deformation of infill is very low or even absent.

8. The wall ties experienced severe damages but they were enough to guarantee an adequate post-peak resistance of the veneer wall. The damages observed consisted of: (1) pull-out of wall tie from embedment bed joint and in more demanding cases the (2) wall tie fracture when veneer wall is subjected to out-of-plane loading under tension direction and (3) buckling of wall tie when the veneer wall is subjected to out-of-plane loading under compression direction. The damage found in veneer and infill wall was very reduced.

9. Based on the results obtained, it is highlighted that the detailing of wall construction and correct application of wall ties is crucial for its adequate seismic performance. On the other hand, the suitable load transference and interaction between wythes are very important aspects to consider in seismic performance, providing a suitable structural design for resisting the loading.

Chapter 7

Design Recommendations

Abstract:

In majority of cases, seismic design of the masonry veneer walls systems is not a current practice, which becomes a real problem considering that these elements can cause severe damages under earthquake actions or other imposed lateral actions. The main goal of this chapter is to present an overview about existing seismic design approaches of masonry veneer system presented in different codes, according its rules and guidelines. The key values obtained from the seismic design procedures described in this chapter are displacements, forces and the behaviour factors that should be used as capacity limits for each performance level analysis in order to maintain primordial function of veneer stability.

7.1. Introduction

As mentioned in Chapter 2, masonry brick veneer is a popular exterior wall cladding used in diverse types of buildings and considered as a non-resistant element, for which no accurate design guidelines are available. Some of these buildings are located in high seismic hazard zones as in case of some south European countries. In the majority of cases, seismic design of these constructive systems is not a current practice, which becomes a real problem considering that these elements can be much vulnerable under earthquakes.

The design of masonry structures, including the masonry veneer walls, should be based on standardized guidelines and it has been developed over the years. The Structural Engineering Institute of the American Society of Civil Engineers (ASCE/SEI) has already published the 3rd edition of manual Minimum Design Loads for Buildings and Other Structures (SEI/ASCE 7-02 and ASCE/SEI 7-10) [158, 159], which provide guidelines about structures general design. In order to specify masonry structures, the ASCE/SEI, the American Concrete Institute (ACI) and The Masonry Society (TMS) work together as a joint committee, producing the Masonry Standards Joint Committee (MSJC) [160]. This committee has published design recommendations for masonry structures based on specific requirements. These were accredited by the American National Standards Institute (ANSI). The seismic assessment of masonry structures is a focus of the manual of Seismic Evaluation and Retrofit of Existing Buildings published by ASCE, created by the first time in 2003 (ASCE/SEI 31-03 [161]) and improved in following editions (ASCE/SEI 41-06 (2006), ASCE/SEI 41-13 (2013) and ASCE/SEI 41-17 (2017) [162-164]). The Federal Emergency Management Agency (FEMA) has also published important Guidelines for the Seismic Rehabilitation of Buildings in 1997 (FEMA 273 [165]). Eurocode 6 (EC6) [30] also present procedures for the design of masonry structures, but the seismic assessment/design is detailed in Eurocode 8 (EC8) [78].

The main goal of this chapter is the revision of existing seismic design approaches for design masonry veneer walls provided in mentioned codes. Thus, design guidelines to ensure the seismic safety of masonry veneer walls are provided. Procedures recommended by different standards are based on methods of analysis in accordance with principles of mechanics. The designer may choose the most appropriate design procedure for a suitable seismic design according to the type of building. The design recommendations include limit values of

strength and deformations that should be verified for each performance level, as well as behaviour factors that can be used in determination of design strengths.

It should be underlined that despite the quantification of the seismic demand on non-structural elements is out of the scope of this work, methods for obtaining these demands are presented.

7.2. Design approaches for masonry veneer walls according to the standards

As seen in the previous section, despite there are no clear guidelines for the design of structural masonry in different codes, the same does not apply to non-structural elements, namely masonry veneer walls. Commonly, brick masonry veneer walls are considered as non-structural elements and they are no explicitly designed for seismic actions.

For the knowledge of the author, MSJC code [160] is the international standard that more directly mentions design recommendation for brick veneer masonry walls. It provides two different approaches for masonry veneer walls design, being essentially based on two concepts: (1) the veneer wall is considered to be a non-structural element of the building; and (2) the veneer wall is considered to be load-resisting element of the building. The designer may choose to consider the veneer as non-structural or as a structural element.

The first assumption implies to follow several recommendations for non-structural elements, namely: (a) the loads shall be distributed through the anchors and transferred from the veneer walls to the backing system by using principles of mechanics; (b) the out-of-plane deflection of the backing shall be limited to keep veneer wall stability; (c) it is allowable that the brick veneer walls crack under service loads but it is not required that they have flexural resistance to safety limit state; (d) differential movement should be considered in the design, detailing, and construction. In addition, some construction guidelines are also provided: (a) the wall system should be designed, detailed, and constructed to prevent water penetration into the building and (b) the requirements for corrosion protection and fire resistance must be included.

The second approach implies that the masonry veneer shall be designed to resist the imposed loads. For that, masonry walls and connections should be designed based on limit design stresses and deformation requirements. The structural masonry wall classified in the majority of cases as unreinforced masonry wall (URM) should be design in order to ensure the safety in terms of maximum stresses installed. The required strength to resist seismic forces in

combination with gravity and other loads shall comply with the earthquake resistance requirements provided by SEI/ASCE 7-02 [158].

For strong winds and high seismic risk regions, there are higher demanding requirements to improve performance of the brick veneers according to the first and second design approaches, namely; (a) supporting at each floor reduces the size of potentially damaged areas of the brick veneer; (b) increasing number of anchors improves veneer stability and reduces the possibility of falling debris; (c) adding expansion joints allow greater building deformation without veneer damage and limit stress developed in the veneer wall; (d) the application of joint reinforcement and horizontal movement joints enhances post-cracking strength and controls cracking; and (e) joint reinforcement provides ductility and post-cracking strength.

Regarding to the attachment of the veneer walls to the backing system, wall ties shall be studied for loads and conditions representing their use in order to obtain their strength. Nevertheless, there are some specific design requirements presented in MSJC code [160], namely: (a) each type of wall tie has physical requirements that must be met (material quality, durability and mechanical properties); (b) minimum embedment requirements have been set for each anchor type to ensure adequate bond adherence against push through or pull-out of the mortar joint (c) maximum air space dimensions of masonry should be taken into account in the selection of wall tie; (d) anchors should allow in-plane movement of the wall but should also resist out-of-plane loads; (e) the number of ties should be calculated according to the required load and capacity of ties.

In both approaches, it is recommended that the designer should provide additional technical and construction guidelines: (a) moisture resistance, thermal properties, fire resistance, acoustic properties, strength and durability of the bricks, vertical support and heights of the veneer wall; (b) definition of appropriate ties and appropriate spacing; (c) proper detailing of flashing and weep holes, air cavity and moisture barriers, vertical and horizontal movement joints and insulation; (d) climatic conditions and exposure; (e) maintenance plans which includes annual inspections.

Other few recommendations for design and detailing are provided in other standards. Quantitative and qualitative deformation limits are empirically recommended for each level of performance in FEMA 273 [165]. Eurocode 6 [30] states that when lateral loads are applied on veneer walls, they should be transferred to the backing through the wall ties. The number of connections should be designed based on imposed lateral load and the strength capacity of each connection, being also recommended a minimum number of wall ties per

unit area. Eurocode 8 [78] dos not provide specific guidelines to calculate the strength capacity of non-structural elements but presents recommendations for the calculation of the seismic action and suggests performance levels (Damage Limitation (DL), Significant Damage (SD) and (c) Near Collapse (NC)) to be achieved when designing the new structure .

7.2.1. Performance levels

As aforementioned, existing literature suggests performance-based design (PBD) as the most appropriate path towards seismic assessment and design since it establishes a direct relationship between demand and performance of a structural system or component [166-169]. PBD is based on defining several levels of seismic performance for structural and non-structural elements. For example, FEMA 273 guidelines [165], ASCE/SEI 41-13 [162] and ASCE/SEI 7-10 [159] define three performance levels for the seismic design for structural components: a) Immediate Occupancy (IO), b) Life Safety (LS), and c) Collapse Prevention (CP), see Figure 7.1. For non-structural elements, the definition is little different, but the idea remains the same: a) Operational (O), b) Position Retention (PR) and c) Life Safety (LS) performance level. The position retention level corresponds to immediate occupancy level. As shown in Figure 7.1, the IO level corresponds to a building that remains safe to immediate occupancy, with minor damages on components; the LS level corresponds to a structure that remains stable but with moderate to extensive damage and in CP level, the life safety is at risk, being the structure remains only standing. The additional level is the operational performance level, which accounts for negligible damage on nonstructural components, meaning an extremely low risk to life safety, and ensures that all important systems for normal operation shall work. All performance levels defined for non-structural components are in damage control range, taking into account that these elements do not contribute for the resistance of buildings. In this same range, it is possible to include two performance levels of structural components (IO and LS levels), aiming to control the damage of buildings. The last performance level of structural components (CP level) is regarding to safety limit of elements, aiming to ensure their structural stability but extensive damage.

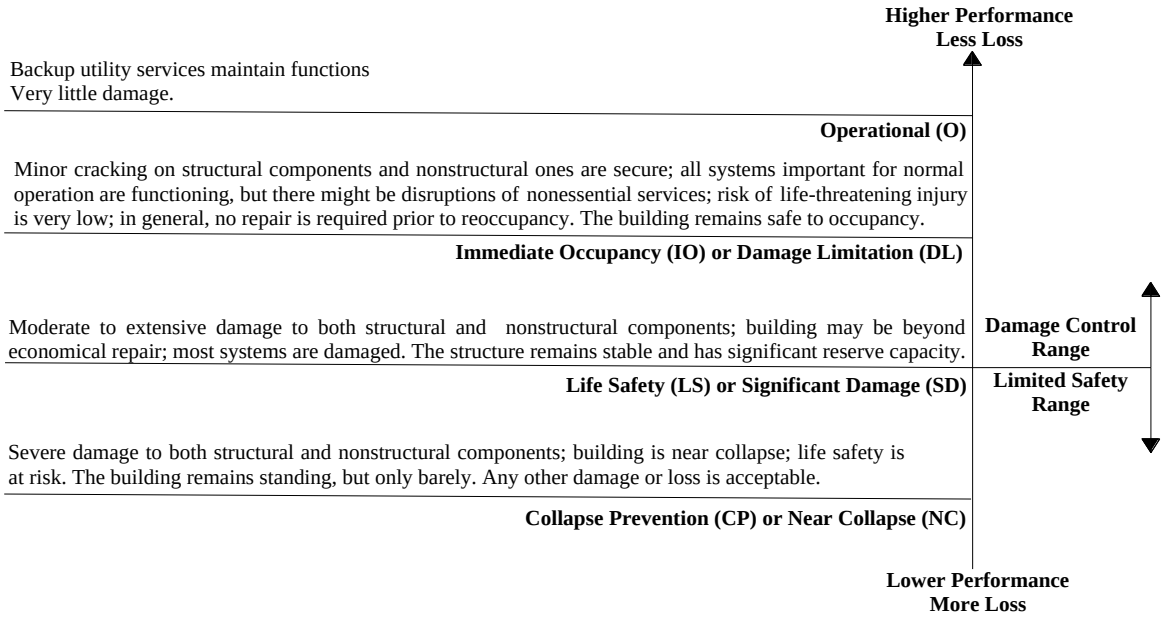

Figure 7.1 – Seismic performance levels

It should be mentioned that the different performance levels can be assigned according to the importance of the building and related to different earthquake hazard levels. For example, according to FEMA 273 [165], important buildings should be designed for an immediate occupancy level associated to a 475 year-recurrence period. For the same buildings, the life safety performance level is associated to a 2475 year-recurrence period.

EC8 [78] associates also the scenarios of different limit states to distinct earthquake hazard levels: (a) the Damage Limitation (DL) should be considered for a return period of 225 years (20%); (b) Significant Damage (SD) should be considered for a return period of 475 years (10%) and (c) Near Collapse (NC) can be achieved for seismic events associated to return period of 2475 years (2%). The value inside brackets represents the probability of exceedance of the seismic event in 50 years. The DL correspond to IO level of ASCE/SEI, the SD corresponds to LS level and NC corresponds to CP level, as described in Figure 7.1.

7.2.2. Veneer walls considered as non-structural elements

As aforementioned, the veneer walls can be considered as non-structural elements and do not formally contribute to resistant function of building. However, to these elements should be applied performance levels objectives as described before (Operational, Position Retention and Life Safety levels), in order to control the damage of structure. The codes

present the method to calculate the seismic actions on structures and provide performance objectives (stress limits and drifts limits) that should be in accordance with that.

ASCE/SEI 41-13 [162] and ASCE/SEI 7-10 [159] present expressions to calculate the seismic imposed actions in veneer walls or at the level of certain connection. The horizontal seismic design force (F_p) to be considered on the non-structural component's center of gravity and distributed relative to the component's mass distribution can be calculated through the expression 7.1:

$$F_p = \frac{0.4 a_p S_{XS} W_p (1 + \frac{2x}{h_{eff}})}{\frac{R_p}{I_p}} \quad (7.1)$$

Where,

F_p is the component seismic force applied horizontally at the center of gravity of the component or distributed according to the mass distribution of the component;

a_p is the component amplification factor;

S_{XS} is the spectral response acceleration parameter at short periods for any seismic hazard level (Chapter 2 of ASCE/SEI 41-13 [162]);

W_p is the weight of the wall or of a specific area of the wall;

h_{eff} is average roof elevation of structure, relative to ground elevation;

R_p is the component response modification factor;

I_p is the component importance factor, that can be 1.0 for Life Safety (LS) and Position Retention (PR) and 1.5 for Operational (O) non-structural performance levels.

x is center of gravity in height from the ground of the component (veneer wall or level of the tie).

ASCE/SEI 41-13 [162] and ASCE/SEI 7-10 [159] consider that the seismic force should be in a range limited by two values F_p *(maximum)* and F_p *(minimum)*. The maximum force that can be considered to be applied in the masonry veneer wall is given by expression 7.2:

$$F_p(maximum) = 1.6\, S_{XS}\, I_p\, W_p \quad (7.2)$$

The minimum force that can be considered to be applied in the masonry veneer wall is given by expression 7.3:

$$F_p(minimum) = 0.3\, S_{XS}\, I_p\, W_p \quad (7.3)$$

EC8 [78] also provides an expression to be used in the calculation of the seismic force to be considered in the design of non-structural components through expression 7.4:

$$F_p = \frac{S_a W_a \gamma_a}{q} \tag{7.4}$$

Where,

S_a is the seismic coefficient applicable to non-structural elements, (EC8 [78]);

γ_a is the importance factor of the element;

q is the behaviour factor of the element;

W_a is the weight of the element.

All parameters are always according with International System Units.

ASCE/SEI 41-13 [162] recommends that the design bending strength of masonry can be defined based on known allowable stress values increased by a factor of 1.4. Examples of allowable bending stress values for clay masonry are presented in MSJC code [160].

The non-structural components of veneer system should be evaluated in terms of deformation limits. These elements should be also included in the numerical models in order to determine the lateral displacements that occurs in structure due to seismic forces and displacement imposed. According to ASCE/SEI 41-13 [162] and ASCE/SEI 7-10 [159], the relative displacements (D_p) and the drift ratios (D_r) should be calculated in selected levels in accordance with following expressions:

$$D_p = (\delta_X - \delta_Y) \tag{7.5}$$

$$D_r = (\delta_X - \delta_Y)/(X - Y) \tag{7.6}$$

where,

D_p is the relative seismic displacement;

D_r is the drift ratio;

X is the height of upper support attachment at level x measured from the ground;

Y is the height of lower support attachment at level y measured from the ground;

δ_X is the lateral displacement at level x of structure;

δ_Y is the lateral displacement at level y of structure.

ASCE/SEI 41-13 [162] states that the deformations experienced by non-structural components should be evaluated to different performance levels, namely Life Safety, Position Retention and Operational non-structural performance levels according the

acceptance criteria presented in codes. The evaluation of allowable deformation is based on drift ratios limits for each performance level and are summarized in Table 7.1. Besides the values provided by ASCE/SEI 41-13 [162], other standards such as EC8 [153] and MSJC [152] indicates also limit values for non-structural walls. The deformation limits are given as target values or can be calculated according to expression involving the storey height (h_{eff}). EC8 [153] suggests a reduction factor, ν to take into account the lower return period of the seismic action associated with the damage limitation requirement. In Portugal, the values of this parameter can be 0.4 or 0.55 according to type 1 or type 2 seismic action (EC8 [78]).

Table 7.1 – Drift limits corresponding to different performance levels in non-structural elements

Source code	Deformation limits for performance levels	
ASCE/SEI 41-13 [162]	LF: $D_r = 0.02\%$	(7.7)
	PR: $D_r = 0.02\%$	(7.8)
	O: $D_r = 0.01\%$	(7.9)
EC8 [78]	$D_r = 0.005 h_{eff}/\upsilon$	(7.10)
MSJC [160]	$D_p = h_{eff}/600$	(7.11)
	$D_p = 7.6mm$	(7.12)

7.2.3. Veneer walls considered as structural elements

In case of veneer walls are considered as a structural element, it is necessary to classify them regarding the importance class. The veneer walls can be considered as primary or secondary components through a careful analysis on the stiffness of the elements regarding the global building stiffness. ASCE/SEI 41-13 [162] suggests that the primary components are required to resist the seismic forces in combination with gravity load and accommodate deformations to comply with a performance level. Secondary components are required to accommodate deformations but are not required to resist the seismic forces. If the total initial lateral stiffness of secondary components in a building exceeds 25% of the total initial lateral stiffness of primary components, some secondary components shall be reclassified as primary to reduce the total stiffness of secondary components to less than 25% of the primary components.

In addition, the components should be classified as “brittle” or “ductile”, which conditioned the use of force-based or displacement-based design criteria, respectively. When force-based design is used, the design is carried out by comparing imposed and design strength. This is widely applied by practitioners, especially when linear analysis procedures are allowed.

Displacement-based design is used when the ductility of the element can be explored, which occurs when post-peak behaviour is known.

The brick masonry of veneer walls present commonly a "brittle" failure mode when submitted to shear and flexural. According to the rules of ASCE/SEI 41-13 [162], the design for this type of element is always based on the elastic behavior range of the elements.

Therefore, the design of brick veneer walls, when considered as a structural element, is based on the comparison between the design strength, Q_{CL}, and imposed stresses, Q_{UF}:

$$kQ_{CL} > Q_{UF} \tag{7.7}$$

Where, k can be seen as a safety factor called a knowledge factor and defined in ASCE/SEI 41-13 [162]. This value is generally considered as 0.75.

As mentioned before, Q_{UF} is the imposed stresses derived from the global analysis of the building to which the brick veneer is attached to. For this, different analysis procedures can be followed, namely static and dynamic procedures. In both cases nonlinear and linear can be carried out: linear static procedure (LSP), nonlinear static procedure (NSP), linear dynamic procedure (LDP) nonlinear dynamic procedure (NDP). For a particular case of out-of-plane actions, ASCE/SEI 41-13 [162] recommends using nonlinear dynamic procedure (NDP) for determining the imposed stresses. The adoption of static and dynamic procedures, depends on the importance of higher mode effects. Dynamic procedures are required for tall buildings and for buildings with torsional irregularities or non-orthogonal systems. It should be noted that inclusion of both primary and secondary components provides a more accurate assessment in nonlinear analyses. For linear procedures, the code limits the amount of lateral resistance that can be provided by secondary components. The main reason for this limitation is to minimize the potential for sudden loss of seismic-force-resisting components to produce irregular structural response that is difficult to evaluate reliably.

According to ASCE/SEI 41-13 [162], the veneer walls classified as unreinforced walls should be evaluated for in-plane and out-of-plane actions. The in-plane resisting mechanisms for URM walls include toe crushing and diagonal tension. The out-of-plane stability of URM walls shall be evaluated through flexural strength for out-of-plane forces by considering components to span vertically between diaphragm levels.

Under in-plane loading, the brick veneer walls shall be evaluated to different resisting mechanism that can develop, namely toe-crushing or diagonal tension. The strength values associated to each resisting mechanism can be calculated according to ASCE/SEI 41-13

[162] through suggested expressions. Therefore, flexure predominates, the resistance is given by:

$$Q_{CL}{}^{IP} = \left((\alpha P_D + 0.5 P_W) \left(\frac{L}{h_{eff}} \right) \left(1 - \frac{f_a}{0.7 f'_m} \right) \right) \tag{7.8}$$

Where,

$Q_{CL}{}^{IP}$ is the shear strength based on toe crushing or diagonal tension;

h_{eff} is the height of the wall;

L is the length of wall or wall pier;

P_D is the superimposed dead load at the top of the wall under consideration;

P_W is the self-weight of the wall;

α is the factor equal to 0.5 for fixed-free cantilever wall, or equal to 1.0 for fixed-fixed wall;

f_a is the axial compression stress caused by gravity loads;

f'_m is the masonry compressive strength.

When shear predominates in the in-plane response of the walls, the resistance is given by:

$$Q_{CL}{}^{IP} = f'_{dt} A_n \beta \sqrt{1 + \frac{f_a}{f'_{dt}}} \tag{7.9}$$

Where:

A_n is the area of net mortared f a wall;

β is 0.67 for L/h_{eff} < 0.67, L/h_{eff} when 0.67 ≥ L/h_{eff} ≤ 1.0, and 1.0 when L/h_{eff} > 1.0;

f'_{dt} is the masonry diagonal tension strength.

According to ASCE/SEI 41-13 [162] flexural cracking in URM walls caused by out-of-plane inertial loading shall not be permitted for the Immediate Occupancy. The flexural cracking occurs when flexural strength of masonry is achieved. According to MSJC [160], the flexural strength, $Q_{CL}{}^{OOP}$ for clay masonry (hollow clay units and general purpose mortar) is 0.33MPa.

For Collapse Prevention Performance Level, stability need to be checked for walls spanning vertically with a height-to-thickness ratio (h_{eff}/t_{eff}) higher than that given in Table 11-5 of ASCE/SEI 41-13 [162]. The ratios depend on the type of wall and building (one-story buildings or multistory building: walls in upper of top story) and seismic hazard.

MSJC [160] also proposes that under earthquakes, the masonry veneer shall be designed so that story drift does not exceed the allowable values provided in building codes. For this

verification, the lateral drift (D_r) can be calculated based on expression 7.6. The allowable story drift can be obtained from SEI/ASCE 7-02 [158] given by expression 7.10, where h_{eff} is the height of the wall. The deflection amplification factor (C_d) is provided by SEI/ASCE 7-02 [158] according type of structure. Some other examples for allowable relative displacements and drifts are provided in Table 7.2, including the values presented in EC8 [78] and FEMA 273 [158]. The latter standard presents different limits for lateral drifts associated to different performance levels.

Table 7.2 – Examples of alowable drifts

Source code	Design performance objectives	
SEI/ASCE 7-02/ MSJC [158, 160]	$D_r = 0.025 h_{eff} \times C_d$	(7.10)
EC8 [78]	$D_r = 0.010 h_{eff}/v$	(7.11)
FEMA 273 [165]	IO: $D_r = 0.3\%$	(7.12)
	LS: $D_r = 0.6\%$	(7.13)
	CP: $D_r = 1\%$	(7.14)

7.2.4. Connections

As concluded in Chapter 6, the efficiency of veneer walls depends greatly of its connections to the masonry infill walls. Therefore, the adequate design and detailing play the major role in the performance of the brick veneer walls.

EC6 [30] refers that the imposed loads on the brick veneer walls should be divided by number of ties to obtain the force to be considered per each tie. Then, the required capacity should be compared with strength capacity of connection in order to ensure the stability of the system.

Regarding MSJC [160] recommendations, the connections of veneer walls are considered masonry anchors in terms of design. The design of masonry anchors is not so developed in comparison with other materials such as concrete. Nevertheless, there are guidelines in this code in order to compute the design strength corresponding to brick masonry breakout of wall ties (headed anchors in code) under tensile loads. As far as compression loading of connections is concerned, the codes do not present any recommendation.

The tensile strength of the tie-masonry connections under tension can be governed by two failure modes, namely sliding of the tie from the masonry or tensile fracture of the tie. If the

strength of the connection is governed by the tensile bond adherence of the wall ties to the masonry, the resistance of the connection can be calculated based on Expression 7.15:

$$N_c{}^{pull} = 0.33 A_{pt} \sqrt{f'_m} \quad (7.15)$$

where,

$N_c{}^{pull}$ is the strength capacity of the connection governed by tie-masonry connection breakout;

A_{pt} is the projected area of masonry for wall ties;

f'_m is the masonry compressive strength;

l_b is the effective embedment length of wall tie.

The projected area of the wall ties in the masonry is given by:

$$A_{pt} = \pi {l_b}^2 \quad (7.16)$$

If the strength of the connection is governed by the tensile resistance of the wall ties, the resistance of the connection can be calculated based on Expression 7.17:

$$N_c{}^{tie} = \sigma_d A_t \quad (7.17)$$

Being,

$N_c{}^{tie}$ is the strength capacity governed by steel tensile failure;

σ_d is the strength design of steel material obtained dividing the strength capacity of material by a suitable partial factor (in steel it is considered equal to 1.15);

A_t is the cross section area of wall tie.

These expressions were applied to the connections with tie T2 and tie T4 wall used in the brick veneer wall studied in Chapter 6, considering the air cavity widths of 75 and 100mm. The value of compressive strength of masonry considered for calculation of the strength capacity of connection governed by masonry breakout should be the lowest value between masonry veneer and masonry infill wall. For the masonry infill, a compressive strength equal to 0.9 MPa was considered following the recommendations Pereira et. al (2010) [65]. For the masonry veneer, a compressive strength of about 3.95 MPa was adopted, following the results obtained in the characterization of materials in Chapter 3. The lowest embedment length is 60mm. Thus, taking into account that the failure mode that governed the tensile behavior of the majority of connections was breakout of the tie from the masonry, the pull-out strength capacity of connection is about 3.54 kN. If this value is compared with pull-out strength of connections obtained in chapter 4 and 5 ($F^{\exp\_con}$), as shown in Table 7.3, it is

observed that the in most of cases, the calculated strength is higher than the value obtained in the experimental tests. Based on these results, it appears that the expression 7.15 predicts values in the unsafety side.

Table 7.3 – Relation between theoretical value and obtained values

	T2 in width cavity of 100mm	T2 in width cavity of 75mm	T4 in width cavity of 100mm	T4 in width cavity of 75mm
N_c/F^{exp_con}	118%	66%	164%	120%

The values of the strength connection calculated through expression 7.17, considering that it is governed by tension fracture of the ties, were obtained by adopting the capacity of steel is equal to 400MPa. The tensile strength obtained for wall tie T2 is about 8kN and for tie T4 is about 2.5KN. This means that the failure of the connection in case of tie T4 can occur through rupture of the tie, which was effectively observed in some experimental tests.

7.3. Safety assessment of connections based on experimental static cyclic response

According to ASCE/SEI 41-13 [162] and EC8 [78], the safety evaluation of connections can be also performed based on its nonlinear static behaviour when it is known from an experimental campaign. From the backbone curves that can be derived from the cyclic tests of assemblies under tensile-compression loading, it is possible to define key groups of values (force, displacement and behaviour factor) that can be associated to different performance levels. In the present work, this procedure was applied to the results obtained in the experimental campaign on cyclic tensile-compression tests on tie-masonry assemblages (Chapter 4 and Chapter 5).

The initial step of the procedure is the definition of the backbones curves, being built by multilinear envelopes based on the experimental curves. There are different methodologies proposed by codes for obtaining this curve. The methodology suggested by ASCE/SEI 41-06 [164] or the one proposed by Frumento et al. (2009) [170] incorporate strength degradation due to cyclic loading. According to ASCE/SEI/SEI 41-06 [164], the backbone curve shall be defined by connecting, with linear segments, the intersections between the first cycle curve for the *i*-th deformation level with the second cycle curve of the (*i–1*)th deformation level, for all *i* levels. Following Frumento et. al (2009) guidelines, the

backbones curves result from connecting, with linear segments, the points of maximum force per cycle, meaning that there will be a backbone curve per cycle. If the test procedure is composed by two or three cycles per displacement level, two or three backbone curves are drawn per specimen, respectively. ASCE/SEI 41-13 [162] proposes that the backbone curve shall be drawn by connecting the points corresponding to the maximum displacement for first cycle corresponding to a certain increment of deformation.

Based on backbone curves, it is necessary the define the idealized curves that replace the backbone curves. The idealized curves can have several linear branches, namely two linear branches (bilinear curves) and three linear branches (trilinear curves), which are recommended when the post-peak behaviour is necessary to be described.

The bilinear curves approximate the experimental behaviour as an elastic-perfectly plastic behaviour, which is expressed by two linear branches, connecting the origin (zero displacement and zero force) to an idealized elastic limit, and the latter to an idealized ultimate limit, as shown in Figure 7.2 (a).

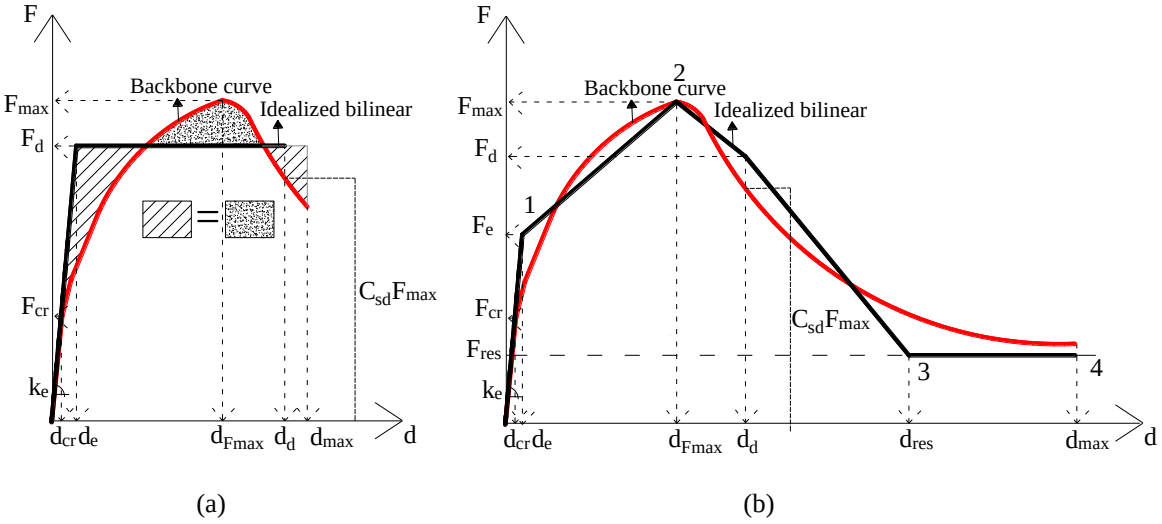

Figure 7.2 – Definition of points: (a) Bilinear and backbone curves' areas and (b) trilinear idealization

These two force-displacement limits are determined by equalizing the total energy under the experimental envelope curve, A_{env}, and under the bilinear diagram, A_{bil}, and by defining three deformation limit states on the experimental force-displacement backbone, namely: (1) deformation corresponding to the crack initiation, (2) deformation corresponding to maximum force, (3) maximum displacement. The definition of the crack limit should be based on physical evidence of cracking, and it should reflect stiffness changes beyond the initial stiffness, k_0. EC8 [78] recommends that the first branch of bilinear idealizations should reflect cracked stiffness, taking the denomination of effective stiffness, $k_e = \frac{F_{cr}}{d_{cr}}$,

where F_{cr} and d_{cr} are the force and displacement corresponding to the onset of cracking. The yielding force, F_d, is obtained by a simplified expression 7.18, from equalization of areas presented in Figure 7.2:

$$F_d = k_e \left(d_{max} - \sqrt{{d_{max}}^2 - \frac{2\,A_{env}}{k_e}} \right) \tag{7.18}$$

where,

d_{max} is the maximum displacement;

k_e is the effective stiffness;

A_{env} is the total energy under the envelope curve;

Then, the idealized bilinear curve can be expressed by Expression 7.19:

$$F(d) = \begin{cases} k_e\, d & for \quad 0 \le d \le d_e \\ F_d & for \quad d_e \le d \le d_d \end{cases} \tag{7.19}$$

where,

F_d is the yielding force calculated based on expression 7.18;

d_d is the displacement corresponding to a certain loss of resistance ($C_{sd}F_{max}$) in the post-peak regime. In general, the coefficient C_{sd} is taken as the displacement corresponding to a force degradation of 20%. Therefore the parameter takes usually the values equal to 0.8 [170, 171].

d_e is the intersection of $F = F_d$ with $F = k_e d$;

d is the general displacement.

The three linear curves are commonly applied when there is the need to describe the pre- and post-peak behaviour. The procedure used herein to define the three linear curves is suggested by Moreira (2015) [172], which combines criteria established for the bilinear curve like the elastic limit and the energy balance. The backbone curve is divided in two parts, before and after the maximum load, originating two areas under the diagrams ($A_{env}^{pre-peak}$ and $A_{env}^{post-peak}$), as shown in Figure 7.3 (a). In the same way, the trilinear curves are also divided in two areas ($A_{tri}^{pre-peak}$ and $A_{tri}^{post-peak}$), as shown in Figure 7.3 (b). For trilinear curves, there are two values of stiffness to consider in the pre-peak regime, one defining the elastic behaviour (pre-cracking) and the other describes the post-cracking regime until the achievement of the peak force. This results in a better approximation between experimental and idealized curves in case on clear nonlinear regime before peak. It was applied once gain a reduction factor C_{sd} to obtain the point of stiffness change in the

post-peak branch (d_d, F_d), based on energy balance. The force corresponding to the maximum displacement is calculated by considering that the area defined in the pre-peak branch, $A_{env}^{post-peak}$, is equal the area under the post-peak branch, $A_{tri}^{post-peak}$.

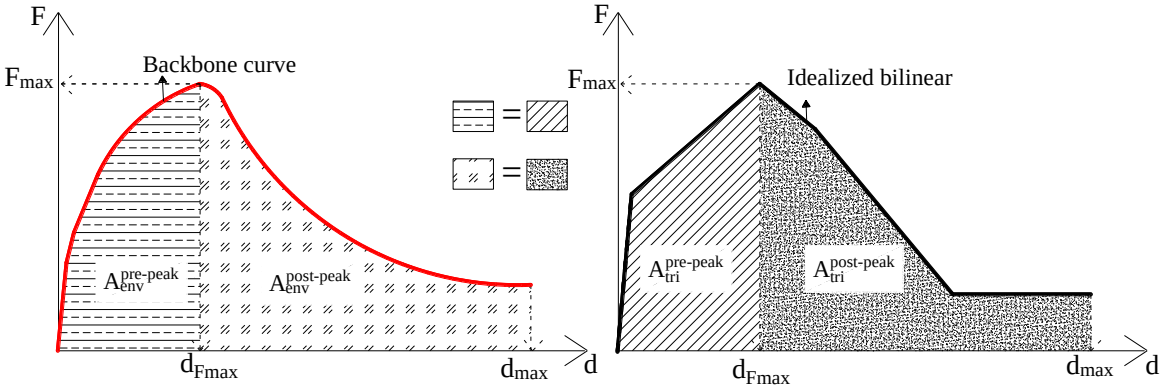

(a) (b)

Figure 7.3 – Areas of (a) backbone curve and (b) trilinear diagram

The general procedure do define the key points defining the idealized trilinear curve can be summarized as follows [172]:

1. Definition of the maximum force and the corresponding displacement (d_{Fmax}, F_{max}) from the experimental envelope;
2. Definition of the cracking force F_{cr} and the corresponding displacement d_{cr} on the experimental envelope;
3. Calculation of the elastic stiffness, k_e:

$$k_e = \frac{F_{cr}}{d_{cr}} \tag{7.20}$$

4. Calculation of the areas below the experimental envelope, before and after the peak force, $A_{env}^{pre-peak}$ and $A_{env}^{post-peak}$ (Figure 7.3);
5. Definition of the elastic displacement by considering equal areas of envelop and trilinear curve before peak load, $A_{env}^{pre-peak} = A_{tri}^{pre-peak}$:

$$d_e = \frac{2\,A_{env}^{pre-peak} - F_{max} \times d_{Fmax}}{d_{Fmax} \times k_e - F_{max}} \tag{7.21}$$

6. Calculation of the elastic force F_e:

$$F_e = k_e \times d_e \tag{7.22}$$

7. Determination of d_{max} from the backbone curve;
8. Obtainment of F_{dmax} by considering $A_{env}^{post-peak} = A_{tri}^{post-peak}$ $A_{env}^{post-peak} = A_{tri}^{post-peak}$:

$$F_{dmax} = \frac{2A_{env}^{post-peak}}{(d_{max} - d_{Fmax})} - F_{max} \tag{7.23}$$

9. Estimation the displacement d_d from the experimental envelope, corresponding to a force degradation of 20% (0.8 F_{max});
10. Calculation the ultimate force, F_d, corresponding to d_d:

$$F_d = F_{max} + \frac{(F_{max} - F_{dmax}) \times (d_{Fmax} - d_d)}{(d_{max} - d_{Fmax})} \quad (7.24)$$

If the post-peak presents a considerable residual strength, this should be considered in the trilinear idealization. In that cases the post-peak branch is divided in two segments: one for softening and another one to represent the residual capacity, as shown in Figure 7.2 (b). It is necessary to define the residual force, F_{res}, according to the force corresponding to the plateau of residual branch of backbone curve. Then, it is necessary to calculate an idealized residual displacement limit, d_{res}, which would correspond to the beginning of the residual linear segment (see Figure 7.2 (b)), by balancing $A_{env}^{post-peak}$ with the area below the two post-peak linear branches.

The last step consists in the classification of connections in terms of importance class (primary or secondary components) and type of behaviour (brittle or ductile) according to ASCE/SEI 41-13 [162]. The importance class is defined according through a analysis on the stiffness of the elements regarding the global building stiffness, as mentioned before. The type of behaviour can be obtained by approximation of obtained idealized curves to the types of curves presented in Figure 7.4 adapted from ASCE/SEI 41-13 [162]. Points 1, 2 and 3 of curves are limits of distinct phases of the behaviour of the connection. The elastic phase goes from 0 to 1, the strain hardening is comprehended between 1 and 2, and the strength degradation phase develops between 2 and 3. The Type 1 and Type 2 curves is representative of ductile behaviour. The primary component that present this ductile behaviour should be designed based on deformation criteria if the plastic range is such that $d \geq 2g$ for type 1 curve and $e \geq 2g$ for type 2 curve; otherwise, they shall be designed according force criteria. Secondary component actions exhibiting the ductile behaviour should be designed based on deformation criteria for any d/g ratio in type 1 curve and for condition $f \geq 2g$ in type 2 curve; otherwise, they shall be designed based on force criteria. Curves matching type 3 represent brittle or non-ductile behaviour, therefore the elements (primary and secondary) with this behaviour should be designed according force criteria.

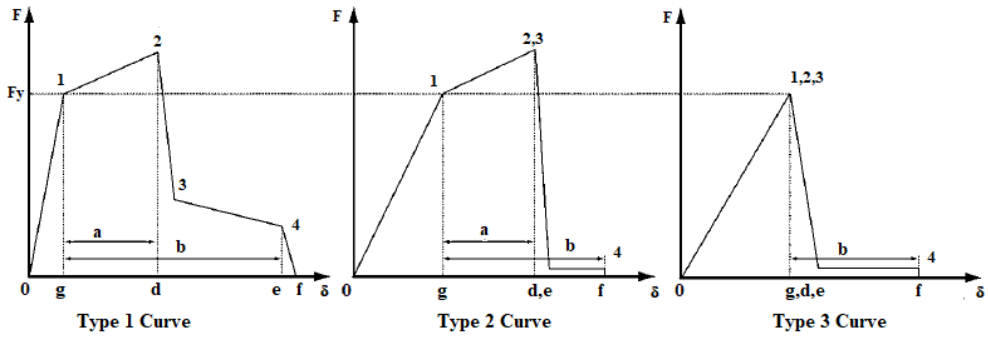

Figure 7.4 – Component force versus deformation curves [adapted from ASCE/SEI 41-13 [162]]

7.3.1. Application to connections with ties T2 and T4

The application of the design guidelines of connections was carried out to connections with ties T2 and T4, regarding to which experimental cyclic response are available. The experimental results regard the connections with ties T2 and T4 and with air cavity width of 100mm and 75mm. To obtain the backbones curves, it was decided to follow the methodology proposed by ASCE/SEI 41-13 [162]. The obtained curves are presented in Figure 7.5.

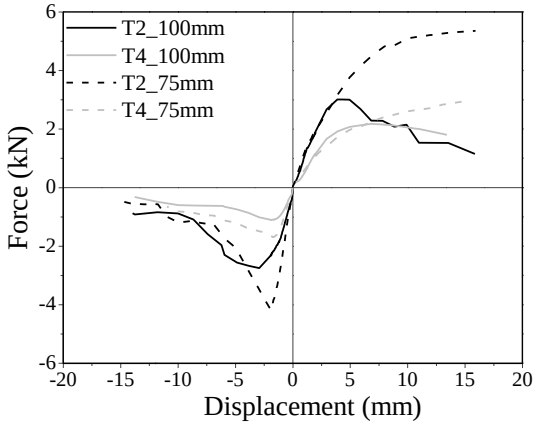

Figure 7.5 – Backbones of connections with T2 and T4 wall ties in air cavity width of 75 and 100mm

Taking into account the shape of the experimental envelopes (Figure 7.5), it was decided to consider the bilinear curve as good approximation for cyclic tension-compression behaviour of connections with air cavity width with 75mm because the post-peak behaviour can be considered as a plateau. For the remaining cases the trilinear curves were adopted. The experimental envelops and the idealized bilinear and trilinear curves are shown in Figure 7.6 for the connections with tie T2 and tie T4 and for air cavity width of 100mm and 75mm. It is stressed that given the different behavior, bilinear or trilinear curves can be adopted for tension and compression regimes.

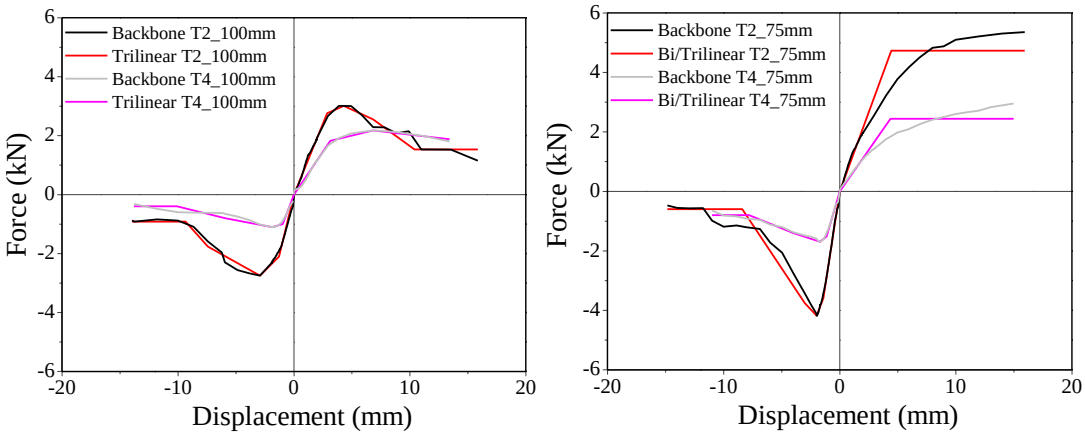

Figure 7.6 – Backbones and equivalent bilinear and trilinear idealizations of connections is study

Regarding to the classification of connection in terms of importance class, these elements can be considered as primary or secondary components in function of structural importance defined by designer, as discussed before. Thus, the procedure will be presented for two types.

In terms of behaviour models, it was possible to classify them as ductile behaviours according to the classification of ASCE/SEI 41-13 [162] (Figure 7.4). The design can be developed based on deformation criteria since the required conditions presented were verified in obtained idealized curves.

Three performance objectives levels proposed by ASCE/SEI 41-13 [162], namely Immediate Occupancy (IO), Life Safety (LS) and Collapse prevention (CP) are considered. According to ASCE/SEI 41-13 [162], IO performance level is defined by the deformation at which visible damage occurred but it cannot be greater than 0.67 times the deformation corresponding to the LS performance level, considering the connections both as primary components or secondary components. The LS performance level for primary components is defined by 0.75 of the deformation at point corresponding to the maximum force (d_{Fmax}, F_{max}), and for secondary components is defined as 0.75 of the deformation at point corresponding to the maximum displacement (d_{max}, F_{res}). The CP performance level is defined by the displacement corresponding to maximum force (d_{Fmax}, F_{max}), but not greater than 0.75 displacement corresponding to residual force (d_{res}, F_{res}) for primary components. This takes advantage of the capacity of the component to still carry seismic loads after the peak load but before complete failure. For secondary components, this last limit is defined by deformation corresponding to residual force (d_{max}, F_{res}).

Following the recommendations of ASCE/SEI 41-13 [162], the deformations for each performance level were then calculated considering the connections as a primary or secondary element. For each deformation state, a correspondent design strength (Q_{CE}) is

defined based on the idealized curves, see Table 7.4. Another seismic parameter that can be calculated following the procedure of the code is the modification factor (*m*-factor) and it can be used when the deformation criteria is not applied. Seismic codes consider this modification factor in designing the loads in order to consider the ability of an element to dissipate energy considering its nonlinear behaviour characteristics without collapse. Mean values of the mechanical properties can be reduced by the mentioned modification factor to obtain design forces. The factor is determined by the displacement at the performance level to the yield displacement (d_e, F_e) ratio and multiplied by 0.75. The obtained results are presented in Table 7.4. Taking into account that the post-peak behaviour of connections with 75mm of air cavity width is characterized by a plateau, the capacity limits were the same for primary and secondary components category.

Table 7.4 – Limit deformation values and behaviour factors for each performance level (based on ASCE/SEI 41-13 [162])

			Secondary component			**Primary component**		
			Deformation limit (mm)	Q_{CE} (kN)	*m*-factor	Deformation limit (mm)	Q_{CE} (kN)	*m*-factor
T2_100mm	Tensile Behaviour	IO	7.97	2.29	2.08	2.16	1.90	0.56
		LS	11.90	1.53	3.10	3.23	2.67	0.84
		CP	15.87	1.15	4.13	4.30	3.01	1.12
	Compression Behaviour	IO	7.01	1.59	4.10	1.47	2.04	0.86
		LS	10.47	0.88	6.12	2.19	2.33	1.28
		CP	13.96	0.88	8.16	2.92	2.75	1.71
T4_100mm	Tensile Behaviour	IO	6.74	2.18	1.61	3.43	1.92	0.82
		LS	10.07	2.06	2.40	5.12	2.07	1.22
		CP	13.42	1.80	3.21	6.83	2.18	1.63
	Compression Behaviour	IO	6.93	0.62	5.36	0.93	0.87	0.72
		LS	10.34	0.60	8.01	1.39	1.06	1.08
		CP	13.79	0.32	10.67	1.86	1.11	1.44
T2_75mm	Tensile Behaviour	IO	8.00	4.83	1.56	8.00	4.83	1.56
		LS	11.95	5.21	2.33	11.95	5.21	2.33
		CP	15.93	5.35	3.11	15.93	5.35	3.11
	Compression Behaviour	IO	7.45	1.21	3.96	0.99	1.72	0.53
		LS	11.12	0.56	5.91	1.49	3.61	0.79
		CP	14.83	0.47	7.88	1.98	4.19	1.05
T4_75mm	Tensile Behaviour	IO	7.53	2.27	1.67	7.53	2.27	1.67
		LS	11.24	2.66	2.49	11.24	2.66	2.49
		CP	14.99	2.95	3.32	14.99	2.96	3.32
	Compression Behaviour	IO	5.52	1.20	3.69	0.85	1.14	0.57
		LS	8.24	0.92	5.50	1.27	1.53	0.85
		CP	10.99	0.65	7.34	1.69	1.69	1.13

The m-factors for the IO limit are very conservative, because of the difference in displacements between the cracking limit and the idealized elastic limit. The higher values obtained for m-factors for LS and CP performance levels for connections T2_75mm and T4_75mm under tension loading reflect the ductility observed experimentally.

An alternative design procedure for analyzing ductile components is proposed in EC8-Part 3 [173]. It recommends that for ductile elements, compliance with the requirements of each performance level should be made through verification of deformations.

In order to determine the deformation limit values, three performance levels are also considered as described before, DL (Damage Limitation), SD (Significant Damage) and NC (Near Collapse). For each limit state, EC8-Part 3 [173] suggests DL, SD, and NC deformation limits should be taken as d_e, $0.75 \times d_d$, and d_d, respectively. The obtained results based on idealized curves are presented in Table 7.5. For each obtained deformation, a correspondent force was determined based on curves and it is referred as F_{lim} in Table 7.5, being equivalent to Q_{CE} in ASCE/SEI 41-13 [162]. For determination of limit stats in connections characterized by a plateau and replaces by bilinear curves (T2/T4_75mm), it was considered the displacement d_d the last displacement of curve d_{max} because there is no strength loss in post-peak behaviour.

On the other hand, EC 8 [78] also presents an alternative design method using a behaviour factor (q-factor) in alternative/complement of using the deformation approach. Similarly, to the m-factor introduced in ASCE/SEI 41-13 [162], this is an elastic procedure that uses a design response spectrum reduced by factor q, which intends to account for the cyclic deformation and energy dissipation effects. q-factor defines a relation between an elastic force and design force taking into account the nonlinear behaviour of element. Mean values of the mechanical properties, divided by the appropriate confidence factor should be taken for ductile elements. For NC and SD limit states, the capacity of the ductile component should be determined from the deformations, instead of strength. On the other hand, capacity relative to the DL limit state should be based on strength for both ductile and brittle components. Structural behaviour factor, q, (Expression 7.25) can be also expressed in terms of the global ductility factor, μ, (Expression 7.26) as follows:

$$q = (2\mu - 1)^{1/2} \tag{7.25}$$

$$\mu = d_d/d_y \tag{7.26}$$

The obtained values of ductility and q-factor are also presented in Table 7.5.

Table 7.5 – Limit deformation values and behaviour factors for each performance level (based on EC8 [78, 173])

			Deformation limit (mm)	F_{lim} (kN)	q factor	μ factor
T2_100mm	Tensile Behaviour	NC	6.84	1.41	1.93	2.36
		SD	5.13	1.38		
		DL	2.90	0.48		
	Compression Behaviour	NC	7.41	1.99	2.94	4.81
		SD	5.56	1.97		
		DL	1.54	1.06		
T4_100mm	Tensile Behaviour	NC	13.42	0.77	2.59	3.86
		SD	10.07	0.76		
		DL	3.48	0.25		
	Compression Behaviour	NC	5.95	1.07	3.34	6.07
		SD	4.46	1.06		
		DL	0.98	0.64		
T2_75mm	Tensile Behaviour	NC	15.93	3.22	2.48	3.6
		SD	11.95	2.53		
		DL	4.45	1.26		
	Compression Behaviour	NC	2.99	3.44	1.73	4.81
		SD	2.24	3.83		
		DL	1.50	2.82		
T4_75mm	Tensile Behaviour	NC	14.99	1.98	2.42	3.43
		SD	11.24	1.74		
		DL	4.37	0.90		
	Compression Behaviour	NC	3.99	1.38	2.46	6.07
		SD	2.99	1.49		
		DL	1.13	1.41		

The representation of deformation values for each performance level are plotted in Figure 7.7 for each connection typology considering the two possibility of importance class (primary and secondary elements) and both analyzed codes. The marked points correspond only to the displacement limit of each connection in each performance level. The nomenclature used in subtitle is constituted by “tie typology_ air cavity width_ type of importance_ Code name”. The tie typology can be T2 or T4 and the air cavity width can be 100 or 75mm. The type of importance is divided in “P” for connections considered as primary components or “S” for connections considered as secondary components. The codes is defined by ASCE for ASCE/SEI 41-13 [162] and EC8 [78]. Comparing the deformations limits, two different methodologies it is possible to conclude that the results from EC8 [78] is less conservative than the limits established in ASCE/SEI 41-13 [162] for primary components category, and more conservation regarding to limits for secondary components category, as shown in Figure 7.7.

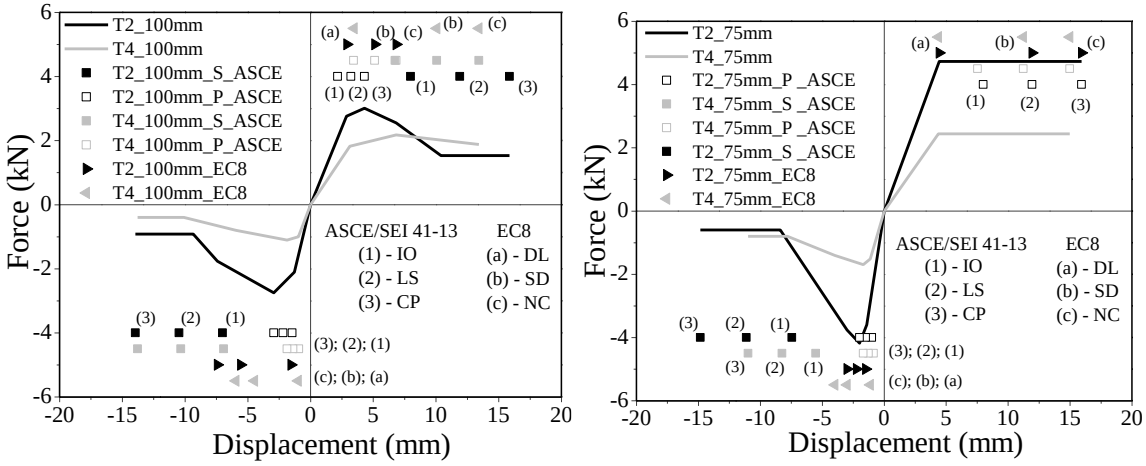

Figure 7.7 – Equivalent bi/trilinear idealized curves and deformations limits for connections in study

7.4. Conclusions

A seismic design methodology should be always composed by analysis and verifications, according to the guidelines and procedures of codes. Basically, a comparison between imposed actions and limit capacity values corresponding to each performance levels should be performed in order to assure that the minimum of the capacities is higher than the seismic demand and the performance objectives are achieved.

The main goal of this chapter was to carry out an overview of different design approaches that be applied to veneer walls mentioned in different codes, namely FEMA 273 [165], ASCE/SEI 41-13 [162], ASCE/SEI 7-10 [159], EC8 [78] and MSJC codes [160]. The focus was to provide the limit capacity values (forces, displacements and behaviour factors) based on codes, that can be used in seismic verifications of masonry veneer walls.

Besides the brick masonry veneer walls, connection takes a major role in its the out-of-plane behaviour. Therefore, when design of masonry veneers is required, major attention should be taken to the connections. The experimental monotonic envelops of different types of connections allowed the development of analytical idealized curves that can be used in the design of connections. The displacement and strength limit values and behaviour factor were calculated for each performance level based on codes rules and experimental data.

Chapter 8

Conclusions and Further Developments

8.1. Main conclusions

In general, the seismic response of masonry structures (structural or non-structural) is complex and need to be very well understood for a safe and economical design in order to contribute for earthquake-resistant construction to protect people and buildings. In this scope, brick veneer walls have been roughly studied and a better insight on the seismic behaviour is needed. This constructive typology has been used in recent decades in different places of the world, United States, Europe and Australia and some of these zones present moderate to high seismic activity, such as south of Europe. Nonetheless, seismic vulnerability has been verified in this constructive solution and inappropriate failure damages during seismic activity has been frequently recorded. This opens multiple research topics in the context of improvement of seismic performance to community research and motivated the work carried out in this thesis.

The masonry veneer walls prototypes considered in this study was composed by brick veneer leaf connected through wall ties to brick infill walls enclosed in reinforced concrete frames. To accomplish the challenge of achieving a better insight on the seismic behaviour of brick veneer walls attached to brick masonry infills, seismic behaviour of the system, the work carried out focused mainly on experimental characterization of components of the brick veneer walls, namely connections under different loading configurations and masonry veneer walls attached to brick infill walls under out-of-plane loadings. The experimental work in complemented with a review on the design procedures existing in codes intend to assure the seismic safety of brick veneer walls.

From the work carried out and discussed in the previous chapters dealing with the connections submitted to cyclic tension-compression and shear loads, the main conclusion can be pointed out:

1. Cyclic tension-compression and shear behaviour of connections depend mostly on the type of tie. Shape and geometry of ties revealed to be the most important factors influencing strength of the connections. Tie surface roughness and geometry at the ends influence the bond strength between the tie and mortar at bed joints and, thus, the tensile strength of the connection. Tie thickness influences in a great extent the compression and shear strength, stiffness and dissipative energy capacity as it controls the strength and the trend for second order effects develop such as buckling. Robust ties lead to connections with higher initial

stiffness, higher dissipation of energy, and had higher load envelopes than the ones constructed with thin ties;

2. The compressive behaviour is also influenced mainly by air cavity width. The influence of embedment length of ties and mortar strength effect could be also observed. The tensile behaviour is influenced mainly by embedment length. The air cavity width has a neglected effect on the connection under tension. The effect of all variables together, namely more resistant mortar, higher embedment length and lesser air cavity width caused an improvement of almost the double of resistance in almost all connections in tension behaviour. The same does not happen in compression behaviour that presented a great difference in rigid wall ties, but in flexible ties the difference is not so evident. Only the air cavity width can provide more effect on compression behaviour because change the buckling free length. Under compression loading, the connection behaviour is more dependent on the tie buckling capacity than on the tie-mortar bond adherence.

3. The strength of connections where the tie is connected to bricks with horizontal perforations through chemical anchorages is influenced by the mechanical properties of the bricks mainly in the direction perpendicular to the horizontal perforations. This solution is very attractive and suitable to façade rehabilitation, but attention should be taken to the resistance of brick units in the perpendicular direction to perforations;

4. The prior shear damage reduced substantially (until 80%) the maximum strength and initial stiffness on tension-compression behaviour of connections.

5. Tie pull-out, tie buckling or tie fracture were the predominant failure modes in cyclic tension-compression and shear loading. The interaction between cyclic tension and compression loading results in the combination of different failure modes. The connection failure mode is mostly characterized by pull-out of the ties from the bed joint mortar of brick veneer leaf. This failure mode is attributed to lower compressive strength of mortar of the brick never prims, resulting in low bond strength between tie and mortar. Regarding to compression behaviour, the cross section of ties determines if plastic deformation of the ties due to buckling develops (T2, T3, T4 and T5) or, instead, if penetration of wall tie on mortar bed joint occurs (T1 and T6). As concerns the shear behaviour, the behaviour is governed by tie bending deformation, and the interaction between tie and mortar is less determinant;

From the work carried out and discussed in Chapter 6 dealing with the behaviour of brick veneer walls under out-of-plane loads, it is possible to conclude that:

1. The maximum out-of-plane resistance was recorded in walls with lower spacing of ties either constructed with T2 or T4 wall ties, which were the ties selected to build the veneer

walls given its better performance under tension-compression loads. The out-of-plane resistance in tension of the brick veneer walls built with T2 is similar to the walls built with ties T4. In compression behaviour, the highest strength was achieved in walls constructed with ties T2 and it is very similar to tension resistance. This is attributed to the symmetric response of this type of tie under cyclic tension-compression;

2. The combined effect of in-plane and out-of-plane influenced greatly the system performance, as far as strength and stiffness are concerned due to cracks localized mainly at the unit-mortar and interfaces;

3. The wall with flashing at veneer base deformed very little under out-of-plane tension due to additional friction caused at veneer base, and consequently the plastic deformations were also low;

4. The pinching effect was more visible in lower resistant walls and in walls with prior in-plane damage. Equivalent viscous damping values of walls were influenced by pinching effect. Thus, the walls with lower values of damping showed more severe pinching. This can be related with the energy of dissipation because this was reduced due to pinching, decreasing its ratio with input energy;

5. The walls with wall tie T2 were considered more dissipative solutions because mostly of these solutions have higher out-of-plane capacity under compression direction. Nevertheless, both of wall ties seems showing a good dissipative and avoiding brittle and dangerous ruptures. It is evident that brittle failures should be avoided since the connections become inefficient and can occur the failure of veneer wall;

6. The deformation of infill wall is dependent on the capacity that wall ties have to transfer loading to the backing system. More deformation of infill wall is associated to the higher load transfer from the brick veneer though the ties. Walls with T4 wall tie did not exhibit great transference capacity, as happen with wall tie T2. Walls constructed with lesser air cavity width and with lesser spacing showed a better transference capacity than walls constructed with higher air cavity width and lesser number of connections. It means that in case of seismic events, the most resistant configurations work better than other layouts taking into account that they result in higher stress redistribution capacity;

7. The wall ties experienced severe damages after failure, nonetheless, in most cases, the wall ties were still able to work and guarantee an adequate resistance of the wall. Similarity to observed in connections locally, the failure damage patterns consisted in: (1) pull-out of wall tie from mortar bed joint; (2) wall tie rupture in more demanding cases when veneer

wall is subjected to out-of-plane loading under tension direction and (3) buckling of wall tie when the veneer wall is subjected to out-of-plane under compression direction;

Briefly, the tests performed on masonry veneer system pointed out the dominant influence of the connections on the global behaviour of the wall as well as its influence on the backing system. Connections represent the dissipative mechanism of the veneer walls as well as their weakest point. The adherence of wall tie on mortar bed joint should be adequate because the wall ties can show poor performance in case of improper installation. The quality of material is also important, the loss of strength should be avoided due to corrosion. Failure can occur at the connections, but, thanks to the configuration and layout of system, once a connection fails a stress redistribution occurs and the wall still has a remaining bearing capacity. Certainly, if the veneer walls are properly installed in a building, the seismic resistance of global structure will increase because all elements work and resist together and dissipate more energy without having dangerous and hazardous ruptures. To take into account veneer walls in seismic design, state limits and standard procedures should be incorporated on the building design in order to address more control and knowledge about its structural performance.

8.2. Limitations of study and further developments

Taking into account that the masonry veneer walls system has many details in its construction that really can influence its performance, it was needed to select some important aspects to be used in construction of prototypes. The main issues concerned to wall ties typologies (6 types), tie spacing (3 layouts), air cavity width (2 configurations), embedment length of wall ties on mortar bed joint (2 lengths) and presence of flashing on construction details. Indeed, the study is limited because other important aspects were not explored such as (1) the presence of openings, (2) different boundary conditions of veneer wall, (3) presence of connections to concrete frame and analysis on a (4) full-scale prototype building. The boundary conditions considered in the experimental work represent a solid panel of a veneer wall, without lateral and top fixed boundaries, which is can be seen as a limitation in the most of cases. This feature can underestimate the resistance of wall because it is known that the fixed boundaries on a veneer panel can slightly improve the lateral responses. Other aspect is related to the type of loading considered. In spite of the thesis workplan envisaged the study of brick veneer walls under dynamic loads, for time and technical constraints, it was not possible to carry out this work. In real seismic events, real inertia forces are imposed

to the brick veneer walls and it believed that the interaction between brick infill enclosed walls and brick veneer walls is much better represented and it would be an opportunity to assess in a more realistic ways the ability of the brick-ties to transfer this load to the infill wall.

Therefore, it is suggesting that the further developments can be planned in future research:

- Assessment of dynamic behaviour of masonry veneer walls based on shake table testing considering a building prototype. Also, varying parameters related to all the structural components that are part of the connection is essential, and it should be achieved by combining existing and further experimental data.

- Development of numerical analysis of masonry veneer walls to simulate the seismic behaviour of masonry veneer buildings using nonlinear static (pushover) and nonlinear dynamic analyses. Parametric and fragility analysis can be carried out in order to evaluate the influence of important parameters: wall ties characteristics (stiffness, embedment depth), layout of connections, air cavity width, masonry characteristics (mortar typology, reinforced masonry), stiffness of backing support, action type and actions combination, presence of opens and boundary conditions.

- Development and update design guidelines for brick veneer walls attached to RC frame with masonry infills based on the insight gathered in the numerical simulation.

REFERENCES

References

[1] Santos, S. P., *Enclosure Masonry Wall Systems Worldwide.*, 2007.

[2] Silva, J. M. d. *Alvenarias não estruturais Patologias e Estratégias de Reabilitação*. in *Seminário sobre Paredes de Alvenaria, P.B. Lourenço & H. Sousa (Eds.).*, 2002.

[3] Gouveia, J. P., F. d. M., Lourenço, P. B., *Alvenaria estrutural: Aplicação a um caso de estudo* in *4ª Jornadas Portuguesas de Engenharia de Estruturas*., 2006.

[4] Mesquita, D., *Viabilidade técnico-económica do tijolo face à vista em fachadas de edifícios em Portugal*., 2007, Instituto Superior Técnico.

[5] Ehlinger, L. P., *Brick Veneer.* Journal of performance of constructed facilities, 2011.

[6] Magenes, G., Bracchi, S., Graziotti, F., Mandirola, M., Manzini, C. F., Morandi, P., Palmieri, M., Penna, A., Rosti, A., Rota, M., and Tondelli, M., *Preliminary damage survey to masonry structures after the May 2012 Emilia earthquakes*.,Vol. 1., 2012.

[7] Ceci, A. M., Contento, A., Fanale, L., Galeota, D., Gattulli, V., Lepidi, M., and Potenza, F., *Structural performance of the historic and moderns buildings of the University of L´Aquila during the seismic events of April 2009.* Engineering Structures, 2010, 32: p. 1899-1924.

[8] Papanicolaou, C. G., Triantafillou, T. C., Papathanasiou, M., and Karlos, K., *Textile reinforced mortar (TRM) versus FRP as strengthening material of URM walls: out-ofplane cyclic loading.* Materials and Structures, 2007, 41 (1): p. 143-157.

[9] Bothara, J. and Brzev, S., *A Tutorial: Improving the Seismic Performance of Stone Masonry Buildings*., 2011, Oakland: EERI.

[10] Martins, A., Vasconcelos, G., and Costa, A. C., *Comportamento sísmico de paredes de alvenaria de fachada - uma breve revisão* in *JPEE- Jornadas Portuguesas de Engenharia de Estruturas*., 2014, Lisboa

[11] Memari, A. M., Burnett, E. F. P., and Kozy, B. M., *Seismic response of a new type of masonry tie used in brick veneer walls.* Construction and Building Materials, 2002, 16 (7): p. 397-407.

[12] Klingner, R. E., Shing, P. B., McGinley, W. M., McLean, D. I., Okail, H., and Jo, S., *Seismic performance tests of masonry and masonry veneer.* Journal of ASTM International, 2010, 7 (3).

[13] *Technical Notes on Brick Construction 44B, Wall Ties for Brick Masonry*., 2003, Brick Industry Association.

[14] Reneckis, D. and LaFave, J. M., *Seismic Performance of Anchored Brick Veneer*, in *Report Nº NSEL-016*, Newmark Structural Laboratory Report Series, 2009, p. 217.

[15] Zisi, N., *The Influence of Brick Veneer on Racking Behavior of Light Frame Wood Shear Walls*., PhD thesis, 2009, The University of Tennessee, Knoxville.

[16] Okail, H., *Experimental and analytical investigation of the seismic performance of low-rise masonry veneer buildings.*, PhD thesis, 2010, University of California, San Diego: Ann Arbor. p. 254.

[17] Jo, S., *Seismic Behavior and Design of Low-rise Reinforced Concrete Masonry with Clay Masonry Veneer*., PhD thesis, 2010, The University of Texas at Austin.

[18] Teguh, M., *Experimental Evaluation of Masonry Infill Walls of RC Frame Buildings Subjected to Cyclic Loads.* Procedia Engineering, 2017, 171: p. 191-200.

[19] Murty, C. V. R. and Jain, S. K., *Beneficial influence of masonry infill walls on seismic performance of RC frame buildings*, in *12WCEE 2000*, 2000., New Zealand.

[20] Akhoundi, F., *Strategies for Seismic Strengthening of Masonry Infilled Reinforced Concrete Frames*. PhD thesis, 2016, University of Minho

[21] Furtado, A., Arêde, A., Varum, H., and Rodrigues, H. *Experimental study of the out-of-plane behaviour of masonry infill walls with and without previous in-plane damage*. in *Brick and Block Masonry – Trends, Innovations and Challenges – Modena, da Porto & Valluzzi (Eds).*, 2016.

[22] Drysdale, R. G. and Hamid, A. A., *Masonry Structures Behavior and Design*., 2008.

[23] Mendes, F., *Durabilidade de fachadas*., Dissertação de mestrado, 2009, Universidade do Porto

[24] Mendonça, P., *Habitar sob uma segunda pele.*, Tese de doutoramento, 2005, Universidade do Minho

[25] *Masonry Design Manual* Fourth Edition ed., 2007.

[26] AFNOR, *NF DTU 20.1* in *P1-1. Ouvrages en maçonnerie de petits éléments — Parois et murs; Partie 1-1 : Cahier des clauses techniques types*. octobre 2008: France.

[27] *Technical Notes on Brick Construction, Anchored Brick Veneer, Wood Frame Constrution*., 2002, Brick Industry Association.

[28] Reneckis, D. and LaFave, J. M. *Seismic Design of Anchored Brick Veneer*. in *15 WCEE 2012, 2012, Lisboa*.

[29] Cerâmica Vale da Gândara, *Manual de Aplicação de tijolo face à vista e de pavers cerâmicos*. 2012.

[30] *EN 1996-1-1*, in *Eurocode 6 - Design of masonry structures - Part 1-1: General rules for reinforced and unreinforced masonry structures*., 1996, European Committee for Standardization (CEN)

[31] *Technical Notes on Brick Construction 18A, Accommodating Expansion of Brickwork*., 2006, Brick Industry Association.

[32] Lynch, G. C. J., *Brickwork: History, Technology and Practice*. Vol. 2., 2015.

[33] Products, A. B., *Wall Ties and Restraint Fixings for the Construction Industry*., 2012.

[34] *TMS 402-08/ACI 530-08/ASCE 5-08, in Building Code Requirements for Masonry Structures. The Masonry Society, Boulder, Colorado, the American Concrete Institute, Farmington Hills, Michigan, and the American Society of Civil*. 2008: Engineers, Reston, VA. Reported by the Masonry Standards Joint Committee (MSJC)

[35] *TMS 602-08/ACI 530.1-08/ASCE 6-08 in Specification for Masonry Structures, The Masonry Society, Boulder, Colorado, the American Concrete Institute, Farmington Hills, Michigan, and the American Society of Civil Engineers*. 2008: Reston, VA.

[36] BS, *BS 5628*, in *Code of practice for use of masonry*., 1992.

[37] Vicente, R. S., Rodrigues, H., Varum, H., Costa, A., and Silva, J. A. R. M. d. *Performance of masonry enclosure walls: lessons learned from recent earthquakes*. in *Earthquake engineering and engineering vibration*, 2011.

[38] Lourenço, P. B. and Medeiros, P., *Learning from Failure of a Long Curved Veneer Wall: Structural Analysis and Repair*. Journal of Performance of Constructed Facilities, 2013: p. 53-64.

[39] Borchelt, J. G. *Building code requirements for brick veneer in seismic areas*. in *Sísmica 2004 - 6º Congresso Nacional de Sismologia e Engenharia Sísmica*. 2004. Brick Industry Association.

[40] Morandi, P., Hak, S., and Magenes, G., *Simplified Out-of-plane Resistance Verification for Slender Clay Masonry Infills in RC Frames*. Dipartimento di Ingegneria Civile ed Architettura, Università degli Studi di Pavia ed EUCENTRE.

[41] Choi, Y.-H. and LaFave, J. M., *Performance of corrugated metal ties for brick veneer wall systems.* J. Mater. Civ. Eng., 2004, 16(3): p. 202-211.

[42] Zisi, N. V. and Bennett, R. M., *Shear Behavior of Corrugated Tie Connections in Anchored Brick Veneer–Wood Frame Wall Systems.* Journal of Materials in Civil Engineering., 2011: p. 121-130.

[43] Mertens, S., Smits, A., and Grégoire, Y. *Experimental parametric study on the performance of wall ties*. in *9th International Masonry Conference*. 2014, Guimarães.

[44] Ribeiro, S., Vicente, R., Varum, H., Graça, J., Lobo, B., and Ferreira, T. *Development of retrofitting solutions: remedial wall ties for masonry enclosure brick walls*. in *9th International Masonry Conference 2014 in Guimarães*., 2014.

[45] McGinley, W. and Hamoush, S., *Seismic Masonry Veneer: Quazi-Static Testing of Wood Stud Backed Clay Masonry Veneer Walls.* Structures Congress, 2008: p. 1-10.

[46] Reneckis, D., LaFave, J. M., and Clarke, W. M., *Out-of-plane performance of brick veneer walls on wood frame construction.* Engineering Structures, 2004, 26(8): p. 1027-1042.

[47] Okail, H. O., Shing, P. B., Klingner, R. E., and McGinley, W. M., *Performance of clay masonry veneer in wood-stud walls subjected to out-of-plane seismic loads.* Earthquake Engineering and Structural Dynamics, 2010, 39: p. 1585–1609.

[48] Liang, J., *Development of a multihazard resistant panelized brick veneer wall system*. 2006, Pennsylvania State University.

[49] Thurston, S. J. and Beattie, G. J., *Seismic performance of brick veneer houses Phase 1. Cyclic and elemental testing of clay brick veneer construction*., 2008.

[50] Reneckis, D. and LaFave, J. M., *Out-of-Plane Seismic Performance and Detailing of Brick Veneer Walls.* Journal of Strucutral Engineering, 2010: p. 781-793.

[51] Paton-Cole, V. P., Gad, E. F., Clifton, C., Lam, N. T. K., Davies, C., and Hicks, S., *Out-of-plane performance of a brick veneer steel-framed house subjected to seismic loads.* Construction and Building Materials, 2012, 28(1): p. 779-790.

[52] Okail, H. O., Shing, P. B., McGinley, W. M., Klingner, R. E., Jo, S., and McLean, D. I., *Shaking-table tests of a full-scale single-story masonry veneer wood-frame structure.* Earthquake Engineering and Structural Dynamics 2011, 40: p. 509–530.

[53] Beattie, G. and Thurston, S., *Twenty years of improvement in the seismic performance of masonry veneer construction.* Australian Journal of Structural Engineering, 2008, 11(3).

[54] Thurston, S. J. and Beattie, G. J., *Seismic performance of brick veneer houses: Shake table tests on a clay brick veneer specimen,* 2008.

[55] Thurston, S. J. and Beattie, G. J., *Seismic performance of brick veneer houses: Cyclic racking of a two-storey clay brick veneer building*, 2008.

[56] Liang, J. and Memari, A. M., *Performance of a Panelized Brick Veneer Wall System under Lateral Loads.* Open Journal of Civil Engineering, 2012, 2: p. 132-146.

[57] Desai, N. and McGinley, W. M., *A study of the out-of-plane performance of brick veneer wall systems in medium rise buildings under seismic loads.* Engineering Structures, 2013, 48(0): p. 683-694.

[58] Marziale, S. A. and Toubia, E. A., *Analysis of brick veneer on concrete masonry wall subjected to in-plane loads.* Structures 2015, 2: p. 1-7.

[59] Reneckis, D. and LaFave, J. M., *Out-of-plane seismic performance and fragility analysis of anchored brick veneer.* Structural Safety, 2012. 35(0): p. 1-17.

[60] *Abaqus, Inc. (2006). ABAQUS 6.6-2*. Providence, R.I.

[61] *OpenSees platform; PEER, Center at the University of California at Berkeley.*

[62] Desai, N., *A study of the behavior of veneer wall systems in medium rise buildings under seismic loads*, PhD thesis 2011, University of Louisville: Ann Arbor. p. 359.

[63] Lapish, E. B. and Allen, D. *Variability of Tie Loads in Brick Masonry Veneer Constructions.* in *Proceedings of 4th Canadian Masonry Symposium, Fredericton*, 1982.

[64] Lintz, J. M. and Toubia, E. A., *In-plane loading of brick veneer over wood shear walls.* . Masonry Soc. J., 2013, 31(1): p. 15-27.

[65] Pereira, P., Aguiar, J. B., Camões, A., and Lourenço, P. B. *The Portuguese masonry's mechanical characterization*. in *8th International Masonry Conference 2010 in Dresden*. 2010.

[66] Pereira, M. F. P., Pereira, M. F. N., Ferreira, J. E. D., and Lourenço, P. B., *Behavior of masonry infill panels in RC frames subjected to in-plane and out-of-plane loads*, in *7th International Conference amcm 2011*, 2011, Poland.

[67] Akhoundi, F., Vasconcelos, G., Lourenco, P., Silva, L., Cunha, F., and Fangueiro, R., *In-plane behavior of cavity masonry infills and strengthening with textile reinforced mortar*. 2018, 156: p.145-160.

[68] *EN 772-16*, in *Methods of test for masonry units - Part 16: Determination of dimensions*. 2005, European Committee for Standardization (CEN).

[69] *BS EN 772-19*, in *Determination of moisture expansion of large horizontally perfurated clay masory units*. 2000, European Committee for Standardization (CEN).

[70] *EN 1015-18*, in *Methods of test for mortar for masonry - Part 18: Determination of water absorption coefficient due to capillary action of hardened mortar*. 2002, European Committee for Standardization (CEN).

[71] *EN 1015-10*, in *Methods of test for masonry - Part 10: Determination of dry bulk density of hardened mortar*, 1999, European Committee for Standardization (CEN).

[72] Brooks, J. J., *Concrete and masonry movements* ed. Elsevier., 2014.

[73] *EN 1936*, in *Natural stone test methods. Determination of real density and apparent density and total and open porosity*, 2007, European Committee for Standardization (CEN).

[74] Haach, V. G., Vasconcelos, G., and Lourenço, P. B., *Influence of aggregates grading and water/cement ratio in workability and hardened properties of mortars.* Construction and Building Materials, 2011, 25(6): p. 2980-2987.

[75] Garbalińska, H. and Wygocka, A., *Microstructure modification of cement mortars: Effect on capillarity and frost-resistance.* Construction and Building Materials, 2014. 51: p. 258-266.

[76] *EN 1015-3*, in *Methods of test for mortar for masonry - Part 3: Determination of consistence of fresh mortar* 1999, European Committee for Standardization (CEN).

[77] *NP EN 772-1*, in *Métodos de ensaios de blocos para alvenaria. Parte 1 - Determinação da resistência à compressão*. 2002, European Committee for Standardization (CEN).

[78] *EN-1998-1*, in *Eurocode 8: Design of structures for earthquake resistance - Part 1: General rules, seismic actions and rules for buildings*. 1998, European Committee for Standardization (CEN).

[79] Cimpor, *Ficha Técnica. AA M5. Argamassa de assentamento de alvenaria.*, 2014.

[80] Cimpor, *Ficha Técnica. AA M10. Argamassa de assentamento de alvenaria.*, 2014.

[81] Cimpor, *Ficha Técnica. FVH. Argamassa de assentamento de alvenaria face à vista hidrofugada*., 2014.

[82] *EN 1015-11*, in *Methods of test for mortar for masonry Ð Part 11: Determination of flexural and compressive strength of hardened mortar*. 1999, European Committee for Standardization (CEN).

[83] Imperatore, S., Rinaldi, Z., and Drago, C., *Degradation relationships for the mechanical properties of corroded steel rebars.* Construction and Building Materials, 2017, 148: p. 219-230.

[84] Bai, Y., Dai, J., and Teng, J. G., *Buckling of steel reinforcing bars in FRP-confined RC columns: An experimental study.* Construction and Building Materials, 2017, 140: p. 403-415.

[85] Černý, M., Glogar, P., and Sucharda, Z., *Mechanical Properties of Basalt Fiber Reinforced Composites Prepared by Partial Pyrolysis of a Polymer Precursor*. 2009, 43: p. 1109-1120.

[86] Chen, W., Hao, H., Jong, M., Cui, J., Shi, Y., Chen, L., and Pham, T. M., *Quasi-static and dynamic tensile properties of basalt fibre reinforced polymer.* Composites Part B: Engineering, 2017, 125: p. 123-133.

[87] *BS EN 1052-1*, in *Methods of test of masonry - Part 1: Determination of compressive strength* 1999, European Committee for Standardization (CEN).

[88] *BS EN 1052-2*, in *Methods of test of masonry - Part 2: Determination of flexural strength*. 1999, European Committee for Standardization (CEN).

[89] *ASTM E519*, in *Standard Test Method for Diagonal Tension (Shear) in Masonry Assemblages*. 2002.

[90] *BS EN 1052-3*, in *Methods of test of masonry - Part 2: Determination of initial shear strength*. 2002, European Committee for Standardization (CEN).

[91] *EN 772-22*, in *Methods of test for masonry units. Determination of freeze/thaw resistance of clay masonry units*. 2006, European Committee for Standardization (CEN).

[92] *CSN 72 2452* in *Testing of Frost Resistance of Mortar (in Czech)*, 1968: Prague.

[93] Nunes, C. and Slížková, Z., *Freezing and thawing resistance of aerial lime mortar with metakaolin and a traditional water-repellent admixture.* Construction and Building Materials, 2016, 114: p. 896-905.

[94] Cultrone, G., Sebastián, E., Elert, K., de la Torre, M. J., Cazalla, O., and Rodriguez–Navarro, C., *Influence of mineralogy and firing temperature on the porosity of bricks.* Journal of the European Ceramic Society, 2004, 24(3): p. 547-564.

[95] Perrin, B., Vu, N. A., Multon, S., Voland, T., and Ducroquetz, C., *Mechanical behaviour of fired clay materials subjected to freeze–thaw cycles.* Construction and Building Materials, 2011, 25(2): p. 1056-1064.

[96] Pospíchal, O., Kucharczyková, B., Misák, P., and Vymazal, T., *Freeze-thaw resistance of concrete with porous aggregate.* Procedia Engineering, 2010, 2(1): p. 521-529.

[97] Arizzi, A., Viles, H., and Cultrone, G., *Experimental testing of the durability of lime-based mortars used for rendering historic buildings.* Construction and Building Materials, 2012, 28(1): p. 807-818.

[98] Martins, L., Vasconcelos, G., Lourenço, P. B., and Palha, C., *Influence of the Freeze-Thaw Cycles on the Physical and Mechanical Properties of Granites.* Journal of Materials in Civil Engineering, 2015, 28(5).

[99] Veiga, R., *As Argamassas na Conservação (Mortars in Conservation)*, in *Actas das 1a as Jornadas de Engenharia Civil da Universidade de Aveiro*. 2003: Lisbon.

[100] Cao, J. and Chung, D. D. L., *Damage evolution during freeze–thaw cycling of cement mortar, studied by electrical resistivity measurement.* Cement and Concrete Research, 2002, 32(10): p. 1657-1661.

[101] Nunes, C., Slížková, Z., and Krivankova, D., *Frost resistance of lime-based mortars with linseed oil* in *XIII Bilateral Czech/German Symposium*. 2012.

[102] Marzouk, H., Jiang, D., *Effects of freezing and thawing on the tension properties of high-strength concrete.* ACI Mater. J. , 1994, 91 (6): p. 577– 586.

[103] Biolzi, L., Guerrini, G. L., and Rosati, G., *Frost durability of very high performance cement-based materials.* J. Mater. Civil Eng. , 1999, 11(2): p. 167-170.

[104] Rutherford, J. H., Langan, B. W., and Ward, M. A., *Use of control specimens in freezing and thawing testing of concretes.* Cem., Concr. Aggreg., 1994, 16(1): p. 78-82.

[105] Bordeleau, D., Pigeon, M., and Banthia, N., *Comparative study of latexmodified concretes and normal concretes subjected to freezing and thawing in the presence of a deicer salt solution.* ACI Mater. J., 1992, 89(6): p. 547-553.

[106] Bakharev, T. and Struble, L. J. *Microstructural features of freeze – thaw deterioration of concrete*. in *Proceedings of the 1994 MRS Fall Meeting on Microstructure of Cement-Based Systems/Bonding and Interfaces in Cementitious Materials*, 1995. Pittsburgh.

[107] Akhras, N. M., *Detecting freezing and thawing damage in concrete using signal energy*. Cem. Concr. Res. , 1998, 28(9): p. 1275-1280.

[108] Uranjek, M. and Bokan-Bosiljkov, V., *Influence of freeze–thaw cycles on mechanical properties of historical brick masonry.* Construction and Building Materials, 2015, 84: p. 416-428.

[109] Lu, Z., Zhou, X., and Zhang, J., *Study on the performance of a new type of water-repellent admixture for cement mortar.* Cement and Concrete Research, 2004, 34(11): p. 2015-2019.

[110] Zhu, Y.-G., Kou, S.-C., Poon, C.-S., Dai, J.-G., and Li, Q.-Y., *Influence of silane-based water repellent on the durability properties of recycled aggregate concrete.* Cement and Concrete Composites, 2013, 35(1): p. 32-38.

[111] Vikan, H. and Justnes, H., *Influence of vegetable oils on durability and pore structure of mortars*, 2006: p. 417-430.

[112] Chandra, S., *History of Architecture and Ancient Building Materials in India*, ed. T.B. International. 2003, New Delhi.

[113] Fang, S., Zhang, H., Zhang, B., and Li, G., *A study of Tung-oil–lime putty—A traditional lime based mortar.* International Journal of Adhesion and Adhesives, 2014, 48: p. 224-230.

[114] Ventolà, L., Vendrell, M., Giraldez, P., and Merino, L., *Traditional organic additives improve lime mortars: New old materials for restoration and building natural stone fabrics.* Construction and Building Materials, 2011, 25(8): p. 3313-3318.

[115] Monteiro, P. J. M. and Mehta, P. K., *Concrete: Microstructure, Properties and Materials*, ed. E.t. edition, 2006: Mc Graw Hill.

[116] Çavdar, A., *Investigation of freeze–thaw effects on mechanical properties of fiber reinforced cement mortars.* Composites Part B: Engineering, 2014. 58: p. 463-472.

[117] Shang, H. S. and Song, Y. P., *Experimental study of strength and deformation of plain concrete under biaxial compression after freezing and thawing cycles.* Cement and Concrete Research, 2006, 36(10): p. 1857-1864.

[118] Zhang, P. and Li, Q.-f., *Effect of polypropylene fiber on durability of concrete composite containing fly ash and silica fume.* Composites Part B Engineering, 2013, 45: p. 1587-1594.

[119] Richardson, A. E., Coventry, K. A., and Wilkinson, S., *Freeze/thaw durability of concrete with synthetic fibre additions.* Cold Regions Science and Technology, 2012, 83–84: p. 49-56.

[120] *EN 12371*, in *Natural stone test methods. Determination of frost resistance.* 2010, European Committee for Standardization (CEN).

[121] Lanas, J., Sierra, R., and Alvarez, J. I., *Study of the mechanical behavior of masonry repair lime-based mortars cured and exposed under different conditions.* Cem. Concr. Res. 36, 2006, 36: p. 961-970.

[122] Popovics, S., *Effects of uneven moisture distribution on the strength and wave velocity in concrete.* Ultrasonics, 2005, 43: p. 429–34.

[123] Kahraman, S., *The correlations between the saturated and dry P-wave velocity of rocks,*. Ultrasonics, 2007, 46 (4): p. 341-348.

[124] Vasconcelos, G., Lourenco, P. B., Alves, C. A. S., and Pamplona, J., *Ultrasonic evaluation of the physical and mechanical properties of granites.* Ultrasonics 2008, 48 (453-66).

[125] *EN 14579*, in *Natural stone test methods – determination of sound speed propagation.*, 2004, European Committee for Standardization (CEN).

[126] *ASTM G57*, in *Standard Method for Field Measurement of Soil Resistivity Using the Wenner Four- Electrode Method*., 2006.

[127] Cao, J. and Chung, D. D. L., *Minor damage of cement mortar during cyclic compression monitored by electrical resistivity measurement.* Cem. Concr. Res., 2001. 31(10): p. 1519-1521.

[128] *EN 12390-3*, in *Ensaios de betão endurecido. Parte 3: Resistência à compressão dos provetes de ensaio* 2003, European Committee for Standardization (CEN).

[129] *NP EN 12390-2*, in *Ensaios de betão endurecido. Parte 2: Execução e cura dos provetes para ensaios de resistência mecânica*. 2003, European Committee for Standardization (CEN).

[130] Nahataa, Y., Kholiaband, N., and Tankc, T. G., *Effect of Curing Methods on Efficiency of Curing of Cement Mortar*, APCBEE Procedia, 2014, 9: p. 222-229.

[131] Silva, B., *Análise de influência do tipo de cura na resistência à compressão de corpos-de-prova de concreto*, in *Instituto Tecnológico de Aeronáutica*., 2009.

[132] Cunha, M., *Influência da interface da cinética de embebiçao e secagem de paredes com múltiplas camadas* 2013, Universidade do Porto.

[133] Elert, K., C. Rodriguez-Navarro, Pardo, E. S., Hansen, E., and Cazalla, O., *Lime Mortars for the Conservation of Historic Buildings.* Studies in Conservation, 2002. 47: p. 62-75.

[134] Silva, P. C., Ferreira, R. M., and Figueiras, H., *Medições de resistividade elétrica avaliada em provetes de betão: influência do método de ensaio e das condições de cura*, in *Encontro Nacional Betão estrutural* 2012, 2012, Porto.

[135] Martins, A., Vasconcelos, G., and Campos Costa, A., *Brick masonry veneer walls: An overview.* Journal of Building Engineering, 2017. 9: p. 29-41.

[136] Magenes, G. and Calvi, G. M., *In-plane seismic response of brick masonry walls.* Earthquake Engineering and Structural Dynamics;, 1997. 26: p. 1091-1112.

[137] Polensek, A. and Laursen, H. I., *Seismic behavior of bending components and intercomponent connections of light framed wood buildings*. 1984.

[138] Stewart, W. G., *The seismic design of plywood-sheathed shear walls*. 1987, Univ. of Canterbury, Christchurch, New Zealand.

[139] Dolan, J. D., *The dynamic response of timber shear walls.* 1989, University of British Columiba, B.C., Canada.

[140] Ceccotti, A. and Vignoli, A. *Engineered timber structures: An evaluation of their seismic behaviour*. in *Proceedings of International Timber Engineering Conference*. 1990, Japan.

[141] Modena, C., *Seismic behaviour of masonry structures: experimentally based modelling. Part 1 and Part 2.* Masonry International, 1992, 6(2): p. 57-62 (Part 1); 62-68 (Part 2).

[142] Foliente, G. C., *Hysteresis modeling of wood joints and structural systems.* Journal of Structural Engineering, 1995, 126 (6): p. 1013-1022.

[143] Krawinkler, H., Parisi, F., Ibarra, L., Ayoub, A., and Medina, R., *Development of a testing protocol for woodframe structures*. 2000, Consortium of Universities for Research in Earthquake Engineering, Richmond, Calif.

[144] Folz, B. and Filiatrault, A., *A computer program for cyclic analysis of wood shear walls*. 2000, Consortium of Universities for Research in Earthquake Engineering, Richmond, Calif.

[145] Folz, B. and Filiatrault, A., *Cyclic analysis of wood shear walls.* Journal of Structural Enginering 2001, 127(4): p. 433-441.

[146] Pang, W. C., Rosowsky, D. V., ASCE, M., Pei, S., Lindt, J. W. v. d., and ASCE, M., *Evolutionary parameter hysteretic model for wood shear walls.* Journal of structural engineering, 2007, 133 (8): p. 1118–1129.

[147] Belmouden, Y. and Lestuzzi, P., *Analytical model for predicting nonlinear reversed cyclic behaviour of reinforced concrete structural walls.* Engineering Structures, 2007, 29: p. 1263-1276.

[148] Porto, F. D., Grendene, M., and Modena, C., *Estimation of load reduction factors for clay masonry walls.* Earthquake Engineering and Structural Dynamics, 2009, 38: p. 1155-1174.

[149] Nicolini1, L. and Porto, F. d., *Definition of equivalent damping for masonry strucutres in support of displacement based design*, in *15th International Brick and Block Masonry Conference*, 2012: Florianópolis, Brasil

[150] Foschi, R. O., *Load-slip characteristics of nails.* Wood Science, 1974, 7(1): p. 69-76.

[151] Negro, G., Vasconcelos, G., Poletti, E., Magenes, G., and Martins, A. *Modelação numérica do comportamento de ligadores metálicos à tração em paredes de tijolo face à vista* in *10 CNME* 2016, 2016, LNEC.

[152] Akhoundi, F., *Strategies for Seismic Strengthening of Masonry Infilled Reinforced Concrete Frames*. PhD thesis, 2016, University of Minho

[153] Costa, A, F., Costa, C., Rodrigues, H., and Arêde, A. *Characterization of structural characteristics of Portuguese buildings with masonry infill walls stock*. in *9th International Masonry Conference*. 2014, University of Minho, Guimarães, Portugal

[154] *ACI 318-08* in *Building Code Requirements for Structural Concrete (ACI 318-08) and Commentary.* 2008, American Concrete Institute.

[155] *ASTM E72-02* in *Standard test methods of conducting strength tests of panels for building construction*, 2002, American Society for Testing and Materials.

[156] *FEMA 461*, in *Interim Testing Protocols for Determining the Seismic Performance Characteristics of Structural and Nonstructural Components*, 2007, Federal Emergency Management Agency.

[157] Frumento, S., Magenes, G., Morandi, P., and Calvi, G. M., *Interpretation of experimental shear tests on clay brick masonry walls and evaluation of q-factors for seismic design*, Pavia: IUSS Press., 2009.

[158] *SEI/ASCE 7-02*, in *Minimum Design Loads for Buildings and Other Structures* 2002, Structural Engineering Institute of the American Society of Civil Engineers.

[159] *ASCE/SEI 7-10*, in *Minimum Design Loads for Buildings and Other Structures* 2010, Structural Engineering Institute of the American Society of Civil Engineers.

[160] *TMS 402-08/ACI 530-08/ASCE 5-08, in Building Code Requirements for Masonry Structures. The Masonry Society, Boulder, Colorado, the American Concrete Institute, Farmington Hills, Michigan, and the American Society of Civil*. 2008: Engineers, Reston, VA. Reported by the Masonry Standards Joint Committee (MSJC).

[161] *ASCE/SEI 31-03*, in *Seismic Evaluation of Existing Building*. 2010, Structural Engineering Institute of the American Society of Civil Engineers.

[162] *ASCE/SEI 41-13*, in *Seismic Evaluation and Retrofit of Existing Building*. 2010, Engineering Institute of the American Society of Civil Engineers.

[163] *ASCE/SEI 41-17*, in *Seismic Evaluation and Retrofit of Existing Building*. 2010, Engineering Institute of the American Society of Civil Engineers.

[164] *ASCE/SEI 41-06*, in *Seismic Rehabilitation of Existing Building*. 2010, Engineering Institute of the American Society of Civil Engineers.

[165] FEMA, *FEMA 273*, in *NEHRP Guidelines for the seismic rehabilitation of buildings*, 1997, Federal Emergency Management Agency.

[166] Priestley, M. J. N., *Performance based seismic design* in *12WCEE 2000*, 2000, University of California, San Diego.

[167] Oxman, R., *Performance-based Design: Current Practices and Research Issues*. Vol 6. 2008.

[168] Kalay, Y., *Performance-based design*. Vol. 8. 1999. 395-409.

[169] Collins, K. R. and Stojadinovic, B., *Limits states for performance based design* in *12WCEE 2000*. 2000, University of California, San Diego.

[170] Frumento, S., Magenes, G., Morandi, P., and Calvi, G. M., *Interpretation of experimental shear tests on clay brick masonry walls and evaluation of q-factors for seismic design,* 2009.

[171] Tomaževič, M., *Earthquake-resistant design of masonry buildings,* 1999.

[172] Moreira, S., *Seismic retrofit of masonry-to-timber connections in historical constructions*. PhD thesis, 2015, University of Minho

[173] *EN-1998-3,* in *Eurocode 8: Design of structures for earthquake resistance - Part 3: Assessment and retrofitting of buildings*. 1998, European Committee for Standardization (CEN).

APPENDIX

A. Details of cyclic out-of-plane tests of brick veneer walls

A.1. Out-of-plane cyclic tests: deformation capacity

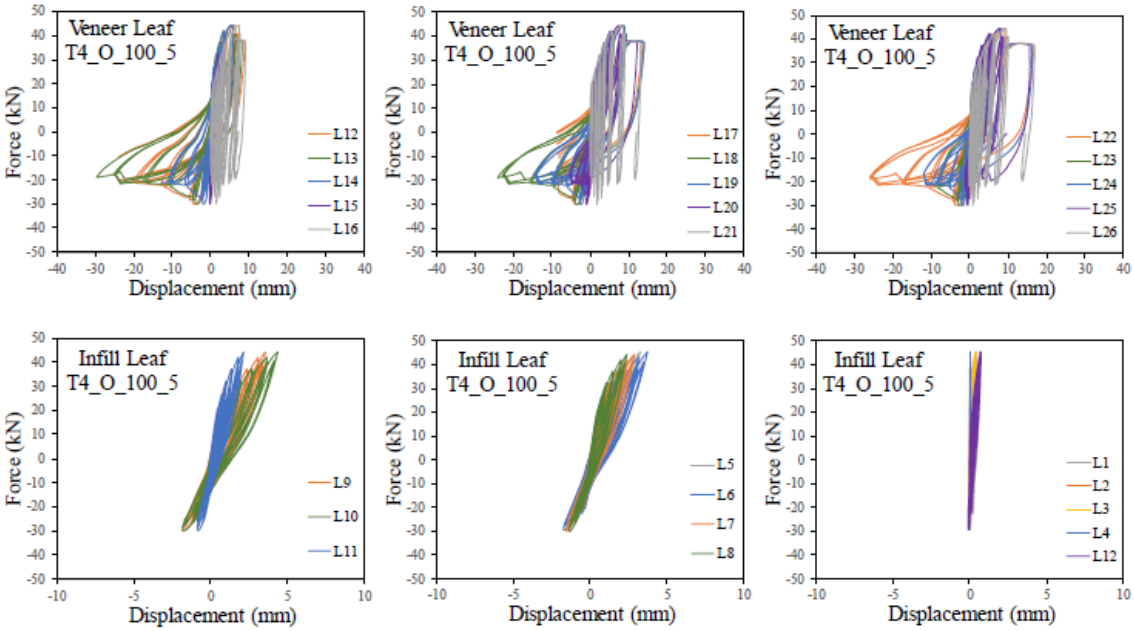

Figure A.1 – Hysteresis responses of infill and veneer leaf of T4_O_100_5 wall

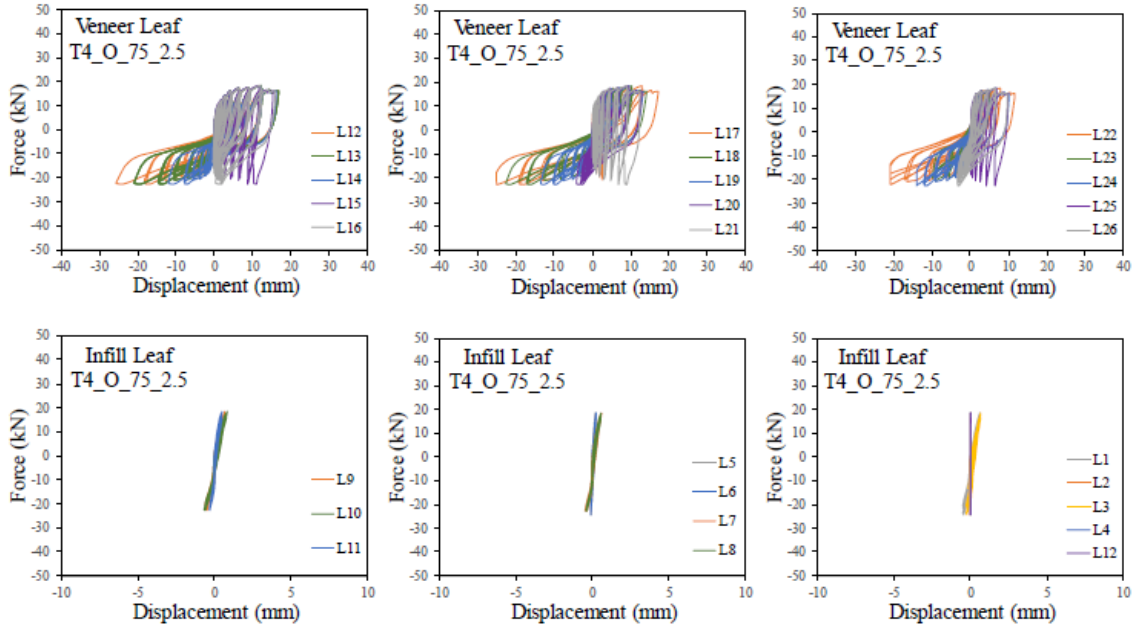

Figure A.2 – Hysteresis responses of infill and veneer leaf of T4_O_75_2.5 wall

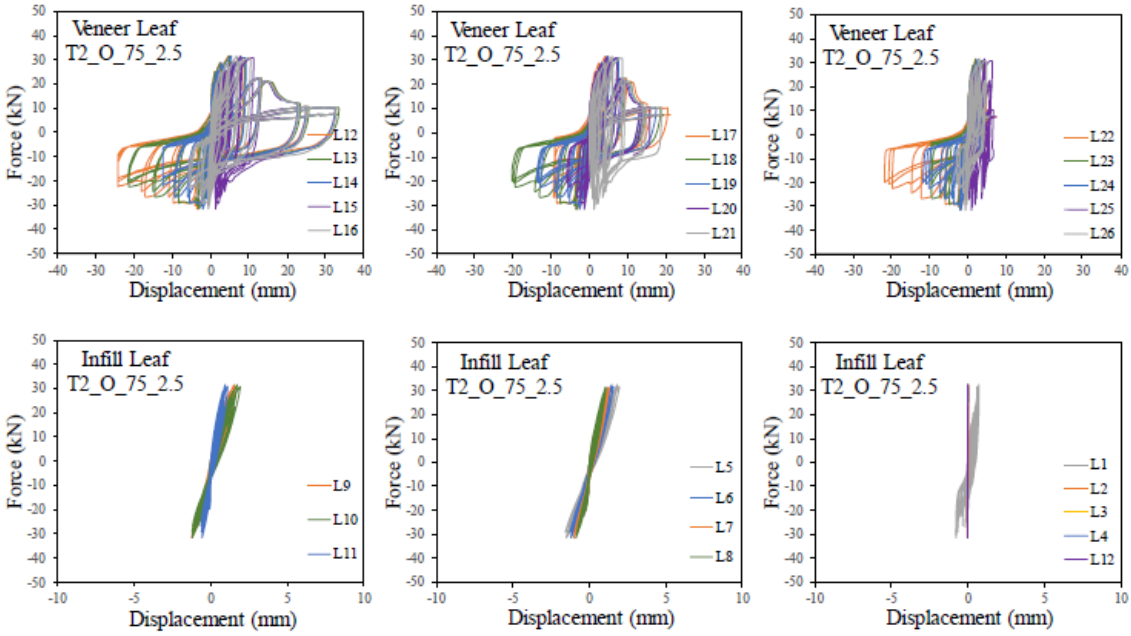

Figure A.3 – Hysteresis responses of infill and veneer leaf of T2_O_75_2.5 wall

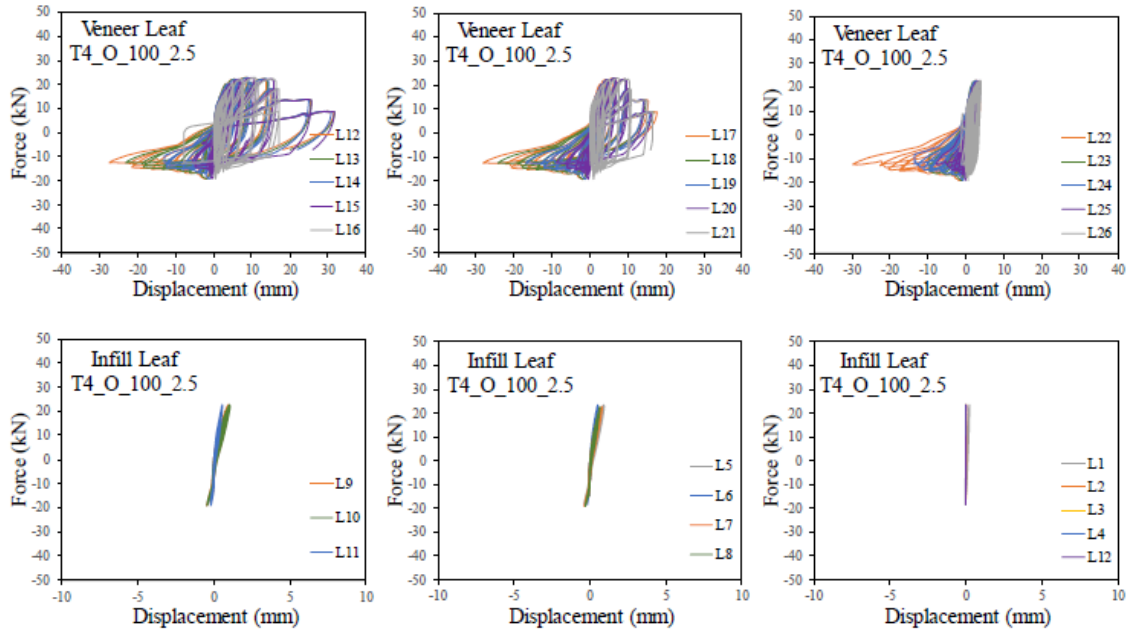

Figure A.4 – Hysteresis responses of infill and veneer leaf of T4_O_100_2.5 wall

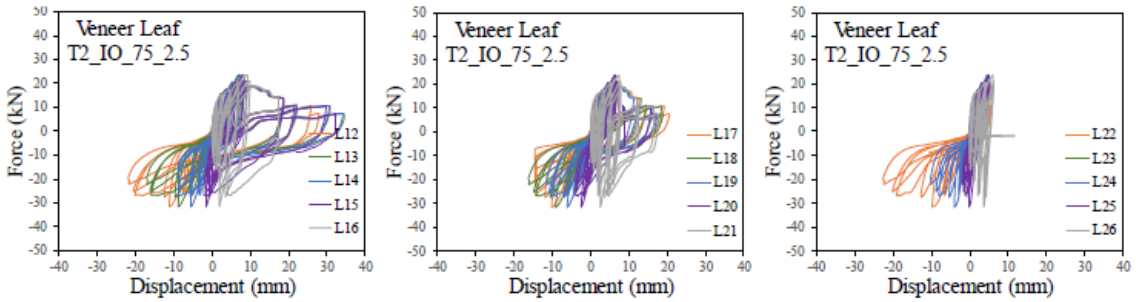

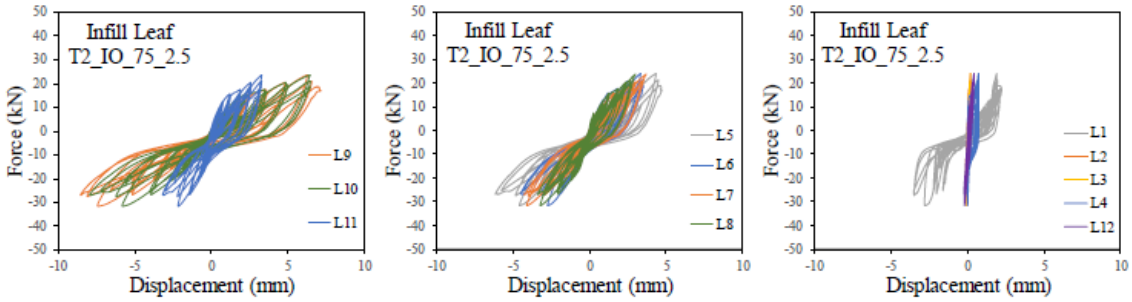

Figure A.5 – Hysteresis responses of infill and veneer leaf of T2_IO_75_2.5 wall

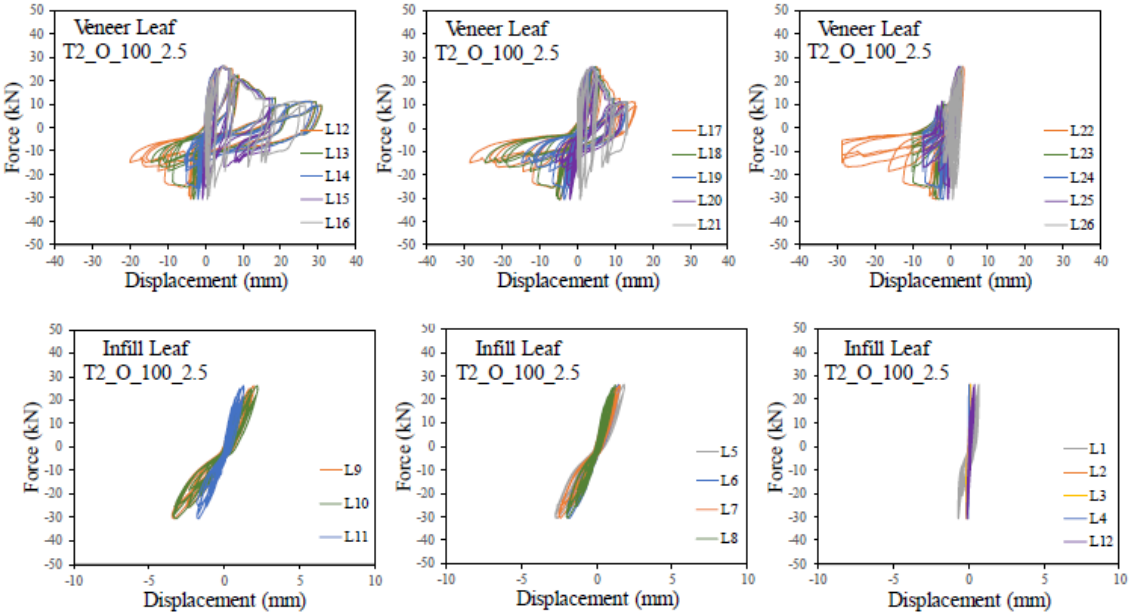

Figure A.6 – Hysteresis responses of infill and veneer leaf of T2_O_100_2.5 wall

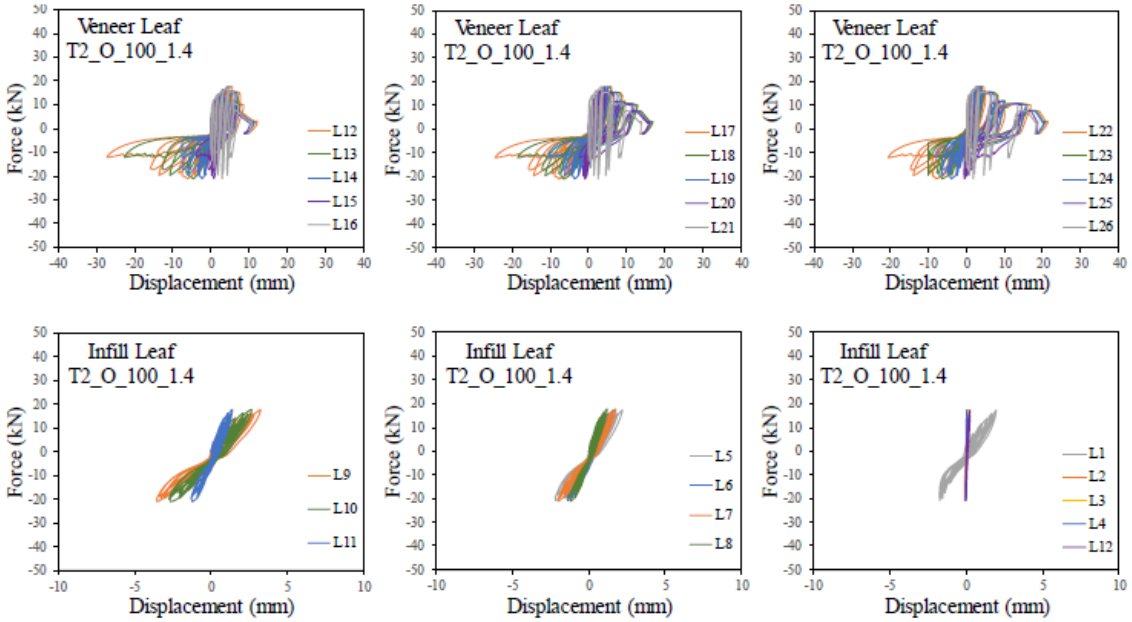

Figure A.7 – Hysteresis responses of infill and veneer leaf of T2_O_100_1.4 wall

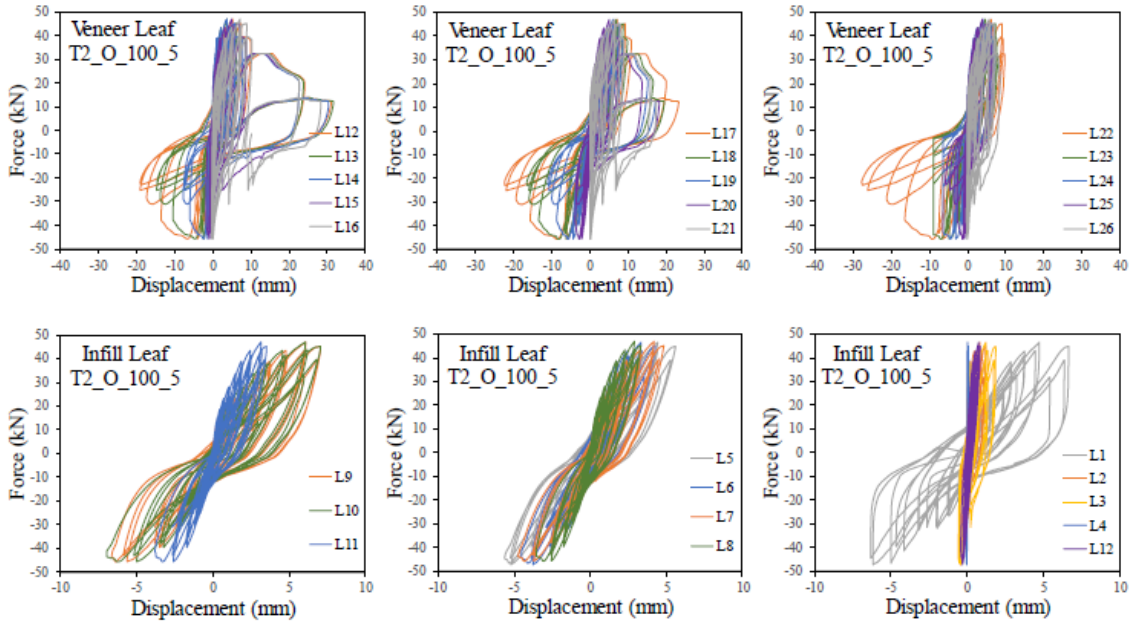

Figure A.8 – Hysteresis responses of infill and veneer leaf of T2_O_100_5 wall

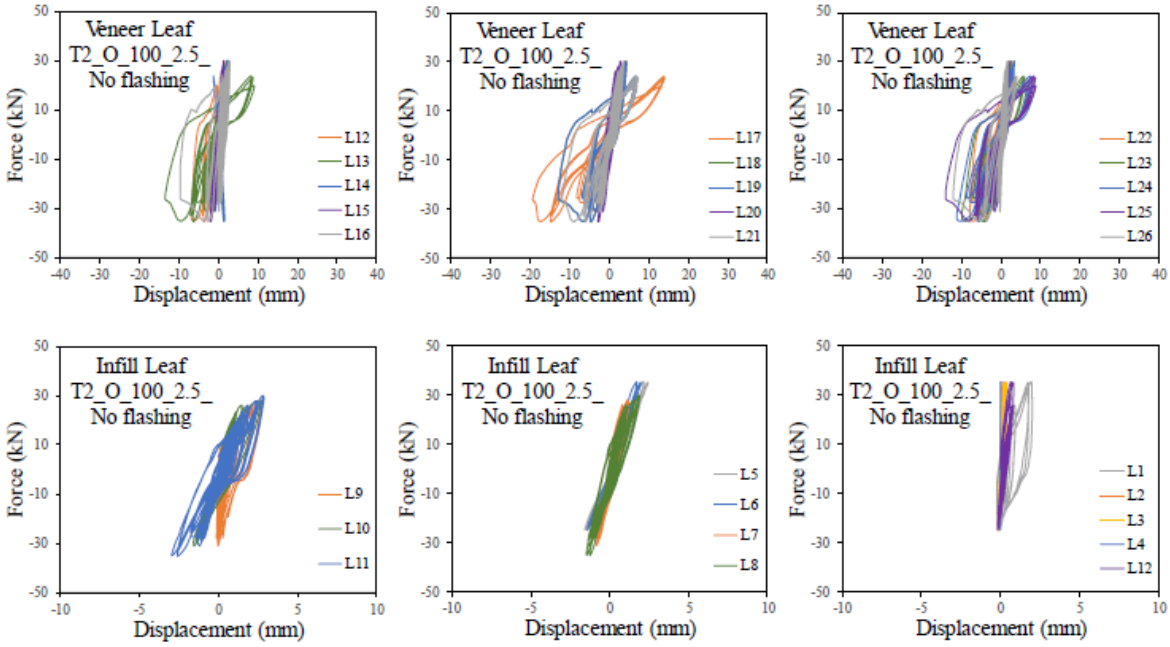

Figure A.9 – Hysteresis responses of infill and veneer leaf of T2_O_100_2.5_No flashing wall

A.2. Out-of-plane cyclic tests: comparison of hysteresis responses

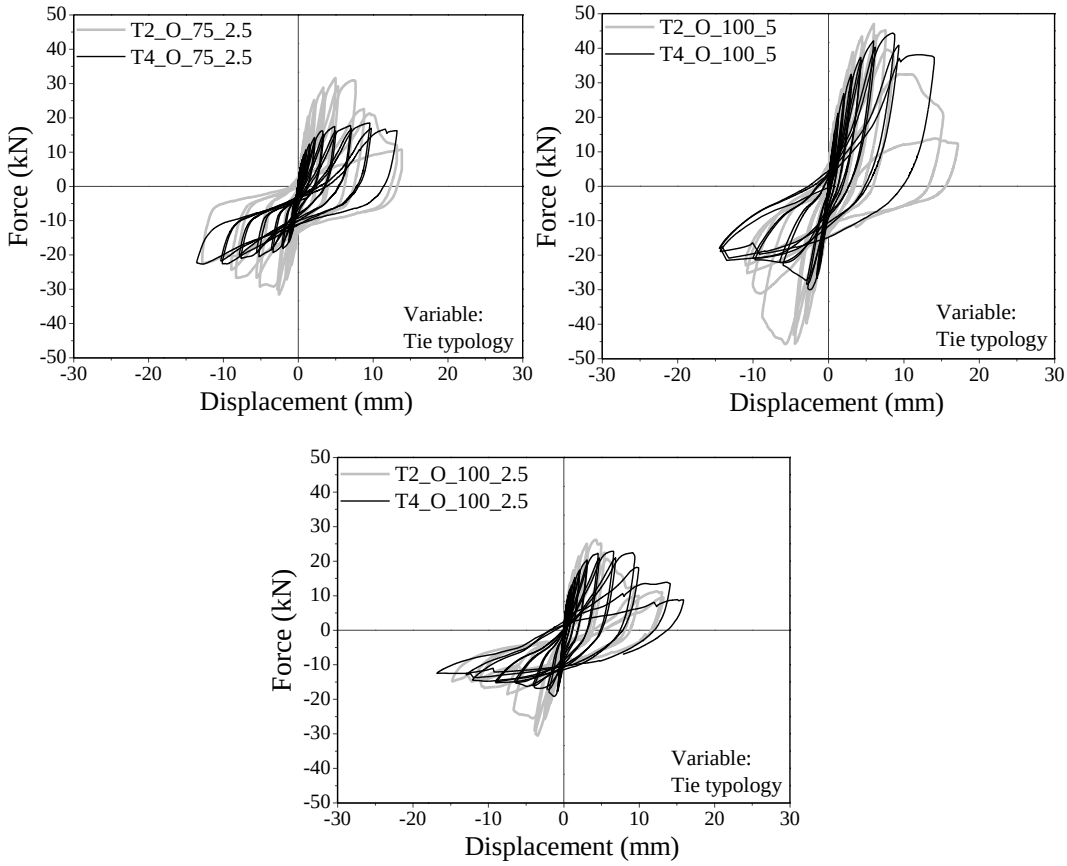

Figure A.10 – Hysteresis responses of walls with different tie typology

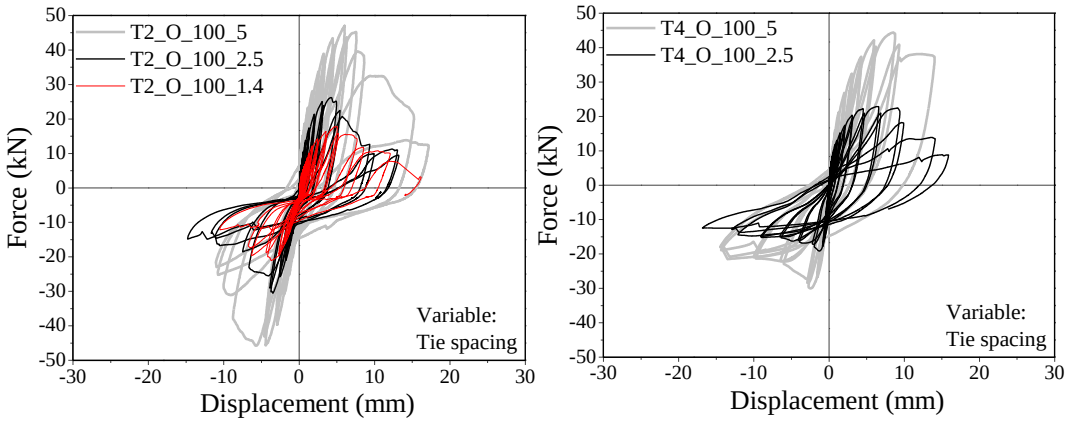

Figure A.11 – Hysteresis responses of walls with different tie spacing

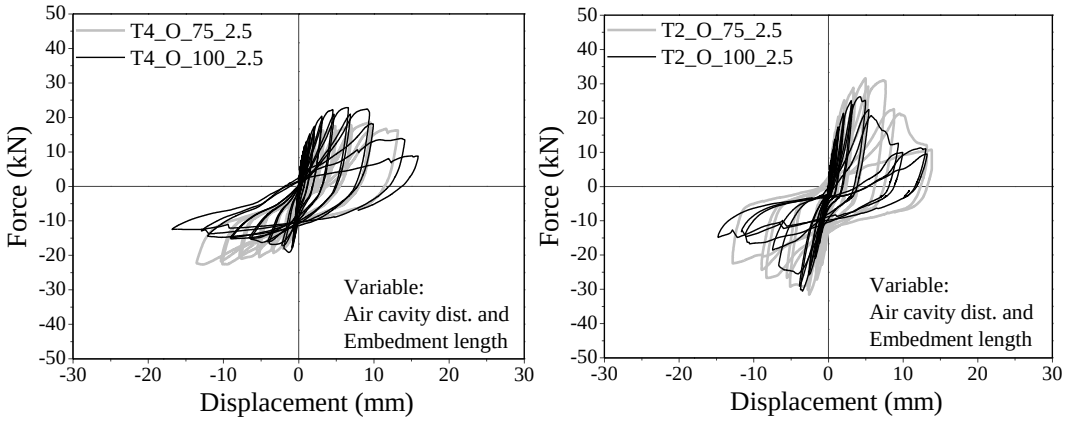

Figure A.12 – Hysteresis responses of walls with different air cavity distance and embedment length

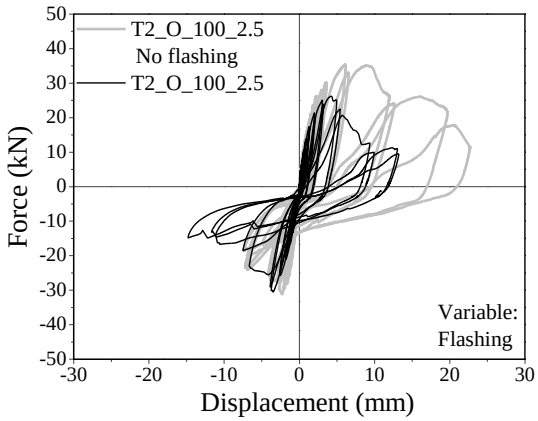

Figure A.13 – Hysteresis responses of walls with and without flashing

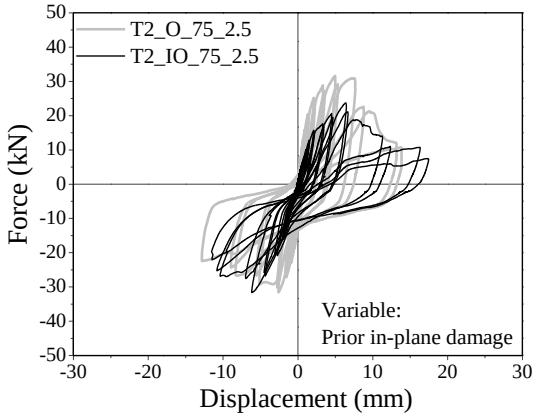

Figure A.14 – Hysteresis responses of walls with and without prior in-plane damage

Este trabalho foi financiado pelo Governo de Portugal e pelo Fundo Social Europeu da União Europeia (EU/FSE), através da Fundação para a Ciência e Tecnologia (FCT), através de uma Bolsa de Doutoramento SFRH/BD/96484/2013, e no âmbito do Programa Operacional Potencial Humano inscrito no Quadro de Referência Estratégico Nacional (POPH/QREN).